FACULTY OF SCIENCES

Anthracene-based crosslinked polymer systems with tunable thermo- and photoreversible properties

Jonas Van Damme

Promotor:
Prof. Dr. Filip Du Prez

Academic year 2017–2018

Submitted to the Faculty of Sciences of Ghent University, in Fulfilment of the Requirements for the Degree of Doctor of Science: Chemistry

GHENT UNIVERSITY

FACULTY OF SCIENCES

ANTHRACENE-BASED CROSSLINKED POLYMER SYSTEMS WITH TUNABLE THERMO- AND PHOTOREVERSIBLE PROPERTIES

Jonas Van Damme

Supervisor: Prof. Dr. Filip Du Prez

A dissertation submitted to the Faculty of Sciences of Ghent University, in fulfilment of the requirements for the degree of Doctor of Science: Chemistry

Academic year: 2017 – 2018

GHENT UNIVERSITY

Exam commission

Prof. dr. Richard Hoogenboom (chair, Ghent University)

Prof. dr. Filip Du Prez (promotor, Ghent University)

Prof. dr. Rint Sijbesma (Eindhoven University of Technology)

Prof. dr. ir. Guy Van Assche (Vrije Universiteit Brussel)

Prof. dr. Sandra Van Vlierberghe (Ghent University)

Prof. dr. Johan Winne (Ghent University)

Research funded by Flanders – Innovation & Entrepreneurship

Onderzoek gefinancieerd door het Agentschap Innoveren & Ondernemen

Dankwoord

Het schrijven van een doctoraat heeft heel wat voeten in de aarde. Bijgevolg dien ik heel wat mensen te bedanken voor hun grote of kleine bijdrage tot dit proefschrift.

Allereerst wens ik mijn promotor, professor Filip Du Prez, te bedanken om mij te accepteren als doctoraatsstudent en met een positieve attitude daarbij te begeleiden van begin tot eind. Mijn leven als student had armzalig geweest zonder de financiële steun van de Universiteit Gent en het Vlaams Agentschap Innoveren & Ondernemen (VLAIO).

Dit project kwam mede in stand door professoren Guy Van Assche en Bruno Van Mele van de FYSC groep (VUB), en werd later ook bijgestaan door Joost Brancart. Hun diepgaande inzichten in de fysicochemische aspecten brachten ongetwijfeld dit onderzoek tot een hoger niveau.

Uiteraard wil ik iedereen bedanken die deze afgelopen jaren gedurende langere of kortere tijd lief en leed heeft gedeeld met me in de PCR groep. In het bijzonder dien ik Otto van den Berg te bedanken, die mijn collega en mentor is geweest in ons onderzoek naar antraceengebaseerde reversibele netwerken. Wij werden bijgestaan in onze queeste door enkele studenten, waaronder Laetitia Vlaminck, Lea Sollka en Akın Gürsoy. De samenwerking met Subrata Chattopadhyay had een andere focus, wat voor een aangename afwisseling zorgde. De sfeer en collegialiteit in de groep is van een ongekend niveau, en zal ik - voor zolang ik niet dementeer - niet vergeten! Met iedereen heb ik herinneringen die ik zal blijven koesteren, gaande van lomp labowerk tot *groovy dancemoves* op conferentiefeestjes. Ik kan proberen iedereen in de (vak)groep op te sommen, maar omdat ik dan mogelijk iemand vergeet (zoals bijvoorbeeld Bernhard), hou ik het algemeen: Bedankt iedereen!

Dan moet ik nog al mijn vrienden (*ja, ik heb vrienden*) en (schoon)familie te bedanken voor hun steun, klein en groot. Uiteraard een dikke merci aan mijn mama, die hopelijk binnenkort

een beetje begrijpt waar ik mee bezig was. Na al die jaren blijf ik van mening dat mijn mama de beste is!

Er is nog iemand die ik zeker niet (nog eens) over het hoofd mag zien. Delphi, je staat altijd voor me klaar en was al die jaren – al dan niet gewild - mijn klankbord, steun en toeverlaat.

Table of contents

Chapter IV: Thermo-degradable and photo-reversible thiol-ene networks

Chapter V: Reversible PU materials: easy removability, remoldability and stress-relaxation

Chapter I: Introduction to the thesis

1. Coatings

1.1 Introduction

Coatings (such as paints) are thin material layers covering surfaces of objects, also known as substrates. The oldest example hereof are ancient rock paintings. While this is an example of a coating which is more important than the surface, often a coating is applied to protect or supplement a more important *substrate*. Such is the case for anti-corrosive coatings, which provides barriers between the surfaces and corrosive chemicals (oxygen and water, acids,..).

In general, coatings are applied to provide the substrate with additional properties. This could be resistance to corrosion, higher scratch resistance, increased or decreased reflection, a pleasant feel, …

Substrates may be flexible materials such as rubbers or even living tissue, but can also be rigid materials such as wood, metal, glass, ceramic, hard plastic or composite. Coating materials may be elastomeric, glassy or crystalline, depending on desired surface properties. Aside from polymeric coating materials, as will be discussed in this thesis, also other materials (e.g. waxes and ceramics) are possible.

Coatings are applied using different techniques and chemistries, although some generalizations are valid for most cases (illustrated in Figure I.1):

- Firstly, the substrate is cleaned, as impurities may lead to film defects, bad adhesion and problems with hardening. Additional preparation steps can also be taken, e.g. roughening the surface to increase adhesion.
- Secondly, the material is deposited on the surface which for organic coatings often is as a liquid *resin*. A resin can be applied by spraying, brushing or dipping the substrate into the resin. Excess material can be removed by doctor blading.
- Thirdly, the resin dries or cures and forms a solid coating. This can be physically and/or chemically driven. Physical hardening occurs by evaporation of solvent. Chemical hardening or cure occurs by polymerization and/or cross-linking of monomers and prepolymers.

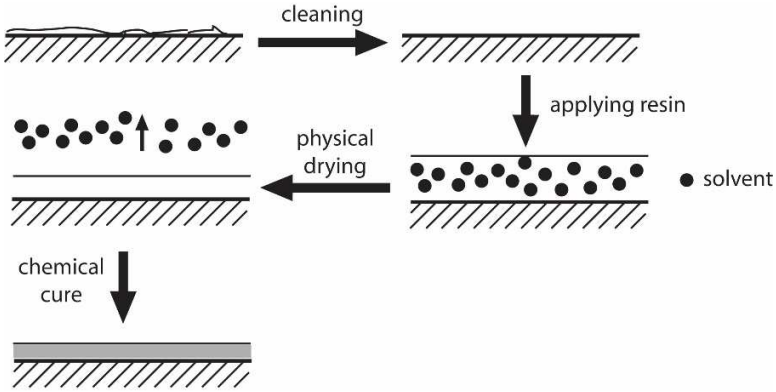

Figure I.1. Simplistic representation of coating process.

1.2 Polymerization and curing chemistries

As there are many different kinds of coating materials, both chemically and physically, a short introduction on some commonly used chemistries is given in this chapter.

Polyurethane coatings are made by the addition reaction of alcohols with isocyanates (Figure I.2).[1] While reaction of diols and diisocyanates leads to linear polymer chains, polymer networks are achieved by cross-linking using polyisocyanates or – as is more often the case - polyols. This stepwise polymerization occurs thermally and usually requires catalysis. Any water present (e.g. moisture from the atmosphere) competes with the alcohol groups. The reaction of water with isocyanates leads to primary amines and carbon dioxide. The formed amines quickly react with isocyanates, forming urea bonds. Therefore, often moisture is avoided and an excess of isocyanates is used. Polyurethane materials are further discussed in chapter V.

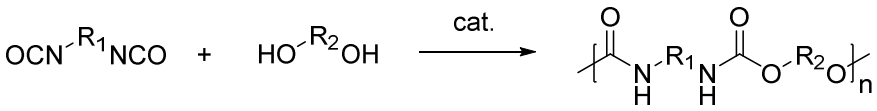

Figure I.2. Catalyzed polymerization to a polyurethane.

Acrylate coatings are made by radical polymerization (Figure I.3).[2] This chain polymerization is initiated by radicals generated by heating or irradiating thermal and light-sensitive initiators, respectively. The latter initiation method is often used for coatings because of the energy-efficient and

fast cure. Using di- or polyfunctional acrylates, polyacrylate networks are made. This reaction is sensitive to oxygen, which reacts with radical chain ends and quenches the polymerization.

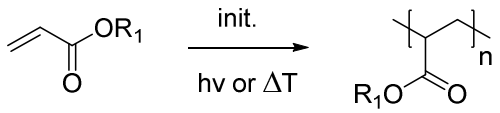

Figure I.3. Light or thermally initiated acrylate homopolymerization.

Epoxy materials are cured by chain homopolymerization of epoxide-containing monomers (Figure I.4) or by stepwise polymerization with amines, (cyclic) anhydrides, phenols or thiols (Figure I.5).[3] Homopolymerization requires an anionic or cationic catalyst and is less frequently used. The stepwise polymerization typically involves heating, with the exception of the highly reactive thiols. Monomers suitable for epoxy-amine chemistry will be described in chapter III. While one of those monomers was used to develop linear chains having pending anthracene groups, the detailed discussion thereof lies out of the scope of this thesis.

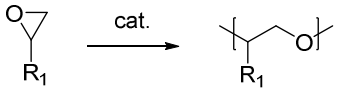

Figure I.4. The catalyzed epoxy homopolymerization.

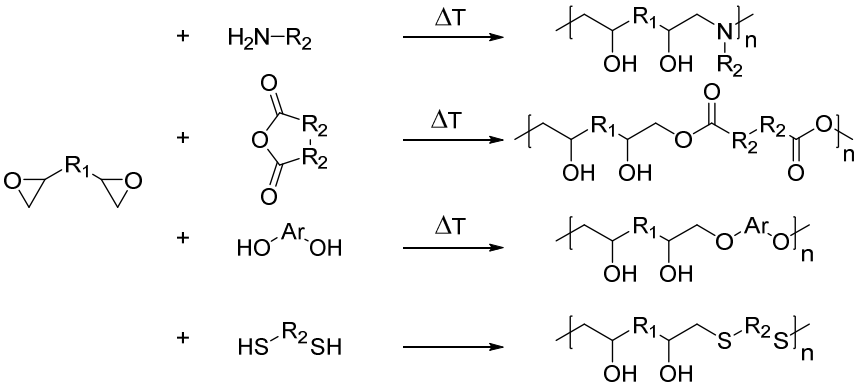

Figure I.5. Epoxy cure with amines, cyclic anhydrides, phenols and thiols.

Thiol-ene coatings are not commonly used in industry, but have great potential because of their reactivity, selectivity and efficiency.[4] The reactions occur between thiols and double bonds, either by

free-radical addition or by catalyzed Michael addition (Figure I.6). Thiol-ene based materials will be further discussed in chapter IV.

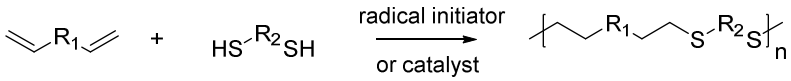

Figure I.6. Thiol-ene reaction (or alkene hydrothiolation).

1.3 Challenges for coatings

Despite the long history and widespread use of coatings, many challenges remain to be tackled. Some are related to adding new functionalities, while others are focused on enhancing lifetimes and reducing ecological impacts. In what follows, several of these challenges are presented.

After application of a coating, it is often desirable that the properties it provides to the substrate remain for a long time. Unfortunately, coatings may fail prematurely. One of the underlying causes leading to coating failure (e.g. by delamination) is stress.[5] Stress occurs due to hindered shrinkage in the material during cure. Permanent cross-linking hinders the occurrence of creep and thus stress-relaxation. Therefore, cross-linked coatings are by definition already in a stressed state. Stress levels may increase during its lifetime by deformations, temperature changes, (solvent) swelling, …

Outdoor coatings are exposed to sunlight, which partially contains ultraviolet light. Irradiation at these wavelengths leads to undesirable side reactions in the coating, often resulting in additional cross-linking, chain scission and color changes[6]. In industrial coating formulations, UV absorbers are often used to limit these effects of solar irradiation.

While high toughness and good adhesion are desirable properties, these properties are a nuisance when attempting to remove a coating from its substrate. This may be necessary for inspection of the substrate, recycling of the substrate or clearing the surface for reapplying a coating. The removal of old coatings is done mechanically by scrubbing or sandblasting and chemically by using solvents and aggressive chemicals.

2. Reversible chemistries in polymer science

2.1 Introduction

As previously mentioned, many challenges remain in coating technology. In this context, the use of reversible cross-links in polymer networks and thermoset coatings has been heavily studied for the past decades. By making controlled alterations to the cross-link density and/or adding dynamic character to the cross-links, these materials can heal from scratches and internal stress can be dissipated, leading to elongated lifetimes. Two mechanisms exist for these reversible bonds: reversible additions and reversible exchanges.[7]

Reversible bonds using a *reversible addition* mechanism exist in either a broken or formed state (Figure I.7). Upon application of a stimulus, the ratio between broken and formed bonds – and thus cross-linking density – can be varied. This change can occur either dynamically, i.e. under simultaneous bond formation and scission, or by exclusively stimulating formation or scission. This mechanism is also called a *dissociative* mechanism, as exchange of binding partners requires dissociation before addition is possible.

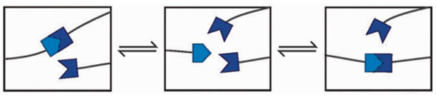

Figure I.7. Schematic representation of reversible addition rearrangement mechanism.[7a]

Reversible bonds following a *reversible exchange* mechanism are essentially always formed (Figure I.8). The release of one binding partner only occurs after the addition of a new partner. As this does not macroscopically change the ratio between broken and formed bonds, no changes in cross-link density occur. This mechanism is always dynamic. This mechanism is also called an *associative* mechanism, as exchange of binding partners requires association of a third partner before dissociation between the first two partners is possible. With temperature increase as trigger to start the associative mechanism, these materials are referred to as *vitrimers*, nowadays a quite active and novel research area that has been reviewed within our department.[7b]

The chemistry used and reported upon in this thesis is one of the many different chemistries following a dissociative mechanism.

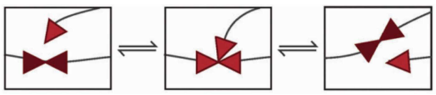

Figure I.8. Schematic representation of reversible exchange rearrangement.[7a]

2.2 Reversible addition chemistries

One of the oldest examples of reversible bonds in polymer networks is disulfide formation and scission (Figure I.9).[8] The oxidation of thiols to disulfide bridges occurs spontaneously in air, but this is often too slow to be of any practical use. By adding oxidants such as hydrogen peroxide, rapid bond formation (and thus cross-linking) is accomplished. By adding reducing agents, disulfide bonds are reduced, and de-crosslinking occurs. It is important to note that thiols also reversibly exchange with disulfide bonds. As a result, bond exchange is often an outcome of multiple mechanisms.

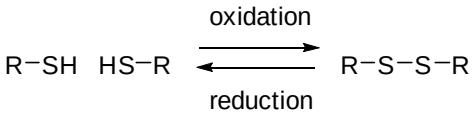

Figure I.9. Disulfide formation and scission following a reversible addition mechanism.

Another example of a well-known reversible addition reaction is the [4+2] Diels-Alder cycloaddition (Figure I.10). Diels-Alder reactions occur between dienes and dienophiles via a concerted mechanism, forming cyclohexene rings. By raising the temperature, the retro-Diels-Alder reaction becomes thermodynamically favored, resulting in the breaking of the bonds and thus a decrease in the connectivity or cross-link density in networks. Adversely, decreasing the temperature leads to an increase in cross-linking density.

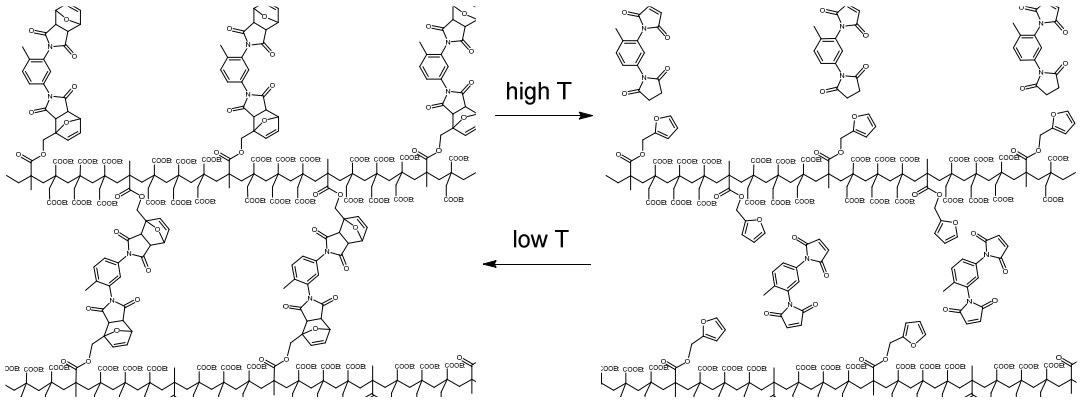

Figure I.10. Reversible (de)crosslinking of a Diels-Alder based coating.[9]

[2+2] Cycloadditions occur similarly, but require photostimulation. Several conjugated double bonds, such as cinnamate esters[10] and coumarines[11], form dimers upon irradiation with UV light (Figure I.11, above). By irradiating the formed (head-head and/or head-tail) dimers with shorter wavelengths, the dimers cleave and reform the parent molecules. This chemistry allows the formation of thermally stable materials without unintentional decrosslinking of the polymer network upon heating.

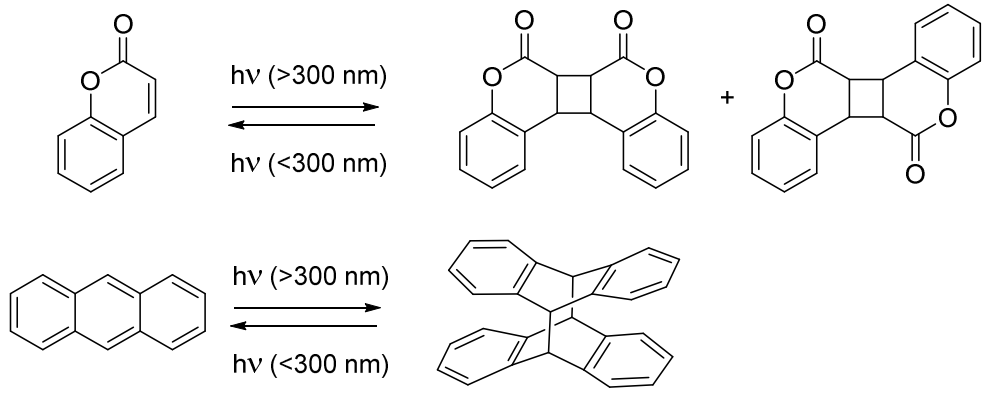

Figure I.11. Reversible dimerization of coumarine (above) and anthracene (below) under UV light.

In the same way, [4+4] cycloadditions are also thermally forbidden and only occur upon photostimulation. Anthracene is the best known example of a molecule undergoing these cycloadditions (Figure I.11, below). The larger aromatic system typically results in the use of higher wavelengths for dimerization and dimer scission compared to the often-used [2+2] cycloaddition systems previously

mentioned here. Also, thermal scission of dimers does occur at high temperatures, albeit via a radical mechanism. Anthracene and its use in polymer science will be discussed more elaborately in the upcoming chapter.

2.3 Reversible exchange chemistries

While no reversible exchange reactions are used in the research presented in this manuscript, an overview of the more relevant chemistries is presented here.

The best known example of a dynamic associative exchange reaction in polymer chemistry, is the transesterification reaction, as demonstrated by Leibler and co-workers.[12] Free alcohol groups present in the material undergo addition/elimination reaction with the ester groups (Figure I.12). This reaction, which occurs upon heating, is accelerated by the use of a catalyst. Transamination of vinylogous urethanes occurs at lower temperatures and requires no catalyst, as demonstrated by Denissen et al. (Figure I.12).[13] As mentioned above, thiols may also exchange with disulfide bonds in an addition/elimination mechanism.[7b, 14] This leads to the formation of a new disulfide bond and another thiol (Figure I.12). More thorough discussions on reversible exchange chemistries are provided in several excellent reviews.[7]

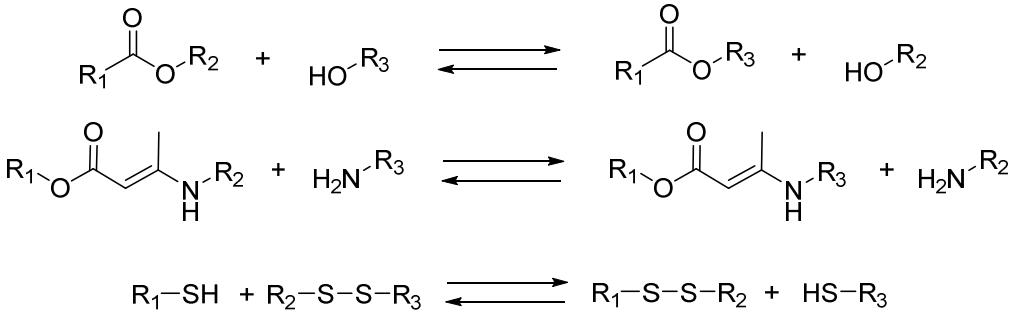

Figure I.12. Transesterification (top), transamidation (middle) and thiol-disulfide (bottom) exchange reactions.

3. Objectives and outline

The objectives of the research presented in this thesis are the development and evaluation of anthracene-based coating materials. More specifically, it will handle the incorporation of anthracene dimerization as reversible cross-linking chemistry. While several other reversible chemistries exist (vide supra),

anthracene is among the least researched in contemporary polymer science. Nevertheless, as anthracene dimerizes under UVA light (at higher wavelengths than coumarine or cinnamate), it is able to dimerize by sunlight exposure. Anthracene also has many positions at which substituents can be present, which are known to influence the absorption properties (see chapter II). In fact, adding substituents can lower the energy required for excitation and dimerization. Because of this, we have chosen to use anthracene as reversible bond and modify it by rationally adding substituents to achieve mild dimerization conditions (higher wavelengths, leading to less side products and degradation). Additionally, we also desired to shift the wavelength required for scission to higher wavelengths and potentially even above 300 nm. While the position and values of the absorption peaks were the main focus (ε above ~10^3 L mol^{-1} cm^{-1}), the absorption tails (ε between ~10^2 to 10^3 L mol^{-1} cm^{-1}) were also important. In fact, when no full dimerization is feasible, the irradiation of medium to thick coatings (e.g. 10-200 micron) at the high absorption wavelengths leads to very limited light penetration and the occurrence of an (abrupt) crosslinking gradient. Also, the influence of the substituents on the thermal stability of the dimers was studied. While the thermal scission of unsubstituted anthracene requires high temperatures (near 200 °C), milder heating requirements would make the thermal scission a viable method for many applications.

The modification of the anthracene moieties was twofold. First, we synthesized 9-substituted anthracenes, as several 9-substituted anthracenes are readily available as synthetic precursors. This position will also function as anchor for a spacer with functional end group, required for incorporation in polymeric materials. Important is also the length of the spacer, as longer spacers should increase the flexibility of the anthracene moiety in the material and increase the solubility of the anthracenes and their dimers. Another followed strategy consisted out of synthesizing 2,6-substituted anthracenes, more specifically derivatives with an electron donor and an electron acceptor in conjugation. The synergistic effect might lead to enhanced intramolecular charge transfer and absorption (and dimerization) in the visible light. The different positioning of the substituents can influence the dimerization kinetics because of steric hindrance. Also, the positioning of the substituents on the benzene rings of the formed dimers would also influence the dimer absorption spectrum and scission to a larger extent.

The anthracenes had to be easily incorporated in materials, preferably by simply adding them as dimers to existing formulations. The focus lied on commonly used approaches, such as polyurethanes and epoxy resins. During material research, the focus lay on the reversible dimerization and the resulting

material (de)crosslinking. Important was to note the influence of the network structures on the final properties with the aim to allow for material property tuneability by anthracene type selection and macromolecular architecture.

This work is subdivided and discussed in this thesis as follows:

In *Chapter I*, a short introduction is given on coatings and some of the challenges in this field. Also, reversible chemistries are briefly discussed with a focus on reversible additions.

In *Chapter II*, the reversible anthracene chemistry is discussed, followed by an extensive review on the existing literature surrounding anthracene-containing polymers. This review starts with discussing the polymers in which anthracenes are non-reactive moieties. In fact, they are often added as conductive or fluorescent groups. Afterwards, the polymers are discussed in which anthracenes are used to accomplish polymerization, post-polymerization modification, (reversible) polymer-polymer coupling and (reversible) cross-linking. These reactions often are Diels-Alder reactions or anthracene photodimerizations.

In *Chapter III*, the synthesis and characterization of novel 9-substituted anthracene derivatives is discussed. These derivatives are suitable for use as additive in formulations and differ mainly by their functional groups at the 9-position. This variation mainly influences the absorption, fluorescence and thermal dimer stability.

In *Chapter IV*, one anthracene derivative is used to develop thermally degradable and photo-recurable thiol-ene networks. The interesting thermomechanical properties resulting from the anthracenes are studied in depth.

In *Chapter V*, polyurethane materials and coatings are made using anthracene derivatives. The properties are tuned by adding non-reversible bonds. The (de)crosslinking is studied and validated for applications as easily removable coating and for stress-relaxation.

In *Chapter VI*, the synthesis and characterization of novel 2,6-substituted anthracenes are discussed, having an electron donor and an acceptor in conjugation. The influence of this alternative substitution pattern is studied, in a similar fashion as in Chapter III. One specific 2,6-substituted anthracene is fully characterized for use in materials.

In *Chapter VII*, the conclusions are discussed and an outlook for future research is given.

4. References

1. (a) Chattopadhyay, D. K.; Raju, K. V. S. N., *Progress in Polymer Science* **2007,** *32* (3), 352-418; (b) Noreen, A.; Zia, K. M.; Zuber, M.; Tabasum, S.; Zahoor, A. F., *Progress in Organic Coatings* **2016,** *91*, 25-32; (c) Noreen, A.; Zia, K. M.; Zuber, M.; Tabasum, S.; Saif, M. J., *Korean Journal of Chemical Engineering* **2016,** *33* (2), 388-400.
2. (a) Nollenberger, K.; Albers, J., *International Journal of Pharmaceutics* **2013,** *457* (2), 461-469; (b) Wang, F.; Hu, J.-q.; Tu, W.-p., *Thermosetting Resin* **2007,** *3*, 012.
3. (a) May, C., *Epoxy resins: chemistry and technology*. CRC press: 1987; (b) Goldschmidt, A.; Streitberger, H.-J., *BASF handbook on basics of coating technology*. William Andrew: 2003.
4. Resetco, C.; Hendriks, B.; Badi, N.; Du Prez, F., *Materials Horizons* **2017,** *4* (6), 1041-1053.
5. Perera, D. Y., *Progress in Organic Coatings* **1996,** *28* (1), 21-23.
6. Zayat, M.; Garcia-Parejo, P.; Levy, D., *Chemical Society Reviews* **2007,** *36* (8), 1270-1281.
7. (a) Kloxin, C. J.; Bowman, C. N., *Chemical Society Reviews* **2013,** *42* (17), 7161-7173; (b) Denissen, W.; Winne, J. M.; Du Prez, F. E., *Chemical Science* **2016,** *7* (1), 30-38.
8. Gyarmati, B.; Némethy, Á.; Szilágyi, A., *European Polymer Journal* **2013,** *49* (6), 1268-1286.
9. Turkenburg, D. H.; Durant, Y.; Fischer, H. R., *Progress in Organic Coatings* **2017,** *111* (Supplement C), 38-46.
10. Oya, N.; Sukarsaatmadja, P.; Ishida, K.; Yoshie, N., *Polym J* **2012,** *44* (7), 724-729.
11. Aguirresarobe, R. H.; Martin, L.; Aramburu, N.; Irusta, L.; Fernandez-Berridi, M. J., *Progress in Organic Coatings* **2016,** *99* (Supplement C), 314-321.
12. Montarnal, D.; Capelot, M.; Tournilhac, F.; Leibler, L., *Science* **2011,** *334* (6058), 965-968.
13. Denissen, W.; Rivero, G.; Nicolaÿ, R.; Leibler, L.; Winne, J. M.; Du Prez, F. E., *Advanced Functional Materials* **2015,** *25* (16), 2451-2457.
14. Pepels, M.; Filot, I.; Klumperman, B.; Goossens, H., *Polymer Chemistry* **2013,** *4* (18), 4955-4965.

Chapter II: Introduction to anthracene and anthracene-containing polymers

Abstract

Anthracene, with its unique properties originating from the linearly fused benzene ring structure, has a long history in polymer science in numerous application areas. The most commonly used reasons are their (tunable) luminescence, easy energy and charge transfer as well as unique photo- and thermoreversible dimerization properties. Aside from [4+4]-photocycloadditions, anthracene is also able to undergo extremely fast Diels-Alder reactions with maleimides. The use of (non)reactive anthracene moieties in polymers is therefore following a constant publication increase that is expected to continue in the future in order to meet the need for more advanced materials. This chapter aims to give a critical overview of the literature dealing with anthracene-containing polymers and provide a solid background on the topic for the reader.

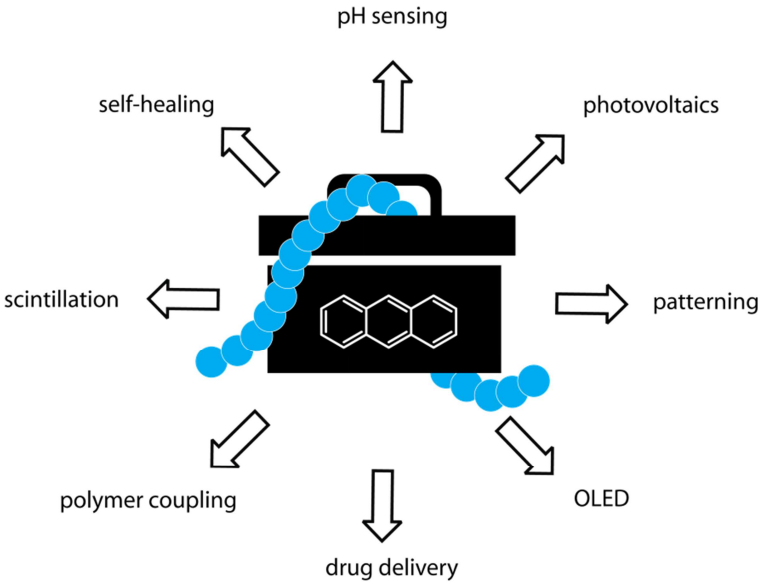

Part of this chapter has been published as:

- Van Damme, J.; Du Prez, F. Anthracene-containing polymers toward high-end applications. *Progress in Polymer Science* **2018** (doi: 10.1016/j.progpolymsci.2018.02.002)

1 Introduction

Polycyclic aromatic hydrocarbons (PAHs) are well-known pollutants produced by incomplete combustion of fuel or biomass. A special class of PAHs are (poly)acenes (Figure II.1), consisting of linearly fused aromatic rings, such as benzene, naphthalene, anthracene, tetracene, pentacene, etc. Most research is done on the shorter acenes, as larger (linear) acene conjugation leads to a faster oxidation by air and thus a more difficult isolation of the compounds.[1] In fact, the aromatic character decreases from the outer rings inward. Increasing the number of rings leads to a property shift from an aromatic molecule to a polyene.

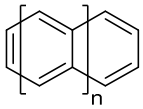

Figure II.1. Schematic representation of acenes, such as naphthalene (n=1), anthracene (n=2), tetracene (n=4), etc.

Anthracene (Figure II.2), consisting of three aromatic rings, makes up a few percentages of coal tar. The separation of anthracene from coal tar is the most economical production route. Anthracene is mostly used after oxidation to anthraquinone as a dye precursor.[2] (Un)substituted anthracenes have so far been used as MALDI matrices,[3] scintillators,[4] electroluminescent devices[5] and fluorophores[6]. Anthracenes have also been introduced in polymer science, mostly for their photophysical properties and reversible cycloadditions.

The focus of this chapter is on the introduction of anthracene and/or its derivatives in polymer chemistry, in combination with the description of the properties and applications of the obtained polymers. In this context, only covalently linked anthracene-polymer systems will be considered. Excellent reviews on anthracene as such and its dimerization are available in literature.[7]

First, a short introduction to anthracene and its properties is given after which the discussion is divided in two main parts corresponding to the use of anthracene as non-reactive or reactive moiety respectively. On the one hand, the use of the intrinsic properties of anthracene for the development of polymers for (fluorescent) detectors and electro-optical applications is explained in detail. On the other hand, polymers in which the anthryl groups are used as reactive species, undergoing mostly reversible dimerization and Diels-Alder reactions, are highlighted.

While mainly publications of the past 15 years have been discussed, also relevant older literature is debated to give a more thorough understanding of the potential of the anthracene structure in polymer chemistry.

2 Anthracene and its properties

2.1 Introduction

Anthracene (Figure II.2) consists of three linearly fused aromatic rings and thus presents an extended π-system with 14 delocalized electrons. Anthracene was first discovered after isolation from coal tar in 1832 by Dumas and Laurent,[8] who named it paranaphthaline. It is a colorless to light brown-yellow solid, which only melts at high temperatures (around 216 °C) because of the planar structure, allowing easy crystallization.

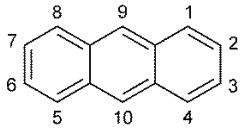

Figure II.2. Anthracene structure.

Because of the extended aromatic π-system, anthracene has a relatively low electronic energy gap (π-π*). Therefore, the molecule can easily be brought to an excited state by irradiation using ultraviolet light.[9] The wavelengths at which anthracene absorbs light can be divided in two groups of absorption maxima (Figure II.3); a first interval between 220 nm and 280 nm and a second between 280 and 390 nm. The absorption maxima are assumed to be occurring from separate states of electronic excitation. Often excitation is only performed with light having wavelengths in the latter absorption maxima interval in order to avoid undesirable side reactions, such as photo-oxidative degradation of the polymer matrix. The high energy content of the short wavelengths leads to the generation of radicals, which in turn results to chain scission and lower molecular weights. Some of the radicals also form new cross-links. This combination leads to a loss of mechanical strength and elasticity, and thus brittle coatings. Another undesirable reaction that may occur is the cycloreversion of the formed anthracene dimers, essentially leading to an equilibrium between dimer formation and scission. Lastly, the high absorption at short wavelengths would often lead to a very limited penetration depth, thus essentially irradiation

only a few microns deep into the material. The absorption maxima can also be shifted to higher wavelengths by adding substituents to the chromophore, which lower the energy gap by raising the HOMO and/or lowering the LUMO.[10]

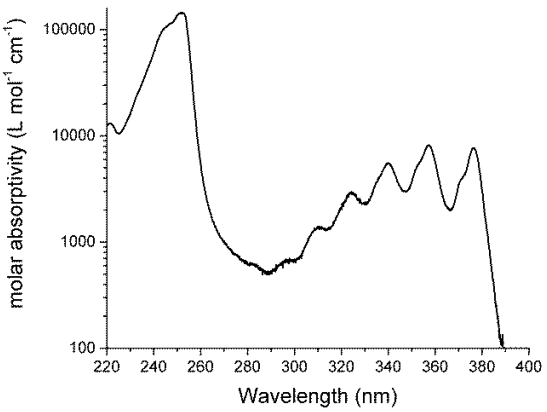

Figure II.3. Ultraviolet absorption spectrum of anthracene in acetonitrile.

2.2 Applications

Because of the extended π-system and rigid structure of the chromophores, most anthracenes are also good fluorophores with high fluorescence quantum yields and nanosecond lifetimes. The combination of typically (easily recognizable) sharp absorption and emission peaks[11] results in the use of anthracenes as fluorescent tags or sensors in many applications such as scintillation,[12] enantiomeric recognition,[13] metal ion detection,[14] (intracellular) pH sensing[15] and DNA binding sensing.[16]

Because the conjugated system of anthracenes allow (easy) charge mobility, the chromophores are also interesting candidates for (photo)electrical applications such as organic light emitting diodes[17] and organic transistors.[18] In some cases, use is made of the rigid aromatic structure of anthracene for supramolecular interactions by efficient π-π stacking.[19]

2.3 Dimerization of anthracene

Another important property of anthracene is its ability to form dimers upon UV irradiation (Figure II.4). This was first discovered by Fritzsche in 1867, when a solution of anthracene led to crystallization upon sunlight exposure.[20] Anthracene was back then called “photene”, while the formed crystals were named

"paraphotene". At the end of the 19th century, cryoscopy experiments proved that these structures were in fact dimers of anthracene.[7c]

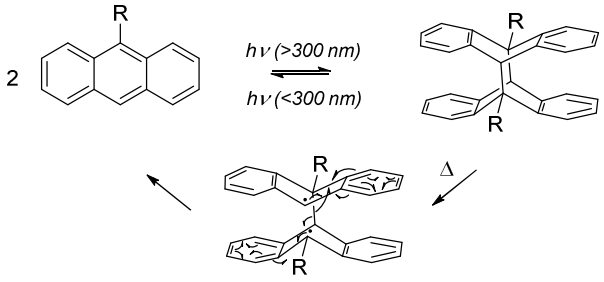

Figure II.4. Reversible anthracene photodimerization.

Several dimer structures are possible, but the most prevalent ones are those by [4+4]-cycloaddition of the middle rings (Figure II.4). The structure of dianthracene was elucidated over the course of the 20th century by X-ray analysis and UV spectrometry.[7a, 7c, 21] Research near the end of the 20th century, showed that 9-substituted anthracenes could dimerize in a head-head or head-tail conformation (Figure II.5). In most cases, head-tail dimers are exclusively formed.[7a]

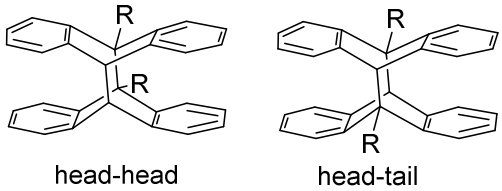

Figure II.5. Head-head and head-tail dimers of a 9-substituted anthracene.

The dimerization mechanism has been extensively discussed in literature. In what follows, the most generally accepted theory is discussed.[22] The dimerization of anthracene is thermally forbidden according to the Woodward-Hoffmann rules, but can occur photochemically.[23] This starts by excitation of anthracene (A) to the first excited state (A*).

$$A \xrightarrow{h\nu} A^*$$

This excited molecule reacts with a molecule in the ground state, forming an excimer ([A A]*). This excimer is short-lived and releases its energy either by light emission or emission-less by photodimerization. [24]

$$A + A^* \longrightarrow [A\ A]^*$$

Decay of the eximer leads to the formation of the photodimer (A_2).

$$[A\ A]^* \longrightarrow A_2$$

That dimerization cannot occur thermally, can be explained by the HOMO and LUMO of anthracene (Figure II.6). These molecular orbitals have no favorable overlap in the ground state. Upon excitation of one of the reaction partners, the HOMO of the excited molecule can react with the LUMO of the unexcited anthracene.

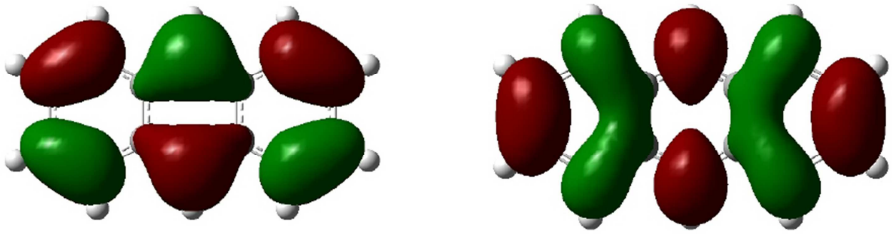

Figure II.6. HOMO (left) and LUMO (right) of anthracene, determined via Unrestricted Hartree Fock calculation in Gaussian (basis set: 6-31G).

The rate at which dimerization occurs is influenced by the position and nature of substituents.[7a, 25] Dimerization typically occurs slower for 9-substituted derivatives. Substitution on both the 9- and 10-position decreases the rate even more, or inhibits it completely. Other positions have little to no significant effect on the dimerization rate. Also the used solvent plays an important role.[7a] Solvents having heavy atoms, such as halogenated solvents, have a negative effect on dimerization.[7c, 26] Heavier atoms have a larger spin-orbit coupling, thus leading to easier intersystem crossing (singlet to triplet state) and thus disappearance of the reactive singlet excited anthracenes.

2.4 Scission of dianthracene

This dimerization is reversible and irradiation of the dianthracenes with UVC light reforms the original anthracenes (Figure II.4).[27] Important to note is the limited penetration depth of UVC, which limits its use to thin materials or dilute solutions. Surprisingly, scission of dianthracenes to the parent anthracenes also occurs *via* a presumably radical pathway at increased temperatures.[7b] Despite the radical nature of the intermediate, this reaction usually occurs cleanly. Studies on the thermal scission of small anthracene dimers proved a significant influence of the 9-substituent on the kinetic parameters (Table II.1).

Calculated from these values, 50 % scission should be accomplished after 10 minutes heating at 208 °C (unsubstituted anthracene), 168 °C (9-methyl A_2 (ht) and 9-ethanol A_2 (ht)) and 124 °C (9-aldehyde A_2 (ht)). Also, the head-head (hh) dimers had a lower activation energy and dissociated at lower temperatures than their head-tail counterparts (ht).

Table II.1. Kinetic parameters of the anthracene dimer scission. Data collected from Bouas-Laurent et al.[7b] and the references therein.

Dimer	Solvent	A (s^{-1})	E_a (kJ mol^{-1})
A_2	Benzene	$6.3\ 10^{13}$	154
9-methyl A_2 (ht)	Tetraline	$1.0\ 10^{16}$	160
9-methyl A_2 (hh)	Ether	$6.3\ 10^{14}$	111
9-ethanol A_2 (ht)	$C_6H_4Cl_2$	$1.6\ 10^{15}$	153
9-ethanol A_2 (hh)	Ether	$1.0\ 10^{15}$	113
9-aldehyde A_2 (ht)	Benzene	$2.0\ 10^{14}$	131

Anthracene photodimers are also cleavable by mechanical stress, allowing their use as mechanophores.[28] This latter reaction is currently of great interest in polymer science for the development of “smart” materials (*vide infra*) as the high fluorescence quantum yield of anthracene allows high sensitivity and detection of early damage and damage deep in the matrix. The extended aromatic system also allows bringing the emission to longer wavelengths, potentially resulting in detection by the naked eye.

2.5 Diels-Alder reactions

Similarly to the photodimerization, the anthracene ring reacts with dienophiles *via* a [4+2]-cycloaddition, also known as a Diels-Alder mechanism.[29] As this Diels-Alder reaction is (thermally) reversible, the thermodynamic equilibrium between cycloadducts and parent molecules can be altered by temperature changes. Higher temperatures are in favor of the retro-cycloaddition (cycloreversion), while lower temperatures shift the equilibrium to the formation of the Diels-Alder adducts.

2.6 Photo-oxidation

Singlet oxygen is a special kind of dienophile that reacts fast with anthracene, forming endoperoxides (Figure II.7).[30] The cycloreversion to the parent anthracene and singlet oxygen occurs upon UV irradiation or heating. This strategy has been used for controlled singlet oxygen release to trigger death of tumor cells,[31] for optical imaging[32] and for the flipping of molecular switches.[33] The cycloreversion competes with homolytic cleavage of the endoperoxides, which leads to the formation of anthraquinones and other byproducts. Therefore, avoiding the presence of oxygen during irradiation is of the utmost importance when quantitative conversion is required.

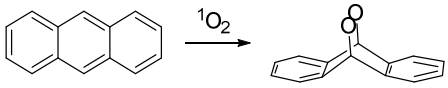

Figure II.7. Endoperoxide formation with singlet oxygen.

3 Polymers containing anthracene as non-reactive moiety

3.1 Anthracene polymers as detector systems

3.1.1 Anthracene polymers as plastic scintillators

Some of the first studies on anthracene-containing polymers were published in the 1950-1970's, often for application as plastic scintillator. Scintillators are materials that emit light upon excitation by ionizing radiation. By detecting the emitted light via conventional methods, the ionizing radiation intensity can be measured.

Plastic scintillators require a primary compound (e.g. polystyrene), which upon high energetic irradiation reaches an excited state and efficiently transfers energy to a secondary, efficient light-emitting compound (e.g. anthracene). This secondary compound is required as the polymer matrix often has low fluorescence quantum yields and self-absorbs its own emissions. Driven by this application, many papers are published on producing luminescent materials by the copolymerization of (un)substituted anthracenes. The (co)polymerization of vinylic and allylic anthracenes *via* various methods have also been intensively investigated.

3.1.1.1 Polymerizations with anthracene

In 1951, Bagat and Boneme discovered that styrene polymerization was hindered by the presence of certain aromatic molecules such as 2-methylanthracene.[34] The resulting polystyrenes had adopted a characteristic fluorescence, indicating introduction of the aromatics into their structures. In 1955, Krenz noticed the improved energy transfer efficiency of a plastic scintillator made by polymerizing styrene in the presence of anthracene.[35] Because of this observation, along with a decreased polymerization rate and the observed fluorescence, he suggested the attachment of anthracene as a polymer end-group. In 1958, Marvel and Wilson reported the copolymerization of anthracene and styrene in soap emulsion.[36] Limited incorporation of anthracene was explained by the low solubility of anthracene and its inhibiting effect. Additionally, Diels-Alder reactions occurred between styrene radicals and the central anthracene rings as side reactions.[37] In 1959, Norrish and coworkers reported the photocopolymerization of styrene with anthracene.[38] Anthracene incorporation occurred *via* the 9- and 10-position, interrupting the aromatic system.[39] The triplet state of anthracene was found to be the initiating species. In 1990, Lissi and Yupanqui reported that anthracenes are not acting as comonomers in the styrene copolymerization, but behave instead as traps for the growing macroradicals.[40] As polyvinyltoluene tended to be a more efficient plastic scintillator than polystyrene, Akezaki copolymerized anthracene with vinyltoluene in 1970.[41] However, anthracene copolymerization did not improve the energy transfer in this case.

Other copolymerizations were also reported, such as the copolymerization of 1,3-butadiene with anthracene[42] and 1- and 2-chloroanthracene by Marvel and coworkers.[43] The Friedel-Crafts arylation of anthracene (*via* the 9- and 10-position, but also the 1- and 4-position) and condensation of 9,10-bis(chloromethyl)anthracene to polybenzyls was reported in 1971 by Montaudo *et al.*.[44] These polymers had both a high melting point and a good solubility in benzene.

3.1.1.2 Polymerizations with vinylic anthracenes

Special interest was given to vinylic anthracene as a monomer, especially 9-vinylanthracene. Bergmann and Katz reported in 1958 that the polymerization thereof occurred faster *via* cationic polymerization than radical polymerization.[45] This is in line with the results of Stolka in 1976, who studied the homopolymerization of 9-vinylanthracene *via* free radical, anionic and cationic polymerization.[46] The highest molecular weight he reported was by cationic polymerization (Mw ~ 20 kg/mol). Michel reported that the cationic polymerization of the 9-vinylanthracene did not occur *via* the vinyl group only,

but also *via* the anthracene ring (Figure II.8).[47] In fact, treating the polymer with trifluoric acid would convert it to poly-(9,10-dimethyleneanthracene).

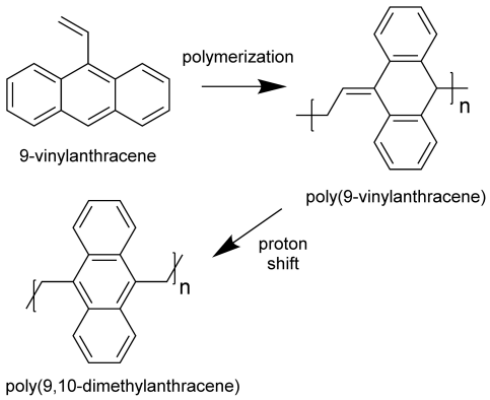

Figure II.8. Polymerization product of 9-vinylanthracene, followed by conversion to poly(9,10-dimethylanthracene).[47]

In 1975, Marechal and coworkers reported that the cationic polymerization of 9-vinylanthracene (**1**, Figure II.9) can occur solely *via* the vinyl group by lowering the temperature and preventing carbocation isomerization.[48] A few years later, they reported the photo-oxidative formation of anthrone and anthraquinone from aging poly-(9-vinylanthracene).[49] Their conclusion provides an alternative explanation for the spectroscopic results of earlier reports, who often claimed the isomerization of the cation during polymerization.

The free radical homopolymerization[50] of 9-vinylanthracene and its copolymerization with styrene[50] and acrylates[51] were further studied and reported by Katz and Relis. In comparison, the polymerization of 1-vinylanthracene (**2**, Figure II.9) occurred faster as there is less sterical hindrance and therefore a higher resonance stabilization of the radical adduct.[50] In 1976, Stolka *et al*. compared the polymerizations of 1-vinylanthracene[46] and 2-vinylanthracene (**3**, Figure II.9)[52] *via* radical, anionic, cationic and Ziegler techniques. Anionic polymerization resulted in polymers with high molecular weights, but did require extremely high monomer purity.

Larger vinylic anthracenes were also studied, albeit to a lesser extent. In 1965, Cherkasov and Voldaikina studied the copolymerization of 2-vinyl-9,10-diphenylanthracene with styrene (**4**, Figure II.9).[53] The blocking of the meso positions by the phenyl groups hindered the undesirable additions to these positions.[53] Stolka *et al.* published the polymerization of 9-vinyl-10-methylanthracene and 2-

propenyl-1-anthracene (**5** and **6**, Figure II.9).[46] The polymerization of 9-(p-vinylphenyl)anthracene was reported by Mukoh and Morishita (**7**, Figure II.9).[54] This monomer polymerized much faster than 9-vinylanthracene, with a rate comparable to that of 1-vinylanthracene, due to easier resonance stabilization.

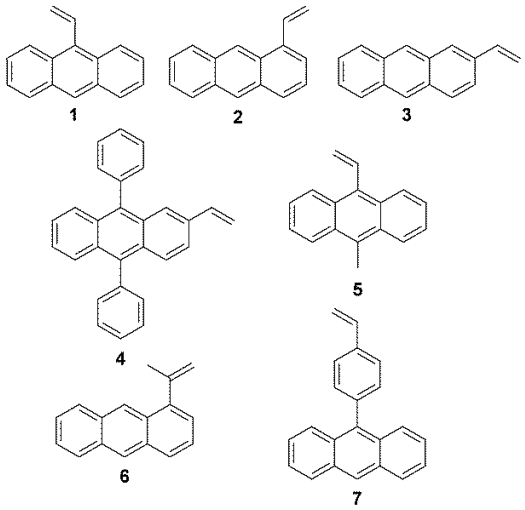

Figure II.9. Structures of the discussed vinylic anthracenes: 9-vinylanthracene (**1**), 1-vinylanthracene (**2**), 2-vinylanthracene (**3**), 2-vinyl-9,10-diphenylanthracene (**4**), 9-vinyl-10-methylanthracene (**5**), 2-propenyl-1-anthracene (**6**) and 9-(p-vinylphenyl)anthracene (**7**).

3.1.1.3 Polymerizations with other anthracene derivatives

Many other polymerizations were performed to make suitable anthracene-containing luminescent polymers starting from other monomers. As a full discussion of the – often old – reports on these polymerizations is beyond the scope of this chapter, only a selection of those alternative polymerizations are described here.

In 1972, Krakovyak *et al.* reported the free radical copolymerization of 9-anthrylmethyl acrylate with methyl methacrylate (MMA).[55] Similar molecular weights as obtained for the homopolymerization of MMA were achieved. In 1985, Simionescu *et al.* reported the initiator-free thermal and radical polymerization of 9-anthrylmethyl acrylate, 9-anthrylmethyl methacrylate, 1'-(9-anthryl)ethyl acrylate and 1'-(9-anthryl)ethyl methacrylate.[56] Radical polymerization at 60 °C was only successful for the methacrylates, while thermal polymerization at 110 °C without radical initiator worked for both types.

Polymerization *via* 1,2-additions occurred for the methacrylates, unlike the double bonds of the acrylates that underwent exclusively Diels-Alder cycloadditions with the anthracene rings (Figure II.10).

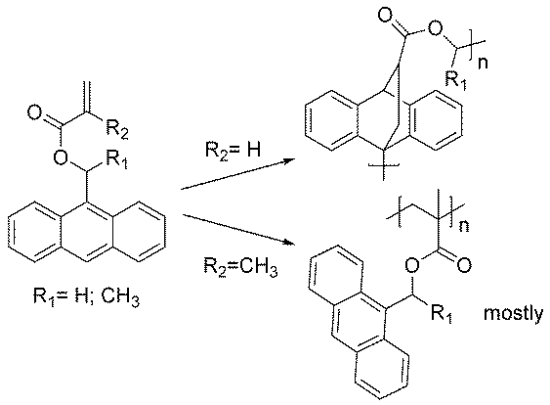

Figure II.10. Polymerization of acrylic anthracene monomers via Diels-Alder reaction and 1,2-type addition.[56]

Dumitrescu *et al.* published the homopolymerization of 9-allylanthracene in 1983 (Figure II.11).[57] Radical polymerization only resulted in oligomers due to the resonance-stabilized radicals formed by reaction with the anthryl group, effectively stopping polymerization. On the other hand, cationic and Ziegler-Natta polymerizations provided normal 1,2 addition, but also 9,10-anthrylenepropylene units.

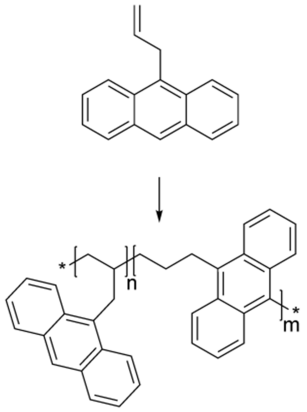

Figure II.11. Polymerization of 9-allylanthracene.

3.1.2 Anthracene polymers as fluorescent probes

Taking advantage of their good fluorescence properties, anthracene moieties have also been attached to polymers for the creation of probes or detectors, providing information on the polymer in which it is

incorporated or on the chemical environment. In the following section, the most important examples of the use of anthracene polymers as (fluorescent) feedback systems are presented.

First, anthracene-containing polymeric probes were used to study segmental dynamics of polymers by fluorescence anisotropy decay experiments.[58] The anthracene moieties show no specific interactions with the polymers and their relatively small sizes seldomly hinder polymeric motions, making them suitable chromophores for such applications. Probes were mostly made by (i) copolymerization with anthracene derivatives, such as 9-vinylanthracene[58c] or p-vinyl-phenyl-9-phenyl-10-anthracene (Figure II.12),[58d, 59] leading to multiple pendent anthracenes per chain; (ii) trapping growing polymer chain ends with symmetrically 9,10-substituted anthracenes ((a) in Figure II.13);[58d, 60] or (iii) by a polymerization initiated by bifunctional 9,10-substituted anthracenes ((b) in Figure II.13).[58a, 61] The latter two options ensure having only a single anthracene molecule in the middle of the polymer chain. As the transition moment associated with excitation and emission of anthracene is oriented according to the 9,10-position, these latter probes have their transition moment aligned along the macromolecular backbone.

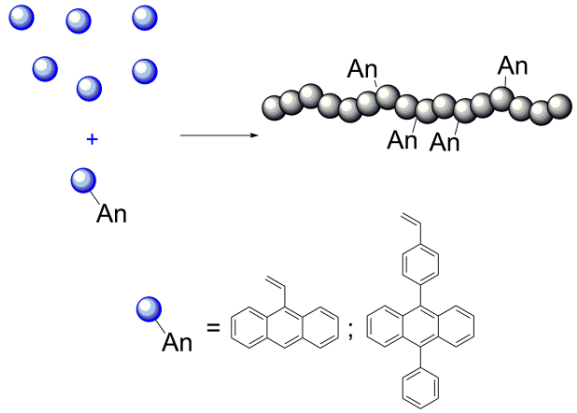

Figure II.12. Fluorescent probe with anthracene side groups by copolymerization with anthracene-based monomers such as 9-vinylanthracene or p-vinyl-phenyl-9-phenyl-10-anthracene.

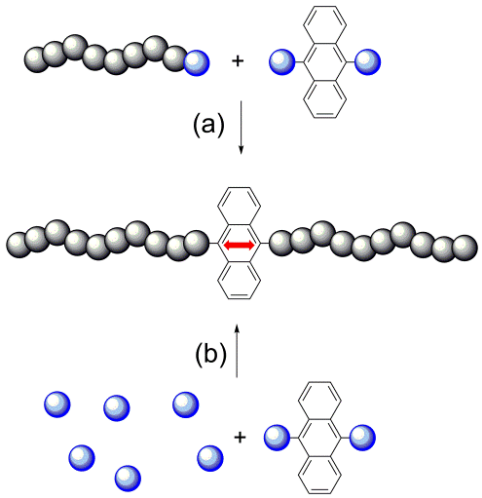

Figure II.13. Fluorescent probe made by (a) trapping growing polymer chain ends with a 9,10-substituted anthracene or by (b) polymerization initiated by a 9,10-substituted anthracene. The transition dipole moment (red arrow) is oriented along the backbone.

Experiments were performed using polarized light pulses, typically slightly above 400 nm, to excite the probe. Light was subsequently emitted by the anthracene, polarized along the transition dipole. Because of this, the emitted light is partially polarized until randomization occurs by molecular motion. These studies were performed for polystyrene,[58] polyisoprene,[60a, b, 62] poly(N-vinylcarbazole),[58c, 60c] polyvinylacetate,[58c] polybutadiene[63] and poly(meth)acrylate copolymers.[58c] This was mostly done in solution, but some studies were also performed in the melt.[60a] Comparison between polymers having anthracene in the middle of the backbone and only at the chain end showed that chain end rotation occurs at least five times faster.[58c] Also, relaxation times of anthracenes in the side chains are much more rapid in comparison to those of anthracenes incoporated in the backbone as they are more sensitive to short-range motions.[58d]

Liu *et al.* reported in 2001 the synthesis of several anthracene-labelled butyl acrylate-methyl methacrylate copolymers, which could be used for labelling emulsion copolymerization and studying polymer diffusion in latex films.[64] The 9-linked anthracenes had methyl groups at the 10-position to avoid competitive reaction at this position during polymerization. The authors observed a higher thermal and acidic stability for polymers labelled with 9-methacryloxy-10-methylanthracene compared to 9-methacryloxymethyl-10-methylanthracene or 9-methacryloxyethyloxymethyl-10-methylanthracene (Figure II.14). Under acidic conditions in combination with heat, anthracene moieties are cleaved,

presumably due to the formation of an An-CH_2^+ cation. Despite this possible side reaction, Tomba *et al.* used the 9-methacryloxymethyl-10-methylanthracene-labelled butyl acrylate-methyl methacrylate copolymer to study the polymer diffusion in latex films in 2009.[65] The anthracene chromophores served as acceptor dye in Förster resonance energy transfer (FRET) measurements.

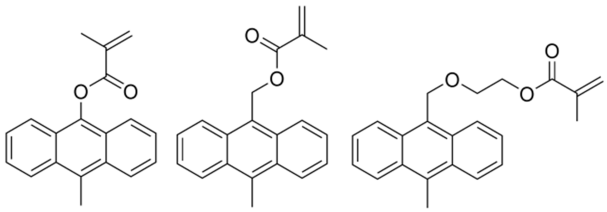

Figure II.14. 9,10-substituted anthracene acrylate monomers: 9-methacryloxy-10-methylanthracene (left), 9-methacryloxymethyl-10-methylanthracene (middle) and 9-methacryloxyethyloxymethyl-10-methylanthracene (right).

Anthracene-containing fluorescent probes have also been used by Horie and coworkers to study the solution-liquid crystal transition of poly(gamma-benzyl-L-glutamate) (PBLG).[66] Anthracene side chain fractions of 0.037 % and 0.11 % were obtained by transesterification with 9-hydroxymethylanthracene. An increasing polymer concentration resulted in sharp decreases in the fluorescence anisotropy ratio (r) due to scattering of incident and emitted light (Figure II.15). Probes with a lower molecular weight had higher r values in liquid state. This was ascribed to aggregation due to the larger amount of chain ends, leading to a lower segmental mobility and thus a higher r.

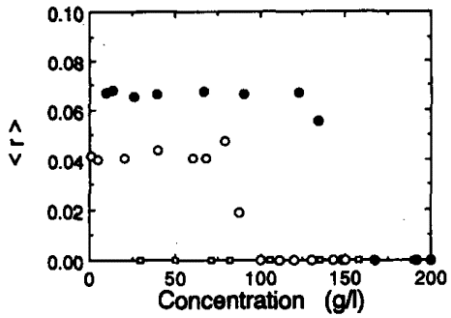

Figure II.15. Solution-liquid crystalline transition of PBLG studied by fluorescence anisotropy studies using a model compound (□), short (●) and longer (○) probes.[66]

In 2004, de Deus et al. reported the use of anthracene side groups in poly(methyl methacrylate) (PMMA) to probe chain relaxations.[67] α, β, γ and even δ transitions were detectable as changes in the

slope of the fluorescence intensity over temperature (Figure II.16). By lowering the amount of anthracene groups, the influence of the bulky groups on the PMMA transitions could be limited.

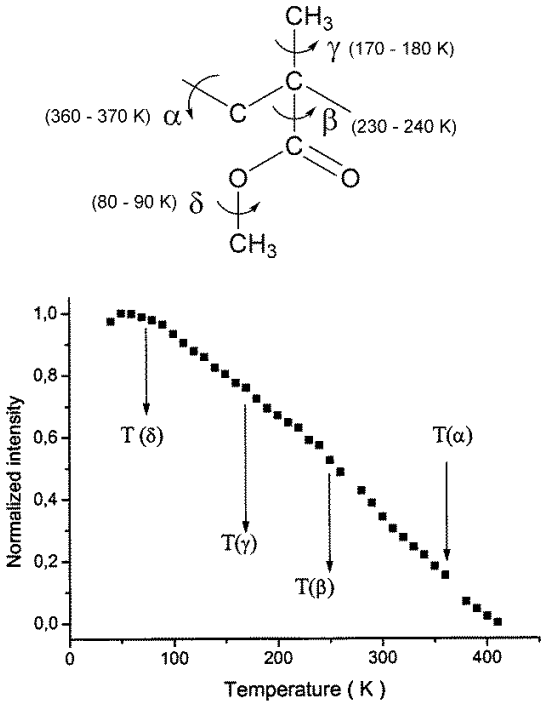

Figure II.16. Structural relaxations in PMMA detected by changes in fluorescence emission.[67]

Very recently, Swift *et al.* used anthracene as an acceptor chromophore in FRET experiments.[68] The energy transfer occurring from spatially neighboring naphthalene units (on a polyacrylamide chain) to anthracene moieties (on a polyacrylamide chain) proves interpolymer complexation. Additionally, by performing FRET experiments on chains having both labels and fluorescence anisotropy experiments, the pH-dependent behavior of both polymers could be fully studied.

3.1.3 External compound detectors

Anthracene-based probes have also been employed to detect external compounds, often by the effects those compounds have on the fluorescence. For example, Petropoulou *et al.* very recently reported the development of a fluorescent ammonia sensing probe, based on poly(9-anthrylmethyl methacrylate).[69] The polymeric probe was blended with PMMA and electrospun, forming 3D grids with large surface areas. Gaseous ammonia forms complexes with the anthracene moieties, which quenches the anthracene

fluorescence. The high surface area to volume ratio of the fibers led to fast responses and detection at concentrations up to 10^5 ppm (Figure II.17).

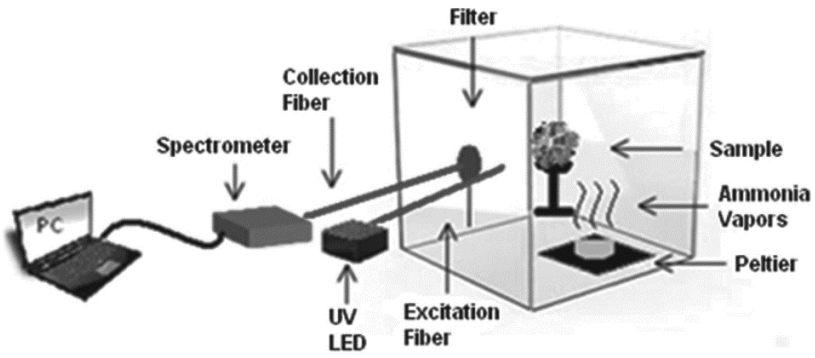

Figure II.17. Ammonia detection setup using the electrospun fluorescent anthracene-containing polymers.[69]

Sandanaraj *et al.* used an anthracene-containing amphiphilic polymer as metalloprotein sensor.[70] The used polymer can bind to many, if not all, proteins. However, quenching of the fluorescence only occurs in the presence of metal ion cofactors.

Shiraishi *et al.* developed an anthracene-labeled poly(NIPAM) copolymer with pH- and temperature-dependent fluorescence.[71] In water at 15 °C, the polymers are dissolved and fluorescence only occurs at low-medium pH when the side chains are protonated ("on-off" type pH sensor). On the other hand, at 34 °C, the polymer acquires a globular conformation that inhibits fluorescence at very low pH values due to scattering by the small-sized globules ("off-on-off"), as shown on Figure II.18. The redox properties of anthracene moieties are (also) pH dependent, allowing the use of poly(vinylanthracene-co-vinylferrocene) as a pH sensor, as reported by Robinson and Lawrence.[72] The anthracene moieties were shown to undergo a Nernstian potential shift with pH, while ferrocene moieties are pH-insensitive and were used as internal reference. The maximal pH for which the potential shift occurs linearly can be increased from 9 to 11 by adding carbon nanotubes to the polymer.[73]

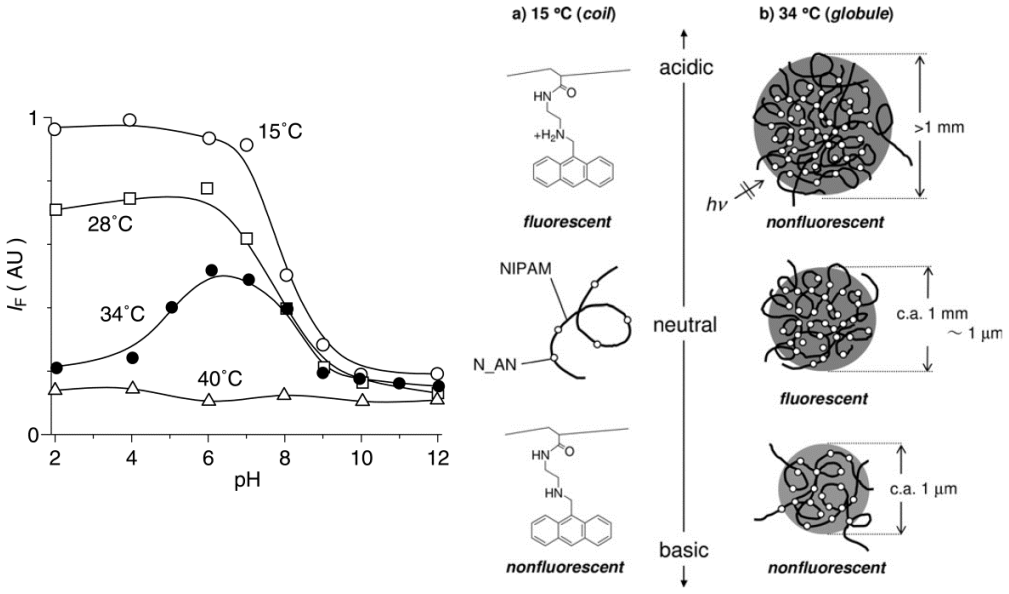

Figure II.18. Fluorescence intensity of labeled poly(NIPAM) at different pH's and temperatures.[71]

Very recently, Yu and Zhao developed CO_2-responsive hyperbranched amphiphilic poly(ether amine)s with anthracene end groups.[74] Bubbling of carbon dioxide in an aqueous solution of those polymers results in the protonation of the tertiary amino groups, increasing the emission intensity, presumably by disruption of the original morphology (Figure II.19). Deprotonation by flushing with nitrogen occurred very slowly, presumably due to restricted diffusion inside the micellar aggregates.

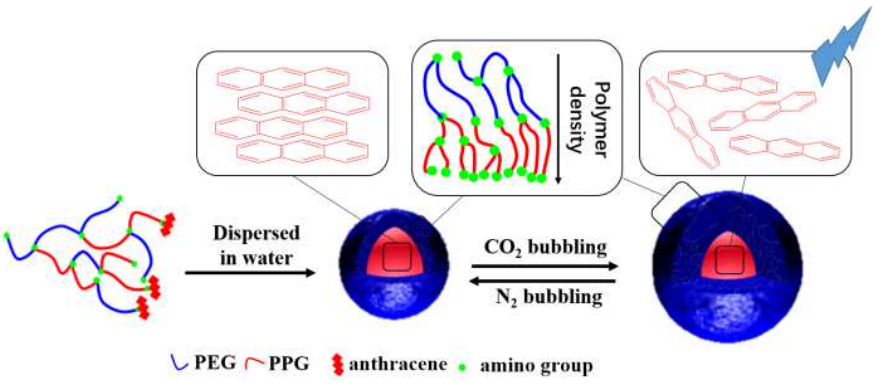

Figure II.19. Suggested mechanism of the fluorescence changes by CO_2-addition.[74]

3.2 Electrical anthracene polymers

The extended aromatic system of anthracene has also resulted in its use for fully or segmented π-conjugated polymers. The energy transfer and conductive properties of these polymers were extensively studied. Besides, anthracene moieties were also applied in polymers for photovoltaics and organic light emitting diodes.

3.2.1 Energy transfer studies

Energy transfer studies were performed on anthracene-containing polymers for applications as plastic scintillators (as discussed in 3.1.1) but also for solar cells. Both intramolecular and intermolecular energy transfer can occur. In the seventies, Holden *et al.* studied the energy transfer from naphthalene groups to anthracene moieties which act as traps.[75] Efficiency was increased by varying the trap concentrations and using a poor solvent to reduce the intermolecular distance. They suggested sequential Förster transfer as the main mechanism. Several years later, Hargreaves and Webber reported excimer formation between pending anthracene units acting as traps for singlet excitons.[76] Equipping the 9-linked anthracenes with a bulky phenyl group at the 10-position, allowed to raise singlet energy migration from about 0 to 2.10^{-5} cm^2/s.

At the beginning of the millennium, Tillman and Hogen-Esch reported more efficient energy transfers for cyclic polystyrene and poly(9,9-dimethyl-2-vinylfluorene) containing a single 9-10-substituted anthracene in the cycle, compared to their linear counterparts.[77] Recently, Morisaki *et al.* studied xanthene-based anthracene-layered polymers, where the anthracenes are in a π-stacked structure and conjugation occurs through space (Figure II.20).[78] The through-space energy transfer along the length of these polymers was validated by covalently linking fluorescence quenchers (e.g. nitrobenzene and ferrocene) at the chain ends. The quencher-capped polymers had up to 52 % lower emission compared to the non-capped polymers, signifying efficient energy transfer from the excited anthracenes to the quenchers. A large excess of non-bound quenchers only decreased emission by 7 %. The efficient energy transfer along the intramolecularly stacked polymers, revealed the potential of these structures as molecular wires. Li and Fox studied the electron transfer between pending anthracene groups (donor) and a polyimide main chain (acceptor).[79]

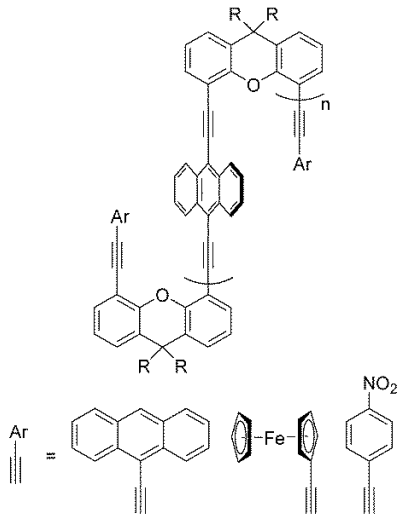

Figure II.20. Synthesis of anthracene-layered polymers with and without quenching end-groups.[78]

3.2.2 Conductivity studies

Similarly to energy transfer studies, many (fundamental) conductivity studies were performed on anthracene-containing polymers, eventually leading to the use of such polymers in a more applied context. One of the earliest reports was in the sixties, when Bolto *et al.* studied electrically conducting polymers prepared by heating sulfur and anthracene at high temperatures.[80] They assumed the presence of mainly disulphide bridges and acquired higher conductivities by lowering the sulfur content and increasing the pressure to promote better π-orbital overlap. Al-Jumah and Fernandez synthesized a poly(arene methide) with anthracene rings by Friedel-Crafts reaction of α,α'-xylene with anthracene, followed by dehydrogenation.[81] Doping with AsF_5 led to an increase in conductivity from ~10^{-12} to 2.8 10^{-5} S/cm. Satoh *et al.* demonstrated the electrochemical homopolymerization of anthracene in a solution of o-dichlorobenzene and a composite electrolyte of $CuCl_2$ and tetrabutylammonium perchlorate.[82] The resulting polyanthracene films already are doped with ClO_4- during synthesis and had conductivities up to 10^{-3} S/cm. The electrical conductivity of the doped polyanthracenes could be increased up to 0.1 S/cm by using boron trifluoride diethyl etherate as an electrolyte instead.[83]

In the sixties, Morimoto *et al.* studied the photoconductivity of poly(9-vinylanthracene) in the context of application in electrophotography.[84] Electrophotography or xerography is a copying technique that relies on electrostatic interactions (to transfer the ink) and photo-stimulated charge dissipation. By (partially) converting the poly(9-vinylanthracene) to poly(9,10-dimethyleneanthracene) - as was initially

discovered by Michel *et al.* (vide supra, Figure II.8) – sped up charge dissipation upon light exposure with a factor up to 1500. The half-decay exposure time of poly(9,10-dimethyleneanthracene) was shown to be similar to the often-used amorphous selenium materials.

The quick and reproducible switching of the conductivity of poly(methylmethacrylate-co-9-anthracenyl-methyl-methacrylate) and its potential for memory applications was demonstrated by Ma *et al.*.[85] Voltage pulses above V_{crit} switched the material "ON", raising its conductivity by a factor 10^5 (Figure II.21). Voltages pulses below V_{hold} switched the material "OFF". At intermediate voltages, the conductivity was either high or low, depending on the previously applied voltage.

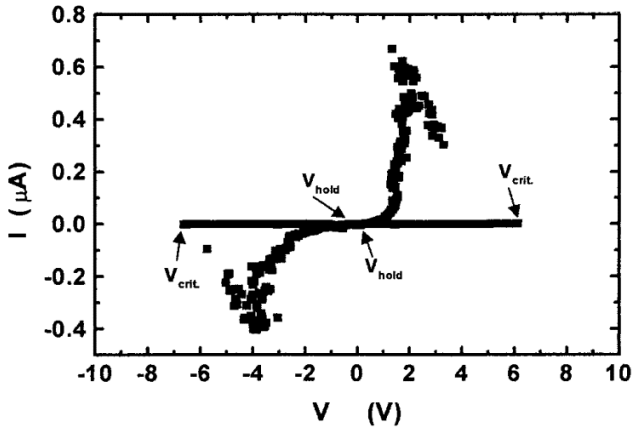

Figure II.21. Anthracene-containing polymer with switchable conductivity.[85]

3.2.3 Energy harvesting and light emission

Multiple times, anthracenes have been successfully used in conjugated polymers designed for solar cells. Indeed, anthracene groups can be used as (weak) donors in donor-acceptor polymers with low band gaps, as demonstrated by Almeataq *et al.*.[86] Anthracene moieties, having 4-dodecyloxybenzene as 9- and 10-substituents, were flanked by donating (di)thienyl groups and alternated with accepting benzothiadiazole moieties (Figure II.22). The limited solubility only allowed processing of lower molecular weight fractions. Band gaps of 1.84 to 1.96 eV and power conversion efficiencies (PCE) of 1.93 to 4.17 % were achieved.

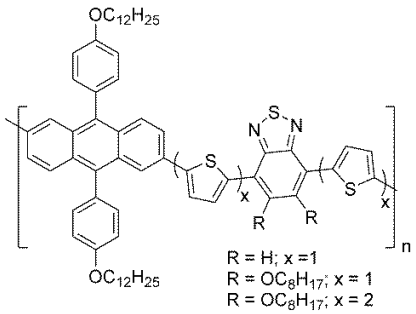

Figure II.22. Donor-acceptor conjugated polymers based on anthracene flanked with (di)thienyl moieties and benzothiadiazole groups.[86]

The weakly donating properties of anthracene also result in deep HOMO levels, which are favorable to achieve high PCE's. Therefore, instead of designing low-band gap polymers, Jung *et al.* recently focused on medium band-gap donor-acceptor polymers with low HOMO levels to achieve higher open-circuit voltages and thus higher PCE's.[87] 9,10-Thienylanthracene donors, flanked by thienyl groups, were alternated with (fluorinated) benzothiadazoles (Figure II.23). The achieved band gaps were 1.78 to 2.1 eV, with maximal PCE's exceeding 8 %.

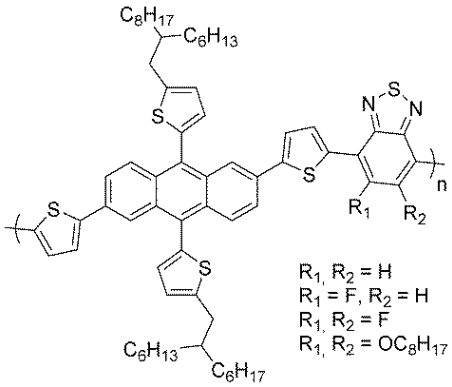

Figure II.23. Synthesis of medium bandgap anthracene-based polymers.[87]

Alternatively, donating anthracene moieties have been used in all-donor polymers, which require blending with (fullerene-based) electron acceptors.[88] The designed poly(arylene-ethynylene)s (Figure II.24) had a maximum PCE of 1.5 %, a high value for bulk heterojunction solar cells based on all-donor polymers.

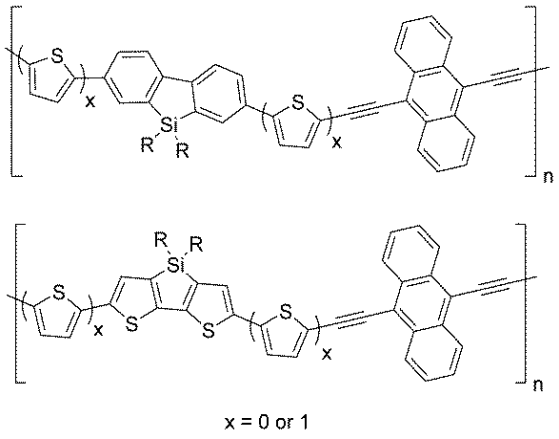

Figure II.24. Synthesized all-donor anthracene-containing polymers. [88]

Anthracenes have also been used as bulky comonomers in blue-light emitting poly(2,8-indenofluorenes).[89] 15 mol% of an anthracene comonomer prevented undesirable aggregation and excimer formation in the random copolymer, which previously led to red-shifting of homopolymer films (Figure II.25).

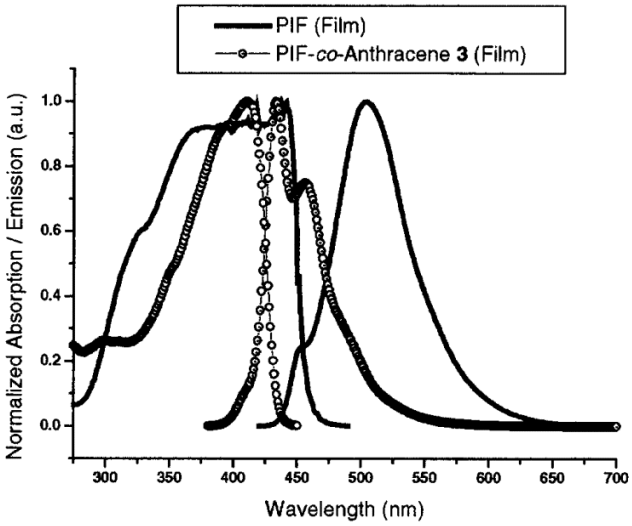

Figure II.25. Absorption and emission spectra of two conjugated blue-emitting polymer films. Random copolymerization of anthracene prevents red-shifting of the film fluorescence due to aggregation.[89]

3.2.4 Electrochromic polymer

Application of an external potential to conducting anthracene-containing polymers can lead to molecular changes resulting in (significant) color changes and thus electrochromic properties.[90]

Anthracene moieties have been electro-copolymerized (*via* their 9- and 10-position) with 3,4-ethylenedioxythiophene (EDOT) directly[91] and by using an EDOT-anthracene-EDOT precursor.[92] The polymer films could repeatedly be switched from one redox state to another in the order of seconds. The acquired color intervals typically span from red to blue, dependent of the oxidation state. Combination of the anthracene-EDOT precursors with other monomers, such as thiophene, selenophene and 3-methylthiophene, allow tuning of the acquired colors at specific oxidation states, as recently demonstrated by Tao *et al.* (Figure II.26).[93]

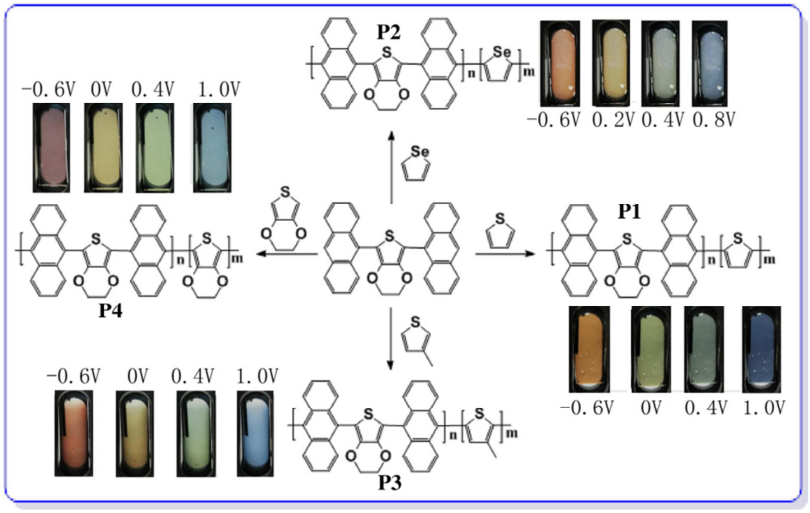

Figure II.26. Electro-copolymerization of anthracene-EDOT-anthracene monomers with different monomers enables to tune the electrochromic properties of the obtained material.[93]

3.3 Other uses as non-reactive moiety

Anthracenes have been incorporated in polymers as non-reactive moieties for many other (niche) applications than those presented above. These alternative applications are however considered out of the scope of this thesis and will therefore not be extensively discussed here. One example hereof is to allow UV-inactive polymers to become removable by using light (laser ablation) having wavelengths in the UV region. Towards this aim, Ishii *et al.* made copolymers of 9-anthrylmethylmethacrylate and

methylmethacrylate.[94] The presence of the (covalently attached) anthracene group allowed absorption of XeF excimer laser irradiation (351 nm), rendering otherwise non-absorbing PMMA ablatable. However, undesirable photo-crosslinking occurred by dimerization of the anthracene side groups.

4 Polymers with anthracene as reactive moiety

Anthracene groups in monomers and polymers have been used as reactive moieties for polymerization, chain extension, polymer modification, coupling, cyclization and crosslinking. The most commonly used reactions are Diels-Alder reactions and photodimerizations.

The principal Diels-Alder reactions involving anthracene are its combination with maleimides or maleic anhydrides. These reactions occur over the central anthracene ring *via* a [4+2] cycloaddition. Anthracene similarly reacts with singlet oxygen, which is formed upon UV-irradiation, forming endoperoxides. While Diels-Alder reactions are technically thermally reversible, these endoperoxides are often undesirable as they undergo other irreversible side reactions.

The anthracene dimerization occurs *via* a [4+4] photocycloaddition upon UV-irradiation at room temperature. This reaction can be reverted by irradiation at lower wavelengths (after UV absorption by the dimers), or thermally, at higher temperatures *via* a presumably radical pathway.

4.1 Polymerization and post-polymerization modification

4.1.1 Post-polymerization modification by Diels-Alder

Several times, the (reversible) cycloaddition of anthracene with dienophiles has been explored as a method for modifying the polymer properties. This strategy has been used for instance by Ishow *et al.* to tune the fluorescence of anthryl-based poly(phenylene ethynylene)s.[95] Diels-Alder reactions of the anthracenes with maleimides led to blue-shifts up to 80 nm, both in absorption and emission (Figure II.27), and increases in fluorescence quantum yield.

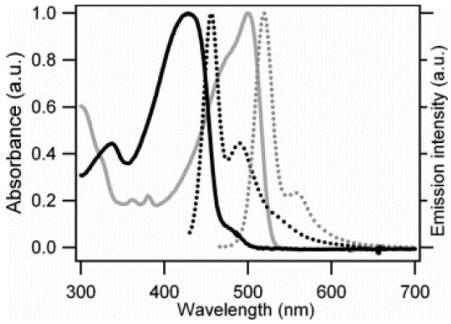

Figure II.27. Diels-Alder reaction of anthracene groups with maleimides leads to blue-shifts in the absorption (full) and fluorescence (dotted) spectra of the material. The pristine polymer is in gray while cycloadducts are in black.[95]

Anthracenes have also been introduced in - otherwise unfunctionalized - polyolefins as functional handles. In a very recent publication, 9-hexenylanthracene and propylene were copolymerized to isotactic polypropylene having pending anthracene groups.[96] The Diels-Alder reaction of those pending groups with maleic anhydride and other dienophiles (Figure II.28) allows to modify the melting and crystallization temperatures, as well as the polarity of the polymer. The reactions can be monitored by fluorescence spectroscopy.

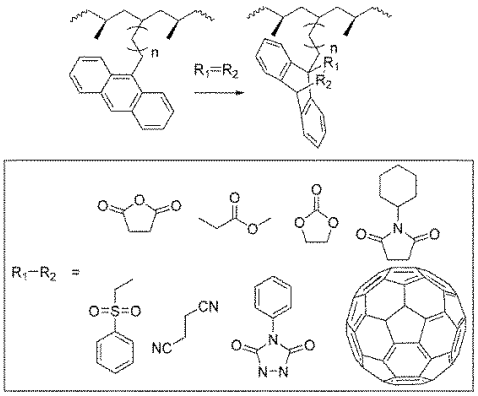

Figure II.28. 9-Hexenylanthracene is copolymerized with propylene. The pending anthracenes react with dienophiles, functionalizing the polymer and tuning its properties.[96]

The reversible nature of the Diels-Alder adducts allows for the functionalization to be only temporary when desired. Indeed, a simple thermal treatment can be used to cleave the adduct. This strategy has been used by Hodge and coworkers to synthesize a soluble precursor of (almost) insoluble conjugated polymers, which facilitates synthesis and casting of the material as a coating.[97] Prior to polymerization,

the 2,6-dibromoanthracene monomer was reacted with maleic anhydride. Soluble precursor polymers with molecular weights up to 5700 g/mol could be polymerized from those modified monomers. In a last step, heating at 260 °C activated the retro-Diels-Alder reaction, resulting in the desired insoluble poly(anthracene-2,6-diyl) and similar copolymer with alternating p-phenylene units. Liu *et al.* recently used this same strategy to prepare donor-acceptor copolymers for solar cells.[98] The 2,6-dibromoanthracene was reacted with maleic anhydride and subsequently turned into the corresponding methylester. After polymerization, the soluble polymers could easily be processed and then thermally treated to reach the desired insoluble donor-acceptor copolymers (Figure II.29).

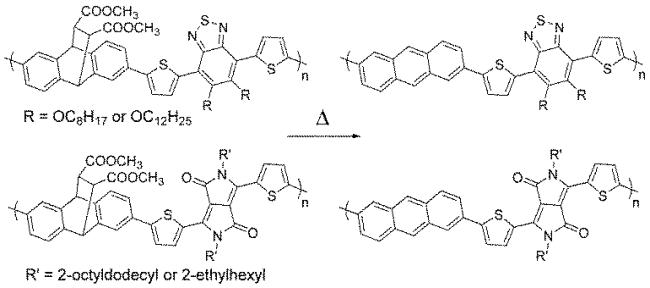

Figure II.29. After deposition of the precursor on a surface, the maleic ester is cleaved upon heating from soluble conjugated precursor molecule, making the polymer well-packed and insoluble.[98]

Gossweiler *et al.* recently incorporated anthracene-phenyltriazolinedione cycloadducts into polymer networks as mechanophores.[99] Those adducts could be triggered to release the phenyltriazolinedione through the force-induced planarization of the anthracene component (Figure II.30). As the adducts are incorporated into the polymer chains only *via* the anthracene 2- and 6-positions, the mechanically activated cycloreversion does not lead to polymer chain scission or decrease in cross-linking. Because of this, the integrity of the polymer network is maintained upon stress, while allowing for an optical or chemical response.

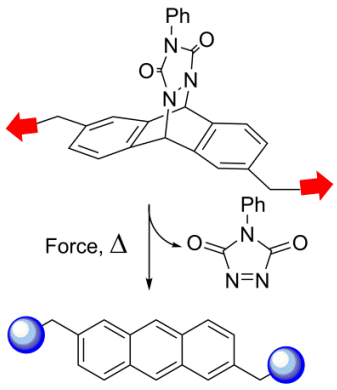

Figure II.30. Flex-activated retro-Diels-Alder reaction.[99]

4.1.2 Post-polymerization modification by dimerization and other chemistries

While the reversible Diels-Alder reaction provides a viable tool for polymer modification, a few other strategies have also been reported.

The dimerization of pendent anthracene groups in water with low molecular weight anthracenes and anthracene-labelled macromolecules was recently studied by Biedermann *et al.*.[100] They reported the use of cucurbit[8]uril (CB[8]), which acts as a host for two anthracene moieties and tethers them in a face-to-face π-π stack arrangement. This host-guest complexation led to higher photodimerization rates and less photodegradation products.

Another post-polymerization modification method was reported by Taylor and Swager.[101] In order to avoid the low solubility of the anthracene-based conjugated polymers, they prepared dihydroacenediol-based precursor polymers instead. Molecular weights up to 160 000 g/mol were achieved, which upon reductive aromatization resulted in the insoluble anthracene-based polymer (Figure II.31). Band gaps down to 1.5 eV and conductivities up to 1.5 S/cm at +0.5 V were achieved.

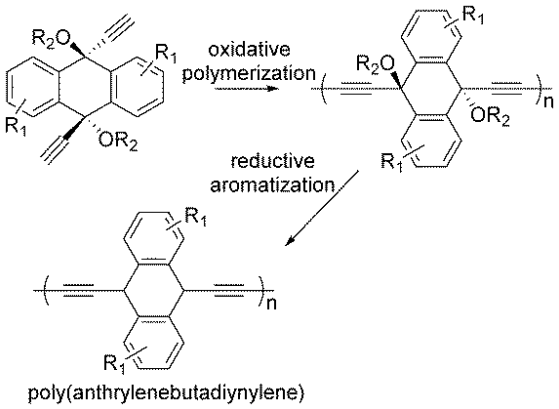

Figure II.31. Strategy for synthesis of conjugated anthracene-containing polymer having a temporary increased solubility.[101]

In another publication, Fudickar and Linker used the reversible endoperoxide formation of 9,10-diphenylanthracene structures under air and UV-irradiation to change the (polymer) solubility and fluorescence (Figure II.32).[102] Such photopatterned films could be visualized under fluorescence microscopy and erased by heating above 100 °C. Unreacted area of monomer films could be removed, allowing etching of the underlying surface. Thomas and coworkers very recently developed water-soluble probes that respond to singlet oxygen, a key reactive oxygen species to many (*in vivo*) reactions.[103] As the aromatic moieties are hydrophobic, a hydrophilic backbone was required. The addition of singlet oxygen to the diarylanthracene groups led to diminution of the fluorescence. However, the use of larger acenes such as tetracene led to probes which reacted faster and are therefore found to be more suitable.

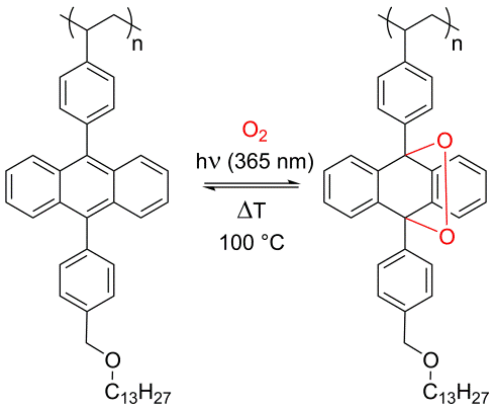

Figure II.32. Reversible reaction of the anthracene to form its corresponding endoperoxide.[102]

Lastly, Modi and Guillet reported the cleaving of the photolabile anthrylmethyl ketone groups using irradiation at 313 nm and a quantum yield of ~0.01.[104] The photolysis produces almost exclusively Norrish I type products. As the formed radicals withdraw protons from their surroundings to form stable products, the authors claimed this strategy to be useful for drug release from polymeric matrices.

4.1.3 Polymerizations by Diels-Alder

Nie and Rotello used the reversible Diels-Alder reaction between bisanthracene ether and C_{60} fullerene to develop a thermally reversible polymer (Figure II.33).[105] As the first and second addition to fullerenes are much faster than a third, no covalent networks should be produced. However, as not all material could be solubilized, the absence of a covalent gel could not be confirmed. Variable temperature UV-vis spectroscopy showed complete depolymerization at 75 °C. Recently, Dang *et al.* reported the polymerization of C_{84} fullerene using a bisanthracene. The spatial separation of the HOMO and LUMO of the polymer might make these polymers useful as charge transfer bipolar materials.[106]

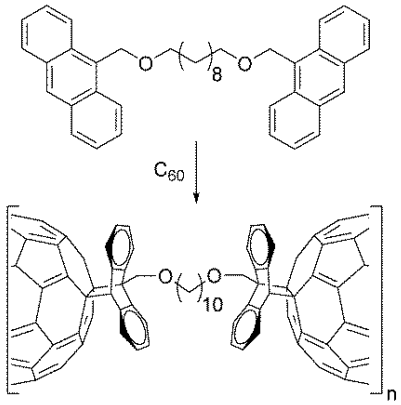

Figure II.33. Diels-Alder polymerization of a bisanthracene with fullerene.[105]

Thermally reversible polymers based on bismaleimides and bisanthracenes were reported by Grigoras.[107] However, the limited solubility of the chains and the reversible nature of the polymerization resulted only in oligomers. Kriegel *et al.* reported the chain extension of 2-anthryl-functional polyesters with bismaleimides.[108] The rapid polyaddition required lower temperatures and thus less energy to achieve high molecular weights compared to polyester synthesis via classical polycondensation.

4.1.4 Polymerizations by dimerization

The cycloaddition of anthracene occurs under mild conditions and does not require any potentially toxic additives or initiators. Thanks to those favorable characteristics, the bisanthracene cycloaddition has very recently been used as mild photopolymerization method by Hizal and coworkers to make tunable biologically active polymers.[109] First a bisanthracenyl-pentafluorophenylester monomer was made, which was photopolymerized for 2 days upon irradiation with 365 nm light (Figure II.34). Afterwards, post-modification could also be achieved by activated ester substitution reactions using various amines. Another recent publication by Ozguc Onal and Nugay reported on the photodimerization to reversibly chain extend telechelic (2-anthryl)-1-phenylethene-capped polyisobutylene.[110] Irradiation of concentrated samples led to doubling up to quadrupling of the molecular weights, as well as unicyclic products. Photoscission occurred in diluted samples with up to 78 % recovery of the anthracene units.

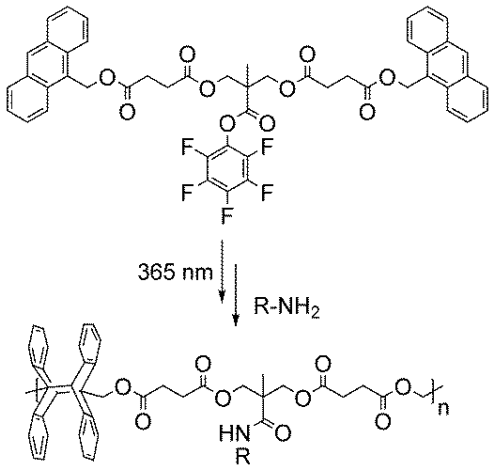

Figure II.34. Bisanthracenes as photopolymerizable monomers under mild conditions.[109]

Polymers with anthracene photodimers in the main chain are photochemically[111] and thermally[112] depolymerizable as shown by Tazuke and Tanabe in the seventies. Concerning the molecular mobility required for dianthracene dissociation, they showed how the scission of the polymers largely depends on segment mobility, rather than on the actual glass transition temperature (T_g). For example, hydrogen bridges in polyurethanes shifted the onset of dissociation to 100 °C, compared to 90 °C in similar polyesters.

Using the anthracene dimerization, Wei *et al.* recently polymerized an anthracene-capped [3]rotaxane, avoiding possible (poly)pseudorotaxane dissociation during polymerization or end capping (Figure

II.35).[113] The formed poly[3]rotaxane could be thermally reverted by mild heating at 60 °C for 20 hours and repolymerized if desired. Telechelic 9-anthryl end-capped poly(ethylene glycol) (PEG) polyrotaxanes have been reversibly dimerized to larger poly(polyrotaxanes) by Okada and Harada.[114] Single 9-anthryl end-capped PEG chains were treated with α-cyclodextrine and then capped using 9-anthracenecarboxylic acid, avoiding dethreading of the α-CD. Irradiation at 340 nm generated poly(polyrotaxane)s, which were 90 % thermally cleavable by heating at 120 °C. As γ-cyclodextrines are large enough to slide over 9-anthryl-groups, but not over their photodimers, Harada and coworkers used the anthracene photodimerization to avoid dethreading of γ-CD.[115]

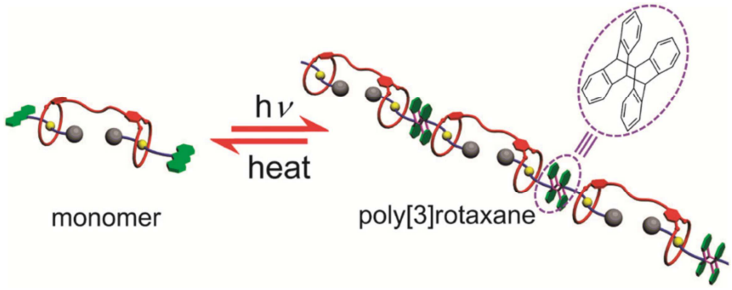

Figure II.35. Depiction of photopolymerizable and thermally cleavable poly[3]rotaxanes.[113]

Yang and coworkers recently developed double dynamic polymers based on supramolecular pillar[5]arene/imidazole host-guest complexes and anthracene dimers (Figure II.36).[116] Short heating times (~ 1 minute) led to temporarily depolymerization due to decomplexation, while long heating times (~ 1 day) led to "permanent" depolymerization by thermal dianthracene scission.

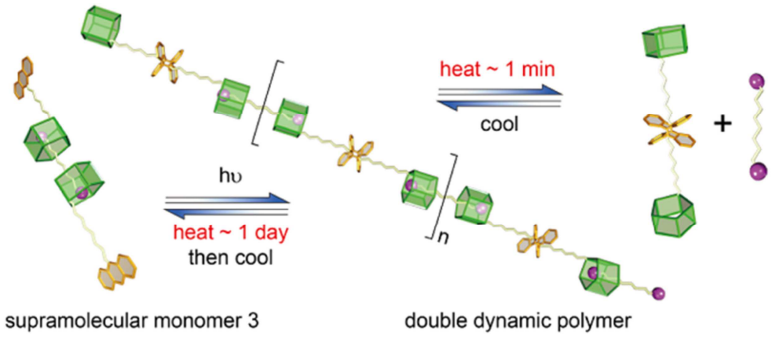

Figure II.36. Double dynamic polymers based on host-guest complexes and anthracene dimerization.[116]

The reversible photopolymerization of anthracene end-capped liquid-crystalline monomers has been used by Kihara and coworkers to develop a rewritable grayscale photopatterning system.[117] While the

unirradiated monomers and oligomers are liquid-crystalline and therefore visible under polarized light, the polymers were amorphous, which allows for photopatterning as shown in Figure II.37. However, due to the high melting point of the liquid crystals, temperatures as high as 230 °C were required during patterning.

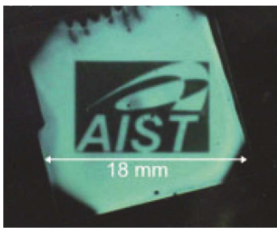

Figure II.37. Polymer film visualized under polarized light after UV-patterning at 230 °C for 30 s. The irradiated areas are dark.[117]

4.2 Polymer-polymer (de)coupling, cyclic polymers and surface grafting

4.2.1 By Diels-Alder

Diels-Alder reactions between anthracene and maleimide structures have been extensively studied as efficient polymer coupling reaction, often referred to as a “click” reaction because of its fast and selective nature. These efficient reactions are desirable when attempting the simple and rapid synthesis of complex polymer architectures. Diels-Alder “click” chemistry have been reviewed by several authors.[118]

In this context, Tunca and coworkers studied the anthracene-maleimide Diels-Alder reactions as chemical tools for making linear block copolymers,[119] star polymers,[120] multiarm[121] and miktoarm[122] star block copolymers, heteroarm H-shaped terpolymers[123] and graft copolymers[124]. In all these publications the maleimide group is initially protected as a Diels-Alder adduct with a furan group, after which the retro-Diels-Alder reaction releases the maleimide moiety upon heating. As the reaction of the maleimide with anthracene is thermodynamically favored over the furan-maleimide cycloaddition, quantitative conversion is acquired without the necessity of furan removal. In combination with the highly efficient Huisgen “click” reaction, they also made regular graft copolymers,[125] heterograft copolymers,[126] ABC triblock structures,[127] 3-arm star block copolymers,[128] multiarm star triblocks,[129] multi-miktoarm star blocks,[130] cyclic structures[131] and block-brush copolymers.[132] Their work demonstrated the good

orthogonality of the maleimide-anthracene Diels-Alder reaction towards the azide-alkyne "click" reaction. Making use of the nitroxide radical coupling as a third reaction, they further synthesized linear tetrablock copolymers,[133] heterograft brush copolymers,[134] 3-miktoarm star terpolymers[135] and tadpole polymers.[136] The thiol-ene reaction was eventually used as a fourth highly efficient reaction for the synthesis of cysteine-terminated linear multiblocks[137] and cysteine-functional heterograft brush copolymers.[138]

The same Diels-Alder chemistry was used by Sanyal and coworkers for making dendronized polymers,[139] diblock and triblock dendrons.[140] Alkayal and Hadjichristidis made α-anthracene-ω-hydroxypolymethylene by polyhomologation and used it with maleimide-capped polymers to make di- and triblocks.[141] Kimura and coworkers used this "click" chemistry to couple poly-L-lactide and poly-D-lactide prepolymers to form di- and triblock copolymers.[142] ABC type miktoarm star copolymers were developed by Yagci and coworkers by starting from an ene-, azide- and anthracene-containing core.[143] The complex star structure was achieved using the efficient thiol-ene as initial reaction, followed by the Huisgen azide-alkyne "click" reaction and eventually the Diels-Alder cycloaddition between anthracene and maleimide. Dendritic star polymers were made in a one-pot approach by Xiong and Xu by coupling PCL, containing a singular central maleimide side group, to a tetrafunctional alkyne-containing core. As maleimides and alkyne groups do not react with each other, an anthracene- and azide-containing coupling agent is used to react with both groups.[144]

The thermal reversibility of anthracene-maleimide adducts was also studied for the decoupling of polymer chains. For example, thermal scission of coupled PMMA chains occurs, but only slowly even at 200 °C, and all cycloadducts are reformed during cooling.[145]

Sumerlin and coworkers very recently published the concept of stimuli-induced macromolecular metamorphosis, in which kinetically formed furan-maleimide bonds are broken upon heating in the presence of anthracene-containing polymers in favor of the thermodynamically more stable anthracene-maleimide bonds.[146] This strategy allowed the transformation of linear amphiphilic and hyperbranched block copolymers to star, comb and hydrophobic block copolymers as shown in Figure II.38.

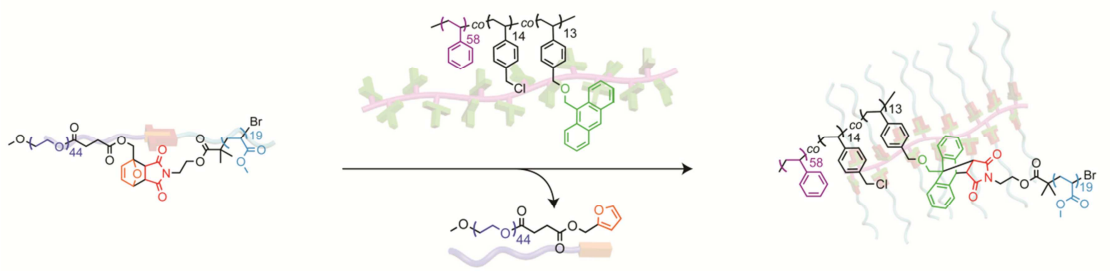

Figure II.38. Macromolecular metamorphosis from linear to comb block copolymer.[146]

The scission of anthracene-maleimide cycloadducts can be mechanically accelerated or suppressed, as recently shown by computational and experimental results by Konda *et al.*.[147] For cycloadducts in which the anthracenes are attached *via* the 2-position, mechanical stress was shown to suppress the cycloreversion reaction. On the other hand, a mechanical acceleration did occur when the polymer chains were attached *via* the 9-position (Figure II.39).

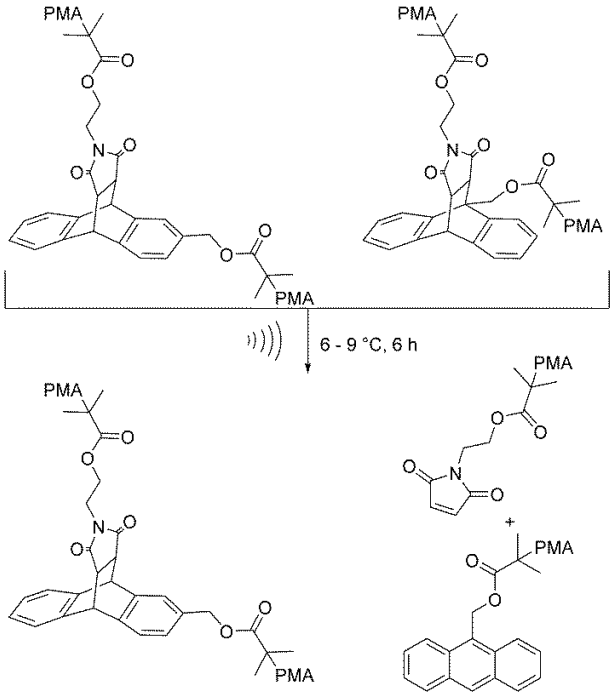

Figure II.39. Polymer chains attached on the 9-position of the anthracene group lead to mechanical acceleration of the cycloreversion. The opposite is true when the chains are attached to the 2-position.[147]

Therefore, the latter cycloadducts have recently been used as mechanophoric bonds in polymers having different architectures, such as linear polymers and three-arm stars (Figure II.40),[148] micelle-forming blocks,[149] "hairy" polymer particles[149b] and linear chains attached to silicone nanoparticles.[150]

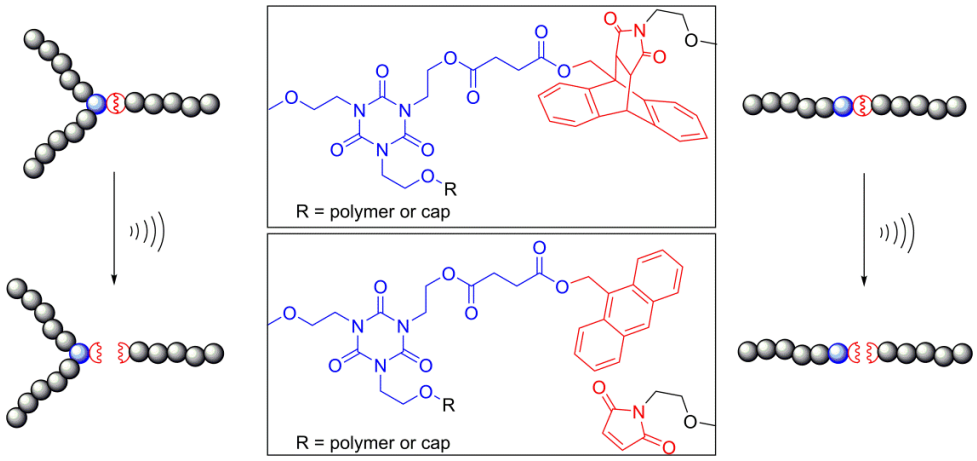

Figure II.40. Mechanophoric response upon ultrasonication of three-arm stars and linear polymers.[148]

An increase of the fluorescence quantum yield, which increases the sensitivity of the mechanophore, has very recently been accomplished by Göstl and Sijbesma by extending the π-system *via* the 9- (and potentially 10-) position (Figure II.41).[151]

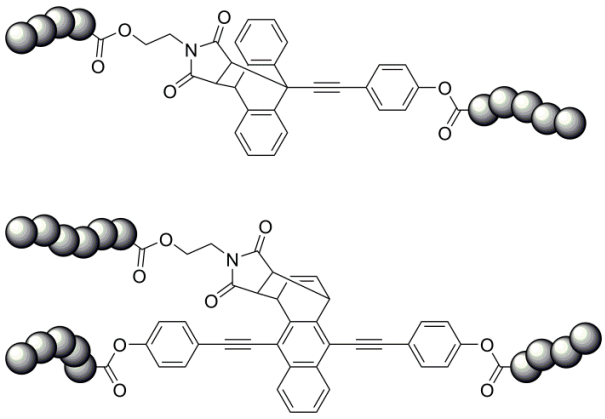

Figure II.41. Mechanically cleavable bonds based the cycloadducts of pi-extended anthracenes and maleimide groups.[151]

4.2.2 By dimerization

The light-driven dimerization of anthracene structures has also been used to make different polymer architectures. The simplest of these structures is the coupling of two identical polymers, as demonstrated by Müllen and coworkers who dimerized end-capped PMMA chains.[152] While this reaction was successful for polymers with low molecular weight, the authors were unable to couple polymers with molecular weights exceeding 8000 g/mol. Coursan and Desvergne found low dimerization quantum yields for all concentrations of ω-anthrylpolystyrenes using 366 nm UV-light (e.g. $\Phi \sim 0.001$ at 10^{-3} mol/L). This result suggests that the anthracene groups are mostly embedded in the polymer skeleton.[153] The coupled product could be dissociated using 280 nm UV-light and this cycle could be repeated up to 10 times without significant side reactions.

Jyo and coworkers reported the photocoupling of 9-anthryl-capped oligodeoxyribonucleotides using a DNA template.[154] In the absence of a template, no coupling occurred. Dimerization rates decreased with shorter linker chain length, larger nucleotide gaps and the presence of one-base-displacements, mainly in central positions. The latter effect allows the use of this system for single-nucleotide polymorphism (SNP) detection. They also showed an increase in photochemical linking efficiency for 1- or 2-substituted anthracenes, compared to the 9-anthryl groups.[155] The optimized system for SNP detection used 1-substituted anthracenes and longer oligodeoxyribonucleotide lengths, resulting in above 90% yield for a one minute irradiation.[156]

Telechelic anthracene-capped PCL has recently been cyclized by photoirradiation by Wang *et al.*.[157] Different ring sizes could be obtained using the same polymer by altering the concentration of the irradiated solution. However, heating at 160 °C for several hours only led to partial reversion to the linear parent polymers. Cyclic poly(catenane)s were made by Okada and Harada by photodimerization of diluted solutions of anthracene-capped α-CD- and PEG-based polyrotaxanes.[114] Reversion to the linear polyrotaxanes occurred at 120 °C with conversions over 90 %. The reversible linear-cyclic topological conversion of polyethers having different anthracene end groups was very recently studied by Tezuka and coworkers.[158] They noticed considerably less undesirable byproducts by photo-oxidation for the electron-poor anthracene units. The polymer could be cyclized by irradiating with UVA light and return to the linear shape by heating at 150 °C for up to 5 topology change cycles (Figure II.42). Ji *et al.* recently made PEG cycles by using the host-guest interactions of the anthracene end-groups with cucubit[8]uril (CB[8]) in water.[159] The supramolecular cycles were fixed covalently by dimerization of

the stacked anthracene groups in the CB[8] hosts, making them analyzable by techniques such as size exclusion chromatography. Tucker and coworkers used the intramolecular dimerization of two anthryl groups in modified DNA strands to reversibly change the binding affinities of the strands with the complementary target strands (Figure II.43).[160]

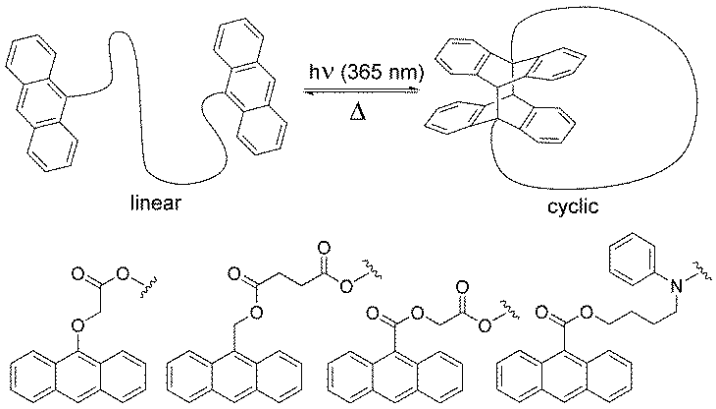

Figure II.42. Reversible linear-cyclic conversion by irradiation and heating.[158]

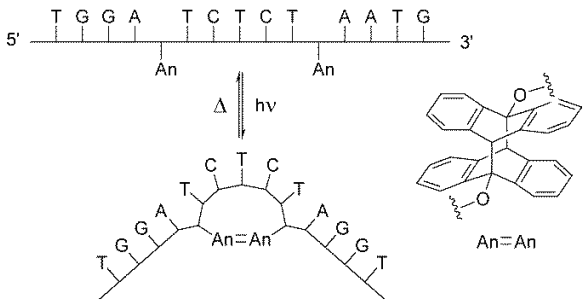

Figure II.43. Reversible intramolecular anthracene dimerization, leading to changing binding affinities of DNA strands.[160]

Anthracene-capped polystyrene and PMMA have been coupled by light-stimulated dimerization to form diblocks by Penelle and coworkers[161]. Aside from the block copolymer, homocoupling products were formed. Scission of the copolymer occurred thermally at 135 °C. The block copolymers were used to obtain microphase separated morphologies.[162] By thermal treatment at 170 °C, morphology and domain sizes could be controlled. Selective washing lead to surfaces with round features or holes. The anthracene dimerization coupling has also very recently been used to make triblocks from diblocks after melt-processing.[163] Anthracene-capped PS-PEO-An diblocks self-assemble into PS spheres in a PEO matrix. Subsequent irradiation of the viscous liquid led to PS-PEO-PS triblock formation and therefore

physical crosslinking of the material. Comparison between these materials, in which the triblocks are photochemically formed after processing, and reference materials, in which triblocks and diblocks are blended before processing, revealed subtle differences. These differences were attributed to the crosslinking gradient throughout the material.

Russell and coworkers photodimerized central pending anthryl groups of triblock structures below T_g, leading to H-type and other high molecular weight branched structures.[164] Upon heating above the T_g, the irradiated material underwent a disorder-to-order transition. A maximal thermal reversion of only 40 % was achieved upon heating to 240 °C.

Yanagimoto *et al.* dimerized 2,3,6,7-substituted anthracenes having dendrimer branches. The dendrimers showed high reactivity in solution, but did not dimerize in the liquid-crystalline state.[165] Surface-block dendrimers were made by photocoupling dendrimer precursors having a 9-substituted anthracene group at the core and long alkyl or oligo(ethylene oxide) chains at the surface (Figure II.44).[166] Aside from the desirable surface-block dimers having a hydrophobic and hydrophilic hemisphere, homo-coupling dendrimers were also made.

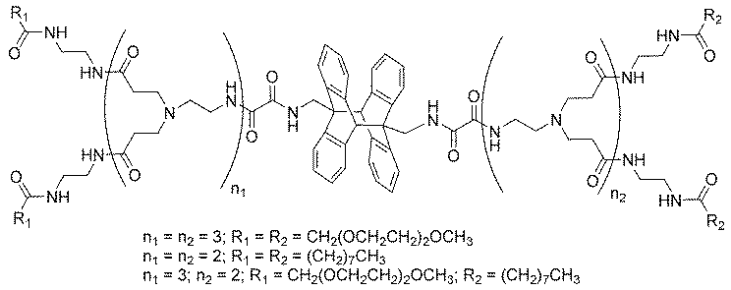

Figure II.44. Surface-block dendrimers made by photocoupling anthracene-based dendrimer precursor.[166]

Very recently, Barner-Kowollik and coworkers used the photodimerization to reversibly pattern anthracene-decorated surfaces with small molecules or polymers.[167] They made use of an electron-rich 9-triazolylanthracene structure attached to the surface, allowing photodimerization to occur at 410 nm during 4 hours. Decoupling occurred over 48 hours using a low intensity UV lamp with the highest emission at 360 nm.

4.2.3 By reaction with thiols

Kim and coworkers recently made use of an anthracene-thiol reaction to form cyclic poly(N-isopropylacrylamide) as shown in Figure II.45.[168] This was done by RAFT polymerization using a 9-anthryl-functionalized chain transfer agent. Aminolysis of the dithioate group led to the α-anthracene-ω-thiol precursor. Radical thiol-ene addition of the opposing groups in dilute solution led to the cyclic polymer.

This is somewhat contradictory to other publications such as the ones of Tunca and coworkers[138] and Yagci and coworkers,[143] where hydrothiolation of a double bond was used as highly efficient coupling reaction in the presence of anthracene. No reference is made to any side reaction, hinting at a much faster reaction of thiols with double bonds than with anthracene.

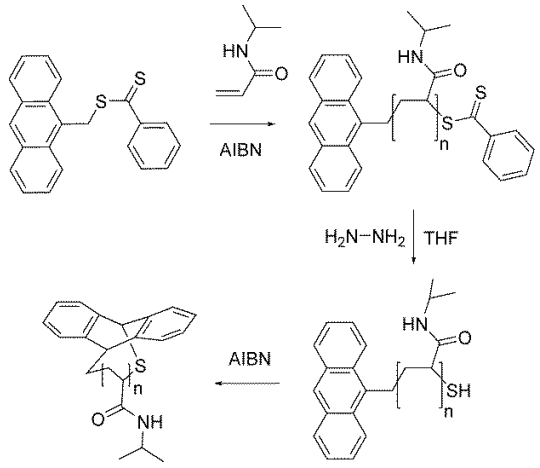

Figure II.45. Synthesis of cyclic poly(N-isopropylacrylamide) using an anthracene-thiol cyclization.[168]

4.3 (De)crosslinking of polymers

4.3.1 (De)crosslinking by Diels-Alder

Jones *et al.* developed PET-like polymers having 2,6-connected anthracenes in the main chain and studied their crosslinking upon adding bis-maleimides.[169] De-crosslinking by the retro-Diels-Alder reaction was shown to only occur in the decomposition temperature range, starting from 250 °C, making the crosslinking essentially permanent. The high reaction rates at mild conditions, thermal stability and orthogonality has led to the use of this “click” reaction for the curing of non-linear optical materials.

This was very recently demonstrated by Gao *et al.*, who used the anthracene-maleimide cycloaddition to crosslink anthracene-containing PMMA with a telechelic anthracene-capped nonlinear optical dye and bis-maleimide.[170] This crosslinking of the electro-optic material between 80 to 120 °C resulted in increased longterm stability. In fact, 85% of the initial electro-optic coefficient remained after 250 hours heating at 80 °C. The maleimide/anthracene cycloaddition has also been used to crosslink star shaped PCL precursors to form shape memory networks via reactive extrusion by Jérôme and coworkers.[171] The high thermal stability of these bonds ensured mechanical integrity when heating above the thermal switching temperature (60 °C). Shi *et al.* used this reaction to crosslink dendrimers having an electro-optical dye in the center and anthracene end groups, using trismaleimides.[172]

Because of the high thermal stability of the anthracene-maleimide adducts, Yoshie *et al.* relied on the mechanical breaking of anthracene-maleimide crosslinks instead for the development of a self-mending polymer network.[173] Upon mechanical stress, the cycloadducts are favorably broken, reforming the parent moieties. Healing of a cut sample at 100 °C for several days allowed recovery of up to ~ 55 % of the initial tensile strength and ~ 90 % of the elongation at break (Figure II.46).

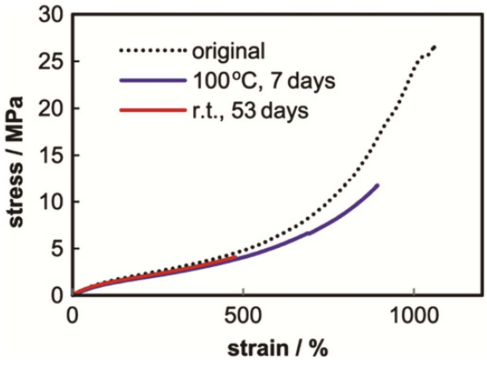

Figure II.46. Healing of a damaged network having anthracene-maleimide crosslinks.[173]

In their recent publication, Sumerlin and coworkers also reported the stimuli-induced macromolecular metamorphosis of densely crosslinked networks.[146] The dense networks were made by kinetically controlled crosslinking of a triblock copolymer bearing pendent furan groups in the center and anthracene end groups with a bis- or tris-maleimide crosslinker. Upon heating, the kinetically more favorable furan-maleimide bonds are broken in favor of anthracene-maleimide bonds, rendering linear polymer or a looser network in case the bis- or tris-maleimide was used, respectively (Figure II.47).

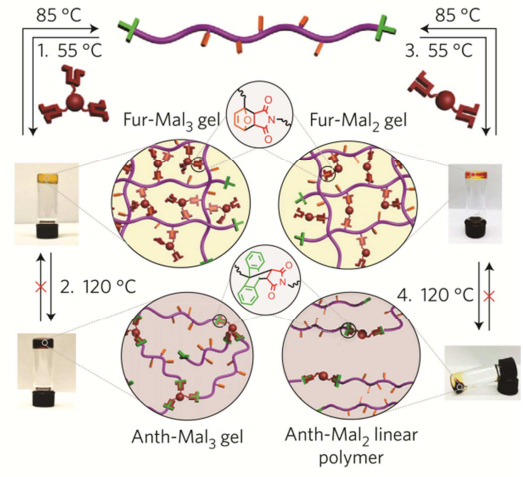

Figure II.47. Stimulus-induced metamorphosis of densely crosslinked networks to loosely crosslinked networks or linear polymers.[146]

Very recently, Kötteritzsch *et al.* developed remendable polymers based on the Diels-Alder cycloaddition of poly(lauryl methacrylate) having pendant 9-anthryl groups with C60-fullerene and phenyl-C61-butyric acid methyl ester.[174] The self-healing of scratches could be tuned between 40 °C and 80 °C, with faster healing occurring for the anthracene compounds having a methyl at the 10-position.

4.3.2 (De)crosslinking by photoirradiation and light-driven/thermal dissociation

4.3.2.1 Inter-and intramolecular crosslinking studies

The dimerization of anthracene has been studied to create (reversible) crosslinks in materials. One of the first studies on these type of systems was by Schröter and Riegger in 1954.[175] 9-Anthracene aldehyde acetal groups were attached to a partially hydrolyzed polyvinylacetate backbone (Figure II.48). UV-light irradiation of the material made it insoluble due to the increase in molecular weight and/or crosslinking by dimerization of the pending anthracene units.

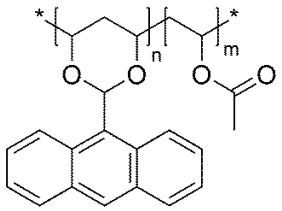

Figure II.48. Anthracene aldehyde acetal of partially hydrolyzed polyvinylacetate.

Polyesters with pendent anthryl groups were irradiated using 370 nm UV irradiation in dilute solution by Tazuke and Banba.[176] Long and flexible chains between anthracene groups led to faster dimerization, fair first-order kinetic linearity and intramolecular reactions. Contrarily, crowded anthracene groups led to slow, head-head cycloadditions and rigid main chains led to mainly slow intermolecular reactions. Irradiation of the photoproducts at 264 nm brings them to a photostationary state with only 60 % anthracene recovery. Photodimerization studies on anthryl-containing polyesters and polyurethanes in the solid state by Tazuke and Hayashi revealed hindrance by the presence of hydrogen bridges, emphasizing the importance of segment mobility in the dimerization process (Figure II.49).[177] De-crosslinking was achieved by thermal treatment at 80-100 °C. The rates at 85 °C were 0.98 for PE(A-8), while only 0.11 and 0.17 for PU(A-6) and PU(A-Xy). The reported activation energies were 83, 128 and 47 kJ kJ mol^{-1}, with pre-exponential factors 1.8 10^5, 5.4 10^7 and 4.5 10^2, respectively.

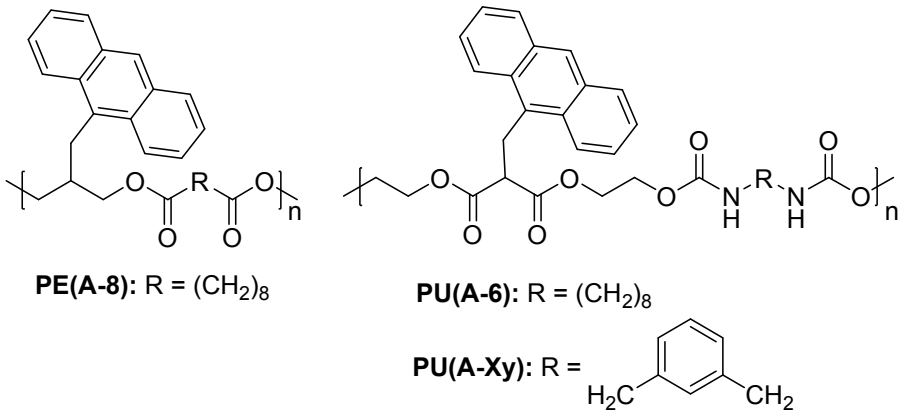

Figure II.49. Structures of the polymers studied by Tazuke and Hayashi.[177]

Similarly, long flexible spacers between anthracene groups and the main chain also facilitated the photodimerization and subsequent thermal de-crosslinking for Schopov and coworkers.[178] The networks were based on the copolymerization of the acrylate functional anthracene monomer shown in Figure II.50, followed by cross-linking through dimerization. After one hour at 130 °C, the free anthracene content of the network reached about 60 % of the initial value.

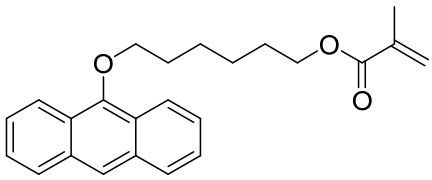

Figure II.50. Monomer synthesized, copolymerized and studied by Schopov and coworkers.[178]

Biedermann *et al.* recently facilitated the crosslinking in aqueous solution by adding CB[8].[100] Each CB[8] molecule keeps two anthracene guests in close proximity while also shielding them from oxygen and other possible reagents when irradiated.

Horie and coworkers studied the intra-molecular crosslinking of anthracene-containing polymers and found that higher amounts of pendant anthracenes did not result in a higher effective crosslinking.[179] The higher group concentration is counteracted by increasing short range reactions between neighboring groups, which results in higher chain segment rigidity and thus lower reactivity (Figure II.51). The remaining unreacted moieties form long range crosslinks in a later stage, which shrinks the polymer coil and suppresses the rotational and segmental translational mobility.

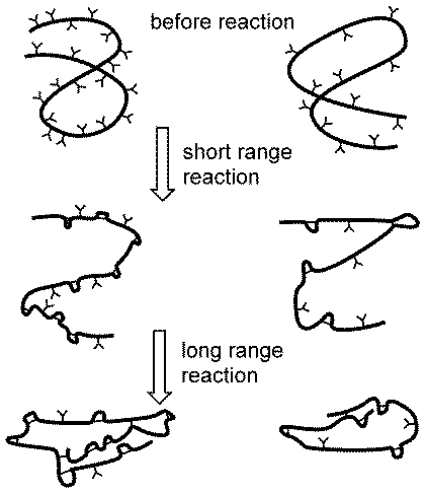

Figure II.51. Intramolecular crosslinking with crowded and uncrowded pending groups. The 'Y's represent the anthracene groups.[179]

Berda and coworkers recently made single-chain nanoparticles by intramolecular crosslinking through anthracene dimerization.[180] High amounts of anthryl side groups led to undesirable interparticle

coupling. Irradiation with UVC light led to partial recovery of anthracene moieties, but was not sufficient to noticeably change the particle morphology.

4.3.2.2 Drug delivery and other biomedical applications

The dimerization of anthracene has often been applied as a tunable photo-crosslinking technique, which does not require a photoinitiator or other additives. The latter is an especially desirable property for biomedical materials, where toxicity of additives might be problematic.

One drug delivery strategy relies on the hindered diffusion of drugs from preloaded hydrogels by increasing their crosslinking density through photodimerization, as demonstrated by Wells *et al.*.[181] Generic amino- and anthracene-capped PEG chains were grafted either on alginate or hyaluronate. After photo-crosslinking, diffusion of guest molecules could be slowed down or even completely stopped (Figure II.52). Similarly, Zheng *et al.* made a photoreversible PEG-based hydrogel.[182] For this, they modified a branched PEG-based polymer with 9-anthracenecarboxylic acid. UVA irradiation of this modified PEG in water led to the formation of a hydrogel with tunable swelling properties. Irradiation of this hydrogel with light of 254 nm led to a 20 % reversion but not to a complete sol-gel-sol process. This partial dimerization and recovery could however be repeated for 14 cycles, indicating good reversibility.

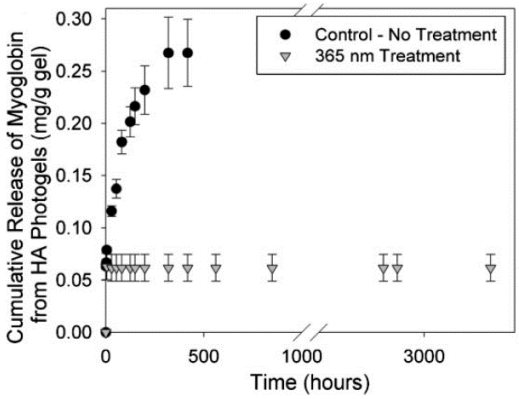

Figure II.52. The increase in cross-linking density of a protein-loaded photogel by photodimerization leads to inhibited protein release.[181]

Matsui *et al.* used the photoreversible dimerization of anthracenes for the development of molecularly imprinted polymer networks based on poly(methacrylic acid) with pendent anthryl groups.[183] As full reversibility was only achieved after the second cycle (irradiation with 365 nm for dimerization and 254

nm for scission of the dimers), a first cycle was performed without template, making a partially crosslinked prepolymer. The prepolymer was allowed to complex with the template drug and again photo-crosslinked (Figure II.53). The template was removed by washing. The imprinted polymer had a binding capacity for the drug nearly twice as large as the non-templated polymer.

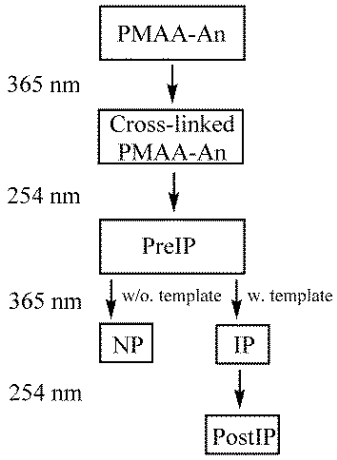

Figure II.53. Imprinting sequence of the poly(methacrylic acid) polymer networks.[183]

Hennink and coworkers recently photo-crosslinked thermally labile micelles for use as drug-delivery vehicles.[184] First a block copolymer was made of N(9-anthranoyloxypropyl) methacrylamide with the monolactate ester of (2-hydroxypropyl) methacrylamide, initiated by a PEG-modified initiator (Figure II.54). The obtained polymer formed micelles in aqueous solution at temperatures above its lower critical solution temperature (LCST). Irradiation with 365 nm light led to crosslinking, which was shown to slow down drug release: 40 % of the drug was released over 10 days instead of 60 % for the un-crosslinked micelles. The micelles could be partially (33 %) de-crosslinked by irradiation with 254 nm light.

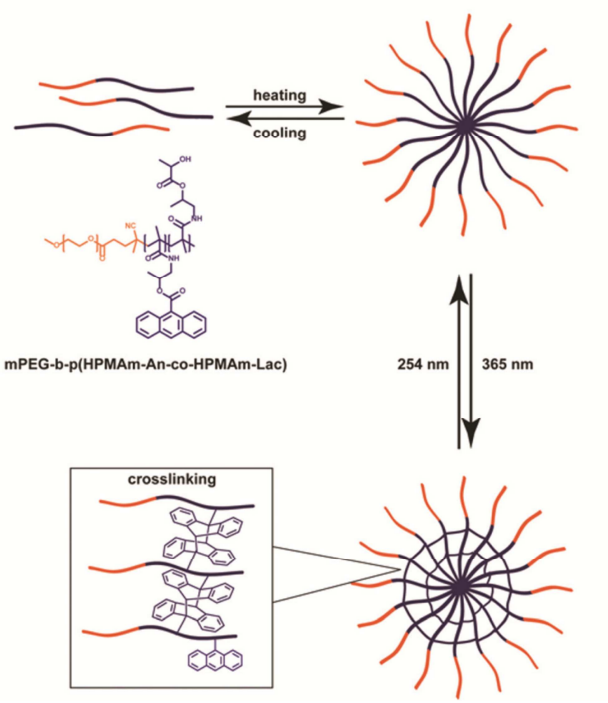

Figure II.54. (Partially) reversibly crosslinked micelles for controlled drug release.[184]

Su *et al.* used the anthracene photodimerization to stabilize hybrid core-shell microspheres.[185] Anthracene-containing polyhedral oligomer silsesquioxane (POSS) was used as a core material and co-assembled by π-π stacking with anthracene-ended hyperbranched poly(ether amine) which formed the shell (Figure II.55). After crosslinking by anthracene dimerization, the POSS core was removed, leaving behind hollow microspheres which are amphiphilic, fluorescent and pH- and temperature-responsive. The hollow spheres allow for the encapsulation and controlled release of guest molecules, monitored by fluorescence of the anthracene moieties.

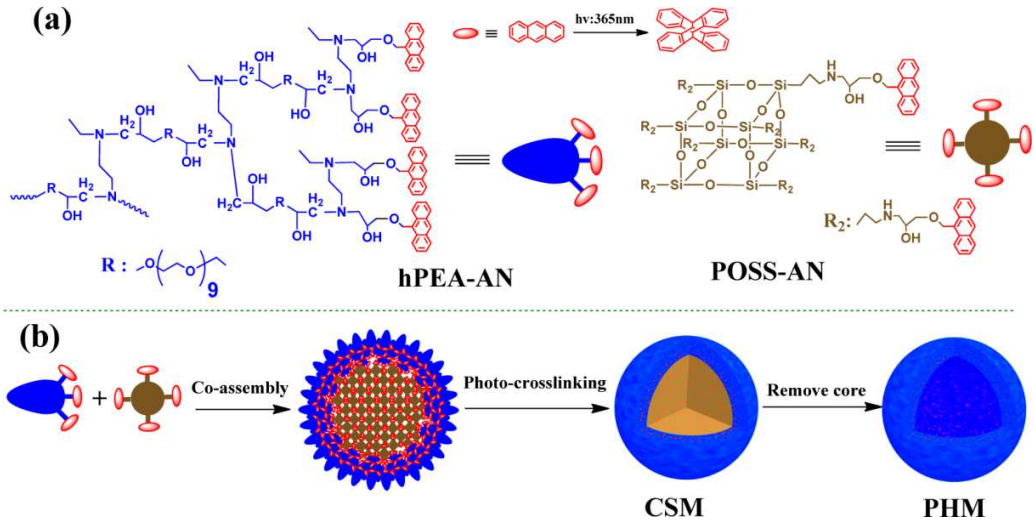

Figure II.55. Synthesis of core-shell particles and their corresponding hollow microspheres.[185]

Very recently, Truong *et al.* used electron-rich 9-substituted anthracenes to cross-link hydrogels suitable for cell encapsulation without requiring an additional cross-linker or catalyst.[186] The bathochromic shift in the absorption spectrum due to the electron-rich 9-substituent allowed cure using visible light (400-500 nm) instead of the more harmful UVA light.

4.3.2.3 Patterning

The light-driven dimerization of anthracene has been used for the photopatterning of polymeric films. In a recent report by Radl *et al.*, anthracene-bearing polynorbornene films were patterned using structured illumination (300 - 450 nm) followed by a development step that dissolves and thus removes the unexposed, uncrosslinked material.[187] This results in a negative-toned pattern, which can be de-crosslinked (and removed) by heating for 90 minutes at 150 °C.

In a follow-up paper, Schlögl and coworkers combined the light-driven dimerization and scission using wavelengths above 300 nm and near 254 nm, respectively.[188] Spin-coated films of linear hydrogenated carboxylated nitrile butadiene rubber having anthryl side groups were patterned by photodimerization a first time. Before development of the negative-toned pattern, the surface underwent a second patterning step, de-crosslinking this time the exposed material, as shown in Figure II.56. Although a de-crosslinking conversion of only about 24 % could be accomplished, the cure/de-cure sequence did allow for the formation of more specialized patterns.

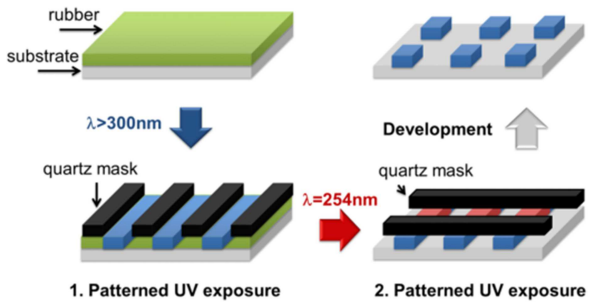

Figure II.56. Patterning by a writing and an erasing step using UV-light.[188]

While the limited penetration depth of short UV irradiation may be hampered when using relatively thick films, this is not an issue for ultrathin samples. Miyashita and coworkers photopatterned such Langmuir-Blodgett (LB) films, having thicknesses down to 22 nm.[189] Irradiation of the poly(N-neopentyl methacrylamide-co-anthrylmethyl methacrylate) films with 254 nm UV light led to decomposition of the chain, leading to positive-toned patterns. Alternatively, irradiation with 365 nm UV light led to crosslinking and negative-toned patterns. The denser packing and high orientation in the LB films led to superior photodimerization and resolution, compared to spin-coated samples. Similar LB films of polymers having swallow-tailed "double" anthracene groups as side chains were studied a decade later.[190] Irradiation using 248 nm light led to negative-toned patterns by photodimerization when shortly irradiated, or positive-toned patterns by decomposition when irradiated longer. Irradiation with less energetic 365 nm UV light only resulted in negative-toned patterns by dimerization.

When starting from structured films, three-dimensional patterned films are achievable as demonstrated by Connal *et al.*.[191] Core-crosslinked star polymer with terminal anthryl groups were deposited in honey-comb structures. Again, combination of photo-crosslinking using long UV and de-crosslinking using short UV allowed writing, erasing and rewriting of the (fluorescent) pattern (Figure II.57).

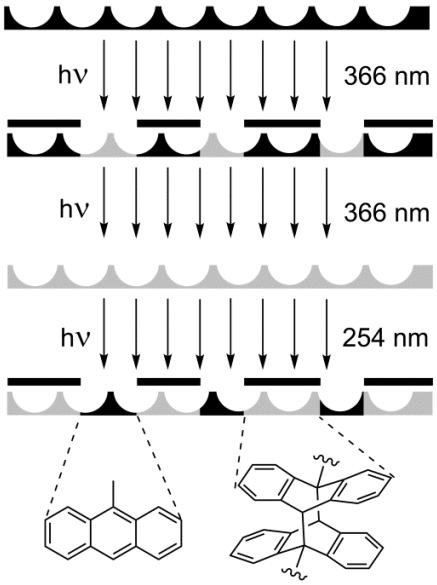

Figure II.57. Photolithography of honeycomb films having fluorescent anthracene groups (first (up): initial honeycomb film; second: patterning with a mask; third: erasing the pattern by removing of the mask; fourth: rewriting on the film).[191]

Photopatterning and nanoparticle adsorption was achieved in a single step by Smith and Watson.[192] For this, they made use of gold nanoparticles and ZrO_2 surfaces, which were both decorated with adsorbed anthracene moieties (9-anthracenethiolate-capped gold nanoparticles and 2-anthroate-functionalized ZrO_2 surfaces). Photoirradiation using 355 nm UV light and a photomask led to nanoparticle adsorption to the surface in controlled patterns.

The fluorescent properties of anthracene have been used to make fluorescent patterns, as demonstrated by Rameshbabu *et al.*.[193] These "dry" photopatterned films do not require any development step to remove material. The polymer was made by polymerization of anthracene with chloromethyl methyl ether *via* a Friedel-Crafts alkylation reaction. This conjugated-non-conjugated spacer-type polymer has a fluorescence quantum yield of 0.8, which is quenched by photodimerization. Photodimerization induces crosslinking and thus leads to a 5 % volume reduction, explaining why the patterns also had moderate height differences of 8 to 14 nm between irradiated and non-irradiated areas (Figure II.58).

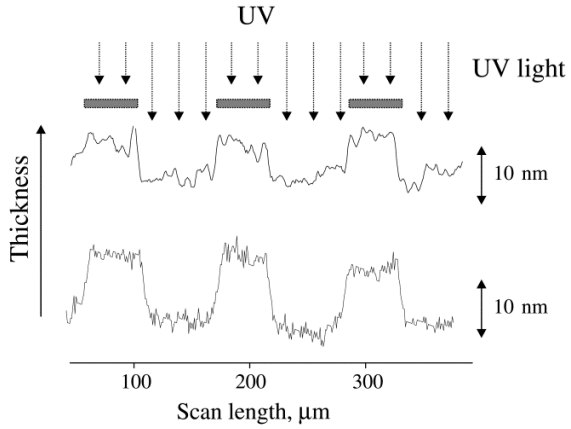

Figure II.58. Depth profile acquired by localized shrinking of a 151 nm film after 30 minutes of irradiation (upper curve) and a 101 nm film after irradiated for 1 hour (lower curve).[193]

Schopov and coworkers used a difference in dopability by disappearance of anthracene groups to create conductive patterns.[194] Segmented polymers having anthracenes in the main chain are dopable with iodine, making them dark and conductive. UVA light irradiation in air led to disappearance of the anthracene groups in favor of benzene-type products. The exact nature of produced compounds was not determined, but presumably mainly endoperoxides and other photo-oxidation products are acquired in combination with some anthracene dimers. This irradiation leads to a local, irreversible loss of dopability, allowing the drawing of patterns as shown in Figure II.59.

Figure II.59. Doped patterned anthracene-containing film.[194]

4.3.2.4 Healing and mechanophoric crack detection

The reversible photodimerization of anthracene has also been validated as a mechanism for the healing of anthracene-containing materials. For example, healable hydrogels of anthryl-capped dendritic PEG macromonomers were made by Froimowicz *et al.*.[195] Photocure conversion was up to 62 % in 10 w% water solution and limited to 35 % in bulk. Scratches were healed by de-crosslinking the hydrogel using short UV, allowing flow to close the material's gap, followed by re-crosslinking to regain mechanical

properties similar to those of the virgin material (Figure II.60). Only a little diminution in the photoreversibility was found after 5 healing cycles.

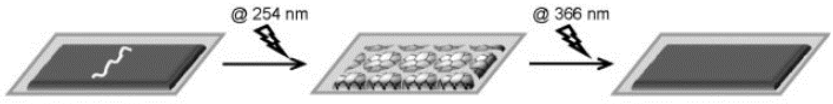

Figure II.60. Healing of a scratch in a hydrogel by de-crosslinking, followed by re-crosslinking.[195]

Anthracene dimers have also been successfully used as damage sensors in polymer networks by Song *et al.*.[196] Mechanical force, applied by grinding the polymer for example, stimulated the reversion of dianthracene crosslinks to free anthracene moieties. This de-crosslinking increased the sol fraction and also the fluorescence, allowing for the detection of the damages. Similarly, mechanically induced cracks in coatings could be visualized by fluorescence microscopy.

The mechanical formation of detectable anthracene groups from dianthracene crosslinks can then be used to heal the damaged material, as recently demonstrated by Schlögl and coworkers.[197] Epoxy prepolymers having pendent anthracene groups were crosslinked to high T_g networks by photodimerization. After damage, healing by dimerization of the mechanically formed free anthracenes occurred above T_g (at 60 °C) which ensured viscoelastic flow. Higher anthracene concentrations in the polymer led to better healing, with force at break recovery up to 100 %. Very recently, Fang *et al.* healed cracks in rubbery anthracene-based polyurethanes by annealing the material for 40 minutes at 130 °C, followed by irradiation at room temperature (Figure II.61).[198] The annealing step caused crack closure by visco-elastic flow and additional dimer scission at the healing zone. Higher healing efficiencies were found for networks having lower T_g's.

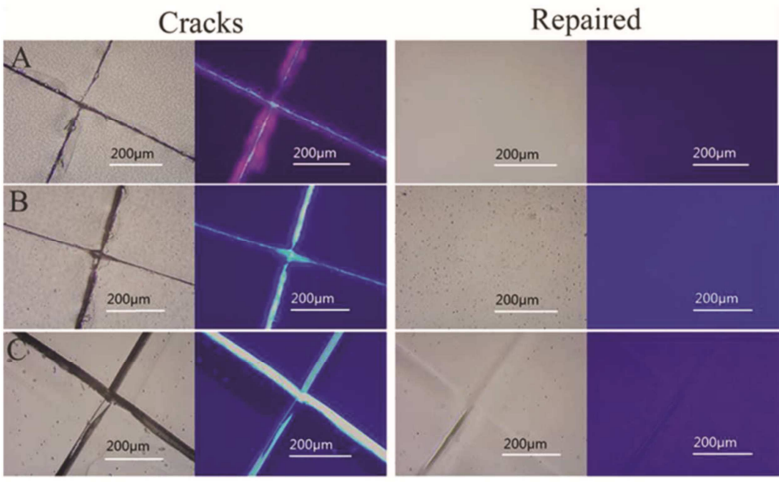

Figure II.61. Micrographs under white light and UV-light of cracked and repaired anthracene-based polyurethane networks. The polymers used for the films B and C have 4 and 8 times more anthracene side groups than the polymer for A.[198]

4.3.2.5 Nanoparticle aggregation

Crosslinking by anthracene dimerization has been used to induce nanoparticle aggregation, as demonstrated by Smith and Watson.[192] Gold nanoparticles with adsorbed 9-anthracene moieties were suspended and exposed to UVA light, leading to aggregates with diameters up to several micrometers. Jiang and coworkers recently used the reversible anthracene dimerization to controllably switch between insoluble aggregated and soluble solitary particles.[199] Soluble gold nanoparticles decorated with pillar[5]arenes were mixed with polymers having anthryl and quaternary ammonium salts end groups, leading to complexation between the salts and pillar[5]arenes and thus anthracene-decorated nanoparticles (Figure II.62). Irradiation in solution resulted in aggregation and possible precipitation of the particles. Disassembly occurred either temporarily under mild and short heating by reducing the binding constants of the complexes, or permanently through dimer scission by heating at 60 °C for 20 hours or by irradiation with UVC light. Reformation of the aggregates could be achieved by irradiation with UVA, and the entire formation /dissociation cycle could be repeated up to 10 times.

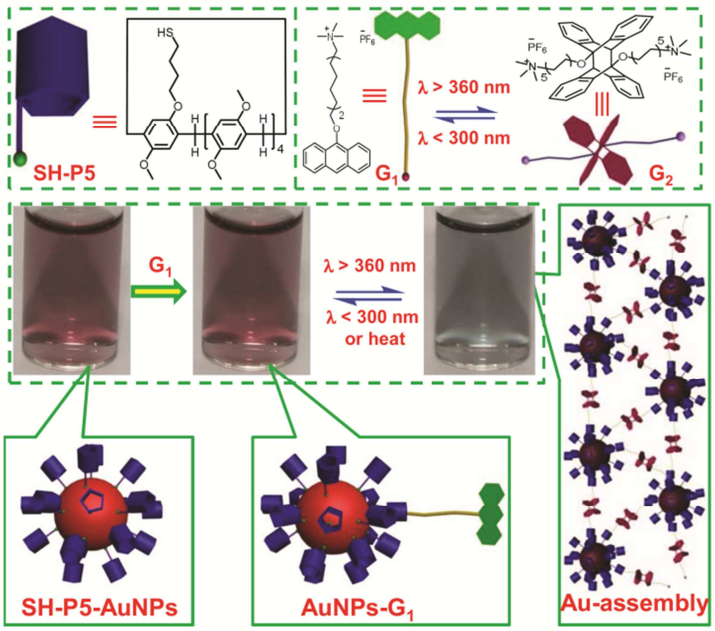

Figure II.62. Synthesis of reversibly assembled gold nanoparticles based on host-guest interactions and anthracene dimerization.[199]

4.3.2.6 Tunable changes in refractive index

Mack and Eisenbach used the photodimerization of segmented anthracene-containing polyurethanes to induce refractive index changes in a material when desired.[200] The photoreactive moieties were incorporated directly in the main chain of the polyurethane, in the crystalline hard segments. The photocure occurred faster and to a higher extent for hexamethylene diisocyanate (HDI)-based polymers, compared to 4,4'-diphenymethylene diisocyanate (MDI)-based ones, presumably because of a different hard segment packing. Refractive index changes up to 0.0041 were obtained. However, these networks did not photocleave upon exposure to UVC light. Kudo *et al.*.[201] acquired large changes in refractive index up to 0.116 by photodimerization of pendent anthryl groups in poly(silsesquioxane)s. The use of anthryl side groups resulted in significantly higher refractive index changes compared to norbornadiene (≤ 0.073) or azobenzene (≤ 0.009) groups.

4.3.2.7 (De)crosslinking for other applications

While the reversible crosslinking by anthracene dimerization has been used multiple times for the previously described applications, it has also occasionally been used for other (more exotic) applications. Jones *et al.* incorporated 2,6-anthracenedicarboxylate units in the main chain of

poly(ethylene terephthalate) (PET) polyesters.[202] While these PET-like material could be crosslinked by UVA light irradiation, no de-crosslinking occurred under UVC irradiation. Recently, López-Vilanova *et al.* used anthracenes to achieve solid state crosslinkable polyethylenes.[203] Poly(ethylene-butyl acrylate) was transesterified with 9-anthracene methanol by reactive extrusion and cured under UVA light. UVC irradiation regenerated up to 42 % of parent anthracenes.

Chujo *et al.* used the photodimerization of pending anthracene groups to photo-crosslink linear water-soluble polyoxazolines to multiresponsive hydrogels.[204] Disulfide bonds between the anthracene groups and the main chains allowed the reductive de-crosslinking of the formed hydrogels using sodium borohydride.

Very recently, Wang and coworkers used solid state crosslinking by anthracene photodimerization to form triple-shape memory materials.[205] This strategy allows the preshaping of the material into complex architectures before cure. The melting point of a poly(tetramethylene oxide) phase at 25 °C and the T_g of a poly(D,L-lactide) blocks at 70 °C were used as shape memory switching temperatures. In another recent shape memory material, the anthracene dimerization was used for shape fixing and the photochemical reversion for shape recovery at room temperature (Figure II.63).[206] The anthryl groups were attached to flexible, amorphous poly(ethylene glycol) soft segments to ensure a good mobility which is required for high photodimerization/scission conversions. Rigid poly(L-lactide) hard segments were used to physically crosslink and stabilize the shape memory material, which had decent shape fixity and recovery values of around 60 % and 80 %, respectively.

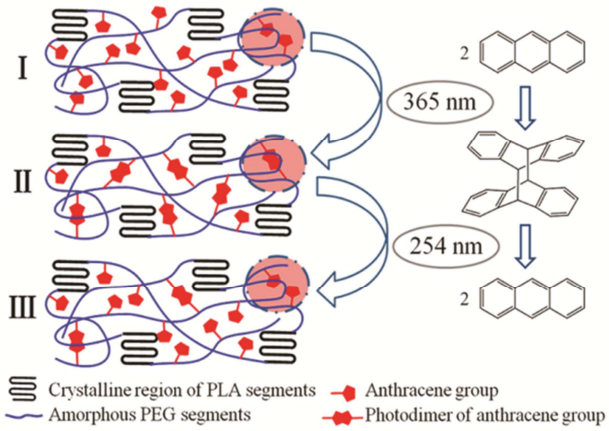

Figure II.63. Scheme of the shape memory mechanism based on the photoreversible dimerization of anthracene groups at room temperature.[206]

Mengel and coworkers made anthracene-capped star polymers as precursors for polyelectrolyte networks.[207] The star architecture was obtained by anionic polymerization using 1-(2-anthryl)-1-phenylhexyllithium as initiator, followed by termination with a trifunctional or octafunctional terminating agent. In the latter case, steric hindrance resulted in 5-armed stars. Salt addition to an aqueous solution induced aggregation and enhanced photoreactivity.

Very recently, Yu *et al.* used the anthracene dimerization to covalently link 2-dimensionally self-assembled DNA networks.[208] First, DNA-triarm precursors having singular anthracene moieties in the centre of each arm were allowed to self-assemble in water into monolayer sheets. After photocuring these sheets, solvent replacement did not redissolve the responsive sheets, but instead led to thick pads due to conformational rearrangements.

5 Conclusion

Anthracene-containing polymers have been studied for a very wide range of applications and are expected to become increasingly important. While they have been intensively studied in the past for plastic scintillators with good performance, no breakthrough developments on anthracene-containing polymers are expected anymore in the context of this field. Indeed, anthracene remains a performant fluorescent moiety and the possibility to tune this reporter molecule is definitely an added value. It should however be noted that many other fluorescent groups exist, which are equally suitable in many applications. The same reasoning holds for the contribution of anthracene groups in the field of conductive polymers: while they provide good properties, they are not unique and therefore replaceable by many other groups without drastic changes on the performance.

Therefore, it is our strong belief that the largest added value of the anthracene moiety in polymer science is as a reactive moiety. It reacts very efficiently and often reversibly with singlet oxygen, which for some applications is considered a nuisance. This reaction can often be prevented or limited by eliminating oxygen, decreasing the reactivity towards oxygen or increasing the dimerization rate. Alternatively, this reaction has also successfully been used for several applications, such as (dry) photopatterning. More often, anthracenes are used for their highly efficient coupling reaction with maleimides and other dienophiles. These Diels-Alder reactions allow for the easy synthesis of very complex structures, but also the reversible modification of (conjugated) polymers. The mechanically

driven retro-Diels-Alder reaction is also expected to be a reoccurring theme for future research, hopefully also picked up by industry in the area of self-healing and dynamic materials. The mild, photostimulated dimerization is the most unique property of anthracene and anthracene-containing polymers. The reversible nature of the dimerization, in combination with the tunability thereof, makes anthracene groups especially interesting in the context of stimuli-responsive, smart materials. Not only can the scission of the anthracene groups be photochemically driven, but also in a thermal and mechanical fashion. These promising tunable reactions will undoubtedly lead to many more upcoming publications, patents and industrial valorisation.

6 References

1. Schleyer, P. v. R.; Manoharan, M.; Jiao, H.; Stahl, F., *Org. Lett.* **2001,** *3* (23), 3643-3646.
2. (a) Senseman, C. E.; Nelson, O. A., *Ind Eng Chem* **1923,** *15* (5), 521-524; (b) Noboru, K.; Nobuyoshi, O.; Yoshitaka, O. Anthraquinone dyestuffs. 1975.
3. (a) Macha, S. F.; Limbach, P. A.; Hanton, S. D.; Owens, K. G., *J. Am. Soc. Mass. Spectrom.* **2001,** *12* (6), 732-743; (b) Streletskiy, A. V.; Goldt, I. V.; Kuvychko, I. V.; Ioffe, I. N.; Sidorov, L. N.; Drewello, T.; Strauss, S. H.; Boltalina, O. V., *Rapid Commun. Mass Spectrom.* **2004,** *18* (3), 360-362.
4. (a) Wright, G. T., *Proc Phys Soc Sect B* **1955,** *68* (11), 929-37; (b) Dijkstra, P.; Wörtche, H. J. Scintillator compositions. 2014.
5. (a) Conley, S. R.; Vreeland, W. B.; Cosimbescu, L. Electroluminescent device with anthracene derivative host. 2005; (b) Kawamura, M.; Ito, M. Anthracene derivatives, luminescent materials and organic electroluminescent devices. 2014.
6. (a) Ansyln, E. V.; Wallace, K. J. Compositions and methods for the detection of chemical warfare agents. 2008; (b) Qian, Y.; Wang, B.; Cui, Y.; Lv, C.; Zhou, Z. Oxadiazole-triphenylamine-anthracene conjugated molecule with three-photon fluorescence characteristic. 2014.
7. (a) Bouas-Laurent, H.; Desvergne, J. P.; Castellan, A.; Lapouyade, R., *Chem. Soc. Rev.* **2000,** *29* (1), 43-55; (b) Bouas-Laurent, H.; Castellan, A.; Desvergne, J. P.; Lapouyade, R., *Chem. Soc. Rev.* **2001,** *30* (4), 248-263; (c) Becker, H. D., *Chem. Rev.* **1993,** *93* (1), 145-172.
8. Dumas, M. J., *Ann. Chim. Phys.* **1832,** *1*, 182-197.
9. Jones, R. N., *Chem. Rev.* **1947,** *41* (2), 353-371.
10. Abou-Hatab, S.; Spata, V. A.; Matsika, S., *J. Phys. Chem. A* **2017,** *121* (6), 1213-1222.
11. Sambursky, S.; Wolfsohn, G., *Trans. Faraday Soc.* **1940,** *35*, 427-432.
12. Bell, P. R., *Phys. Rev.* **1948,** *73* (11), 1405-1406.
13. Szemenyei, B.; Móczár, I.; Pál, D.; Kocsis, I.; Baranyai, P.; Huszthy, P., *Chirality* **2016,** *28* (7), 562-568.
14. (a) Ma, Y.; Chen, H.; Wang, F.; Kambam, S.; Wang, Y.; Mao, C.; Chen, X., *Dyes Pigm.* **2014,** *102*, 301-307; (b) Nguyen, T. V. T.; Seo, Y. J., *Tetrahedron Lett.* **2017,** *58* (10), 941-944; (c) Lee, H. G.; Kim, K. B.; Park, G. J.; Na, Y. J.; Jo, H. Y.; Lee, S. A.; Kim, C., *Inorg. Chem. Commun.* **2014,** *39*, 61-65.
15. Banerjee, A.; Sahana, A.; Lohar, S.; Sarkar, B.; Mukhopadhyay, S. K.; Das, D., *RSC Adv.* **2013,** *3* (34), 14397-14405.

16. Jaividhya, P.; Ganeshpandian, M.; Dhivya, R.; Akbarsha, M. A.; Palaniandavar, M., *Dalton Trans.* **2015,** *44* (26), 11997-12010.
17. (a) Song, J. Y.; Park, S. N.; Lee, S. J.; Kim, Y. K.; Yoon, S. S., *Dyes Pigm.* **2015,** *114*, 40-46; (b) Chen, M.; Zhao, Y.; Yan, L.; Yang, S.; Zhu, Y.; Murtaza, I.; He, G.; Meng, H.; Huang, W., *Angew. Chem. Int. Ed.* **2017,** *56* (3), 722-727.
18. (a) Dadvand, A.; Sun, W. H.; Moiseev, A. G.; Belanger-Gariepy, F.; Rosei, F.; Meng, H.; Perepichka, D. F., *J. Mater. Chem. C* **2013,** *1* (16), 2817-2825; (b) Jiang, L.; Hu, W.; Wei, Z.; Xu, W.; Meng, H., *Adv. Mater.* **2009,** *21* (36), 3649-3653; (c) Zhao, Y.; Yan, L.; Murtaza, I.; Liang, X.; Meng, H.; Huang, W., *Org. Electron.* **2017,** *43*, 105-111.
19. Hisamatsu, S.; Masu, H.; Takahashi, M.; Kishikawa, K.; Kohmoto, S., *Cryst. Growth Des.* **2015,** *15* (5), 2291-2302.
20. Fritzsche, J., *J. Prakt. Chem.* **1867,** *101* (1), 333-343.
21. Ehrenberg, M., *Acta Crystallogr* **1965,** *19*, 698-+.
22. Breton, G. W.; Vang, X., *J. Chem. Educ.* **1998,** *75* (1), 81.
23. Woodward, R. B.; Hoffmann, R., *Angewandte Chemie International Edition in English* **1969,** *8* (11), 781-853.
24. (a) Birks, J., *Rep. Prog. Phys.* **1975,** *38* (8), 903; (b) Lowry, T. H.; Richardson, K. S., *Mechanism and theory in organic chemistry*. Harper & Row New York: 1987.
25. Burnelle, L.; Lahiri, J.; Detrano, R., *Tetrahedron* **1968,** *24* (9), 3517-3531.
26. Bowen, E. J.; Rohatgi, K. K., *Discussions of the Faraday Society* **1953,** *14* (0), 146-150.
27. Chandross, E. A., *J. Chem. Phys.* **1965,** *43* (11), 4175-4176.
28. Koo, B.; Nofen, E.; Chattopadhyay, A.; Dai, L., *Comput. Mater. Sci.* **2017,** *133*, 167-174.
29. Atherton, J. C. C.; Jones, S., *Tetrahedron* **2003,** *59* (46), 9039-9057.
30. Aubry, J. M.; Pierlot, C.; Rigaudy, J.; Schmidt, R., *Acc. Chem. Res.* **2003,** *36* (9), 668-675.
31. Kolemen, S.; Ozdemir, T.; Lee, D.; Kim, G. M.; Karatas, T.; Yoon, J.; Akkaya, E. U., *Angew. Chem. Int. Ed.* **2016,** *55* (11), 3606-3610.
32. Baumes, J. M.; Gassensmith, J. J.; Giblin, J.; Lee, J. J.; White, A. G.; Culligan, W. J.; Leevy, W. M.; Kuno, M.; Smith, B. D., *Nat. Chem.* **2010,** *2* (12), 1025-1030.
33. Zehm, D.; Fudickar, W.; Linker, T., *Angew. Chem. Int. Ed.* **2007,** *46* (40), 7689-7692.
34. Magat, M.; Boneme, R., *CR hebd séances Acad Sci* **1951,** *232* (18), 1657-1659.
35. Krenz, F. H., *Trans. Faraday Soc.* **1955,** *51* (2), 172-183.
36. Marvel, C. S.; Wilson, B. D., *J. Org. Chem.* **1958,** *23* (10), 1479-1482.
37. Cherkasov, A. S.; Voldaikina, K. G., *Polym Sci USSR* **1963,** *4* (4), 688-697.
38. Andersen, V. S.; Norrish, R. G. W., *Proc. R. Soc. London, Ser. A* **1959,** *251* (1264), 1-3.
39. Norrish, R. G. W.; Simons, J. P., *Proc. R. Soc. London, Ser. A* **1959,** *251* (1264), 4-26.
40. Lissi, E. A.; Yupanqui, K., *Eur. Polym. J.* **1990,** *26* (6), 707-710.
41. Ikezaki, K., *Jpn. J. Appl. Phys.* **1970,** *9* (8), 936-945.
42. Marvel, C. S.; Anderson, W. S., *J. Am. Chem. Soc.* **1953,** *75* (18), 4600-4601.
43. Marvel, C. S.; Johnson, J. W., *J. Polym. Sci.* **1956,** *21* (98), 251-255.
44. Montaudo, G.; Finocchiaro, P.; Caccamese, S., *J Polym Sci Part A Polym Chem* **1971,** *9* (12), 3627-3637.
45. Bergmann, E. D.; Katz, D., *J. Chem. Soc.* **1958,** (Sep), 3216-3217.
46. Stolka, M.; Yanus, J. F.; Pearson, J. M., *Macromolecules* **1976,** *9* (5), 715-719.
47. Michel, R. H., *J Polym Sci Part A Polym Chem* **1964,** *2* (6), 2533-2545.
48. Bunel, C.; Cohen, S.; Laguerre, J. P.; Marechal, E., *Polym. J.* **1975,** *7* (3), 320-325.

49. Coudane, J.; Brigodiot, M.; Marechal, E., *J. Macromol. Sci.-Chem.* **1979,** *A13* (6), 827-834.
50. Katz, D., *J Polym Sci Part A Polym Chem* **1963,** *1* (5), 1635-1643.
51. Katz, D.; Relis, J., *J Polym Sci Part A Polym Chem* **1968,** *6* (8), 2079-2083.
52. Stolka, M.; Yanus, J. F.; Pearson, J. M., *Macromolecules* **1976,** *9* (5), 710-714.
53. Cherkasov, A. S.; Voldaikina, K. G., *Polym Sci USSR* **1965,** *7* (1), 191-196.
54. Mukoh, A.; Morishita, H., *J Polym Sci Part C Polym Lett Ed* **1980,** *18* (1), 35-43.
55. Krakovyak, M. G.; Anufrieva, Y. V.; Skorokho, S. S., *Polym Sci USSR* **1972,** *14* (5), 1259-1264.
56. Simionescu, C. I.; Grigoras, M.; Barboiu, V., *J Polym Sci Part A Polym Chem* **1985,** *23* (8), 2089-2098.
57. Dumitrescu, S.; Grigoras, M.; Simionescu, C. I., *Makromol Chem* **1983,** *184* (10), 2033-2040.
58. (a) Ohno, K.; Fujimoto, K.; Tsujii, Y.; Fukuda, T., *Polymer* **1999,** *40* (3), 759-763; (b) Viovy, J. L.; Monnerie, L.; Brochon, J. C., *Macromolecules* **1983,** *16* (12), 1845-1852; (c) North, A. M.; Soutar, I., *J. Chem. Soc., Faraday Trans. 1* **1972,** *68*, 1101-1116; (d) Valeur, B.; Monnerie, L., *J Polym Sci Part B Polym Phys* **1976,** *14* (1), 11-27.
59. Wahl, P.; Meyer, G.; Parrod, J.; Auchet, J. C., *Eur. Polym. J.* **1970,** *6* (4), 585-608.
60. (a) Veissier, V.; Viovy, J. L.; Monnerie, L., *Polymer* **1989,** *30* (7), 1262-1268; (b) Ono, K.; Ueda, K.; Yamamoto, M., *Polym. J.* **1994,** *26* (12), 1345-1351; (c) Aoki, H.; Horinaka, J. I.; Ito, S.; Yamamoto, M.; Katayama, H.; Kamigaito, M.; Sawamoto, M., *Polym. J.* **2001,** *33* (6), 464-468.
61. Kim, C. S.; Oh, S. M.; Kim, S.; Cho, C. G., *Macromol. Rapid Commun.* **1998,** *19* (4), 191-196.
62. (a) Adolf, D. B.; Ediger, M. D.; Kitano, T.; Ito, K., *Macromolecules* **1992,** *25* (2), 867-872; (b) Punchard, B. J.; Adolf, D. B., *Macromolecules* **2002,** *35* (8), 3281-3287.
63. (a) Adams, S.; Adolf, D. B., *Macromolecules* **1998,** *31* (17), 5794-5799; (b) Punchard, B. J.; Kirpatch, A.; Adolf, D. B., *Polymer* **2002,** *43* (23), 6287-6293.
64. Liu, R.; Winnik, M. A.; Di Stefano, F.; Vanketessan, J., *J Polym Sci Part A Polym Chem* **2001,** *39* (9), 1495-1504.
65. Tomba, J. P.; Portinha, D.; Schroeder, W. F.; Winnik, M. A.; Lau, W., *Colloid. Polym. Sci.* **2009,** *287* (3), 367-378.
66. Torii, T.; Yamashita, T.; Ushiki, H.; Horie, K., *Eur. Polym. J.* **1993,** *29* (4), 465-467.
67. de Deus, J. F.; Souza, G. P.; Corradini, W. A.; Atvars, T. D. Z.; Akcelrud, L., *Macromolecules* **2004,** *37* (18), 6938-6944.
68. Swift, T.; Paul, N.; Swanson, L.; Katsikogianni, M.; Rimmer, S., *Polymer* **2017,** *123* (Supplement C), 10-20.
69. Petropoulou, A.; Christodoulou, K.; Polydorou, C.; Krasia-Christoforou, T.; Riziotis, C., *Macromol. Mater. Eng.* **2017,** *302* (8), 1600453 |1-7.
70. Sandanaraj, B. S.; Demont, R.; Aathimanikandan, S. V.; Savariar, E. N.; Thayumanavan, S., *J. Am. Chem. Soc.* **2006,** *128* (33), 10686-10687.
71. Shiraishi, Y.; Miyamoto, R.; Hirai, T., *Tetrahedron Lett.* **2007,** *48* (38), 6660-6664.
72. Robinson, K. L.; Lawrence, N. S., *Anal. Chem.* **2006,** *78* (7), 2450-2455.
73. Lawrence, N. S.; Robinson, K. L., *Talanta* **2007,** *74* (3), 365-369.
74. Yu, B.; Zhao, Y., *Polym. Chem.* **2017,** *8* (28), 4132-4139.
75. Holden, D. A.; Guillet, J. E., *Macromolecules* **1980,** *13* (2), 289-295.
76. Hargreaves, J. S.; Webber, S. E., *Macromolecules* **1984,** *17* (2), 235-240.
77. Tillman, E. S.; Hogen-Esch, T. E., *Macromolecules* **2001,** *34* (19), 6616-6622.
78. Morisaki, Y.; Nakano, T.; Chujo, Y., *J Polym Sci Part A Polym Chem* **2014,** *52* (19), 2815-2821.
79. Li, W.; Fox, M. A., *J. Phys. Chem. B* **1997,** *101* (51), 11068–11076.

80. Bolto, B. A.; Weiss, D. E.; Willis, D.; Bolto, B. A.; Weiss, D. E.; Willis, D., *Aust. J. Chem.* **1965,** *18* (18), 487-491.
81. Al-Jumah, K.; Fernandez, J. E., *Macromolecules* **1987,** *20* (6), 1181-1183.
82. Satoh, M.; Uesugi, F.; Tabata, M.; Kaneto, K.; Yoshino, K., *J. Chem. Soc., Chem. Commun.* **1986,** *0* (12), 979-980.
83. Fan, B.; Qu, L.; Shi, G., *J. Electroanal. Chem.* **2005,** *575* (2), 287-292.
84. Morimoto, K.; Ishida, E.; Inami, A., *J Polym Sci Part A Polym Chem* **1967,** *5* (7), 1699-1704.
85. Ma, D.; Aguiar, M.; Freire, J. A.; Hümmelgen, I. A., *Adv. Mater.* **2000,** *12* (14), 1063-1066.
86. Almeataq, M. S.; Yi, H.; Al-Faifi, S.; Alghamdi, A. A. B.; Iraqi, A.; Scarratt, N. W.; Wang, T.; Lidzey, D. G., *Chem. Commun.* **2013,** *49* (22), 2252-2254.
87. Jung, J. W.; Liu, F.; Russell, T. P.; Jo, W. H., *Adv. Energy Mater.* **2015,** *5* (11), 1500065 |1-6.
88. Grisorio, R.; Suranna, G. P.; Mastrorilli, P.; Allegretta, G.; Loiudice, A.; Rizzo, A.; Gigli, G.; Manoli, K.; Magliulo, M.; Torsi, L., *J Polym Sci Part A Polym Chem* **2013,** *51* (22), 4860-4872.
89. Marsitzky, D.; Scott, J. C.; Chen, J. P.; Lee, V. Y.; Miller, R. D.; Setayesh, S.; Müllen, K., *Adv. Mater.* **2001,** *13* (14), 1096-1099.
90. Beaujuge, P. M.; Reynolds, J. R., *Chem. Rev.* **2010,** *110* (1), 268-320.
91. Tao, Y. J.; Zhang, Z. Y.; Xu, X. Q.; Zhou, Y. J.; Cheng, H. F.; Zheng, W. W., *Electrochim. Acta* **2012,** *77*, 157-162.
92. Yildirim, A.; Tarkuc, S.; Ak, M.; Toppare, L., *Electrochim. Acta* **2008,** *53* (14), 4875-4882.
93. Tao, Y.; Zhang, K.; Zhang, Z.; Cheng, H.; Jiao, C.; Zhao, Y., *Chem. Eng. J.* **2016,** *293*, 34-43.
94. Ishii, T.; Tezuka, Y.; Kawamoto, S.; Uno, T., *J. Photochem. Photobiol., A* **1994,** *83* (1), 55-62.
95. Ishow, E.; Bouffard, J.; Kim, Y.; Swager, T. M., *Macromolecules* **2006,** *39* (23), 7854-7858.
96. Zhang, D.; Pan, L.; Li, Y.; Wang, B.; Li, Y., *Macromolecules* **2017,** *50* (6), 2276-2283.
97. Hodge, P.; Power, G. A.; Rabjohns, M. A., *Chem. Commun.* **1997,** (1), 73-74.
98. Liu, C.; Xu, W.; Guan, X.; Yip, H. L.; Gong, X.; Huang, F.; Cao, Y., *Macromolecules* **2014,** *47* (24), 8585-8593.
99. Gossweiler, G. R.; Hewage, G. B.; Soriano, G.; Wang, Q.; Welshofer, G. W.; Zhao, X.; Craig, S. L., *ACS Macro Lett.* **2014,** *3* (3), 216-219.
100. Biedermann, F.; Ross, I.; Scherman, O. A., *Polym. Chem.* **2014,** *5* (18), 5375-5382.
101. Taylor, M. S.; Swager, T. M., *Angew. Chem. Int. Ed.* **2007,** *46* (44), 8480-8483.
102. Fudickar, W.; Linker, T., *Langmuir* **2010,** *26* (6), 4421-4428.
103. Altinok, E.; Frausto, F.; Thomas, S. W., *J Polym Sci Part A Polym Chem* **2016,** *54* (16), 2526-2535.
104. Modi, P. J.; Guillet, J. E., *J Polym Sci Part A Polym Chem* **1995,** *33* (2), 197-201.
105. Nie, B.; Rotello, V. M., *Macromolecules* **1997,** *30* (13), 3949-3951.
106. Dang, J. S.; Wang, W. W.; Zhao, X.; Nagase, S., *Org. Lett.* **2014,** *16* (1), 170-173.
107. Grigoras, M.; Sava, M.; Colotin, G.; Simionescu, C. I., *J. Appl. Polym. Sci.* **2008,** *107* (2), 846-853.
108. Kriegel, R. M.; Saliba, K. L.; Jones, G.; Schiraldi, D. A.; Collard, D. M., *Macromol. Chem. Phys.* **2005,** *206* (15), 1479-1487.
109. Baysak, E.; Durmaz, H.; Tunca, U.; Hizal, G., *Macromol. Chem. Phys.* **2017,** *218* (18), 1600572 |1-8.
110. Ozguc Onal, C.; Nugay, T., *Des Monomers Polym* **2017,** *20* (1), 514-523.
111. Tazuke, S.; Tanabe, t., *Macromolecules* **1979,** *12* (5), 853-862.
112. Tazuke, S.; Tanabe, T., *Macromolecules* **1979,** *12* (5), 848–853.
113. Wei, P.; Yan, X.; Huang, F., *Chem. Commun.* **2014,** *50* (91), 14105-14108.
114. Okada, M.; Harada, A., *Macromolecules* **2003,** *36* (26), 9701-9703.

115. Okada, M.; Takashima, Y.; Harada, A., *Macromolecules* **2004,** *37* (19), 7075-7077.
116. Xu, J. F.; Chen, Y. Z.; Wu, L. Z.; Tung, C. H.; Yang, Q. Z., *Org. Lett.* **2013,** *15* (24), 6148-6151.
117. Kihara, H.; Motohashi, M.; Matsumura, K.; Yoshida, M., *Adv. Funct. Mater.* **2010,** *20* (10), 1561-1567.
118. (a) Tasdelen, M. A., *Polym. Chem.* **2011,** *2* (10), 2133-2145; (b) Hizal, G.; Tunca, U.; Sanyal, A., *J Polym Sci Part A Polym Chem* **2011,** *49* (19), 4103-4120.
119. (a) Durmaz, H.; Colakoglu, B.; Tunca, U.; Hizal, G., *J Polym Sci Part A Polym Chem* **2006,** *44* (5), 1667-1675; (b) Omurtag, P. S.; Gunay, U. S.; Dag, A.; Durmaz, H.; Hizal, G.; Tunca, U., *J Polym Sci Part A Polym Chem* **2013,** *51* (10), 2252-2259.
120. Dag, A.; Durmaz, H.; Hizal, G.; Tunca, U., *J Polym Sci Part A Polym Chem* **2008,** *46* (1), 302-313.
121. (a) Durmaz, H.; Dag, A.; Onen, C.; Gok, O.; Sanyal, A.; Hizal, G.; Tunca, U., *J Polym Sci Part A Polym Chem* **2010,** *48* (21), 4842-4846; (b) Dag, A.; Durmaz, H.; Tunca, U.; Hizal, G., *J Polym Sci Part A Polym Chem* **2009,** *47* (1), 178-187.
122. (a) Durmaz, H.; Karatas, F.; Tunca, U.; Hizal, G., *J Polym Sci Part A Polym Chem* **2006,** *44* (1), 499-509; (b) Altintas, O.; Hizal, G.; Tunca, U., *Des. Monomers Pol.* **2009,** *12* (1), 83-98.
123. Durmaz, H.; Karatas, F.; Tunca, U.; Hizal, G., *J Polym Sci Part A Polym Chem* **2006,** *44* (13), 3947-3957.
124. (a) Gacal, B.; Durmaz, H.; Tasdelen, M. A.; Hizal, G.; Tunca, U.; Yagci, Y.; Demirel, A. L., *Macromolecules* **2006,** *39* (16), 5330-5336; (b) Dag, A.; Aydin, M.; Durmaz, H.; Hizal, G.; Tunca, U., *J Polym Sci Part A Polym Chem* **2012,** *50* (21), 4476-4483.
125. Durmaz, H.; Dag, A.; Hizal, G.; Tunca, U., *J Polym Sci Part A Polym Chem* **2011,** *49* (5), 1195-1200.
126. Dag, A.; Durmaz, H.; Demir, E.; Hizal, G.; Tunca, U., *J Polym Sci Part A Polym Chem* **2008,** *46* (20), 6969-6977.
127. Durmaz, H.; Dag, A.; Altintas, O.; Erdogan, T.; Hizal, G.; Tunca, U., *Macromolecules* **2007,** *40* (2), 191-198.
128. Durmaz, H.; Dag, A.; Hizal, A.; Hizal, G.; Tunca, U., *J Polym Sci Part A Polym Chem* **2008,** *46* (21), 7091-7100.
129. Durmaz, H.; Dag, A.; Gursoy, D.; Demirel, A. L.; Hizal, G.; Tunca, U., *J Polym Sci Part A Polym Chem* **2010,** *48* (7), 1557-1564.
130. Dag, A.; Durmaz, H.; Kirmizi, V.; Hizal, G.; Tunca, U., *Polym. Chem.* **2010,** *1* (5), 621-623.
131. Durmaz, H.; Dag, A.; Hizal, G.; Tunca, U., *J Polym Sci Part A Polym Chem* **2010,** *48* (22), 5083-5091.
132. Dag, A.; Sahin, H.; Durmaz, H.; Hizal, G.; Tunca, U., *J Polym Sci Part A Polym Chem* **2011,** *49* (4), 886-892.
133. Durmaz, H.; Hizal, G.; Tunca, U., *J Polym Sci Part A Polym Chem* **2011,** *49* (9), 1962-1968.
134. Cakir, N.; Yavuzarslan, M.; Durmaz, H.; Hizal, G.; Tunca, U., *J Polym Sci Part A Polym Chem* **2013,** *51* (4), 899-907.
135. Gunay, U. S.; Durmaz, H.; Gungor, E.; Dag, A.; Hizal, G.; Tunca, U., *J Polym Sci Part A Polym Chem* **2012,** *50* (4), 729-735.
136. Dedeoglu, T.; Durmaz, H.; Hizal, G.; Tunca, U., *J Polym Sci Part A Polym Chem* **2012,** *50* (10), 1917-1925.
137. Candan, O. A.; Durmaz, H.; Hizal, G.; Tunca, U., *J Polym Sci Part A Polym Chem* **2012,** *50* (14), 2863-2870.
138. Candan, O. A.; Kopan, D.; Durmaz, H.; Hizal, G.; Tunca, U., *Eur. Polym. J.* **2013,** *49* (7), 1796-1802.
139. Tonga, M.; Cengiz, N.; Kose, M. M.; Dede, T.; Sanyal, A., *J Polym Sci Part A Polym Chem* **2010,** *48* (2), 410-416.

140. Gok, O.; Yigit, S.; Merve Kose, M.; Sanyal, R.; Sanyal, A., *J Polym Sci Part A Polym Chem* **2013,** *51* (15), 3191-3201.
141. Alkayal, N.; Hadjichristidis, N., *Polym. Chem.* **2015,** *6* (27), 4921-4926.
142. Masutani, K.; Lee, C. W.; Kimura, Y., *Polym. J.* **2012,** *45*, 427-435.
143. Iskin, B.; Yilmaz, G.; Yagci, Y., *Polym. Chem.* **2011,** *2* (12), 2865-2871.
144. Xiong, X. Q.; Xu, Y. H., *Polym. Bull.* **2010,** *65* (5), 455-463.
145. Syrett, J. A.; Mantovani, G.; Barton, W. R. S.; Price, D.; Haddleton, D. M., *Polym. Chem.* **2010,** *1* (1), 102-6.
146. Sun, H.; Kabb, C. P.; Dai, Y.; Hill, M. R.; Ghiviriga, I.; Bapat, A. P.; Sumerlin, B. S., *Nat Chem* **2017,** *9*, 817-823.
147. Konda, S. S. M.; Brantley, J. N.; Varghese, B. T.; Wiggins, K. M.; Bielawski, C. W.; Makarov, D. E., *J. Am. Chem. Soc.* **2013,** *135* (34), 12722-12729.
148. Church, D. C.; Peterson, G. I.; Boydston, A. J., *ACS Macro Lett.* **2014,** *3* (7), 648-651.
149. (a) Li, H.; Göstl, R.; Delgove, M.; Sweeck, J.; Zhang, Q.; Sijbesma, R. P.; Heuts, J. P. A., *ACS Macro Lett.* **2016,** *5* (9), 995-998; (b) Li, H.; Zhang, Y.; Liu, Y.; Sijbesma, R. P.; Heuts, J. P. A.; Zhang, Q., *Polym. Chem.* **2017,** *8* (27), 3971-3976.
150. (a) Li, J.; Shiraki, T.; Hu, B.; Wright, R. A. E.; Zhao, B.; Moore, J. S., *J. Am. Chem. Soc.* **2014,** *136* (45), 15925-15928; (b) Li, J.; Hu, B.; Yang, K.; Zhao, B.; Moore, J. S., *ACS Macro Lett.* **2016,** *5* (7), 819-822.
151. Göstl, R.; Sijbesma, R. P., *Chem Sci* **2016,** *7* (1), 370-375.
152. Bartz, T.; Klapper, M.; Müllen, K., *Macromol. Chem. Phys.* **1994,** *195* (3), 1097-1109.
153. Coursan, M.; Desvergne, J. P.; Deffieux, A., *Macromol. Chem. Phys.* **1996,** *197* (5), 1599-1608.
154. Ihara, T.; Fujii, T.; Mukae, M.; Kitamura, Y.; Jyo, A., *J. Am. Chem. Soc.* **2004,** *126* (29), 8880-8881.
155. Mukae, M.; Ihara, T.; Tabara, M.; Jyo, A., *Org. Biomol. Chem.* **2009,** *7* (7), 1349-1354.
156. Mukae, M.; Ihara, T.; Tabara, M.; Arslan, P.; Jyo, A., *Supramol. Chem.* **2009,** *21* (3-4), 292-295.
157. Wang, H.; Zhang, L.; Liu, B.; Han, B.; Duan, Z.; Qi, C.; Park, D. W.; Kim, I., *Macromol. Rapid Commun.* **2015,** *36* (18), 1646-1650.
158. Yamamoto, T.; Yagyu, S.; Tezuka, Y., *J. Am. Chem. Soc.* **2016,** *138* (11), 3904-3911.
159. Ji, Z.; Li, Y.; Ding, Y.; Chen, G.; Jiang, M., *Polym. Chem.* **2015,** *6* (38), 6880-6884.
160. Manchester, J.; Bassani, D. M.; Duprey, J. L. H. A.; Giordano, L.; Vyle, J. S.; Zhao, Z. Y.; Tucker, J. H. R., *J. Am. Chem. Soc.* **2012,** *134* (26), 10791-10794.
161. Goldbach, J. T.; Russell, T. P.; Penelle, J., *Macromolecules* **2002,** *35* (11), 4271-4276.
162. Goldbach, J. T.; Lavery, K. A.; Penelle, J.; Russell, T. P., *Macromolecules* **2004,** *37* (25), 9639-9645.
163. Huq, N. A.; Ekblad, J. R.; Leonard, A. T.; Scalfani, V. F.; Bailey, T. S., *Macromolecules* **2017,** *50* (4), 1331-1341.
164. Chen, W.; Wang, J. Y.; Zhao, W.; Li, L.; Wei, X.; Balazs, A. C.; Matyjaszewski, K.; Russell, T. P., *J. Am. Chem. Soc.* **2011,** *133* (43), 17217-17224.
165. Yanagimoto, Y.; Takaguchi, Y.; Tsuboi, S.; Ichihara, M.; Ohta, K., *Bull. Chem. Soc. Jpn.* **2006,** *79* (8), 1265-1270.
166. Yanagimoto, Y.; Takaguchi, Y.; Tuboi, S., *Polym. J.* **2006,** *38* (12), 1230-1236.
167. Claus, T. K.; Telitel, S.; Welle, A.; Bastmeyer, M.; Vogt, A.; Delaittre, G.; Barner-Kowollik, C., *Chem. Commun.* **2017,** *53* (10), 1599-1602.
168. Liu, B.; Wang, H.; Zhang, L.; Yang, G.; Liu, X.; Kim, I., *Polym. Chem.* **2013,** *4* (8), 2428-2431.
169. Jones, J. R.; Liotta, C. L.; Collard, D. M.; Schiraldi, D. A., *Macromolecules* **1999,** *32* (18), 5786-5792.

170. Gao, W.; Qin, G.; Liu, J.; Fedorchuk, A. A.; Ozga, K.; Kityk, I. V., *J. Mater. Sci. Mater. Electron.* **2017,** *28* (12), 8480-8486.
171. Defize, T.; Riva, R.; Jérôme, C.; Alexandre, M., *Macromol. Chem. Phys.* **2012,** *213* (2), 187-197.
172. Shi, Z.; Hau, S.; Luo, J.; Kim, T. D.; Tucker, N. M.; Ka, J. W.; Sun, H.; Pyajt, A.; Dalton, L.; Chen, A.; Jen, A. K. Y., *Adv. Funct. Mater.* **2007,** *17* (14), 2557-2563.
173. Yoshie, N.; Saito, S.; Oya, N., *Polymer* **2011,** *52* (26), 6074-6079.
174. Kötteritzsch, J.; Geitner, R.; Ahner, J.; Abend, M.; Zechel, S.; Vitz, J.; Hoeppener, S.; Dietzek, B.; Schmitt, M.; Popp, J.; Schubert, U. S.; Hager, M. D., *J. Appl. Polym. Sci.* **2018,** *135* (10), 45916 |1-14.
175. Schröter, G. A.; Riegger, P., *Kunststoffe* **1954,** *44* (7), 278-80.
176. Tazuke, S.; Banba, F., *J Polym Sci Part A Polym Chem* **1976,** *14* (10), 2463–2478.
177. Tazuke, S.; Hayashi, N., *J Polym Sci Part A Polym Chem* **1978,** *16* (11), 2729–2739.
178. Bratschkov, C.; Karpuzova, P.; Müllen, K.; Klapper, M.; Schopov, I., *Polym. Bull.* **2001,** *46* (5), 345–349.
179. Torii, T.; Ushiki, H.; Horie, K., *Polym. J.* **1993,** *25*, 173-183.
180. Frank, P. G.; Tuten, B. T.; Prasher, A.; Chao, D.; Berda, E. B., *Macromol. Rapid Commun.* **2014,** *35* (2), 249-253.
181. Wells, L. A.; Brook, M. A.; Sheardown, H., *Macromol. Biosci.* **2011,** *11* (7), 988-998.
182. Zheng, Y.; Micic, M.; Mello, S. V.; Mabrouki, M.; Andreopoulos, F. M.; Konka, V.; Pham, S. M.; Leblanc, R. M., *Macromolecules* **2002,** *35* (13), 5228-5234.
183. Matsui, J.; Ochi, Y.; Tamaki, K., *Chem. Lett.* **2006,** *35* (1), 80-81.
184. Shi, Y.; Cardoso, R. M.; van Nostrum, C. F.; Hennink, W. E., *Polym. Chem.* **2015,** *6* (11), 2048-2053.
185. Su, Z.; Yu, B.; Jiang, X.; Yin, J., *Macromolecules* **2013,** *46* (9), 3519-3528.
186. Truong, V. X.; Li, F.; Forsythe, J. S., *ACS Macro Lett.* **2017,** *6* (7), 657-662.
187. Radl, S. V.; Roth, M.; Gassner, M.; Wolfberger, A.; Lang, A.; Hirschmann, B.; Trimmel, G.; Kern, W.; Griesser, T., *Eur. Polym. J.* **2014,** *52*, 98-104.
188. Manhart, J.; Ayalur-Karunakaran, S.; Radl, S.; Oesterreicher, A.; Moser, A.; Ganser, C.; Teichert, C.; Pinter, G.; Kern, W.; Griesser, T.; Schlögl, S., *Polymer* **2016,** *102*, 10-20.
189. Li, T. S.; Chen, J. F.; Mitsuishi, M.; Miyashita, T., *J. Mater. Chem.* **2003,** *13* (7), 1565-1569.
190. Li, T. S.; Xu, W. J.; Tang, C. Q.; Zhang, M.; Wu, Y. J.; Miyashita, T., *J Polym Sci Part B Polym Phys* **2012,** *50* (2), 139-147.
191. Connal, L. A.; Vestberg, R.; Hawker, C. J.; Qiao, G. G., *Adv. Funct. Mater.* **2008,** *18* (20), 3315-3322.
192. Smith, A. R.; Watson, D. F., *Chem. Mater.* **2010,** *22* (2), 294-304.
193. Rameshbabu, K.; Kim, Y.; Kwon, T.; Yoo, J.; Kim, E., *Tetrahedron Lett.* **2007,** *48* (27), 4755-4760.
194. Sinigersky, V.; Müllen, K.; Klapper, M.; Schopov, I., *Adv. Mater.* **2000,** *12* (14), 1058-1060.
195. Froimowicz, P.; Frey, H.; Landfester, K., *Macromol. Rapid Commun.* **2011,** *32* (5), 468-473.
196. Song, Y. K.; Lee, K. H.; Hong, W. S.; Cho, S. Y.; Yu, H. C.; Chung, C. M., *J. Mater. Chem.* **2012,** *22* (4), 1380-1386.
197. Radl, S.; Kreimer, M.; Griesser, T.; Oesterreicher, A.; Moser, A.; Kern, W.; Schlögl, S., *Polymer* **2015,** *80*, 76-87.
198. Fang, Y.; Du, X.; Du, Z.; Wang, H.; Cheng, X., *J. Mater. Chem. A* **2017,** *5* (17), 8010-8017.
199. Zhou, Q.; Zhang, B.; Han, D.; Chen, R.; Qiu, F.; Wu, J.; Jiang, H., *Chem. Commun.* **2015,** *51* (15), 3124-3126.
200. Mack, M. J.; Eisenbach, C. D., *Mol. Cryst. Liq. Cryst.* **2005,** *431* (1), 397-402.
201. Kudo, H.; Yamamoto, M.; Nishikubo, T.; Moriya, O., *Macromolecules* **2006,** *39* (5), 1759-1765.
202. Jones, J. R.; Liotta, C. L.; Collard, D. M.; Schiraldi, D. A., *Macromolecules* **2000,** *33*, 1640-1645.

203. López-Vilanova, L.; Martínez, I.; Corrales, T.; Catalina, F., *Eur. Polym. J.* **2014,** *56*, 69-76.
204. Chujo, Y.; Sada, K.; Nomura, R.; Naka, A.; Saegusa, T., *Macromolecules* **1993,** *26* (21), 5611-5614.
205. Xie, H.; Cheng, C. Y.; Du, L.; Fan, C. J.; Deng, X. Y.; Yang, K. K.; Wang, Y. Z., *Macromolecules* **2016,** *49* (10), 3845-3855.
206. Xie, H.; He, M. J.; Deng, X. Y.; Du, L.; Fan, C. J.; Yang, K. K.; Wang, Y. Z., *ACS Appl Mater Interfaces* **2016,** *8* (14), 9431-9439.
207. Mengel, C.; Meyer, W. H.; Wegner, G., *Macromol. Chem. Phys.* **2001,** *202* (7), 1138-1149.
208. Yu, H.; Alexander, D. T. L.; Aschauer, U.; Häner, R., *Angew. Chem.* **2017,** *129* (18), 5122-5126.

Chapter III: Synthesis and characterization of novel 9-substituted anthracene derivatives

Abstract

A large series of functional 9-substituted anthracenes was synthesized and evaluated for the ability to undergo [4+4]-cycloadditions, forming dimers upon irradiation with UVA, and for their dimers to dissociate thermally. This scission of the dimers was shown to proceed in a clean and efficient way at temperatures between 90 °C and 200 °C. It was shown that the dissociation temperature is significantly influenced by the substituent. The Arrhenius parameters of the scission reactions were determined by fluorescence spectroscopy and correlated to the type of substituent. The absorption and emission maxima of the prepared monomeric anthracenes red-shift with increasing electron-donating power of the 9-substituent. For the introduction of the derivatives in polymer coatings, the reader is referred to the next two chapters.

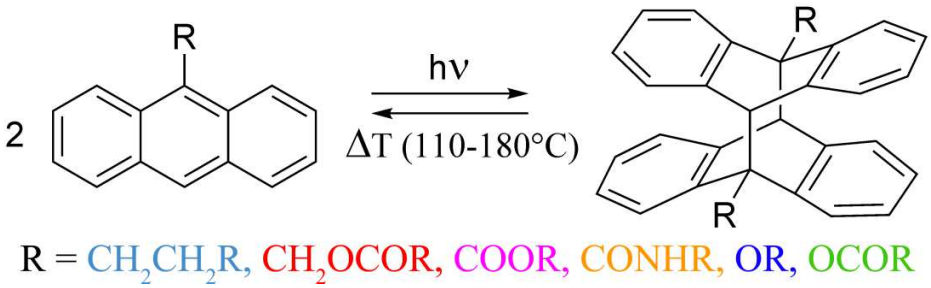

The findings in this chapter have been published as:

- Van Damme, J.; Vlaminck, L.; Van Assche, G.; Van Mele, B.; van den Berg; O.; Du Prez, F. Synthesis and evaluation of 9-substituted anthracenes with potential in reversible polymer systems. *Tetrahedron* **2016**, *72* (29), 4303-4311

Some of the results presented in this chapter are also included in articles:

- Van Damme , J.; van den Berg, O.; Brancart, J.; Vlaminck, L.; Huyck, C.; Van Assche, G.; Van Mele, B.; Du Prez, F. Anthracene-based Thiol-Ene Networks with Thermo-Degraable and Photo-Reversible Properties. *Macromolecules* **2017**, *50*, 1930-1938
- Van Damme, J.; van den Berg, O.; Vlaminck, L.; Brancart, J.; Van Assche, G.; Du Prez, F. Anthracene-based polyurethane networks: tunable thermal degradation, photochemical cure and stress-relaxation, accepted
- Chattopadhyay, S.; Van Damme, J.; van den Berg, O.; Du Prez, F. Anthracene-based colloidal polymer nanoparticles: their photochemical ligation and waterborne coating applications. *Part. Part. Syst. Charact.* **2018,** DOI: 10.1002/ppsc.201800030

Collaborations:

In this work, dr. Kevin De Bruycker assisted by performing DFT calculations on several model molecules. For the work on the simulations of a coating system by sunlight, mathematical and strategic advice was given by prof. Guy Van Assche and dr. Joost Brancart. Dr. Otto van den Berg provided several synthesis and characterization ideas. The practical workload was shared with master students Laetitia Vlaminck and Akın Gürsoy.

1 Introduction

As discussed in the previous chapter, the dimerization of anthracene **1** occurs under the influence of either artificial near-UV radiation (UVA) or sunlight (Figure III.1).[1] The formed dimers are typically crystalline with a very low solubility, which upon irradiation with short wavelength UV (UVC) or heating form the starting anthracenes. As both [4+4]-cycloaddition and cycloreversion are only photochemically allowed,[2] the thermal scission must follow a radical mechanism. Upon simultaneous stimulation of dimerization and scission, a photodynamic equilibrium can be established. This photostationary state can be tuned by the reaction parameters (e.g. light wavelengths, intensity and temperature), changing the relative reaction rates. In cross-linked polymer systems, this would allow having dynamic exchange of bonds while maintaining a high connectivity and thus network integrity.

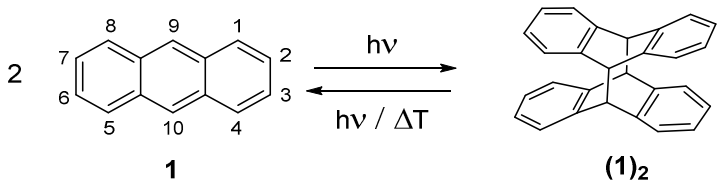

Figure III.1. Reversible dimerization of anthracene.

Thus far, many anthracene derivatives have been shown to share the dimer forming properties with their parent compound anthracene,[3] provided that there is no significant steric hindrance that could interfere with the formation of a dimer, such as bulky substituents on the 9- and 10-position of the central ring. For example, introduction of two phenyl moieties on both the 9- and 10-position of anthracene leads to a complete loss of the dimerization ability.[4] However, this substitution pattern also blocks non-radiative decay of the excited state of anthracene, leading to very efficient fluorescence and to fluorescence quantum yields approximating unity.[5]

The dimerization of anthracene has been used for (reversible) polymerization[6] and reversible crosslinking in various fields ranging from self-healing polymer materials[7] to surface patterning[8] and controlled drug release.[9] The dimerizable anthracene moieties provide control over polymerization or crosslinking degree by the application of UV-light to form dimers, while heat or UVC are applied to breakup dimers into the original anthracene derivatives. The anthracenes used in literature are often esters based on 9-anthracene methanol.[7, 10] While other 9-substituted anthracene monomers have also been reported, such as aromatic ethers,[3a] they are usually synthesized on a smaller scale.

In order to quantify and predict the behavior of anthracene derivatives and their corresponding dimer species with regard to UV-exposure and thermal stability, both as bare building blocks and in crosslinked networks, quantitative data regarding the scission of anthracene dimers is required. Unfortunately such data are currently only available for a small selection of anthracene derivatives.[11] Moreover, thermodynamic data are mostly limited to the dimer dissociation enthalpy of a few non-functional 9-substituted anthracene dimers that cannot be used for the synthesis of linear or crosslinked polymer systems.[12]

In this chapter, the synthesis of a series of anthracene derivatives and their corresponding dimers, substituted at the 9-position with moieties having a different degree of electronegativity, is described with the aim to understand the relationship between the (photo)chemical properties of these structures and their chemical structure. Each derivative is subsequently spectroscopically characterized with regard to absorption and fluorescence emission in chloroform, acetonitrile and ethanol. Using the absorption data, simulations are made of sunlight-driven anthracene dimerization. The dimerization, photo-oxidative stability and dimer photoscission are studied. Lastly, the kinetic parameters determining the thermal reversion are then obtained in order to be able to predict the behavior of the prepared derivatives for their later application in functional crosslinked polymer materials (chapters IV and V).

2 Results and discussion

2.1 Synthesis of anthracene derivatives

As explained in the introductory section, the aim of this study is to create a toolbox of well-characterized functional anthracene derivatives that will be used in the forthcoming study to construct polymer materials with reversible crosslinks. For this reason, synthetic efforts and commercial accessibility played a major role in the selection of the type of anthracene derivative. Since the 9-position is the most reactive position towards electrophilic aromatic substitution,[13] the synthesis of 9-substituted anthracene compounds is typically more upscalable than for other substituted anthracenes, making material applications more viable. Examples of available low-cost anthracene derivatives and precursors include anthracene methanol **2**, anthrylcarboxylic acid **22**, 9-anthraldehyde **5**, which can be prepared using the Vilsmeier reaction[14] and anthrone, which can be prepared by partial reduction of anthraquinone.[15]

2.1.1.1 9-CH_2R anthracene derivatives

The first series, consisting of '9-CH_2' anthracene derivatives, i.e., compounds with a methylene unit attached to the anthracene structure, was synthesized either by esterification of anthracene methanol **1** with freshly distilled undecenoyl chloride **3** in pyridine to form ester **4** or by a Grignard reaction of 9-anthraldehyde **5** with allylmagnesium chloride **6** or undecen-10-en-1-ylmagnesium bromide **7**, followed by reduction of the formed benzylic alcohol with triethyl silane and trifluoroacetic acid (Figure III.2) with formation of **10** and **11**, respectively. A similar compound with amine end group (suitable for reaction with epoxy resin) was also prepared starting from 9-anthraldehyde **5**. The 9-anthraldehyde (**5**) was reacted with an excess of nitromethane in the presence of ammonium acetate to prepare 9-(2-nitrovinyl)anthracene (**12**). This product was reduced using lithium aluminium hydride and subsequently worked up with a HCl solution to form 2-(anthracen-9-yl)ethan-1-ammonium chloride (**13**). This stable salt was stored as such and was treated with KOH solution to form fresh 2-(anthracen-9-yl)ethan-1-amine (**14**) upon demand.

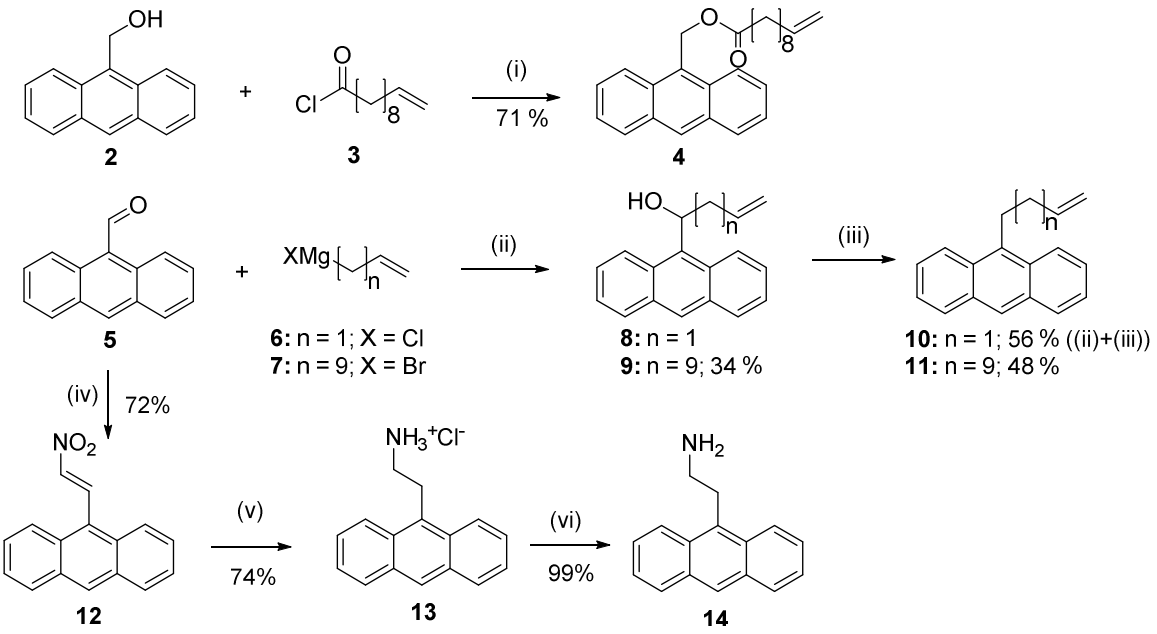

Figure III.2. (i) C_5H_5N, 5 min, 0 °C; overnight, rt, (ii) (1) THF, 5 min, 0 °C; 1 h, rt, (2) NH_4Cl, (iii) CH_2Cl_2, Et_3SiH, CF_3COOH, overnight, rt; (iv) CH_3NO_2, NH_4OAc, 2h, 100 °C; (v) (1) $LiAlH_4$, H_2SO_4, THF, rt, overnight, (2) 1 M HCl; (vi) 10 % KOH.

2.1.1.2 9-vinyl anthracene derivatives

Anthracene derivatives with a double bond at the 9-position were synthesized using a palladium catalyzed vinylation of aromatic halides, also known as a Heck reaction (Figure III.3).[16] Reaction of 9-bromoanthracene **15** and 10-undecenol **16** or 10-undecenoic acid **17** with palladium acetate as catalyst and tri(o-tolyl)phophine as ligand led to the formation of derivative **18** and **19**, respectively. However, because of some reproducibility issues, challenging purification and possible occurrence of side reactions due to the double bond, these derivatives were excluded in the upcoming characterization.

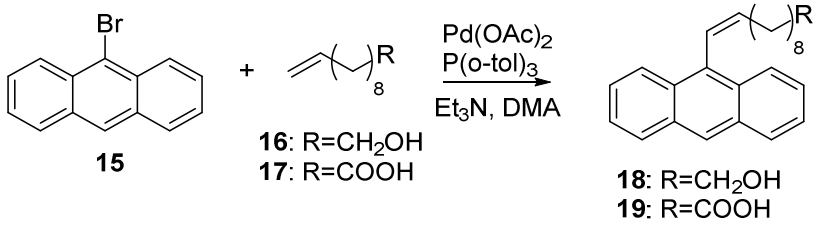

Figure III.3. Heck reaction leading to 9-vinyl anthracenes.

2.1.1.3 9-carbonyl anthracene derivatives

In a third series, consisting of electron-poor 9-carbonyl anthracene derivatives, the synthesis of an aromatic ketone **20** was first attempted by Friedel-Crafts acylation on the central anthracene ring with an acid chloride (**3**) and aluminium trichloride (Figure III.4).[17] While kinetic control should lead to 9-substitution, thermodynamic reaction conditions would mainly lead to substitution on the less hindered position, such as the 2-position. However, no significant conversion was observed after 5 minutes at 0 °C using an excess of aluminium trichloride. Performing this reaction for longer times and at room temperature in different solvents (dichloromethane, carbondisulfide, nitrobenzene) led to tar formation without achieving the desired product. This might be due to interference of the double bond present in the 10-undecenoyl chloride **3**. This hypothesis is supported by the disappearance of the ^{1}H-NMR double bond peaks and by literature.[18] Alternatively, aromatic ketone **21** was succesfully produced in high yield (99 %) by Swern oxidation of the intermediate **9**. This intermediate was produced by the Grignard reaction of anthraldehyde **5** with undecen-10-en-1-ylmagnesium bromide **7** (Figure III.2).

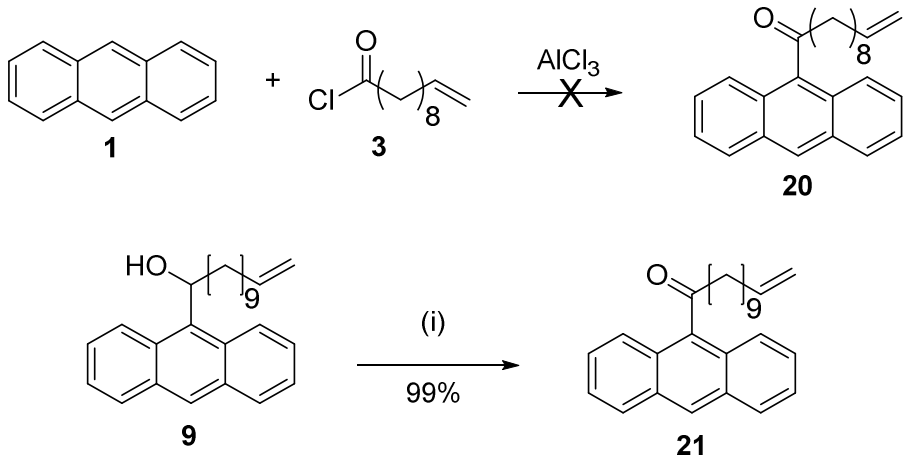

Figure III.4. (i) (1) CH_2Cl_2, $C_2O_2Cl_2$, DMSO, 30 min, −78 °C, (2) Et_3N

Starting from 9-anthrylcarboxylic acid **22**, aromatic amides and esters could be synthesized. First, 9-anthrylcarboxylic acid **22** was converted to the corresponding acid chloride **23** by reaction with thionylchloride as previously reported.[19] Reaction of **23** with 10-undecen-1-ol yielded the aromatic ester **24** with terminal double bond (Figure III.5). Bases such as triethylamine or pyridine could not be used, since steric hindrance of the carbonyl position by the anthracene moiety leads to the formation of stable quaternary acylammonium salts that are hardly reactive towards alcohols, severely lowering the yield when tertiary amines are added.[20] Similarly, the non-functional aromatic amide **25** was synthesized by adding 2 equiv of butylamine to **23** in dichloromethane.

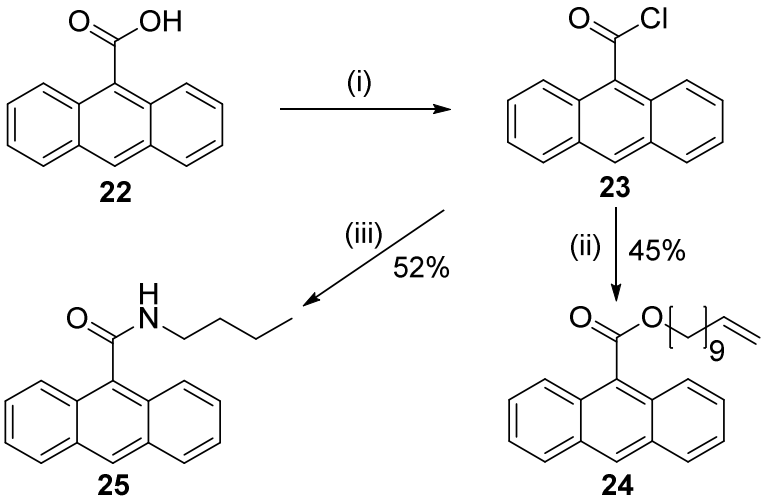

Figure III.5. (i) $SOCl_2$, 2 h, reflux, (ii) 10-undecen-1-ol, CH_2Cl_2, overnight, rt, (iii) n-butyl amine, CH_2Cl_2, overnight, rt.

2.1.1.4 9-OR anthracene derivatives

A third type of derivative, consisting of anthracenes with an oxygen at the 9-position, was synthesized starting from anthrone **26**. 9-Alkoxyanthracenes were synthesized by acid catalyzed etherification of alcohols with **26** as described in literature (Figure III.6).[21] By using an excess of either 1,6-hexanediol or 1,12-dodecanediol, a functionalized anthracene derivative with either a short **27** or a long spacer **28** was synthesized. Upon dimerization of **27** or **28**, diols are created that can be used as such as building blocks in polyurethanes (see chapter V). The acid catalyzed etherification was also attempted using 10-undecenol to yield **29**. However, only low conversion was observed, presumably due to side reactions between the acids and the double bond. An alternative approach consists of protecting the double bond prior to reaction, followed by deprotection afterwards or by performing a base mediated proton abstraction at the methylene bridge of anthrone, followed by alkylation of the formed anion with alkyl halides.[22] By adding undecenoyl chloride **3** instead of alkyl halides to anthrone **26**, after addition of a (strong) base and allowing enol rearrangement, ester **30** was synthesized in good yield (84 %).

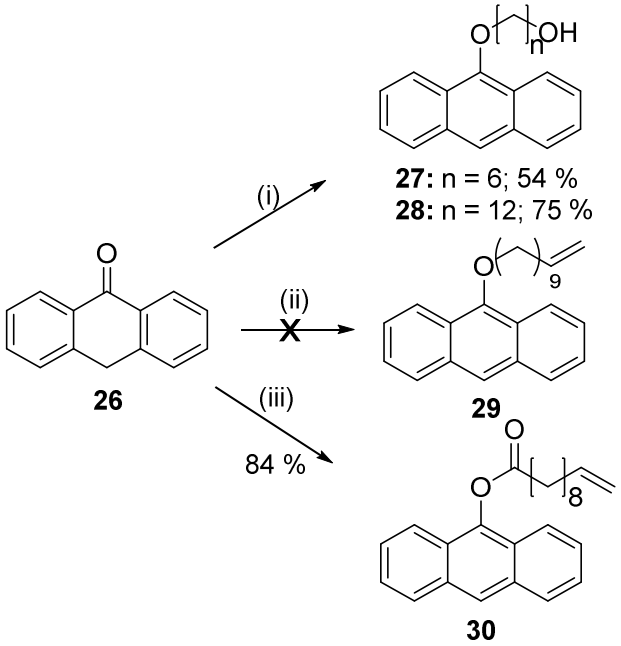

Figure III.6. (i) C_7H_8, diol, H_2SO_4 (cat.), overnight, reflux; (ii) C_7H_8, 10-undecenol, H_2SO_4 or p-TsOH (cat.), overnight, reflux; (iii) (1) Et_3N, 1 h, reflux, (2) 10-undecenoyl chloride **3**, 2 h, reflux.

2.1.1.5 9-SR anthracene derivatives

Similar to the synthesis of the anthracene ethers, thio-ether derivatives were synthesized. As the reaction based on anthrone **26** is much slower with thiols, 9-methoxyanthracene **36** was synthesized as intermediate (Figure III.7). Due to the low boiling point of methanol, the produced water cannot be removed by azeotropic evaporation. Therefore, trimethyl orthoformate was used instead. Unfortunately, this reaction proved to be irreproducible with unpredictable yields up to 43 %.

First thioether **38** was successfully synthesized by reacting **36** with an excess of 1-octanethiol **37** in toluene using methanesulfonic acid as catalyst. Second, we attempted to synthesize an alcohol functional thio-ether **39**. Prior to this, 11-mercapto-1-undecanol **35** had to be synthesized. This was done by a radical thiol-ene reaction using 10-undecenol **31** and thioacetic acid **32**, followed by thioester scission using propylamine **34**. However, reaction of **36** with **35** resulted in low conversion. Upon purification by column chromatography, no pure product was achieved. As a result, **38** was used for characterization instead.

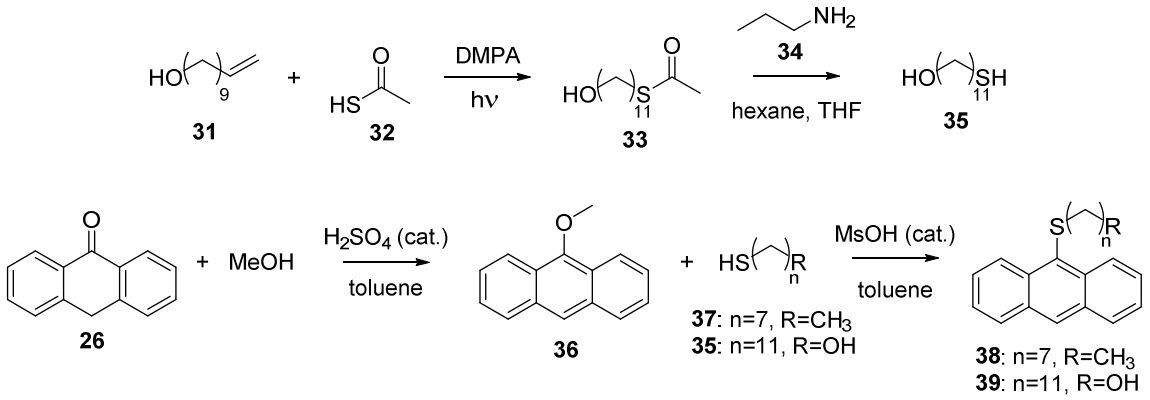

Figure III.7. Synthesis of 11-mercapto-1-undecanol and thioethers **38** and **39**.

2.1.1.6 9-NR_2 anthracene derivative

Lastly, the synthesis of anthracene derivatives with amines at the 9-position were attempted. For this, first the 9-aminoanthracene **42** was made in high yield following a procedure published in literature (Figure III.8).[23] However, difficulties arose when attempting to react **42** to an amide **43**, a secondary **44** or tertiary amine **45** (Figure III.9).

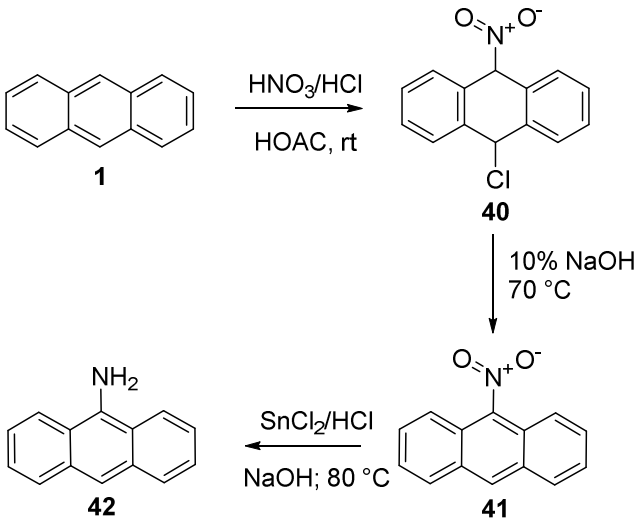

Figure III.8. Synthesis of 9-aminoanthracene.

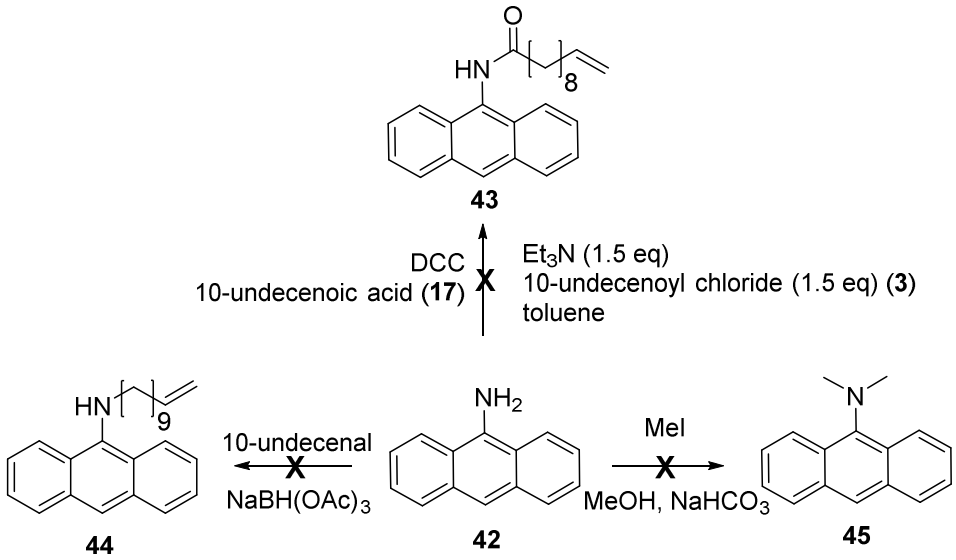

Figure III.9. Failed attempts at reacting **42**.

Later it was found out that **42** oxidizes readily to anthraquinone monoimide **46** in the presence of oxygen (Figure III.10).[24] Unlike most other anthracenes, this reaction occurs with triplet oxygen instead of singlet oxygen and therefore cannot be stopped by storing in the dark. Due to these issues and doubts on the toxicity and carcinogenicity of this compound, this route was abandoned.

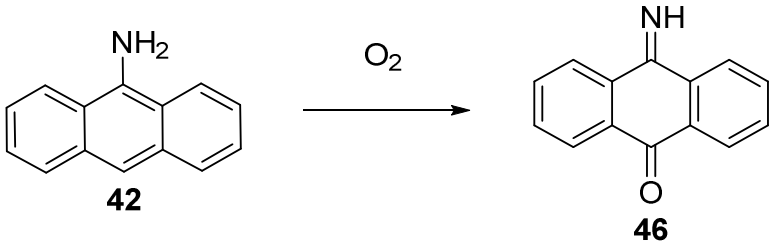

Figure III.10. Oxidation of 9-aminoanthracene **42** to anthraquinone monoimide **46**.

2.2 Functional group modification

In order to implement the synthesized anthracene derivatives as building blocks for stepgrowth polymers (e.g., polyurethane synthesis), alcohol groups are desired. Terminal double bonds, present in many derivatives, can be hydrothiolated with alcohol-containing thiols to form monofunctional or multifunctional alcohols. However, as thiols can also undesirably react with the central anthracene ring,[25] derivatives were first dimerized under UVA irradiation prior to reaction. Derivative **4** was dissolved in THF/hexane and irradiated (using mercury lamps with primary emission at 365 nm) to form dimer **$(4)_2$**, which precipitated during reaction (Figure III.**11**). After recrystallization in hexane, **$(3)_2$** was dissolved in THF and radically reacted with 2-mercaptoethanol or thioglycerol using DMPA as a photoinitiator to form diol **$(47)_2$** and tetraol **$(48)_2$**, respectively (Figure III.12).

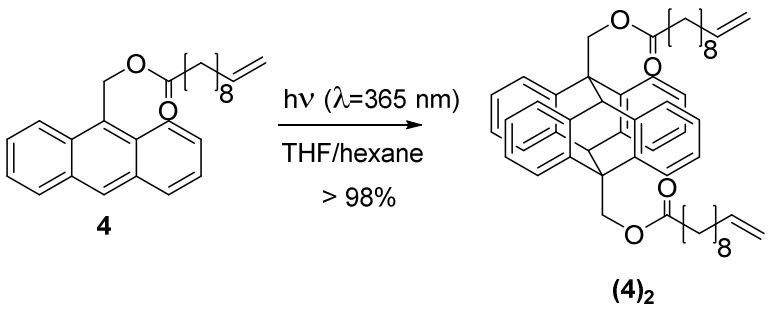

Figure III.11. Dimerization of **4**.

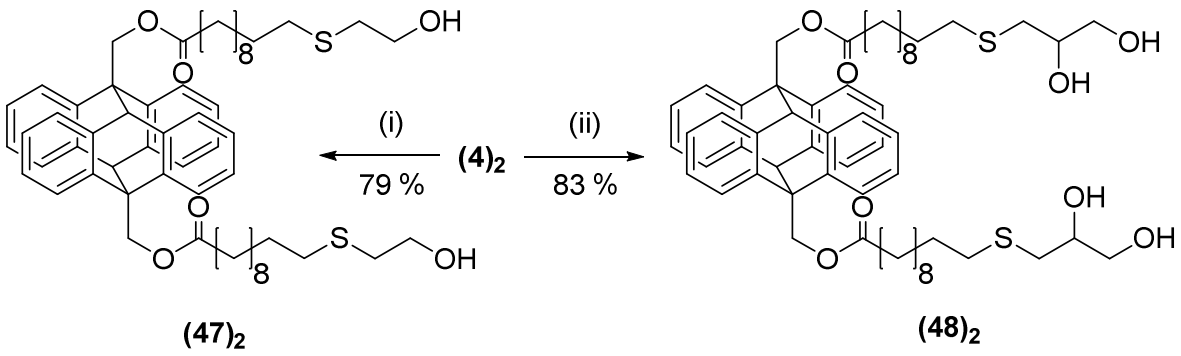

Figure III.12. (i) 2-mercaptoethanol, THF, DMPA, 1 h, rt, hν, (ii) 1-thioglycerol, THF, DMPA, 1 h, rt, hν.

A dianthracene ether tetraol was also prepared by modification of the monofunctional anthracene **28** (Figure III.13). This novel anthracene dimer **(50)$_2$** was synthesized in high yield by mesylation of the alcohol group of **28**, followed by a substitution with 2,2-bis(hydroxymethyl)propionic acid under alkaline conditions, and a dimerization step under UVA irradiation.

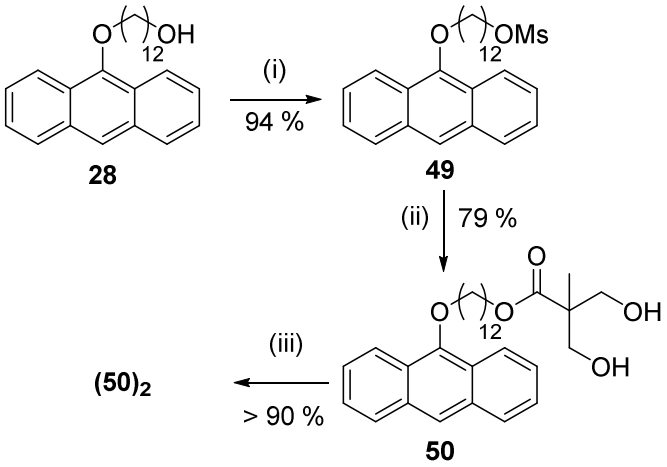

Figure III.13. Synthesis of dimer tetraol **(50)$_2$**. (i) Et_3N, MsCl, THF, rt, 3 h; (ii) K_2CO_3, 2,2-bis(hydroxymethyl) propionic acid, DMF, 80 °C, overnight; (iii) 365 nm, THF.

2.3 UV–vis absorption and fluorescence behavior

The UV–vis and fluorescence properties of anthracenes may vary depending on the surrounding solvent or (polymer) matrix. Therefore, the absorption wavelengths, λ_{max}, and Stokes shifts of the anthracene

derivatives were determined in three different solvents, respectively chloroform (aprotic) (Figure III.14 and Table III.1), acetonitrile (aprotic) (Table III.2) and ethanol (protic) (Table III.3). In general, the λ_{max} of the anthracene chromophore (e.g., at 359 nm in chloroform) shifts to higher wavelengths (e.g., 365–376 nm in chloroform) by the presence of a substituent, which lowers the HOMO–LUMO gap. This shift of λ_{max} increases as the electron donating power of the substituent increases. The highest shift is therefore found for the strongest electron donating substituents such as thioether **38** and 9-alkoxyethers **27** and **28**.[26]

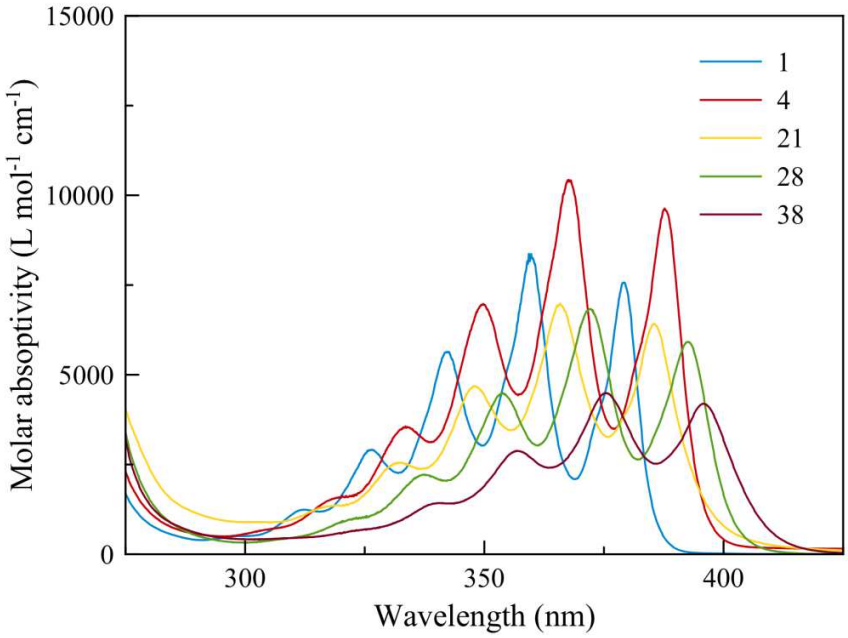

Figure III.14. Molar attenuation coefficient of several anthracene derivatives in chloroform.

Table III.1. Spectroscopic data of anthracene derivatives (ordered from low to high λ_{max}) in chloroform. [a] The Stokes shift is taken as the difference of wavelength or wavenumber between the absorption and fluorescence maxima.

	λ_{max} (nm)	ε_{max} (10^3 M^{-1} cm^{-1})	Φ_f	Stokes shift[a] (nm)	Stokes shift[a] (10^3 cm^{-1})
1	359	8.31	0.11	45	3.1
24	365	7.09	0.49	97	5.8
25	365	7.10	0.13	52	3.4
21	366	7.00	0.02	51	3.4
30	367	6.86	0.21	45	3.0
4	368	10.3	0.27	48	3.1
9	369	7.21	0.25	49	3.2
10	370	8.72	0.39	48	3.1
18	370	10.6	-	-	-
11	371	7.36	0.40	47	3.0
27	372	7.08	0.33	51	3.2
28	372	6.85	0.39	52	3.3
38	376	4.50	-	-	-

Table III.2. Spectroscopic data of anthracene derivatives (ordered from low to high λ_{max}) in acetonitrile. [a] The Stokes shift is taken as the difference of wavelength or wavenumber between the absorption and fluorescence maxima.

	λ_{max} (nm)	ε_{max} (10^3 M^{-1} cm^{-1})	Φ_f	Stokes shift[a] (nm)	Stokes shift[a] (10^3 cm^{-1})
1	357	8.17	0.19	44	3.1
24	363	8.2	0.36	100	5.9
25	362	7.2	0.12	45	3.0
21	364	5.61	0.01	44	3.0
30	364	10.6	0.20	46	3.1
4	365	8.91	0.24	46	3.1
9	366	2.95	0.15	49	3.2
10	368	12	0.40	46	3.0
11	368	7.97	0.40	46	3.0
27	369	6.68	0.17	51	3.3
28	369	8.34	0.15	52	3.3

Table III.3. Spectroscopic data of anthracene derivatives (ordered from low to high λ_{max}) in ethanol. [a] The Stokes shift is taken as the difference of wavelength or wavenumber between the absorption and fluorescence maxima. [b] Incomplete fluorescence integration due to overlap with the excitation beam.

	λ_{max} (nm)	Φ_f	Stokes shift[a] (nm)	Stokes shift[a] (10^3 cm^{-1})
1	357	>0.21[b]	42	3.0
24	362	0.23	106	6.2
25	363	0.14	47	3.1
21	364	0.03	53	3.5
30	364	0.21	45	3.0
4	365	0.51	46	3.1
9	367	0.13	48	3.2
10	367	0.36	46	3.0
18	-	0.52	-	-
11	368	0.32	46	3.0
27	369	0.29	49	3.2
28	369	0.21	49	3.2
38	-	0.25	-	-

The absorption red-shift encountered for 9-carbonyl anthracenes such as ester **24**, amide **25** and ketone **21** is not due to intramolecular charge displacement stabilization by an electron withdrawing carbonyl (mesomeric effect), as steric hindrance inhibits the carbonyl to be in plane with the anthracene ring.[27] Instead, the absorption shift should only be ascribed to the inductive effect of the substituents, lowering the energy gap.

Absorption spectra in acetonitrile and ethanol had lower wavelength maxima (2–3 nm difference) compared to chloroform (Table III.1). This change in absorption wavelength is attributed to a different stabilization of the excited and ground state by the solvents.

The relative order in energy gap size is confirmed by DFT calculations (basis set 6.311G*, using Spartan) on several anthracenes (Table III.4). In order to limit the amount of conformers, the alkyl chain

length was shortened for calculation. This is done by assuming that the influence of the chain length on the light absorption by the anthracene rings is negligible. This assumption is supported by the observation that variation in the absorption wavelengths of similar anthracenes is within the range of experimental uncertainty.

Table III.4. HOMO, LUMO and energy gap E calculations. [a] HOMO and LUMO are calculated for the derivatives having shorter chain lengths (3–5 carbons), using 6.311G* as a basis set. [b] Calculated as E=LUMO–HOMO. [c] Calculated as E=hc/λ_{max}.

	HOMO[a]	LUMO[a]	Ecalcd[b]	Echloroform[c]	Eethanol[c]
	(eV)	(eV)	(eV)	(eV)	(eV)
"24"	−5.73	−2.22	3.51	3.40	3.42
"4"	−5.61	−2.11	3.50	3.37	3.40
"11"	−5.35	−1.86	3.49	3.35	3.37
"28"	−5.34	−1.86	3.48	3.33	3.36

Molar attenuation coefficients (ε) in chloroform at λ_{max} vary between ~6.85×10^3 (**28** and **29**) and 10.3×10^3 L mol^{-1} cm^{-1} (**4**), while that for unsubstituted anthracene was 8.3×10^3 L mol^{-1} cm^{-1}. In acetonitrile, the molar attenuation coefficients varied between 2.95×10^3 (**9**) and 12×10^3 L mol^{-1} cm^{-1} (**10**). Both absorption wavelength maxima and molar attenuation are important factors in polymer applications when considering the penetration depth of light upon irradiation and the choice of the UV source.

The absorption spectra of several anthracene dimers were also measured (Figure III.15). Compared to the reported UV-absorption spectrum of the virtually insoluble unsubstituted dianthracene **(1)$_2$**, no significant absorption wavelength shifts were found. This may be due to the inability of resonance, rendering the aromatic systems less electron rich.

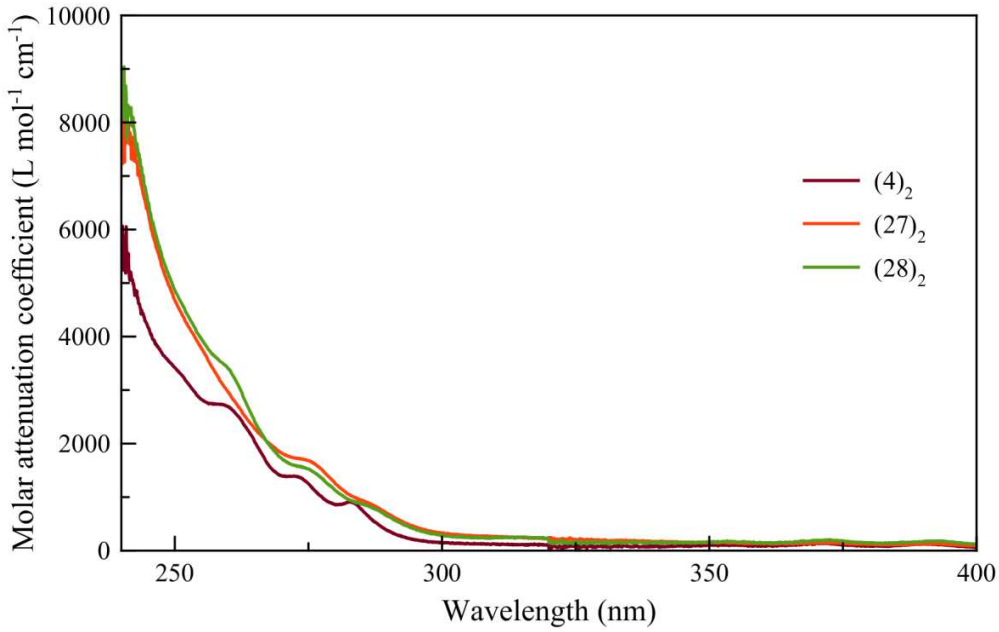

Figure III.15. Molar attenuation coefficient of several dimers in ethylacetate.

Aside from dimerizing (in concentrated solution) upon irradiation, excited anthracene molecules are also known to decay via fluorescence. As is shown in Table III.1, Table III.2 and Table III.3, the formed derivatives have medium (0.49) to low (0.01) fluorescence quantum yield Φ_f in dilute solutions of chloroform, acetonitrile or ethanol. The very low values of 0.01–0.03 are found for the aromatic ketone **21**. This lack of fluorescence at room temperature for 9-anthryl alkyl ketones has been previously observed by Lai and Lim[28] and Hirayama,[29] and has been ascribed to a very efficient non-radiative decay. The highest fluorescence quantum yield is found for aromatic ester **24**, having a similar quantity of radiative and non-radiative decay. Additionally, **24** has exceptional high Stokes shifts (97–106 nm) in comparison to the other derivatives (44–52 nm), along with high broadening of the vibrational bands, leading to a diffuse emission. Werner and Hercules[27] ascribed this effect for 9-anthroic esters (and 9-anthrylcarboxylic acid **22**) to rotation of the carbonyl to a coplanar excited-state configuration with intramolecular hydrogen bonding. Ghoneim *et al.*[30] contradict this conclusion and ascribed this effect to twisted intramolecular charge transfer.

2.4 Simulations

To verify the viability of the anthracene dimerization in polymeric films having thicknesses of 100 nm to a few hundred microns, the dimerization under sunlight was simulated. This is possible as the solar emission spectrum (Figure III.16)and the absorption of anthracene are well documented. Using the previously determined absorptions of the synthesized derivatives, the relative dimerization rates in such conditions can be determined.

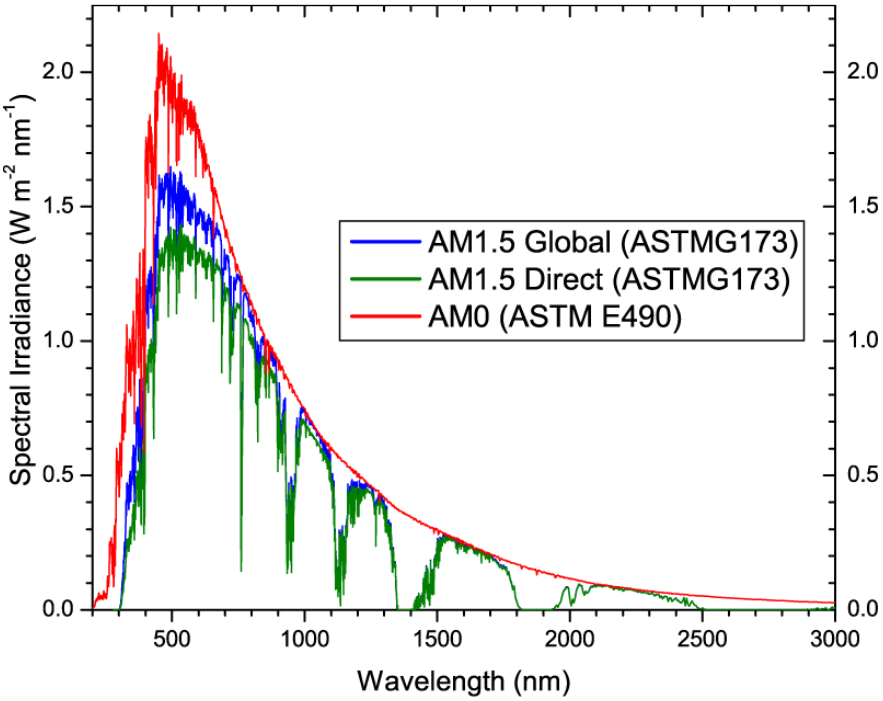

Figure III.16. ASTM solar spectrum reference spectrum used for the simulation.

2.4.1 Assumptions

In order to successfully simulate the anthracene dimerization, certain assumptions had to be taken into account.

First, the absorption of light by anthracene leads to a change in the anthracene concentration in all of the exposed material. As we can safely assume that there is only a spectral overlap of sunlight with anthracene monomers and not with any dimers, any influence of dimer formation to the absorption is not taken into account. This simplifies the situation to a mere decrease in anthracene concentration.

$$A \xrightarrow{h\nu} A^*$$

$$A^* + A \xrightarrow{\Phi_{dim}} D$$

Second, upon absorption of a photon, anthracene reaches an excited state after which it can react with another anthracene in the ground state, forming a dimer. However, this dimerization is only one of the many events which can occur upon excitation of an anthracene. Luckily, this is also the only (significant) pathway which leads to a change in anthracene concentration in the absence of oxygen. The efficiency at which an event occurs is often expressed as the quantum yield Φ. The quantum yield is defined as the amount of events occurring after absorption of a photon and for most events is maximum 1. As one photon leads to the dimerization of two anthracene molecules, the maximal quantum yield is 2. The quantum yield of dimerization Φ_{dim} is assumed here to be independent of the wavelength. Also, to the best of our knowledge, the dimerization quantum yield of a bulk polymeric anthracene system is never reported. Therefore, an arbitrary quantum yield of 2 is chosen, meaning that all absorbed photons lead to a dimer. The results can therefore only be interpreted as a theoretical minimal time required for conversion.

2.4.2 Derivation

First the retrieved solar spectrum J_{ov} is converted into more convenient units, from W/m^2 to mol/m^{2}s per nm (equation 1). This is done by dividing J_{ov} by the energy for one mol photons ((hc/λ)*N_A) of wavelength λ, with h the Planck constant (6.626 10^{-34} J s), c the speed of light (2.998 10^8 m s^{-1}) and N_A Avogado's number.

$$I_{ov} = \frac{\lambda}{hcN_A} J_{ov} \qquad \text{Equation 1}$$

As light will travel through a film or coating, it is obvious that this light intensity will decrease (Figure III.17). The photon flux at deeper laying material will be diminished, leading to a gradient in the material. As not only the absorption by the entire material is relevant, but also the absorption at different depths in the material, $dI_\nu(x,t)$ should be calculated for different layers with thickness dx.

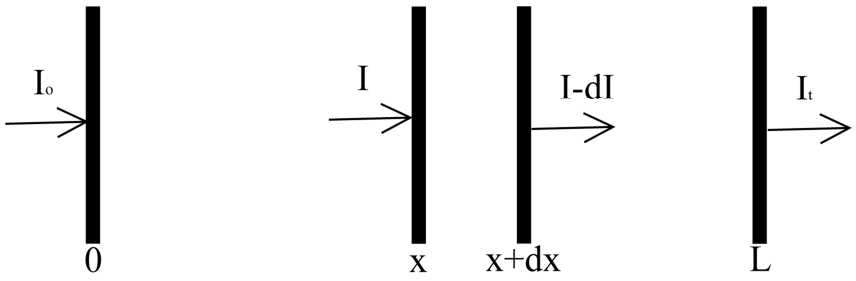

Figure III.17. Scheme of incident light I_o through an absorbing layer of thickness L with transmitted light I_t. I is the incident light at a slice of thickness dx at depth x, with I-dI the transmitted light.

This calculation is done based on the law of Lambert-Beer (equation 2), with $I_\nu(x,t)$ the photons transmitted through the upper layer (in mol m^{-2} s^{-1} nm^{-1}) with thickness x, anthracene concentrations $C(x,t)$ (in mol m^{-3}) and ε_ν the molar absorptivity (in m^2 mol^{-1}). The absorbed photon flux $dI_\nu(x,t)$ in thin layer x → x+dx (in mol m^{-2} s^{-1}) is derived in equation 3.

$$I_\nu(x,t) = I_{o\nu} 10^{-\varepsilon_\nu \int_0^x C(x,t)\,dx} \qquad \text{Equation 2}$$

$$dI_\nu(x,t) = I_\nu(x,t)\,(1 - 10^{-\varepsilon_\nu\, C(x,t)\,dx}) \qquad \text{Equation 3}$$

As dx approaches 0, we can approximate $10^{-\varepsilon_\nu C(x,t)dx} \approx 1 - \varepsilon_\nu\, C(x,t)\, dx$.

$$dI_\nu(x,t) = I_\nu(x,t)\, \varepsilon_\nu\, C(x,t)\, dx \qquad \text{Equation 4}$$

The rate of local anthracene disappearance because of dimerization is given in equations 5 to 8, with Φ_ν the quantum efficiency of dimerization (up to 2) and $I_{abs,\nu}(x,t)$ the number of photons absorbed in the volume of layer x → x+dx.

$$-\frac{dC(x,t)}{dt} = \int \Phi_\nu\, I_{abs,\nu}(x,t)\, d\nu \qquad \text{Equation 5}$$

$$-\frac{dC(x,t)}{dt} = \int \Phi_\nu\, \frac{dI_\nu(x,t)}{dx}\, d\nu \qquad \text{Equation 6}$$

$$-\frac{dC(x,t)}{dt} = \int \Phi_\nu\, I_\nu(x,t)\, \varepsilon_\nu\, C(x,t)\, d\nu \qquad \text{Equation 7}$$

$$-\frac{dC(x,t)}{dt} = \int \Phi_\nu\, I_{o\nu} 10^{-\varepsilon_\nu \int_0^x C(x,t)\,dx}\, \varepsilon_\nu\, C(x,t)\, d\nu \qquad \text{Equation 8}$$

Using Visual Basic for Applications (VBA) in Excel, these calculations were performed in an iterative fashion. First the concentrations were calculated at every layer at time t, after which these concentrations were used to calculate the concentrations at time t+dt. Pictures of the data-input cells, data output form and the VBA code are given in the experimental section.

2.4.3 Results

In a first set of simulations, the dimerization of unsubstituted anthracene was studied. As concentration we used 2 mol L^{-1}, which corresponds to a weight percentage of approximately 29% anthracene. The conversions at several thicknesses is shown in Figure III.18.

While dimerization occurs rapidly at the upper layers of several microns, it is obvious that the dimerization hardly takes place at deeper levels. However, the dimerization at these depths quickly increase when the upper laying anthracenes are largely converted to non-absorbing dimers. According to these simulations – which assume high efficiency and perfect polymer kinetics, allowing full conversion – the layer below 200 µm is completely converted after only 9 minutes. While this value is unrealistic, it does indicate that the intensity of sunlight is sufficient to accomplish dimerization in coatings of relevant thickness (up to several hundreds of microns). Under these conditions, the time required for full conversion scales linearly with thickness (e.g. 250 and 500 seconds for 100 and 200 µm).

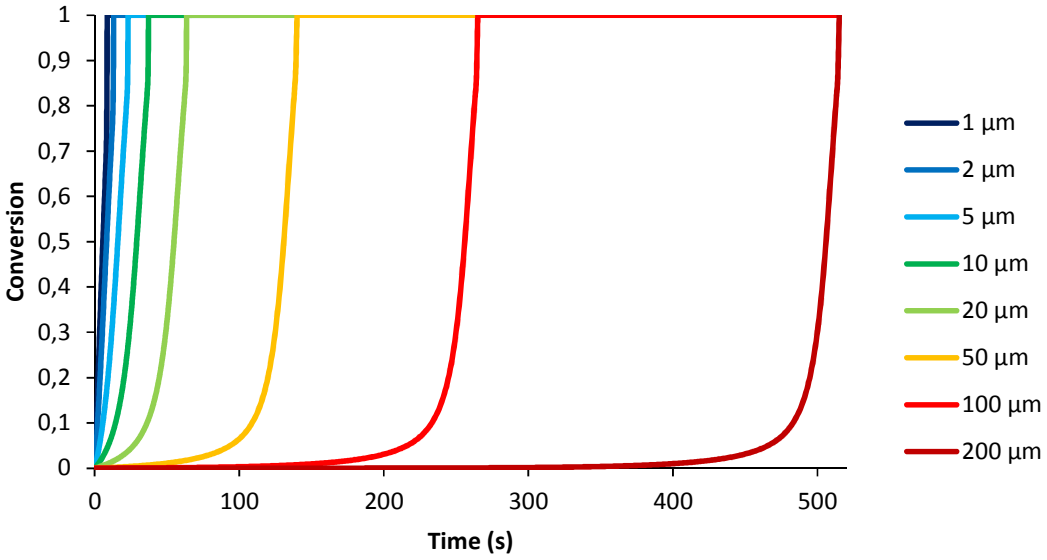

Figure III.18. Simulated dimerization of unsubstituted anthracene (2 mol L^{-1}) using sunlight and a quantum efficiency of 2.

However, due to kinetic and topological reasons, it is likely that no complete conversion is achieved. Figure III.19 and Figure III.20 show the same simulations when a conversion above 0.75 or 0.50 is not reachable. As the remaining anthracenes absorb the incident sunlight, the dimerization is significantly slower at deeper levels. In fact, the time required to achieve maximum conversion at a layer is no longer linearly dependent of the depth (Figure III.21). This indicates the importance of having a high maximal dimerization rate when attempting to develop thick coatings.

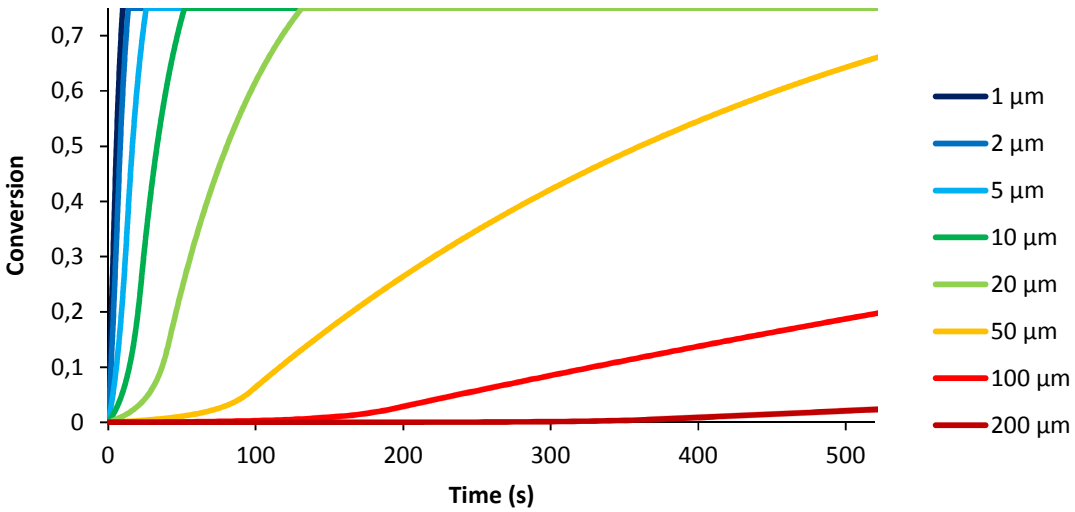

Figure III.19. Simulated dimerization of unsubstituted anthracene (2 mol L^{-1}) using sunlight and a quantum efficiency of 2. Maximum conversion is set at 0,75.

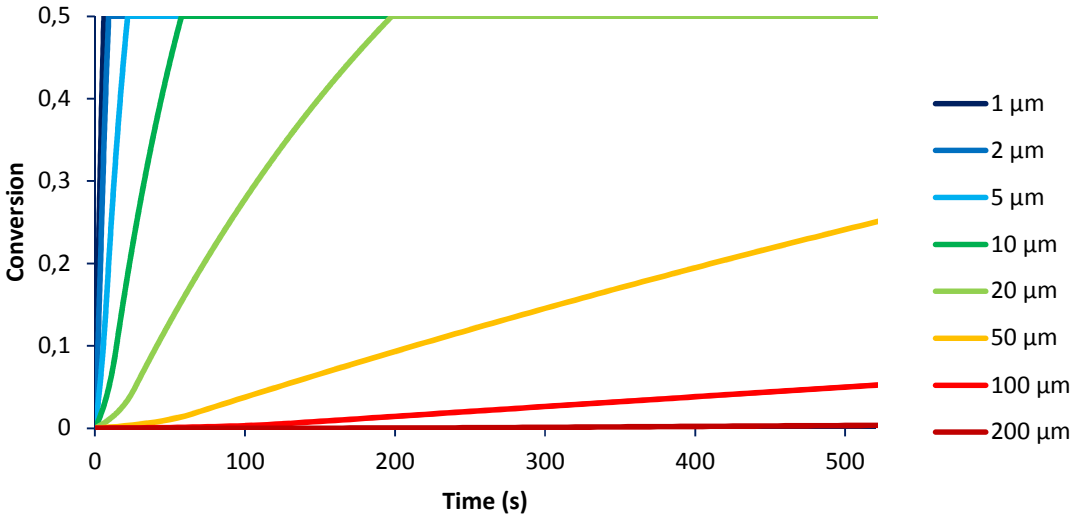

Figure III.20. Simulated dimerization of unsubstituted anthracene (2 mol L^{-1}) using sunlight and a quantum efficiency of 2. Maximum conversion is set at 0,5.

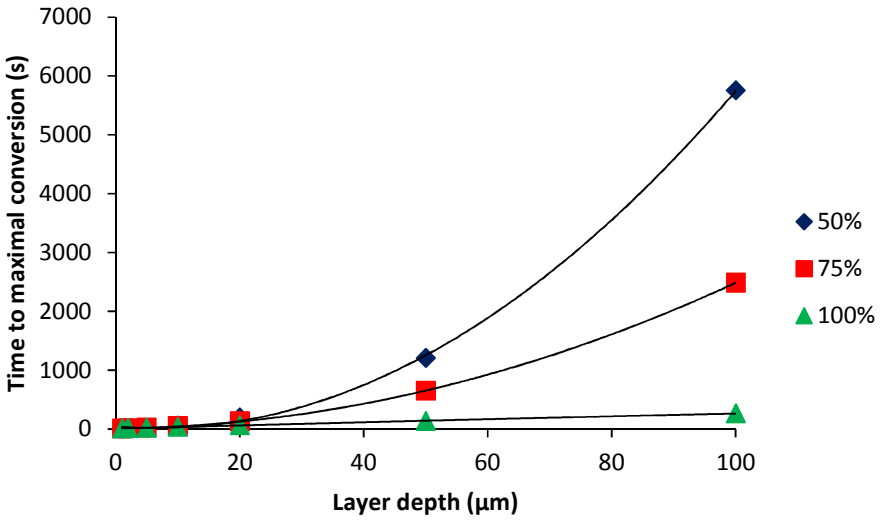

Figure III.21. Time required to achieve maximal conversion for systems having maximal conversion of 100 %, 75 % and 50 %.

The anthracene dimerization conversion at different times has also been plotted against the depth of the material layers (Figure III.22 and Figure III.23). From these plots it becomes clear that the dimerization results in a conversion gradient throughout the material. For high maximal conversion systems (Figure III.22), there is a fully dimerized zone, followed by a small zone with a steep conversion gradient and a zone with almost no dimer. Upon longer radiation times, this gradient zone migrates to deeper levels. When there is a lower maximal conversion (Figure III.23), the originally formed zone with steep gradient in the material moves increasingly slower throughout the material over time and becomes increasingly broader and less steep. Therefore, we can conclude that the maximal conversion in a dimerizing coating influences the type of gradient (sharp conversion cutoff or gradual gradient) throughout the material.

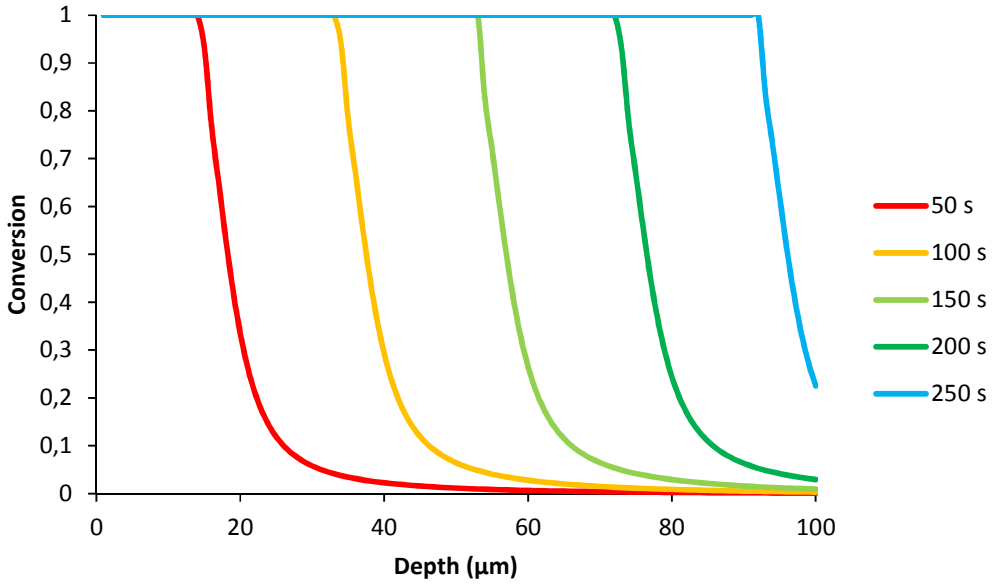

Figure III.22. Simulated dimerization of unsubstituted anthracene (2 mol L^{-1}) using sunlight and a quantum efficiency of 2.

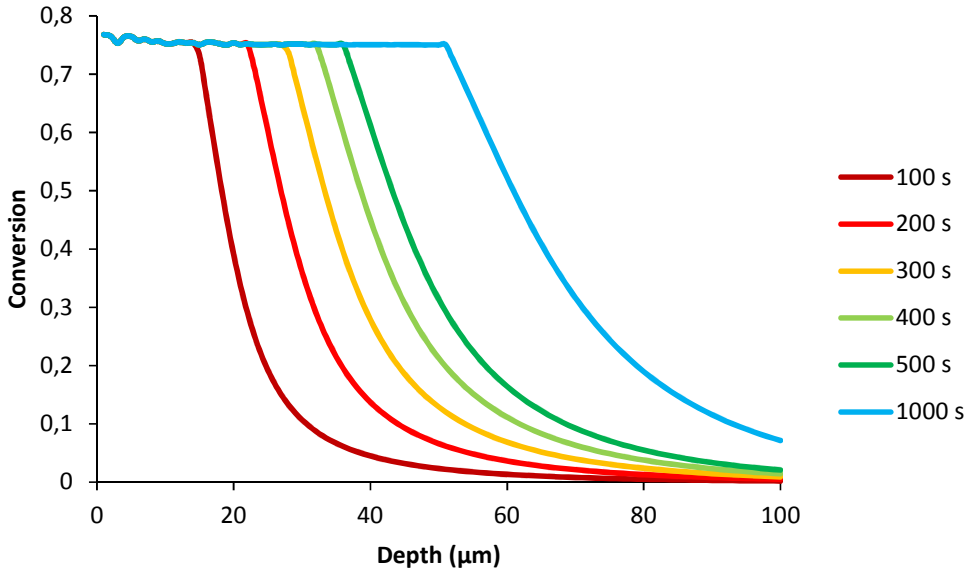

Figure III.23. Simulated dimerization of unsubstituted anthracene (2 mol L^{-1}) using sunlight and a quantum efficiency of 2. Maximum conversion set at 75 %.

By using the measured absorption spectra, a comparison can be made between the synthesized derivatives (Figure III.24). For this, we simulated the dimerization at 100 µm thickness with a maximum

dimerization conversion of 75 %. The dimerization occurs similarly for each derivative, but the time required for reaching the maximal conversion is derivative dependent (**25** < **4** < **18** ~ **21** ~ **10** < **27** < **38** < **11** ~ **28** ~ **24** < **30** < **1**). The relative slow dimerization of unsubstituted anthracene **1** is explained by the limited spectral overlap. The fastest dimerization is found for the amide **25**, which has no functional group at the end and therefore as such cannot be incorporated in polymer systems. The second fastest dimerization is found for anthracen-9-yl methyl-undec-10-enoate **4**, making this derivative the preferred derivative for developing sun-light curable materials. This was the starting point for the development of thiol-ene based materials, discussed in chapter IV.

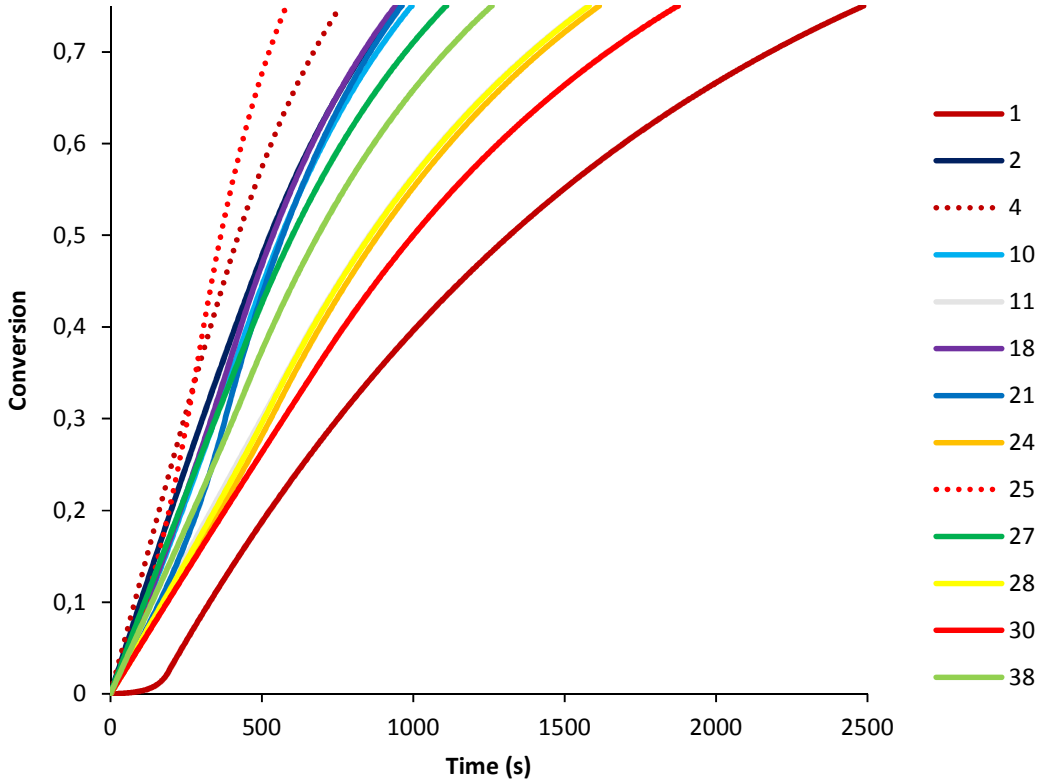

Figure III.24. Simulated dimerization conversion of numerous anthracene compounds by sunlight at 100 µm depth, 2 M concentration, 75 % maximal conversion.

2.5 Photo-oxidative stability

As the long-term stability of these derivatives is also important for application, we left glass vials of dilute solutions of several anthracenes in chloroform exposed to sunlight for 10 weeks. While these vials

were capped to limit solvent evaporation, no oxygen was removed and thus photo-oxidation could occur freely. While (in hindsight) this system is not perfect for comparing oxidation kinetics (in which case an open quartz vial under air stream would be better), it is similar to real-life situations of stored anthracene solutions exposed to artificial lighting and daylight. The samples were afterwards concentrated in *vacuo* and studied using ^{1}H NMR (Figure III.25). For all derivatives, anthraquinone was detected, which is a well-known photo-oxidation product. Other (unknown) byproducts were also present in the solutions. The best result was found for **24**, which had only 1 % anthraquinone, 81 % unreacted anthracene and 11 % dimer. This increased oxidative stability for such esters was also found by Yamamoto *et al.* and is attributed to a decrease in reactivity as diene in the Diels-Alder reaction with singlet oxygen.[31] Therefore, **24** is favored when long-term oxidative stability is desired. The second best result was found for **4**, having 63 % remaining anthracene and 4 % dimer. While this product is less stable than **24**, the synthesis route of **4** is straightforward and significantly cheaper.

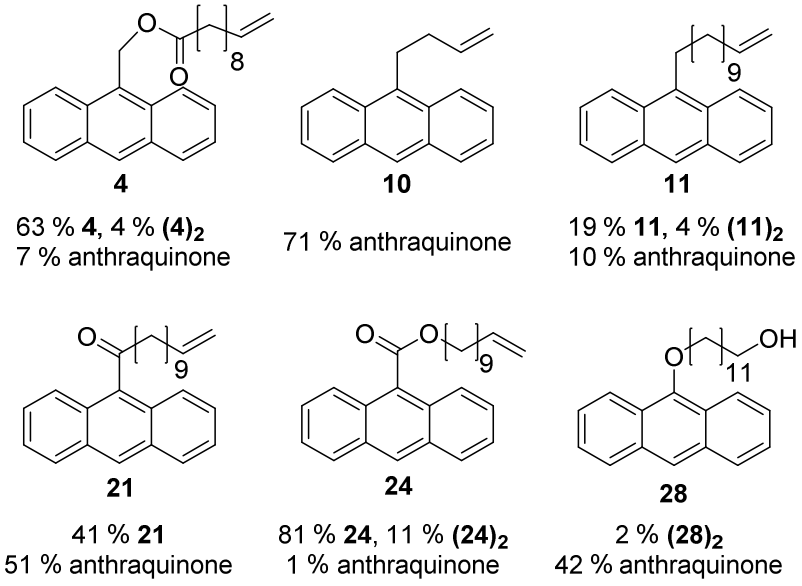

Figure III.25. Monomer, dimer and anthraquinone content of long-term stored solutions (via ^{1}H-NMR)

2.6 Dimerization

The kinetics of dimerization were tested by irradiation of solutions of 10 mM anthracene monomer in hexane under inert atmosphere (Figure III.26). The samples were irradiated with twelve 9 W standard UVA-lamps with an emission maximum at 365 nm and were analyzed using ^{1}H NMR.

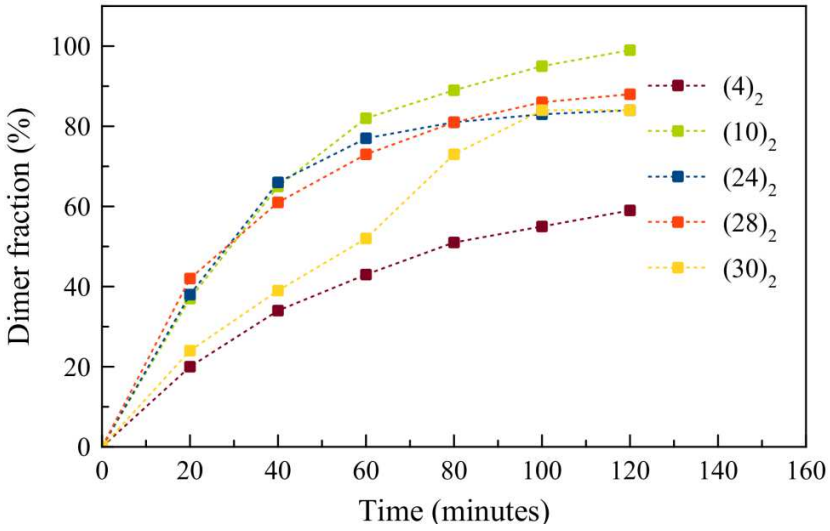

Figure III.26. Dimerization of anthracenes (10 mM in hexane).

Amide **25** did not properly dissolve in hexane and could therefore not be tested. Upon irradiation, the aromatic ketone **21** formed more byproducts than dimers. This formation of side products limits the reversibility of dimerization, and therefore anthryl ketones are not deemed useful for the envisioned applications.

As can be seen in Figure III.26, 59–99 % dimerization was acquired after 2 h of UVA irradiation (~5 mW cm^{-2}). These dimerization rates are in the order of those previously reported in literature for anthracenes in solution[2] or in polymers having high chain mobility.[3c, 7-9]

As expected, the dimerization rate can be increased by using higher concentrations and light intensity. This is shown by the dimerization of **4** in the melt, using a photo-DSC equipment with a high intensity UV lamp having 12 W cm^{-2} intensity. After 25 min, 72 % conversion was confirmed by ^{1}H NMR (Figure III.27).

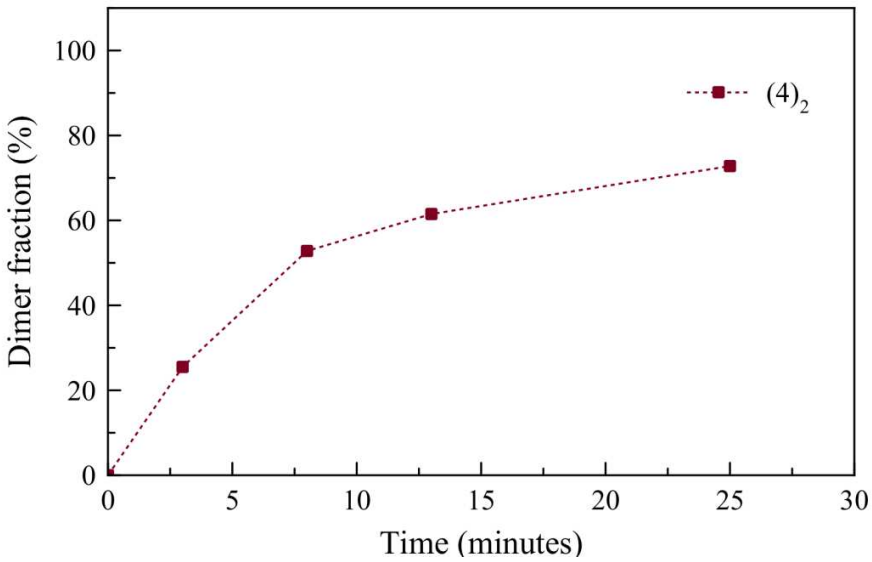

Figure III.27. DSC pans filled with 5 to 10 milligrams of **4** were irradiated at 70 °C with 12 W/cm^{-1} UVA under nitrogen atmosphere in a photo-DSC apparatus (Q2000, TA Instruments), equipped with a photo-calorimetric accessory (PCA Novacure 2100, EXFO). UV light was delivered by a 100-W high-pressure mercury lamp.

2.7 Photochemical dissociation

Upon irradiation of anthracene dimers using short wavelength UV light, anthracene dimers cleave into the parent compounds. This photochemical dissocation of the synthesized derivatives was studied by observing the changes in the UV-vis absorption spectrum (Figure III.28). All samples, in sealed quartz cuvettes, were irradiated using commercial lamps of 254 nm (11 lamps of 9 W each). The derivatives were dissolved in acetonitrile to a concentration of 2.8 µM. This low concentration is required in order to limit competitive dimer formation, resulting in the formation of an equilibrium between anthracenes and dianthracenes. Also, the low concentration is required to allow significant UV-light penetration depth, as not only the dianthracenes but also the formed anthracenes absorb at the irradiation wavelengths. Lastly, too low and too elevated concentrations would both lead to a low signal-to-noise ratio, making measurement results less reliable. Initial attempts using 10, 1 and 0.1 mg L^{-1} concentrations of **(1)$_2$** in acetonitrile proved that 1 mg L^{-1}, or 2.8 µM, is a suitable concentration. The highest signal-to-noise ratio was found when measuring the longitudinal absorption maximum of the formed anthracene (<300 nm).

While it is assumed that the dianthracenes do not form side products, it is known that the formed anthracenes are photo-oxidizable. This was also seen from the measurement results as a fast increase in anthracene concentration due to dianthracene scission, followed by a steady drop due to oxidation until all anthracene is consumed. Therefore, the exclusion of oxygen was attempted by (i) argon flushing and sealing the cuvette sample and (ii) freeze-pump-thaw cycles, followed by solution transfer under inert atmosphere (in a glove box) and sealing the quartz cuvette sample. However, these laborious procedures did not result in significant improvement.

The results for several derivatives **$(1)_2$**, **$(4)_2$**, **$(24)_2$**, **$(28)_2$**, **$(30)_2$ and $(47)_2$** are given in Figure III.29. It should be noted that irradiation occurred in 5 second intervals, including lamp ignition. Therefore, the actual irradiation time is lower and the dimerization thus occurs faster upon continuous irradiation, as can be seen in the differences between intervals of 5 and 15 seconds for **$(47)_2$** in Figure III.29.

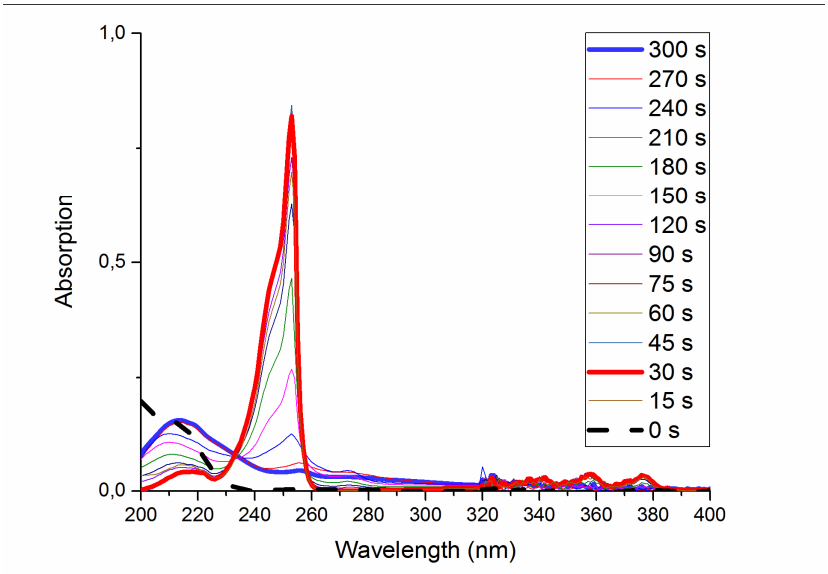

Figure III.28. UV-vis absorption spectrum upon irradiation of a 2.8 µM solution of dianthracene **$(1)_2$** in acetonitrile. UV source: 11 x 254 nm lamps (9 W each)

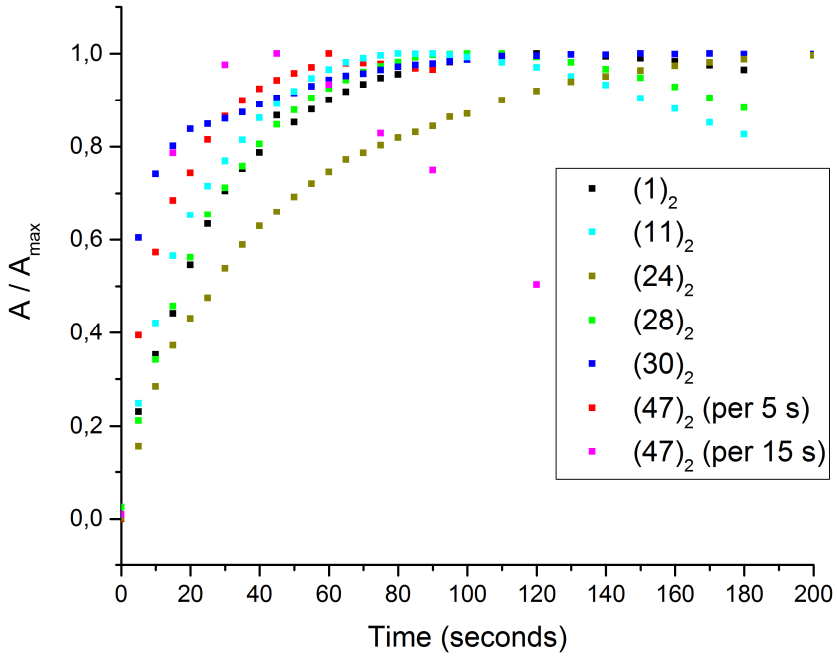

Figure III.29. Change in absorption at anthracene peak maximum upon irradiation of dimer solutions (254 nm). Regular irradiation time intervals were 5 seconds.

Dissociation occurred quickly for all derivatives and maximum scission was accomplished after 1 to 3 minutes. The calculated conversion at this maximum is typically high (~ 94 %), based on the previously measured molar absorptivities. To precisely determine the conversion, a technique less prone to measuring and weighing errors is recommended, such as NMR spectroscopy. However, this is highly impractical as it would require more mass and thus larger solution volumes which need to be concentrated prior to measurement. After reaching the maximum conversion, the anthracene concentration is decreasing. This decrease occurred faster for **(11)$_2$**, **(28)$_2$** and **(47)$_2$**, compared to unsubstituted anthracene dimer **(1)$_2$**. Alternatively, the anthracene content in **(24)$_2$** and **(30)$_2$** decreased much slower, presumably due to higher photo-oxidative stability, making them more suitable for applications involving photoscission.

The (small) differences in photoscission rates are attributed to the difference in absorption properties of the dimers, but to also the absorption maxima of the produced anthracenes. As mentioned above, this reaction was performed using lamps having an emission maximum of 254 nm. This is extremely close to the maximum absorption of the derivatives: **1** has its maximum at 252 nm, **24** at 253 nm, **30** at 254 nm, **47** at 255 nm, **28** and **11** at 256 nm.

It should be noted that these fast scission rates occurred on dilute samples. More concentrated and/or thicker samples would cleave much slower due to the limited penetration depth of the used UV-light.

2.8 Thermal dissociation of dianthracene derivatives

The dissociation of dianthracene to anthracene can occur either photochemically by using UVC (*vide supra*) or thermally by heating.[32] Photochemical dissociation may give rise to an equilibrium between anthracene and dianthracene, as anthracene also absorbs UVC wavelengths. Additionally, UV irradiation may cause side reactions, limiting the use of this reversible system when many cycles are desirable. The thermal dissociation, however, does not result in an equilibrium between anthracene and its dimer and often occurs in a clean and complete way.

The purified anthracene dimers were heated at a constant rate (10 K min^{-1}) and kept isothermal at different temperatures for 10 min under inert atmosphere in a thermogravimetrical analysis (TGA) equipment. Afterwards, the ^{1}H NMR spectra of the samples were measured if no mass loss was observed, ensuring quantitative analysis (Figure III.30). Dissociation occurred without any side reactions for most derivatives.

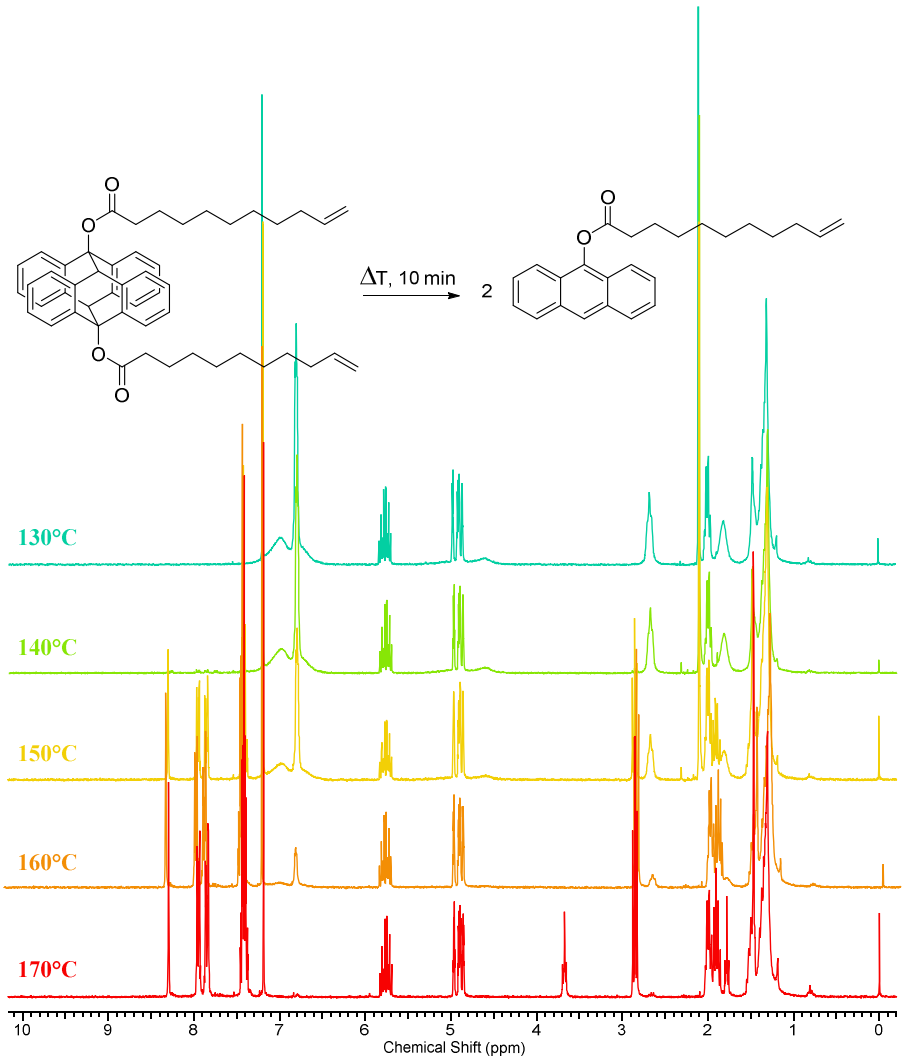

Figure III.30. Thermal dissociation of dimer **(30)$_2$** in bulk.

As observed in Figure III.31, the thermal dissociation of the derivatives greatly depends on the substituent and can thus happen over a broad temperature window (from around 110 to 180 °C). The thermal dissociation results for the dimers **(4)$_2$** and **(47)$_2$** are very similar, which indicates that the further extension of the chain length and change of the end functionality does not influence the thermal dimer dissociation in a significant way. However, the thermal dissociation of the short dimer **(10)$_2$** greatly differs from that of the longer **(11)$_2$**. Indeed, dimer **(11)$_2$** shows a gradual dissociation occurring over a large temperature range (110–160 °C), while **(10)$_2$** remains stable up to 150 °C and is completely dissociated after 10 min at 180 °C. It should also be noted that **(10)$_2$**, unlike **(11)$_2$**, becomes liquid around 182 °C and differential scanning calorimetry shows an endothermic peak at 193 °C immediately

followed by an exothermic signal due to scission of the dimer. Either some dissociation occurred first, forming liquid monomer which dissolves the remaining dimer, or true melting occurs followed by fast dissociation as a result of better thermal contact or lower stability as a liquid. This is in contrast with **(11)$_2$**, which is liquid at 115 °C, before a significant amount of dissociation occurs.

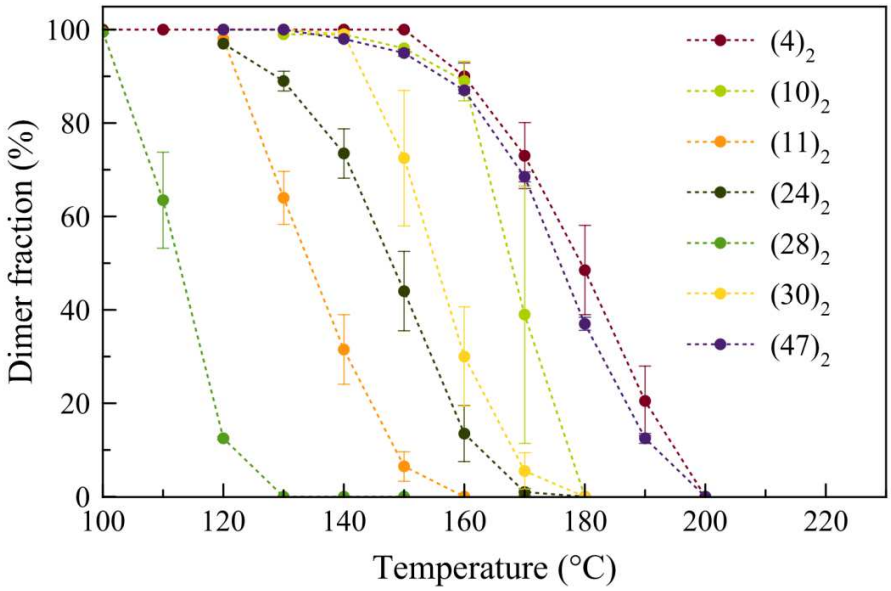

Figure III.31. Thermal dissociation of anthracene dimers in bulk after 10 min, measured by ^{1}H NMR. Error bars show the standard error calculated on 3 repeated experiments per point.

To eliminate the possibly stabilizing effect of crystallinity, the thermal dissociation was also studied in a high boiling solvent solution (tributyrin). The anthracenes generated upon scission were detected by fluorescence spectroscopy of the diluted samples in dichloromethane. As an overnight reaction leads to full scission at the measured temperatures, conversions were normalized to the last (overnight) sample. The rate constants (k) of **(4)$_2$**, **(10)$_2$**, **(11)$_2$**, **(24)$_2$**, **(28)$_2$** and **(30)$_2$** were calculated from the slopes of ln (D_0/D) versus time, in which D is the calculated and D_0 is the original dimer concentration. The ln k values at different temperatures are depicted in the Arrhenius plot in Figure III.32. The reaction rates found for **(10)$_2$** and **(11)$_2$** were identical, confirming that their difference in bulk thermal stability can be ascribed to **(10)$_2$** being crystalline and **(11)$_2$** being liquid upon scission.

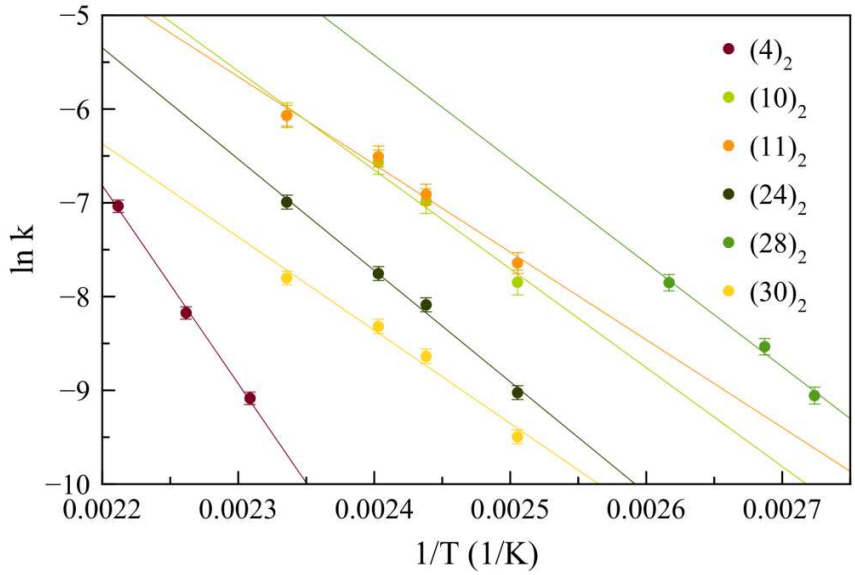

Figure III.32. Arrhenius plot for the thermal dissociation of **(4)$_2$**, **(10)$_2$**, **(11)$_2$**, **(24)$_2$**, **(28)$_2$** and **(30)$_2$** in tributyrin. Error bars show the standard error from linear fitting the concentration vs time.

From the slopes in the Arrhenius plot (Figure III.32), the activation energies E_a for thermal dissociation were calculated, along with the corresponding pre-exponential factor A (Table III.5). Activation energies ranged between ~78 and 176 kJ/mol. However, the variation in lnA is very high (15.5–39.7), which we assumed would be similar for all derivatives, since they should follow the same mechanism. Therefore, and as the uncertainties on the measurements are relatively high, the activation energies should be interpreted with care. In an attempt to achieve more reliable data, plotting was repeated without linearization. Presumably, exponential plotting would lead to smaller errors. The results thereof are also shown in Table III.5. While slightly different results are achieved, the errors and the variation in the pre-exponential factor are still high. The reliability of the current study can be improved in future work by performing more kinetic experiments at different temperatures. Also, the kinetics of the dimer scission should be studied on mixtures of the dimers to exclude the influence of possible impurities in the samples.

Table III.5. Activation energies E_a and lnA-values of thermal scission of anthracene dimers. Error margins show the standard error. *Values determined by fitting exponential plots.

	9-substituent	E_a (kJ/mol)	lnA	E_a (kJ/mol)*	lnA*
(4)$_2$	–CH_2OCOR	176±8	39.7±2.2	178±5.9	40.3±40.8
(10)$_2$	–CH_2R	87.7±9.0	18.7±2.6	95.5±3.1	21.0±20.9
(11)$_2$	–CH_2R	77.8±7.6	15.9±2.2	99.0±6.6	21.8±22.4
(24)$_2$	–COOR	98.7±5.1	20.8±1.5	81.8±5.9	15.9±16.4
(28)$_2$	–OCH_2R	92.0±9.5	21.1±3.1	87.0±5.4	19.6±20.1
(30)$_2$	–OCOR	82.6±8.3	15.5±2.4	71.0±7.1	12.1±12.8

Using the Arrhenius parameters E_a and A from the thermal scission in solution, the results from the bulk scission were simulated and are shown in Figure III.33 and Figure III.34. The calculated theoretical bulk conversions showed good similarity to the actual experimental bulk dissociation. The only exception is for **(10)$_2$**, which is the only derivate having its melting point above the dissociation temperature (as determined using DSC, Figure III.35). It can therefore be assumed that the thermal dissociation of anthracenes is not influenced by concentration, as long as there is no crystallization occurring. The effect of this crystallization on the thermal scission behavior has been further studied in depth by Joost Brancart of the Vrije Universiteit Brussel and the findings thereof are presented in his doctoral thesis.

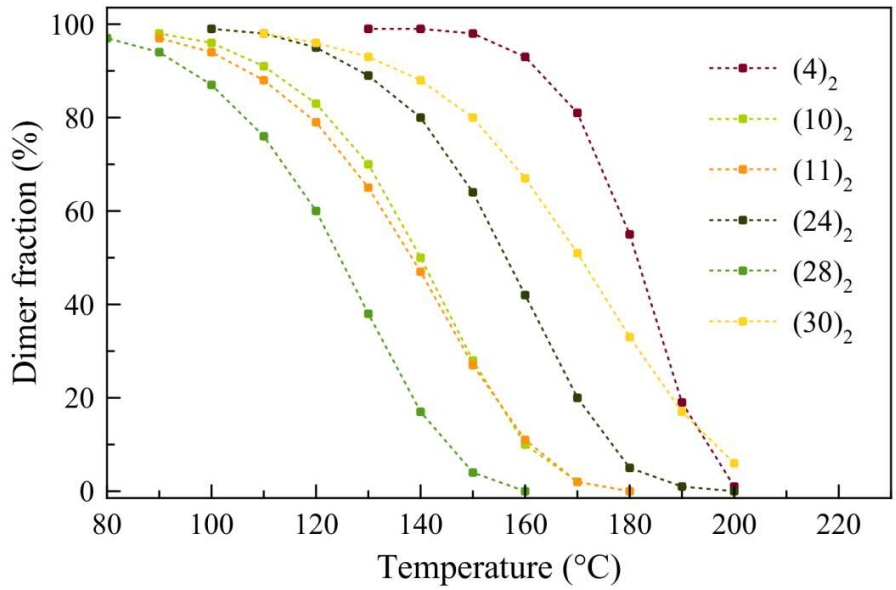

Figure III.33. Bulk thermal dissociation simulation with calculated fractions using the experimentally determined Arrhenius parameters.

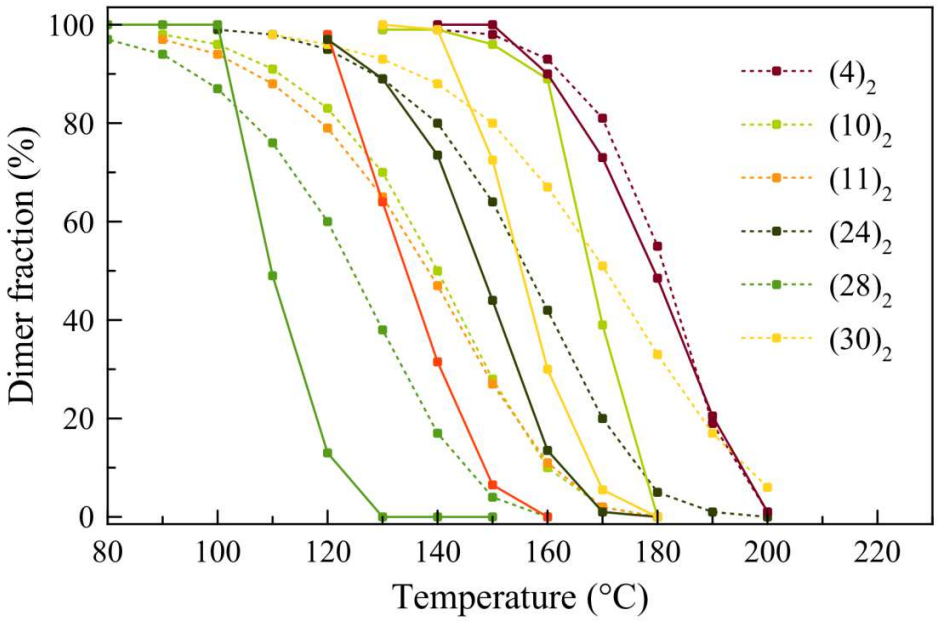

Figure III.34. Experimental (full lines) and calculated (dotted lines) fractions after bulk thermal dissociation.

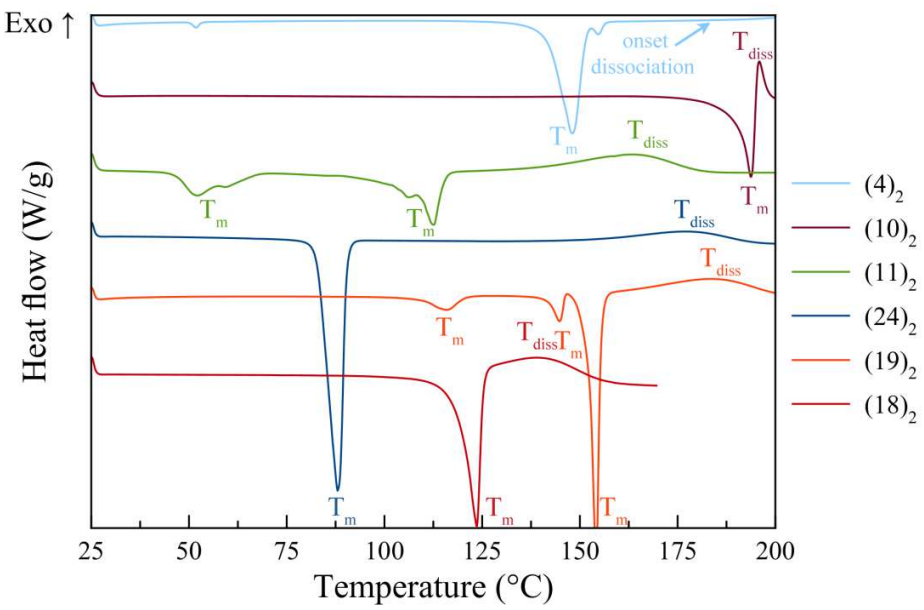

Figure III.35. DSC thermograms from the anthracene derivatives. Indicated are the endothermic melting temperatures (T_m), the thermal dissociation peaks (T_{diss}) and the onset of the scission of **$(4)_2$**.

While the using derived Arrhenius parameters of **$(4)_2$** resulted in a good similarity between the simulated and scission behavior (Figure III.31 and Figure III.33), these data are the least reliable. This is because the scission (in solution) was only studied at three different temperatures. As this compound is incorporated in materials later on, an alternative method to determine the Arrhenius parameters was attempted. This was done based on the proton NMR data of the controlled bulk thermal scission of **$(4)_2$**. The derived pre-exponential factor *ln A* was 32.5, while the activation energy E_a was 148 kJ/mol. These results are lower but more reliable than the previously reported results (*ln A* = 38.7 and E_a = 176 kJ/mol). In Figure III.36, the superior resemblance between the experimental data and the performed simulations using those new data are shown.

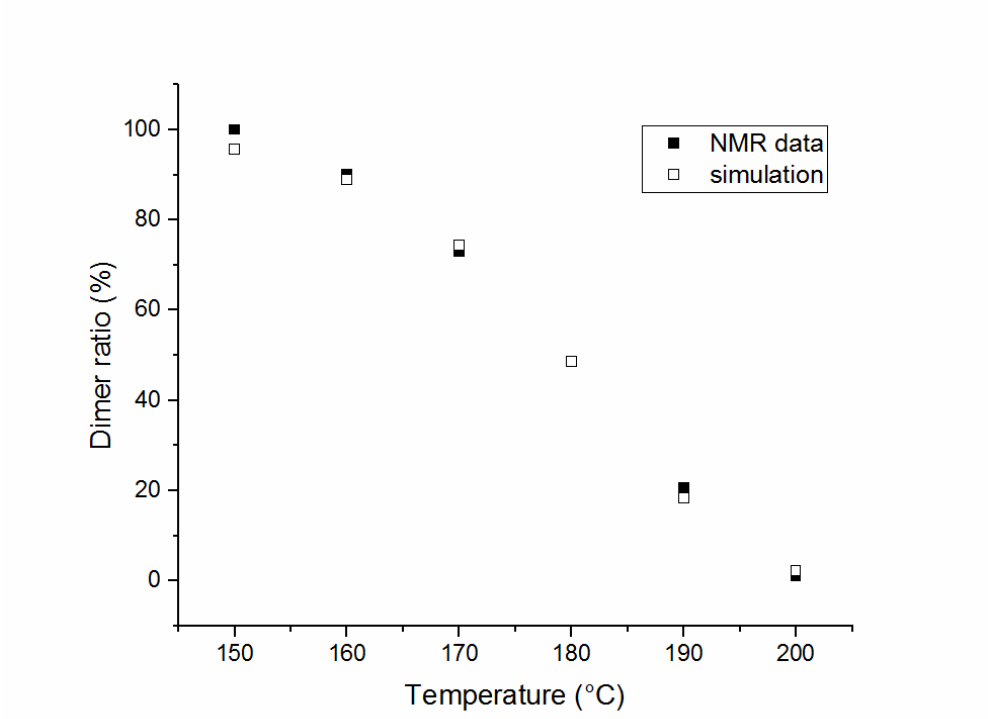

Figure III.36. Percentage of remaining **(4)$_2$** after 10 min of heating at the indicated temperatures, as determined by ^{1}H NMR and simulated using the new derived Arrhenius parameters.

Lastly, it should be noted that there is no correlation found between the thermal and photochemical scission of the studied anthracene dimers. This is explained by the different reaction mechanisms. The photochemical scission occurs via a photostimulated concerted cycloreversion. This mechanism is thermally forbidden and therefore the thermal scission of the dimers must occur in a different, presumably radical fashion.

3 Conclusion

A range of novel 9-substituted functional anthracene compounds, with direct applications in polymer science as reversible bonds or crosslinks, was successfully synthesized in several reaction steps from inexpensive, readily available precursors. Synthesis of derivatives with different substituents (methylene, ether, carbonyl, ester, amide) at the 9-position resulted in a variation in absorption and thus dimerization wavelengths. The (modest) increase in λ_{max} after substitution ranged from 6 to 13 nm. Additionally, the absorption wavelength varies several nanometers when changing the polarity of the

surrounding media. While the influence of the type of substituent on the dimerization kinetics is modest, the thermal dissociation rates of the dimers in bulk and solution changed significantly. By different substitution at the 9-position only, thermal dissociation temperatures could be varied up to 70 °C. This difference in thermal stability of anthracene dimers enables the development of polymer materials having reversible bonds, which are formed by UVA irradiation, and break at a tunable temperature. This research will be presented in a forthcoming chapter.

4 Experimental section

4.1 Materials and instruments

All chemicals were purchased from either Sigma–Aldrich, TCI Europe or Acros Organics and were used as such. IR spectra were recorded with a Perkin Elmer FTIR SPECTRUM 1000 and a PIKE Miracle ATR unit. NMR spectra were recorded with a Bruker AVANCE 300 (300 MHz), Bruker Avance-III (400 MHz) or Bruker DRX500 (500 MHz) NMR spectrometers. LC-MS analyses were performed on an Agilent Technologies 1100 series LC/MSD system with a diode array detector (DAD) and single quad MS. Analytical reversed phase HPLC-analyses were performed with a Phenomenex Luna C18 (2) column (5 μm, 250 mm×4.6 mm) and a solvent gradient (75–100 % acetonitrile in H_2O in 15 min), the eluted compounds were analyzed via UV detection (214 nm). A Mettler-Toledo TGA/SDTA 851e under nitrogen atmosphere was used as an oven for the thermal dissociation of bulk dimers. The uncertainties on the results were calculated as the differences between both results divided by $2\sqrt{2}$. UV dimerization occurred under inert atmosphere in a Metalight Classic from Primotec, with 12 double 365 nm UV lamps of 9 W each (intensity measured in the middle $\sim$ 5 mW cm^{-2}). Higher intensity irradiation occurred in a TA Instruments Q9000 DSC apparatus, equipped with a PCA Novacure 2100 EXFO. The irradiation source was a 100 W mercury lamp, and a 300–500 nm bandpass filter was used. UV–vis absorption was measured with a Specord 200 from AnalitykJena from 200 nm to 600 nm with a speed of 5 nm s^{-1}, a slit of 2 nm and $\Delta\lambda$=0.1 nm. Melting points were determined using the IA9000 melting point apparatus from Electrothermal at a heating rate of 1 °C/min. Differential scanning calorimetry (DSC) was performed using a DSC1/700 Mettler-Toledo apparatus. The used heating rate was 10 K/min and all measurements were done under nitrogen flow. For fluorescence analysis, a Cary Eclipse Fluorescence Spectrophotometer from Agilent with a Xenon flash lamp was used. Excitation occurred at the absorption peak maxima (in chloroform and acetonitrile) or at 372 nm (in ethanol) and the fluorescence

spectrum was measured between 380 nm and 600 nm with a 2.5 nm slit and a scan rate of 600 nm min^{-1}. The concentration of the samples were chosen to ensure a transmission of 95–99 % at the emission wavelength. 9,10-Diphenylanthracene in ethanol (Φ_f = 0.95) was used as standard[33] in the quantum yield calculations using following equation,

$$\Phi = \Phi_R \frac{Int}{Int_R} \frac{1-10^{-A_R}}{1-10^{-A}} \frac{\eta^2}{\eta_R^2}$$

where '*Int*' is the integrated area under the fluorescence curve, A the absorption, η the refractive index of the medium and Φ the fluorescence quantum yield. Subscript 'R' is used when referring to the standard. The uncertainties on the activation energies and pre-exponential factors were determined using Excel's LINEST function.

4.2 Anthracen-9-ylmethyl-undec-10-enoate (4)

A solution of 32.3 g 9-anthracene methanol (0.155 mmol, 1 equiv) in dry pyridine (300 mL) under inert atmosphere was cooled in an ice bath, while adding 50 mL of distilled undecenoyl chloride (0.23 mmol, 1.5 equiv). After a night of stirring at room temperature, the reaction mixture was washed with water (100 mL) and brine (100 mL). The combined aqueous phases were extracted with diethyl ether (3×50 mL). The combined organic phases were dried over magnesium sulfate and concentrated in vacuo. Chromatography over silica, eluting with a gradient from heptane to chloroform, resulted in anthracen-9-ylmethyl-undec-10-enoate **4** as a yellow solid (41.9 g, 71 %); Mp=49–50.5 °C; R_f (25 % $CHCl_3$/hexane) 0.42; ^{1}H NMR (400 MHz, $CDCl_3$): δ (ppm)=1.15–1.40 (m, 10H, $CH_2CH_2CH_2CH_2$), 1.62 (quin, *J*=7.2 Hz, 2H, $COCH_2CH_2$), 2.02 (q, *J*=7.3 Hz, 2H, CH_2CHCH_2), 2.34 (t, *J*=7.5 Hz, 2H, $COCH_2CH_2$), 4.90–5.03 (m, 2H, CH_2CHCH_2), 5.73–5.88 (m, 1H, CH_2CHCH_2), 6.17 (s, 2H, CCH_2O), 7.47–7.54 (m, 2H, $CH_2CCCHCHCH$), 7.56–7.61 (m, 2H, $CH_2CCCHCHCH$), 8.05 (d, *J*=8.4 Hz, 2H, $CHCCHCH$), 8.35 (dd, *J*=8.9 Hz, *J*=0.8 Hz, 2H, $CCCHCH$), 8.52 (s, 1H, $CCHC$); ^{13}C NMR (100 MHz, $CDCl_3$): δ (ppm)=25.0 (CH_2), 28.9 (CH_2), 29.0 (CH_2), 29.1 (CH_2), 29.2 (CH_2), 29.3 (CH_2), 33.8 (CH_2), 34.3 (CH_2), 58. 7 (CH_2), 114.1 (CH_2), 124.0 (CH), 125.1 (CH), 126.4 (C), 126.6 (CH), 129.1 (CH), 131.1 (C), 131.4 (C), 139.2 (CH), 174.2 (C); IR ν_{max} cm^{-1}: 2922, 2848, 1726, 1386, 1318, 1278, 1244, 1210, 1158, 1060; LC-MS (*m*/*z*) 191.1 $[C_{15}H_{11}]^+$; GC–MS (*m*/*z*) 191.1 $[C_{15}H_{11}]^+$, 374.2 $[M]^+$; HRMS (*m*/*z* for $[MH]^+$): calcd: 375.232; found: 375.231; *only traces of the molecular ion were found in LC-MS*

and HRMS, probably due to very efficient fragmentation forming $[C_{15}H_{11}]^+$. *In GC–MS both the molecular ion and fragment product were found.*

4.3 1-(Anthracene-9-yl)dodec-11-en-1-ol (9)

In a 250 mL flask under inert atmosphere, bromine (3.3 mL, 0.064 mol, 0.6 equiv) was added to magnesium flakes (5.4 g, 0.22 mol, 2 equiv). The mixture was heated to reflux for 30 min, after which the flask was cooled in an ice bath. Dry diethyl ether (25 mL) was quickly added, followed by 11-bromo-undec-1-ene (25 mL, 0.11 mol, 1 equiv). The reaction mixture was heated to reflux for 1 h until the magnesium flakes had disappeared. To the grignard reagent (0.11 mol, 1.2 equiv) a solution of anthraldehyde (19 g, 0.092 mol, 1 equiv) in dry diethyl ether (50 mL) was added until the reaction stopped. The reaction mixture was washed with a saturated ammonium chloride solution (50 mL), after which it was extracted with ether. The collected organic phases were dried with sodium sulfate and concentrated in vacuo. Purification by chromatography over silica (eluent: chloroform) was required to obtain the pure 1-(anthracene-9-yl)dodec-11-en-1-ol **9** as a yellow oil (11.3 g, 31 mmol, 34 %); R_f($CHCl_3$) 0.5; ^{1}H NMR (300 MHz, $CDCl_3$): δ (ppm)=1.22–1.76 (m, 14H, $CH_2CH_2CH_2$), 1.54–1.73 (m, 2H, $CH_2CH_2CH_2$), 2.03 (q, *J*=7.3 Hz, 2H, CH_2CH_2CH), 4.90–5.04 (m, 2H, $CHCH_2$), 5.75–5.87 (m, 1H, CH_2CHCH_2), 6.27 (dd, *J*=8.3 Hz, *J*=6.1 Hz, 1H, CH_2CHOH), 7.43–7.52 (m, 4H, $CHCHCHCH$), 7.97–8.04 (m, 2H, $CCHCH$), 8.38 (s, 1H, $CCHC$), 8.53–8.83 (m, 2H, $CCCHCH$); IR ν_{max} cm^{-1}: 2924, 2852, 1722, 1454, 1382, 1344, 1292, 1156, 1054; LC-MS (*m*/*z*) 343.2 $[M-|-OH]^+$; HRMS (*m*/*z* for $[M-|-OH]^+$): calcd: 343.2426; found: 343.2427.

4.4 9-(But-3-en-1-yl)anthracene (10)

9-Anthraldehyde (10.8 g, 52.4 mmol, 1 equiv) was dissolved in dry tetrahydrofuran (60 mL), put under inert atmosphere and cooled with an ice bath. Allylmagnesium chloride solution was slowly added (26.4 mL, 2 M in THF, 52.8 mmol, 1.01 equiv). The reaction mixture stirred at room temperature for 1 h. Ammonium chloride was added and the reaction mixture was dried using sodium sulfate. The crude 1-(anthracen-9-yl)but-3-en-1-ol **8** was obtained after concentration in vacuo.

The crude 1-(anthracen-9-yl)but-3-en-1-ol (13 g, 52 mmol, 1 equiv), was dissolved in dichloromethane (60 mL). To the solution, triethylsilane (9.75 mL, 61 mmol, 1.15 equiv) was added. The reaction mixture was cooled with an ice bath and trifluoroacetic acid (6.5 mL, 83 mmol, 1.6 equiv) was added. The reaction mixture was stirred overnight at room temperature and concentrated in vacuo. The crude

product was purified using chromatography over silica (gradient: heptane; heptane:chloroform 3:2) to give **10** as a yellow solid. Mp=67–68 °C; R_f ($CHCl_3$) 0.62; ^{1}H NMR (500 MHz, $CDCl_3$): δ (ppm) = 2.55–2.61 (m, 2H, CCH_2CH_2CH), 3.70–3.75 (m, 2H, CCH_2CH_2CH), 5.10 (dd, *J*=10.1 Hz, *J*=1.6 Hz, 1H, CH_2CHCH_2), 5.22 (dq, *J*=17.1 Hz, *J*=1.7 Hz, 1H, CH_2CHCH_2), 6.08 (ddt, *J*=17 Hz, *J*=10.3 Hz, *J*=6.6 Hz, 1H, CH_2CHCH_2), 7.47–7.50 (m, 2H, $CH_2CCCHCH$), 7.50–7.55 (m, 2H, $CH_2CCCHCHCH$), 8.02 (d, *J*=8.2 Hz, 2H, CHCCHCH), 8.27 (d, *J*=8.7 Hz, 2H, $CH_2CCCHCH$), 8.36 (s, 1H, CCHC);^{13}C NMR (125 MHz, $CDCl_3$): δ (ppm)=27.4 (CH_2), 35.1 (CH_2), 115.0 (CH_2), 124.4 (CH), 124.8 (CH), 125.5 (CH), 125.8 (CH), 129.2 (CH), 129. 6 (C), 131.7 (C), 134.2 (C), 138.3 (CH); IR ν_{max} cm^{-1}: 3054, 2896, 1622, 1436, 1350, 1318, 1242, 1154, 1006; GC–MS (*m*/*z*) 232 $[M]^+$.

4.5 9-(Dodec-11-en-1-yl)anthracene (11)

Crude **9** (9.24 g, 75% pure, 19.2 mmol, 1 equiv) was dissolved in 30 mL dichloromethane. To the solution, triethylsilane (4.75 mL, 29.4 mmol, 1.5 equiv) was added. The reaction mixture was cooled in an ice bath and trifluoroacetic acid (3.2 mL, 42 mmol, 2.2 equiv) was slowly added. The reaction mixture was stirred overnight at room temperature and concentrated in vacuo. The crude product was purified using chromatography over silica (eluent dichloromethane:hexane). 4.64 g pure **11** was obtained as a yellow oil (53 %). ^{1}H NMR (500 MHz, $CDCl_3$): δ(ppm) = 1.27–1.47 (12H, $CH_2CH_2CH_2$), 1.6 (quin, *J*=15.2 Hz, *J*=7.4 Hz, 2H, $CH_2CH_2CH_2$), 1.83 (quin, *J*=15.8 Hz, *J*=7.9 Hz, 2H, $CCH_2CH_2CH_2$), 2.06 (q, *J*=7.9 Hz, 2H, CH_2CH_2CH), 3.61 (t, *J*=8.2 Hz, 2H, CCH_2CH_2), 4.95 (ddt, *J*=10.2 Hz, *J*=2.2 Hz, *J*=1.1 Hz, 1H, CH_2CHCH_2), 5.02 (dq, *J*=17.1 Hz, *J*=1.8 Hz, 1H, CH_2CHCH_2), 5.84 (ddt, *J*=17 Hz, *J*=10.2 Hz, *J*=6.7 Hz, 1H, CH_2CHCH_2), 7.45–7.54 (m, 4H, CCHCHCHCHC), 8.02 (d, *J*=7.8 Hz, 2H, CHCCHCH), 8.28 (d, *J*=8.9 Hz, 2H, $CH_2CCCHCH$), 8.34 (s, 1H, CCHC);^{13}C NMR (125 MHz, $CDCl_3$): δ (ppm)=28.1 (CH_2), 29.0 (CH_2), 29.2 (CH_2), 29.5 (CH_2), 29.6 (CH_2), 29. 7 (CH_2), 30.4 (CH_2), 31.4 (CH_2), 33.8 (CH_2), 114.1 (CH_2), 124.5 (CH), 124.8 (CH), 125.3 (CH), 125.5 (CH), 129.2 (CH), 129.5 (C), 131.7 (C), 135.5 (C), 139.3 (CH); IR ν_{max} cm^{-1}: 2920, 2850; GC–MS (*m*/*z*) 191 $[C_{15}H_{11}]^+$, 344 $[M]^+$.

4.6 11-(Anthracen-9-yl)-undec-10-en-1-ol (18)

In a 250 mL flask, 9-bromoanthracene (10 g, 39 mmol, 1 equiv.) was dissolved in dimethylacetamide (40 mL) and triethylamine (40 mL). The reaction mixture was placed under inert atmosphere and heated to 100 °C. To this solution, 10-undecenol (8.5 mL, 42 mmol, 1.1 equiv.), palladium acetate (110 mg, 4.9

mmol, 0.125 equiv.) and tris(*ortho*-tolyl)phosphine (220 mg, 7.2 mmol, 0.185 equiv.) are added. After overnight stirring at 100 °C, TLC confirmed quantitive reaction of the 9-bromoanthracene. After cooling to room temperature, the reaction mixture was washed with water (40 mL), and extracted with diethyl ether (3 x 40 mL). The combined organic phases were dried on magnesium sulfate and concentrated *in vacuo*. Purification by column chromatography (gradient: hexane:dichloromethane 1:3 to dichloromethane) resulted in the pure 11-(anthracen-9-yl)unde-10-en-1-ol as a brown-red oil (5.8 g, 16.7 mmol, 43 %). ^{1}H NMR (500 MHz, $CDCl_3$): δ (ppm) = 1.03 – 2.11 (m, 14H, C*H*$_2$), 2.43 (m, 2H, CHCHC*H*$_2$), 3.55 (m, 2H, C*H*$_2$OH), 5.26-5.76 (m, 2H, AnC*H*C*H*), 7.40 (m, 4H, CHC*H*C*H*CH), 7.93 (d, 2H, CHCC*H*CH), 8.19 (d, 2H, CCC*H*CH), 8.27 (s, 1H,CC*H*C); LC-MS (*m/z*) 374.2 $[MH]^+$; HR-MS (*m/z* for $[MH]^+$): calcd.: 347.2369; found: 347.2368

4.7 11-(Anthracen-9-yl)undec-10-enoic acid (19)

In a 100 mL flask, 9-bromoanthracene (6 g, 23 mmol, 1 equiv.) was dissolved in dimethylacetamide (24 mL) and triethylamine (24 mL). The reaction mixture was placed under inert atmosphere and heated to 100 °C. To this solution, 10-undecenoic acid (4.7 mL, 26 mmol, 1.1 equiv.), palladium acetate (60 mg, 2.9 mmol, 0.125 equiv.) and tris(*ortho*-tolyl)phosphine (120 mg, 4.3 mmol, 0.185 equiv.) are added. After overnight stirring at 100 °C, TLC confirmed quantitive reaction of the 9-bromoanthracene. After cooling to room temperature, the reaction mixture was washed with water (40 mL), and extracted with diethyl ether (3 x 20 mL). The combined organic phases were dried on magnesium sulfate and concentrated *in vacuo*. Purification by column chromatography (eluent: chloroform: methanol 98:2) resulted in the pure 11-(anthracen-9-yl)unde-10-enoic acid as a brown-red oil (3.3 g, 9.1 mmol, 39 %). ^{1}H-NMR (300 MHz, $CDCl_3$): delta (ppm) = 1.03 – 2.06 (m, 12H, C$\underline{H}_2$), 2.27 (m, 4H, CHCHC*H*$_2$ + C*H*$_2$CO), 4.89 (m, 1H, AnCHC*H*), 5.73 (m, 1H, AnC*H*CH), 7.40 (m, 4H, CHC*H*C*H*CH), 7.93 (d, 2H, CHCC*H*CH), 8.19 (d, 2H, CCC*H*CH), 8.26 (s, 1H,CC*H*C); LC-MS (*m/z*) 360.2 $[MH]^+$

4.8 1-(Anthracen-9-yl)dodec-11-en-1-on (20) attempts

In a 100 mL flask, undecenoyl chloride (3.0 mL, 16 mmol, 1 equiv.) was mixed with anthracene (2.79 g, 16 mmol, 1 equiv.) and aluminum chloride (4.14 g, 31.4 mmol, 2 equiv.) in anhydrous carbon disulfide (50 mL). The flask was cooled using an ice bath and the reaction mixture was stirred for 5 minutes. Then, the reaction was quenched in ice and sodium bicarbonate. The aqueous phase were extracted with diethyl ether and dried using sodium sulfate. Concentration in vacuo resulted in the starting compounds.

In a 50 mL flask, undecenoyl chloride (20 mL, 105 mmol, 1 equiv.) was mixed with anthracene (18.6 g, 105 mmol, 1 equiv.) and aluminum chloride (27.6 g, 210 mmol, 2 equiv.) in anhydrous carbon disulfide (150 mL). After 1 hour of stirring at room temperature, no reaction was observed. Similar synthesis in nitrobenzene and dichloromethane also gave no results.

4.9 1-(Anthracen-9-yl)dodec-11-en-1-one (21)

Oxalylchloride (0.30 mL, 3 mmol, 1.1 equiv) in dry dichloromethane (5 mL) in a 50 mL flask, was cooled to −78 °C, after which a solution of dimethylsulfoxide (0.50 mL, 6.1 mmol, 2.2 equiv) in dry dichloromethane (5 mL) was added. After 2 min of stirring, a solution of 1-(anthracene-9-yl)dodec-11-en-1-ol **9** (1.0 g, 2.8 mmol, 1 equiv) in dry dichloromethane (10 mL) was added dropwise over 5 min. The reaction mixture was stirred for 15 min, and an excess of triethyl amine (2 mL) was added. The mixture was stirred for another 5 min and was warmed up to room temperature. Water (50 mL) was added, and the mixture was extracted with dichloromethane (3×50 mL). The combined organic phases were washed respectively with brine (20 mL), water (20 mL), 5% bicarbonate solution (20 mL) and water (20 mL). The combined organic phases were dried on magnesium sulfate and concentrated in vacuo to a red oil (5.8 g, 2.8 mmol, >99 %); ^{1}H NMR (500 MHz, $CDCl_3$): δ (ppm) = 1.17–1.70 (m, 12H, $CH_2CH_2CH_2$), 1.89 (quin, J=7.5 Hz, 2H, CH_2CH_2CO), 2.04 (q, J=6.8 Hz, 2H, CH_2CHCH_2), 3.07 (t, J=7.5 Hz, 2H, CH_2CO), 4.92–4.96 (m, 1H, $CHCH_2$), 4.97–5.04 (m, 1H, $CHCH_2$), 5.82 (ddt, J=17 Hz, J=10.3 Hz, J=6.7 Hz, 1H, $CHCH_2$), 7.47–7.54 (m, 4H, $CHCHCHCH$), 7.77–7.83 (m, 2H, $CHCHCHCH$), 8.02–8.06 (m, 2H, $CCCHCH$), 8.49 (s, 1H, $CCHC$); ^{13}C NMR (125 MHz, $CDCl_3$): δ (ppm)=23.9 (CH_2), 29.0 (CH_2), 29.1 (CH_2), 29.3 (CH_2), 29.5 (CH_2), 33.8 (CH_2), 46.5 (CH_2), 114.2 (CH_2), 124.4 (CH), 125.5, (CH), 126.7 (CH), 127.0 (C), 127.2 (CH), 128.1 (CH), 128.8 (CH), 131.1 (C), 134.1, (CH), 136.9 (C), 139.2 (CH), 210.6 (C); IR ν_{max} cm^{-1}: 2924, 2852, 1696, 1444, 1160; LC-MS (m/z) 359.2 $[MH]^+$; HRMS (m/z for $[MH]^+$): calcd: 359.2371; found: 359.2363.

4.10 Undec-10-en-1-yl anthracene-9-carboxylate (24)

9-Anthracenecarboxylic acid (1.50 g, 6.75 mmol, 1 equiv) was dissolved in thionyl chloride (20 mL). A drop of dimethylformamide was added and the solution was heated to reflux for 2 h according to literature.[19] The excess thionyl chloride was removed from **13** in vacuo after cooling to room temperature.

Dry dichloromethane (20 mL) and 10-undecen-1-ol (1.5 mL, 7.5 mmol, 1.1 equiv) were added to **23** and the reaction mixture was stirred for 1 h in an ice bath. The ice bath was then removed and the reaction mixture was stirred overnight at room temperature. Potassium carbonate (1.00 g, 17.5 mmol, 1.1 equiv) was added and the reaction was stirred for another 3 h. The solution was filtered over a silica plug and concentrated in vacuo. After column chromatography over silica (eluent: chloroform), the pure undec-10-en-1-yl anthracene-9-carboxylate **14** was acquired as a yellow oil (1.13 g, 3.02 mmol, 45 %); R_f ($CHCl_3$) 0.66; ^{1}H NMR (500 MHz, $CDCl_3$): δ(ppm) = 1.24–1.44 (m, 10H, $CH_2CH_2CH_2$), 1.50 (quin, *J*=7.8 Hz, 2H, $OCH_2CH_2CH_2$), 1.89 (quin, *J*=7.5 Hz, 2H, OCH_2CH_2), 2.04 (q, *J*=6.9 Hz, 2H, CH_2CHCH_2), 4.63 (t, *J*=6.8 Hz, 2H, OCH_2CH_2), 4.94 (dt, *J*=10.2 Hz, *J*=1 Hz, 1H, CH_2CHCH_2), 5.00 (dq, *J*=17.1 Hz, *J*=1.7 Hz, 1H, CH_2CHCH_2), 5.84 (ddt, *J*=17 Hz, *J*=10.3 Hz, *J*=6.7 Hz, 1H, CH_2CHCH_2), 7.48–7.52 (m, 2H, CHCHCH), 7.53–7.57 (m, 2H, CHCHCH), 8.05 (t, *J*=9.9 Hz, 4H, CCCHCH), 8.54 (s, 1H, CCHC); ^{13}C NMR (125 MHz, $CDCl_3$): δ(ppm)=26.1 (CH_2), 28.8 (CH_2), 28.9 (CH_2), 29.1 (CH_2), 29.2 (CH_2), 29.4 (CH_2), 29.5 (CH_2), 33.8 (CH_2), 66.0 (CH_2), 114.2 (CH_2), 125.1 (CH), 125.5 (CH), 126.9 (CH), 128.2 (C), 128.4 (C), 128.6 (CH), 129.2 (CH), 131.0 (C), 139.3 (CH), 169.8 (C); IR ν_{max} cm^{-1}: 2922, 2850, 1718, 1446, 1288, 1200; LC-MS (*m*/*z*) 375.3 $[MH]^+$; HRMS (*m*/*z* for $[MH]^+$) calcd: 375.2324; found: 375.2335.

4.11 N-Butylanthracene-9-carboxamide (25)

9-Anthracenecarboxylic acid (1.50 g, 6.75 mmol, 1 equiv) was dissolved in thionyl chloride (20 mL). A drop of dimethylformamide was added and the solution was heated to reflux for 2 h according to literature.[19] The excess thionyl chloride was removed from **23** in vacuo after cooling to room temperature.

Dry dichloromethane (30 mL) and butyl amine (1.08 g, 14.9 mmol, 2.2 equiv) are added to **23** and the reaction mixture was stirred for 1 h in an ice bath. The reaction mixture was then stirred at room temperature for 3 days. The reaction mixture was concentrated in vacuo. The product was purified by chromatography over silica (eluent: chloroform with 1% methanol), giving product **25** (0.97 g, 3.5 mmol, 52%) as a white solid; Mp>250 °C *(solid became dark brown, signifying decomposition before melting)*; ^{1}H NMR (500 MHz, $CDCl_3$): δ (ppm)=1.03 (t, *J*=7.3 Hz, 3H, CH_3), 1.51 (sxt, *J*=7.5, 2H, CH_2CH_3), 1.74 (quin, *J*=7.5 Hz, 2H, $CH_2CH_2CH_3$), 3.72 (td, *J*=7.2 Hz, *J*=6 Hz, 2H, $NHCH_2$), 6.03 (1H, $CONHCH_2$), 7.47–7.57 (m, 4H, CCHCH), 8.02 (d, *J*=8.4 Hz, 2H, CCHCH), 8.09 (d, *J*=8.2 Hz, 2H, CCHCH), 8.49 (s, 1H, CCHC); ^{13}C NMR (125 MHz, $CDCl_3$): δ (ppm)=13.8 (CH_3), 20.3 (CH_2), 31.8

(CH_2), 40.0 (CH_2), 125.1 (CH), 125.5 (CH), 126.7 (CH), 128.0 (C), 128.2 (CH), 128.5 (CH), 131.1 (C), 132.2 (C), 169.5 (C); IR ν_{max} cm^{-1}: 3212, 3044, 2954, 2930, 2872, 2368, 2160, 2024, 1978, 1612, 1568, 1470, 1376, 1292, 1254, 1226, 1156, 1080, 1012; LC-MS (*m*/*z*) 278.2 $[MH]^+$; HRMS (*m*/*z* for $[MH]^+$) calcd: 278.1545; found: 278.1552.

4.12 6-(Anthracen-9-yloxy) hexan-1-ol (27)

In a 500 mL flask equipped with a Dean–Stark water separator, 10.0 g anthrone (51.5 mmol, 1 equiv) was dissolved in 250 mL toluene. 1,6-hexanediol (60.3 g, 515 mmol, 10 equiv) and 2 mL sulfuric acid (≥95%) were added and the solution was heated to reflux. The reaction mixture was stirred overnight and the reaction was monitored by thin layer chromatography. After cooling, the precipitated excess 1,6-hexanediol was removed by filtration and the filtrate was washed with a saturated aqueous sodium bicarbonate solution (300 mL) and water (300 mL). The combined aqueous phases were extracted with diethyl ether, the combined organic phases were dried over magnesium sulfate and concentrated in vacuo. To obtain pure 6-(anthracen-9-yloxy) hexan-1-ol **27** (8.2 g, 54 %) as a yellow-orange oil, the dried mixture was purified via chromatography on silica (eluent: dichloromethane/hexane); R_f (CH_2Cl_2/hexane) 0.16; ^{1}H NMR (400 MHz, $CDCl_3$): δ (ppm) = 1.50–1.60 (m, 2H, $CH_2CH_2CH_2$), 1.65–1.77 (m, 4H, $CH_2CH_2CH_2$), 2.08 (quin, *J*=7.5 Hz, 2H, CH_2CH_2O), 3.65 (t, *J*=6.5 Hz, 2H, CH_2OH), 4.14 (t, *J*=6.7 Hz, 2H, AnthrOCH_2), 7.46–7.53 (m, 4H, CHC*H*C*H*CH), 7.98–8.02 (m, 2H, CHCC*H*CH), 8.12 (s, 1H, CC*H*C), 8.28–8.32 (m, 2H, CCC*H*CH); ^{13}C NMR (100 MHz, $CDCl_3$): δ (ppm)=25.8 (CH_2), 26.1 (CH_2), 30.7 (CH_2), 32.8 (CH_2), 63.0 (CH_2), 76.0 (CH_2), 122.0 (CH), 122.4 (CH), 124.8 (C), 125.1 (CH), 125.5 (CH), 128.5 (CH), 132.5 (C), 151.5 (C); IR ν_{max} cm^{-1}: 3315, 2934, 2854, 1676, 1590, 1442, 1416, 1338, 1282, 1170, 1084, 1008; LC-MS (*m*/*z*): 295.1 $[MH]^+$; HRMS (*m*/*z* for $[MH]^+$): calcd: 295.1693; found: 295.1691.

4.13 12-(Anthracen-9-yloxy) dodecan-1-ol (28)

In a 2 L flask equipped with a Dean–Stark water separator, 12.0 g anthrone (61.7 mmol, 1 equiv) was dissolved in 1 L toluene. 1,12-dodecanediol (125 g, 617 mmol, 10 equiv) and 2.5 mL sulfuric acid (≥95%) were added and the solution was heated to reflux. The reaction mixture was stirred overnight and the reaction was monitored by thin layer chromatography. After cooling, the precipitated excess of 1,12-dodecanediol was removed by filtration and the filtrate was washed with a saturated aqueous sodium bicarbonate solution (300 mL) and water (300 mL). The combined aqueous phases were

extracted with diethyl ether, the combined organic phases were dried over magnesium sulfate and concentrated in vacuo. To obtain purified 12-(anthracen-9-yloxy) dodecan-1-ol **28** (17.7 g, 75.3 %) as a yellow-orange oil, the dried mixture was purified via chromatography on silica (eluent: CH_2Cl_2); R_f (CH_2Cl_2) 0.13; ^{1}H NMR (400 MHz, $CDCl_3$): δ (ppm)=1.26–1.51 (m, 14H, $CH_2CH_2CH_2$), 1.54–1.62 (m, 2H, $CH_2CH_2CH_2$), 1.68 (quin, J=7.5 Hz, 2H, $CH_2CH_2CH_2$), 2.07 (quin, J=7.4 Hz, 2H, CH_2CH_2OH), 3.65 (t, J=6.7 Hz, 2H, CH_2OH), 4.21 (t, J=6.7 Hz, 2H, AnthrOCH_2), 7.45–7.52 (m, 4H, CH*CH*CH*CH*CH), 7.98–8.03 (m, 2H, CHCC*H*CH), 8.22 (s, 1H, CC*H*C), 8.29–8.34 (m, 2H, CCC*H*CH); ^{13}C NMR (100 MHz, $CDCl_3$): δ (ppm)=25.8 (CH_2), 26.3 (CH_2), 29.5 (CH_2), 29.6 (CH_2), 29.7 (CH_2), 30.7 (CH_2), 32.8 (CH_2), 63.1 (CH_2), 76.2 (CH_2), 122.0 (CH), 122.5 (CH), 124.8 (C), 125.0 (CH), 125.5 (CH), 128.4 (CH), 132.5 (C), 151.6 (C); LC-MS (m/z) 379.20 $[MH]^+$; HRMS (m/z for $[MH]^+$) calcd: 379.2633; found: 379.2633.

4.14 9-(Undec-10-en-1-yloxy)anthracene (29) attempt

In a 100 ml flask, equipped with a Dean-Stark apparatus, anthrone (1 g, 5.15 mmol, 1 equiv.) dissolved in toluene (75 mL) was added. Undecenol (8.77 g, 515 mmol, 10 equiv.) were added to this solution. As catalyst, concentrated sulfuric acid (0.5 mL) or *p*-toluenesulfonic acid (0.5 g) was added. The solution was overnight stirred and heated to reflux conditions. TLC runs indicated the formation of a large amount of side products.

4.15 Anthracen-9-yl undec-10-enoate (30)

10 g of anthrone (3.4 mmol, 1 equiv) was dissolved in 20 mL toluene and 0.86 mL of triethyl amine (4.1 mmol, 1.2 equiv). The solution was heated to reflux for 1 h. After cooling to room temperature, 0.87 mL undecenoyl chloride was added (4.1 mmol, 1.2 equiv) and the reaction was heated to reflux for 2 h. The solvent was removed in vacuo, and the crude product was purified by column chromatography (eluent: $CHCl_3$/hexane) to a light yellow oil that crystallized to a white powder (1.32 g, 2.85 mmol, 84 %). Mp = 58–60 °C; ^{1}H NMR (500 MHz, $CDCl_3$): δ (ppm) = 1.24–1.49 (m, 10H, $CH_2CH_2CH_2$), 1.59 (quin, J=7.4 Hz, 2H, $CH_2CH_2CH_2$), 2.00 (quin, J=7.6 Hz, 2H, $COCH_2CH_2$), 2.09 (q, J=7.2 Hz, 2H, CH_2CHCH_2), 2.95 (t, J=7.6 Hz, 2H, $COCH_2CH_2$), 4.96 (ddt, J=10.1 Hz, J=2.1 Hz, J=1.2 Hz, 1H, CH_2CHCH_2), 5.03 (dq, J=17.1 Hz, J=1.8 Hz, 1H, CH_2CHCH_2), 5.85 (ddt, J=17 Hz, J=10.3 Hz, J=6.7 Hz, 1H, CH_2CHCH_2), 7.47–7.54 (m, 4H, CCHC*H*) 7.94 (d, J=8.2 Hz, 2H, CHCC*H*CH), 8.03 (d, J=8.1 Hz, 2H, CCC*H*CH), 8.38 (s, 1H, CC*H*C); ^{13}C NMR (125 MHz, $CDCl_3$): δ(ppm)=25.3 (CH_2),

28.9 (CH_2), 29.1 (CH_2), 29.3 (CH_2), 29.4 (CH_2), 29.4 (CH_2) 33.8 (CH_2), 34.3 (CH_2), 114.2 (CH_2), 121.4 (CH), 124.0 (C), 124.7 (CH), 125.6 (CH), 126.2 (CH), 128.5 (CH), 131.9 (C), 139.2 (CH), 142.1 (C), 172.4 (C); IR ν_{max} cm^{-1}: 3326, 2926, 2854, 1454, 1338, 1292, 1254, 1226, 1164, 1118, 1052; LC-MS (*m*/*z*) 378.3 $[MNH_4]^+$; HRMS (*m*/*z* for $[MNH_4]^+$): calcd: 378.2433; found: 378.2428.

4.16 S-(11-Hydroxyundecyl) ethane thioate (33)

In a Schlenk tube of 20 mL, 10-undecenol (10 mL, 50 mmol, 1 equiv.) was added to thioacetic acid (4.7 mL, 50 mmol, 1 equiv.) and dimethoxy-2-phenylacetophenone (DMPA) (130 mg, 0.5 mmol, 0.01 equiv.). The tube was shaken well to mix the reagents. The tube was irradiated with UV light for 1 hour (365 nm, 12 x 9W). The crude product appeared as white crystals and was not purified before use. ^{1}H NMR (300 MHz, $CDCl_3$): δ (ppm) = 0.81 (m, 3H, C*H*$_3$), 1.29 (m, 16H, C*H*$_2$), 1.50 (m, 2H, C*H*$_2$CH$_2$OH), 2.79 (t, 2H, C*H*$_2$SCOCH$_3$), 3.57 (t, 2H, C*H*$_2$OH), 4.89 (s, 1H, CH$_2$O*H*).

4.17 11-Mercaptoundecan-1-ol (35)

In a flask of 50 mL, the crude S-(11-hydroxyundecyl)ethanethioate (12.3 g, 50 mmol, 1 equiv.) was dissolved in tetrahydrofuran (20 mL) and hexane (10 mL). The reaction was brought under inert atmosphere and propylamine (4.5 mL, 55 mmol, 1.1 equiv.) was added. The reaction was stirred for 1 hour at room temperature. The reaction mixture was quenched using an HCl-solution (20 mL, 1 M) and washed with water (20 mL). The aqueous phases were extracted using diethyl ether (3 x 20 mL). The collected organic phases were dried using magnesium sulfate and concentrated *in vacuo*. Recrystallization in heptane led to pure 11-mercapto-undecan-1-ol as a white solid (7.26 g, 35.5 mmol, 71 %). ^{1}H NMR (300 MHz, $CDCl_3$): δ (ppm) = 1.29 (m, 16H, C*H*$_2$), 1.50 (m, 2H, C*H*$_2$CH$_2$OH), 2.44 (q, 2H, C*H*$_2$SH), 3.57 (t, 2H, C*H*$_2$OH).

4.18 9-Methoxy anthracene (36)

In a 500 ml flask, anthrone (10 g, 52 mmol, 1 equiv.) was dissolved in methanol (150 mL) and toluene (150 mL). After adding trimethyl ortoformate (5.6 mL, 52 mmol, 1 equiv.) and concentrated sulfuric acid (1 mL, >95 %), the solution was heated to reflux conditions. After 4 days, the solution was left to cool to room temperature. The organic solution was washed with sodium bicarbonate solution (60 mL), water (60 mL) and brine (60 mL). The collected aqueous phases were extracted with diethyl ether (3 x 50 mL). The collected organic phases were dried with sodium sulfate and concentrated *in vacuo*. Recrystallization in ethanol led to pure 9-methoxyanthracene as a slightly pink solid (4.6 g, 43 %). ^{1}H

NMR (300 MHz, $CDCl_3$): δ (ppm) = 4.12 (m, 3H, OC*H*$_2$), 7.39 (m, 4H, CHC*H*C*H*CH), 7.91 (m, 2H, CHCC*H*CH), 8.13 (s, 1H, CC*H*C), 8.22 (m, 2H, CCC*H*CH); LC-MS (m/z): 209.1 $[MH]^+$

4.19 Anthracen-9-yl(octyl)sulfane (38)

In a flask of 50 mL, 9-methoxyanthracene (0.75 g, 4.8 mmol, 1 equiv.) was solublized with octane thiol (3 mL, 24 mmol, 5 equiv.) in toluene (20 mL) under inert atmosphere. After adding methane sulfonic acid (5 drops), the reaction mixture was heated to reflux for 10 hours. After cooling to room temperature, the reaction mixture was washed with a 5 % sodium hydroxide solution (20 mL) and extracted with diethyl ether (3 x 20 mL). The combined organic phases were washed with a 5 % sodium hydroxide solution (20 mL) and brine (20 mL). The combined organic phases were dried on magnesium sulfate and concentrated *in vacuo*. The crude mixture was purified by column chromatography (eluent: dichloromethane:heptane 25:75), yielding the pure anthracene-9-yl(ocytl)sulfane as a yellow oil (0.26 g, 0.8 mmol, 17 %). ^{1}H NMR (300 MHz, $CDCl_3$): δ (ppm) = 0.81 (t, 3H, CH_2CH_3), 1.03-1.38 (m, 10H, CH_2), 1.53 (m, 2H, SCH_2CH_2), 2.77 (t, 2H, SCH_2), 7.47 (m, 4H, CHC*H*C*H*CH), 7.95 (d, 2H, CHCC*H*CH), 8.40 (s, 1H, CC*H*C), 8.89 (d, 2H, CCC*H*CH); ^{13}C NMR (125 MHz, $CDCl_3$): δ (ppm) = 14.1 (CH_3), 22.6 (CH_2), 28.9 (CH_2), 29.1 (CH_2), 23.0 (CH_2), 31.8 (CH_2), 37.5 (CH_2), 125.3 (CH), 126.5 (CH), 127.2 (CH), 128.7 (CH), 128.9 (CH), 130.0 (C), 134.6 (C); LC-MS (*m/z*) 240.20 $[MNH_4]^+$.

4.20 11-(Anthracen-9-ylthio)undecan-1-ol (39)

In a 100 mL flask, 9-methoxyanthracene (1.69 g, 8.1 mmol, 1 equiv.) was dissolved with 11-mercapto-undecan-1-ol (4.15 g, 20.3 mmol, 2.5 equiv.) in toluene (60 mL) under inert atmosphere. After adding methanesulfonic acid (5 drops), the reaction mixture was heated to reflux for 20 hours. After cooling to room temperature, the reaction mixture was washed with a 5 % sodium hydroxide solution (50 mL) and extracted with diethyl ether (3 x 50 mL). The combined organic phases were washed with a 5 % sodium hydroxide solution (50 mL) and brine (50 mL). The combined organic phases were dried with magnesium sulfate and concentrated *in vacuo*. ^{1}H NMR spectroscopy showed a conversion of 4.4 %. Purification by column chromatography (eluent: dichloromethane: heptane 25:75) resulted in no product yield.

4.21 9-(2-Nitrovinyl)anthracene (40)

9-Anthraldehyde (30 g, 0.15 mol) was dissolved in nitromethane (100 ml, 1.87 mol). To this mixture, ammonium acetate (5 g, 0.065 mol) was added and the mixture was refluxed for 2 hours. The crude

product was concentrated *in vacuo*. Pure 9-(2-nitrovinyl)anthracene was obtained as a red powder by recrystallization from isopropanol (26 g, 0.10 mol, 72 %). ^{1}H NMR (400 MHz, $CDCl_3$): δ (ppm) = 7.52-7.64 (m, 5H, CHC<u>H</u>C<u>H</u>CH (*2,3,6,7*) + C<u>H</u>CHNO_2), 8.07 (d, J=8.7 Hz, 2H, CC<u>H</u>CH, *4,5*), 8.20 (dd, J=0.9 Hz, 8.7 Hz, 2H, CC<u>H</u>CH, *1,8*), 8.56 (s, 1H, CC<u>H</u>C, *10*), 9.02 (d, J=13.8 Hz, 1H, CHC<u>H</u>NO_2); ^{13}C NMR (100 MHz, $CDCl_3$): δ (ppm) = 123.2 (C), 124.3 (CH), 125.7 (CH), 127.5 (CH), 129.2 (CH), 129.9 (C), 130.5 (CH), 131.2 (C), 135.7 (CH), 142.7 (CH); IR ν_{max} cm^{-1}: 604 (m), 692 (s), 706 (s), 726 (vs), 758 (m), 786 (w), 830 (m), 844 (m), 876 (w), 904 (m), 918 (m), 950 (m), 1070 (m), 1248 (s), 1324 (s), 1348 (m), 1442 (m), 1498 (vs), 1524 (w), 1616 (m), 1624 (m), 1808 (w), 3050 (w); GC-MS (m/z) 249 $[M]^+$

4.22 2-(Anthracen-9-yl)ethan-1-ammonium chloride (41)

Lithium aluminium hydride (23.8 g,0.63 mol) was dissolved in 500 ml dry tetrahydrofuran. The mixture was brought under nitrogen and cooled using an ice bath. Anhydrous sulfuric acid (17 ml, 0.32 mol) was slowly added. A solution of 9-(2-nitrovinyl)anthracene (26 g,0.10 mol) in 50 ml tetrahydrofuran was slowly added at 0 °C. The solution was subsequently heated to reflux temperature for two hours and left to cool to room temperature overnight. Afterwards, isopropanol (100 ml) was carefully added, followed by 10 M HCl (200 ml),after which a white flocculate formed. The flocculate was filtered and washed with water and diethylether, yielding pure 2-(anthracen-9-yl)ethan-1-ammonium chloride as a white powder. (20 g, 74 %). ^{1}H NMR (400 MHz, d6-DMSO): δ (ppm) = 3.07 (dquin, J=5.5 Hz, 11.2 Hz, 2H, oC<u>H_2</u>NH_3Cl), 3.95-4.02 (m, 2H, CC<u>H_2</u>CH_2), 7.52-7.57 (m, 2H, CC<u>H</u>CH, *3, 6*), 7.59-7.64 (m, 2H, CCHC<u>H</u>, *2, 7*), 8.12 (d, J=8.3 Hz, 2H, CC<u>H</u>CH, *4, 5*), 8.37 (br, 3H, N<u>H_3</u>Cl), 8.45 (d, J=8.8 Hz, 2H, CC<u>H</u>CH, *1, 8*), 8.57 (s, 1H, CC<u>H</u>C, *10*); ^{13}C NMR (100 MHz, d6-DMSO): δ (ppm) = 25.4 (CH_2), 39.3 (CH_2), 124.0 (CH), 125.2 (CH), 126.4 (CH), 126.6 (CH), 129.1 (CH), 129.3 (C), 129.5 (C), 131.1 (C); IR ν_{max} cm^{-1}: 630 (w), 702 (w), 734 (vs), 786 (w), 840 (m), 878 (m), 938 (w), 954 (w), 1006 (m), 1016 (w), 1144 (m), 1160 (w), 1264 (w), 1352 (w), 1496 (m), 1594 (w), 2904 (m), 3008 (m)

4.23 2-(Anthracen-9-yl)ethan-1-amine (42)

2-(Anthracen-9-yl)ethan-1-ammonium chloride (2.0 g) was added to a mixture of chloroform (150 ml) and 10% KOH solution (100 ml). The mixture was sonified until all aggregated material dispersed and dissolved as the free amine (~30 minutes needed). The chloroform was washed with water, dried with magnesium sulfate and concentrated *in vacuo* to a yellow powder (1.7 g, 99%). ^{1}H NMR (400 MHz, d6-

DMSO): δ (ppm) = 1.75-1.92 (br, 2H, $CH_2N\underline{H_2}$), 2.88 (t, 2H, J=8.0 Hz, $C\underline{H_2}NH_2$), 3.68 (t, 2H, J=8.3 Hz, $CC\underline{H_2}$), 7.47-7.58 (m, 4H, CCHC<u>H</u>, *2,3,6,7*), 8.06 (d, 2H, J=8.3 Hz, CC<u>H</u>CH, *4,5*), 8.39 (d, 2H, J=8.8 Hz, CC<u>H</u>CH, *1,8*), 8.46 (s, 1H, CC<u>H</u>C, *10*); ^{13}C NMR (100 MHz, d6-DMSO): δ (ppm) = 32.5 (CH_2), 43.7 (CH_2), 124.6 (CH), 125.0 (CH), 125.3 (CH), 125.6 (CH), 128.9 (CH), 129.4 (C), 131.1 (C), 132.8 (C); IR ν_{max} cm^{-1}: 632 (w), 700 (m), 726 (vs), 788 (m), 840 (m), 884 (s), 900 (w), 1008 (m), 1150 (w), 1344 (m), 1444 (m), 1520 (w), 1592 (w), 2916 (w), 3048 (w), 3158 (w), 3344 (w), GC-MS (m/z) 221 $[M]^+$, 233 $[M+12]^+$; LC-MS (m/z) 222.1 $[MH]^+$; HRMS (m/z) for $[MH]^+$calcd: 222.1283; found: 222.1286

4.24 5,12:6,11-bis([1,2]Benzeno)dibenzo[*a*,*e*][8]annulene-5,11(6*H*,12*H*)-diylbis(methylene) bis(11-((2-hydroxyethyl) thio) undecanoate) ($(47)_2$)

A dimer of anthracen-9-ylmethyl undec-10-enoate $(4)_2$ (3.41 g, 4.5 mmol, 1 equiv) was dissolved in a minimal amount of tetrahydrofuran (15 mL). 3.14 mL mercaptoethanol (45 mmol, 5 equiv) and 229 mg DMPA (0.9 mmol, 0.1 equiv) was added. The mixture was irradiated (λ=365 nm) for 1 h under nitrogen gas atmosphere and the reaction was monitored with TLC. The reaction mixture was washed with water (10 mL), after which the aqueous phases were extracted with diethyl ether (3×10 mL). The combined organic phases were dried over magnesium sulfate and the filtrate was concentrated in vacuo. Recrystallization in THF/water was required to obtain $(47)_2$ as a white solid (3.2 g, 79 %); Mp = 121–125 °C; R_f ($CHCl_3$) 0.1; ^{1}H NMR (400 MHz, $CDCl_3$): δ (ppm) = 1.13–1.62 (m, 28H, $CH_2C\mathit{H}_2CH_2$), 1.71–2.04 (m, 4H, $CH_2C\mathit{H}_2CH_2$), 2.13–2.26 (m, 3H, $COC\mathit{H}_2CH_2$), 2.51 (t, *J*=7.3 Hz, 4H, $CH_2C\mathit{H}_2S$), 2.73 (t, *J*=5.9 Hz, 4H, $SC\mathit{H}_2CH_2OH$), 3.72 (t, *J*=5.9 Hz, 4H, $SCH_2C\mathit{H}_2OH$), 3.71+4.4 (s, 2H, CC*H*C), 5.12–5.28 (m, 4H, $CC\mathit{H}_2O$), 6.81–7.14 (m, 16H, CC*H*C*H*C*H*C*H*C); ^{13}C NMR (100 MHz, $CDCl_3$): δ (ppm) = 24.9 (CH_2), 25.1 (CH_2), 28.1 (CH_2), 29.0 (CH_2), 29.1 (CH_2), 29.3 (CH_2), 29.4 (CH_2), 29.7 (CH_2), 31.6 (CH_2), 34.2 (CH_2), 35.4 (CH_2), 55.1 (CH_2), 59.0 (CH), 60.2 (C), 63.5 (CH_2), 68.9 (CH_2), 124.7 (CH), 125.8 (CH), 127.7 (CH), 128.0 (CH), 142.1 (C), 174.5 (C); IR ν_{max} cm^{-1}: 3518, 2922, 2852, 2160, 2028, 1978, 1722, 1454, 1384, 1342, 1246, 1210, 1168, 1060, 1008; LC-MS (*m*/*z*) 887.4 $[M-|-OH]^+$, 922.4 $[MNH_4]^+$; HRMS (*m*/*z* for $[M+OAc]^-$) calcd: 963.4903; found: 963.4907.

4.25 5,12:6,11-bis([1,2]Benzeno)dibenzo[*a*,*e*][8]annulene-5,11 (6*H*,12*H*)–diylbis(methylene) bis(11-((2,3 -dihydroxypropyl) thio) undecanoate ($(48)_2$)

A dimer of anthracen-9-ylmethyl undec-10-enoate $(4)_2$ (7.25 g, 9.5 mmol, 1 equiv) was dissolved in a minimal amount of tetrahydrofuran (20 mL). 8.2 mL thioglycerol (95 mmol, 5 equiv) and 487 mg DMPA (0.9 mmol, 0.1 equiv) was added. The mixture was irradiated (λ=365 nm) for 1 h under nitrogen gas atmosphere and the reaction was monitored with TLC. The reaction mixture was washed with water (10 mL), after which the aqueous phase was extracted with diethyl ether (3×10 mL). The combined organic phases were dried over magnesium sulfate and the filtrate was concentrated in vacuo. Recrystallization in THF/water was required to obtain $(48)_2$ as a white solid (7.88 g, 83 %); Mp = 129.5–134.5 °C; R_f ($CHCl_3$) 0; ^{1}H NMR (400 MHz, $CDCl_3$): δ (ppm) = 1.13–1.95 (m, 32H, $CH_2CH_2CH_2$), 2.18 (m, 3H, CH_2CH_2CO(*ht*)), 2.53–2.89 (m, 9H, CH_2SCH_2 + CH_2CH_2CO(*hh*)), 3.57–3.83 (m, 7.5H, $CHCH_2OH$+ CC*H*C(*ht*)), 4.48 (s, 0.5H, CC*H*C(*hh*)), 5.12–5.27 (m, 4H, CCH_2O), 6.81–7.12 (m, 16H, CC*H*C*H*C*H*C*H*C); ^{13}C NMR (100 MHz, $CDCl_3$): δ (ppm)=24.9 (CH_2), 28.8 (CH_2), 29.0 (CH_2), 29.1 (CH_2), 29.3 (CH_2), 29.7 (CH_2), 32.3 (CH_2), 34.2 (CH_2), 35.9 (CH_2), 55.1 (CH_2), 59.0 (CH), 63.5 (CH_2), 65.5 (CH_2), 69.7 (CH), 124.7 (CH), 125.8 (CH), 127.7 (CH), 128.0 (CH), 142.1 (C), 174.5 (C); IR ν_{max} cm^{-1}: 3378, 2924, 2852, 1726, 1454, 1384, 1344, 1172, 1068, 1026; LC-MS (*m*/*z*) 947.4 $[M-|-OH]^+$, 982.4 $[MNH_4]^+$; HRMS (*m*/*z* for $[M-|-H]^-$) calcd: 963.4903; found: 963.4890; HRMS (*m*/*z* for $[M-|-OH]^+$) calcd: 947.495424; found: 947.4955.

4.26 Anthracene mesylate (49)

Dry triethylamine (3.7 ml, 26 mmol, 2 equiv.) was added to a solution of anthracene ether **28** (5 g, 13 mmol, 1 equiv.) in anhydrous tetrahydrofuran (50 ml). After cooling in an ice bath, methanesulfonyl chloride (1.5 ml, 20 mmol, 1.5 equiv.) was slowly added. The solution was stirred for 3 hours until full conversion confirmed via thin layer chromatography. The solution was washed with water (30 ml). This separated aqueous phase was extracted with ether (3 x 30 ml). The combined organic phases were washed with a saturated bicarbonate solution (30 ml) and brine (30 ml). The organic phase solution was dried with magnesium sulfate. Concentration *in vacuo* yielded the mesylate **49** as a brown oil (5.69 g, 12.5 mmol, 94 %). ^{1}H NMR (300 MHz, $CDCl_3$): δ (ppm) = 1.06-1.85 (m, 18 H, CH_2), 1.98 (m, 2 H,

C*H*$_2$CH$_2$OMs), 2.92 (s, 3 H, C*H*$_3$), 4.14 (m, 4 H, C*H*$_2$OMs + C*H*$_2$OAntr), 7.39 (m, 4 H, CHC*H*C*H*CH), 7.91 (m, 2 H, CHCC*H*CH), 8.13 (s, 1 H, CC*H*C), 8.22 (m, 2 H, CCC*H*CH).

4.27 11-(anthracen-9-yloxy)undecyl 3-hydroxy-2-(hydroxymethyl)-2-methylpropanoate (50)

A solution of mesylate **49** (5.96 g, 12.5 mmol, 1 equiv.) in anhydrous dimethylformamide (15 ml) was slowly added to an ice-cooled mixture of 2,2-bis(hydroxyl)methylpropionic acid (1.65 g, 12.5 mmol, 1 equiv.), potassium carbonate (1.89 g, 13.8 mmol, 1.1 equiv.) and anhydrous dimethylformamide (15 ml). The mixture was stirred overnight at 80 °C. After cooling to room temperature, the salts were filtered off and the filtrate was concentrated *in vacuo*. The resulting orange-brown oil was diluted to 10 w%, using 5% triethylamine in ethyl acetate. After 10 minutes of ultrasonication, the salts were filtered off and the filtrate was concentrated in vacuo to yield anthracene diol **50** as a yellow oil (4.89 g, 10.5 mmol, 79 %). ^{1}H NMR (500 MHz, CDCl$_3$): δ (ppm) = 0.99 (s, 3 H, C*H*$_3$), 1.06-1.69 (m, 18 H, C*H*$_2$), 1.99 (m, 2 H, C*H*$_2$CH$_2$OCO), 3.65 (dd, 2 H, CC*H*$_2$OH), 3.82 (dd, 2 H, CC*H*$_2$OH), 4.10 (t, 2 H, C*H*$_2$OCO), 4.13 (t, 2 H, C*H*$_2$OAntr), 7.39 (m, 4 H, CHC*H*C*H*CH), 7.91 (m, 2 H, CHCC*H*CH), 8.13 (s, 1 H, CC*H*C), 8.22 (m, 2 H, CCC*H*CH). LC-MS (m/z): 495.3 $[MH]^+$

4.28 General dimerization method

Anthracene derivatives are dissolved in a minimal amount of hexane and/or THF. The solution is irradiated using UVC lamps for several hours under inert atmosphere. Dimers were separated from the mixture, either by filtration and recrystallization or column chromatography. All were white to slightly yellow powders. Determined melting points of dimers are either by true melting or liquefaction due to thermal dissociation, possibly followed by dimers dissolving in formed monomers.

4.29 $(4)_2$ (head-head (hh) and head-tail (ht) dimer)

Mp = 154.5–157.5 °C; ^{1}H NMR (400 MHz, CDCl$_3$): δ (ppm) = 0.12–1.64 (m, 23H, CH$_2$C*H*$_2$CH$_2$), 1.87–1.95 (m, 1H, C*H*$_2$CH$_2$CO, *hh*), 1.98–2.09 (m, 4H, C*H*$_2$CHCH$_2$), 2.15–2.25 (m, 3H, C*H*$_2$CO, *ht*), 2.74 (t, *J*=7 Hz, 1H, C*H*$_2$CO, *hh*), 3.78 (s, 1.5H, CC*H*C, *ht*), 4.48 (s, 0.5H, CC*H*C, *hh*), 4.90–5.04 (m, 4H, CH$_2$CHC*H*$_2$), 5.12–5.27 (m, 4H, CC*H*$_2$O), 5.74–5.87 (m, 2H, CH$_2$C*H*CH$_2$), 6.81–7.15 (m, 16H, CC*H*C*H*C*H*C*H*C); ^{13}C NMR (100 MHz, CDCl$_3$): δ (ppm) = 24.9 (CH$_2$), 28.9 (CH$_2$), 29.0 (CH$_2$), 29.0 (CH$_2$), 29.1 (CH$_2$), 29.2 (CH$_2$), 29.4 (CH$_2$), 33.8 (CH$_2$), 34.3 (CH$_2$), 59.0 (CH), 63.4 (CH$_2$), 68.9 (CH$_2$),

114.2 (CH_2), 124.7 (CH), 125.8 (CH), 127.7 (CH), 128.0 (CH), 139.2 (CH), 142.1 (C), 143.9 (C), 174.5 (C); IR ν_{max} cm^{-1}: 2926, 2852, 1724, 1640, 1454, 1382, 1344, 1292, 1242, 1176, 1116, 1070.

4.30 $(10)_2$

Mp = 182–183 °C; ^1H NMR (500 MHz, $CDCl_3$): δ (ppm) = 2.13 (q, *J*=7.3 Hz, 4H, CCH_2CH_2CH), 2.76–2.82 (m, 4H, CCH_2CH_2CH), 3.88 (s, 2H, CC*H*C), 5.10 (d, *J*=10.2 Hz, 2H, CH_2CHCH_2), 5.15 (d, *J*=17.1 Hz, 2H, CH_2CHCH_2), 6.04 (ddt, *J*=16.9 Hz, *J*=10.3 Hz, *J*=6.5 Hz, 2H, CH_2CHCH_2), 6.79–6.93 (m, 12H, CCHC*H*C*H*C*H*C), 6.99 (d, *J*=7.5 Hz, 4H, CC*H*CH); ^{13}C NMR (125 MHz, $CDCl_3$): δ (ppm) = 29.3 (CH_2), 36.2 (CH_2), 56.5 (C), 64.8 (CH), 114.5 (CH_2), 125.2 (CH), 125.3 (CH), 126.2 (CH), 127.5 (CH), 138.6 (CH), 142.7 (C), 143.7 (C); IR ν_{max} cm^{-1}: 3066, 3018, 2930, 2862, 2160, 2032, 1976, 1640, 1472, 1448, 1122, 1046; GC–MS (*m*/*z*) 232 $[M/2]^+$.

4.31 $(11)_2$

Mp = 111.5–114 °C; ^1H NMR (500 MHz, $CDCl_3$): δ (ppm)=1.23–1.43 (m, 28H, $CH_2CH_2CH_2$), 1.47–1.59 (m, 4H, CCH_2CH_2), 2.05 (q, *J*=7.1 Hz, 4H, CH_2CHCH_2), 2.65 (t, *J*=7.9 Hz, 4H, CCH_2CH_2), 3.84 (s, 2H, CC*H*C), 4.94 (d, *J*=10.2 Hz, 2H, CH_2CHCH_2), 5.00 (d, *J*=17.1 Hz, 2H, CH_2CHCH_2), 5.83 (ddt, *J*=17.1 Hz, *J*=10.3 Hz, *J*=6.7 Hz, 2H, CH_2CHCH_2), 6.77–6.89 (m, 12H, CCHC*H*C*H*C*H*C), 6.96 (d, *J*=7.5 Hz, 4H, CC*H*CH); ^{13}C NMR (125 MHz, $CDCl_3$): δ (ppm) = 24.9 (CH_2), 29.0 (CH_2), 29.2 (CH_2), 29.5 (CH_2), 29.5 (CH_2), 29.6 (CH_2), 29.6 (CH_2), 30.7 (CH_2), 33.8 (CH_2), 37.8 (CH_2), 56.6 (C), 65.0 (CH), 114.1 (CH_2), 125.1 (CH), 126.2 (CH), 127.4 (CH), 139.3 (CH), 143.0 (C), 143.9 (C); IR ν_{max} cm^{-1}: 2924, 2852, 2530, 2478, 2160, 2028, 1978, 1734, 1450, 1364, 1328, 1252, 1166, 1096.

4.32 $(24)_2$

Mp = 83.5–85 °C; ^1H NMR (500 MHz, $CDCl_3$): δ (ppm) = 1.18–1.39 (m, 20H, $CH_2CH_2CH_2$), 1.67 (quin, *J*=6.7 Hz, 4H, OCH_2CH_2), 2.02 (q, *J*=7.1 Hz, 4H, CH_2CHCH_2), 4.31 (t, 4H, OCH_2CH_2), 4.93 (dt, *J*=10.1 Hz, *J*=1.1 Hz, 2H, CH_2CHCH_2), 4.93 (dq, *J*=17.1 Hz, *J*=1.8 Hz, 2H, CH_2CHCH_2), 5.74 (s, 2H, CC*H*C), 5.74 (ddt, *J*=17.1 Hz, *J*=10.3 Hz, *J*=6.7 Hz, 2H, CH_2CHCH_2), 6.65 (dd, *J*=7.5 Hz, *J*=1.4 Hz, 2H, CC*H*CH), 6.79–6.86 (m, 4H, CCHC*H*), 7.00 (dd, *J*=7.1 Hz, *J*=1.6 Hz, 2H, CC*H*CH); ^{13}C NMR (125 MHz, $CDCl_3$): δ (ppm) = 26.1 (CH_2), 28.4 (CH_2), 28.9 (CH_2), 29.1 (CH_2), 29.1 (CH_2), 29.3 (CH_2), 29.4 (CH_2), 33.8 (CH_2), 55.0 (CH), 66.2 (C), 114.1 (CH_2), 125.5 (CH), 126.1 (CH), 126.5 (CH), 128.2 (CH), 139.2 (CH), 141.9 (C), 142.7 (C), 174.5 (C); IR ν_{max} cm^{-1}: 3072, 3024, 2922, 2852, 2160,

2030, 1978, 1722, 1640, 1454, 1198, 1104, 1006; LC-MS (*m*/*z*) 766.4 $[MNH_4]^+$; HRMS (*m*/*z* for $[MNH_4]^+$) calcd: 766.4835; found: 766.4830.

4.33 $(27)_2$

Mp = 117–119 °C; ^{1}H NMR (400 MHz, $CDCl_3$): δ (ppm) = 1.42–1.55 (m, 10H, $CH_2CH_2CH_2$), 1.65 (quin, *J*=6.8 Hz, 4H, $COCH_2CH_2$), 1.87 (quin, *J*=7 Hz, 4H, CH_2CH_2OH), 3.53 (t, *J*=7 Hz, 4H, $COCH_2$), 3.69 (t, *J*=6.5 Hz, 4H, CH_2OH), 4.46 (s, 2H, CCHC), 6.82–6.90 (m, 8H, CCHCH), 7.00–7.06 (m, 8H, CCHCH); ^{13}C NMR (100 MHz, $CDCl_3$): δ (ppm) = 25.8 (CH_2), 26.0 (CH_2), 30.5 (CH_2), 32.8 (CH_2), 63.0 (CH_2), 64.0 (CH), 65.0 (CH_2), 89.3 (C), 125.1 (CH), 125.6 (CH), 125.8 (CH), 127.6 (CH), 141.0 (C), 142.1 (C); IR ν_{max} cm^{-1}: 3341, 2934, 2858, 1452, 1292, 1254, 1202, 1154, 1118, 1052; HRMS (*m*/*z* for $[MNH_4]^+$) calcd: 606.3583; found: 606.3574.

4.34 $(28)_2$

Mp = 118–118.5 °C; ^{1}H NMR (500 MHz, $CDCl_3$): δ (ppm) = 1.24–1.47 (m, 36H), 1.54–1.62 (m, 4H, $COCH_2CH_2$), 1.85 (quin, *J*=7.2 Hz, 4H, CH_2CH_2OH) 3.53 (t, *J*=7.1 Hz, 4H, $COCH_2$), 3.65 (t, *J*=6.7 Hz, 4H, CH_2OH), 4.46 (s, 2H, CCHC), 6.82–6.89 (m, 8H, CCHCH), 7.00–7.07 (m, 8H, CCHCH); ^{13}C NMR (125 MHz, $CDCl_3$): δ (ppm) = 25.3 (CH_2), 25.8 (CH_2), 26.2 (CH_2), 29.5 (CH_2), 29.6 (CH_2), 32.8 (CH_2), 63.1 (CH_2), 65.1 (CH_2), 89.2 (C), 125.1 (CH), 125.8 (CH), 127.5 (CH), 141.0 (C), 142.2 (C); IR $\nu_{max}$$cm^{-1}$: 3324, 2920, 2850, 1452, 1290, 1256, 1202, 1154, 1118, 1056; HRMS (*m*/*z* for $[MH]^+$) calcd: 757.5196; found: 757.5181.

4.35 $(30)_2$

Mp = 150–151 °C; ^{1}H NMR (400 MHz, $CDCl_3$): δ (ppm)=1.27–1.62 (20H), 1.78–2.00 (m, 4H, $COCH_2CH_2$), 2.07 (q, *J*=6.9 Hz, 4H, CH_2CHCH_2), 2.70–2.80 (m, 4H, $COCH_2CH_2$), 4.57–4.74 (1.35H, CCHC), 4.95 (dt, *J*=10.2 Hz, *J*=1 Hz, 2H, CH_2CHCH_2), 5.02 (dq, *J*=17.1 Hz, *J*=1.7 Hz, 2H, CH_2CHCH_2), 5.09–5.22 (0.65H, CCHC), 5.84 (ddt, *J*=17 Hz, *J*=10.3 Hz, *J*=6.6 Hz, 2H, CH_2CHCH_2), 6.66–7.33 (16H, CCHCHCHCHC); ^{13}C NMR (100 MHz, $CDCl_3$): δ (ppm) = 25.2 (CH_2), 29.0 (CH_2), 29.1 (CH_2), 29.4 (CH_2), 29.4 (CH_2), 33.8 (CH_2), 114.2 (CH_2), 125.6 (CH), 126.2 (CH), 139.2 (CH); IR ν_{max} cm^{-1}: 3066, 3032, 2924, 2850, 2160, 2020, 1978, 1744, 1640, 1452, 1376, 1294, 1210, 1154, 1118, 1010; HRMS (*m*/*z* for $[MNH_4]^+$) calcd: 738.4522; found: 738.4537.

4.36 $(50)_2$

^{1}H NMR (300 MHz, $CDCl_3$): δ (ppm) = 1.00 (s, 6 H, C*H*$_3$), 1.06-1.71 (m, 36 H, C*H*$_2$), 2.01 (m, 4 H, C*H*$_2$CH$_2$OCO), 3.55 (t, 4H, COC*H*$_2$), 3.66 (dd, 4 H, CC*H*$_2$OH), 3.84 (dd, 4 H, CC*H*$_2$OH), 4.11 (t, 4 H, C*H*$_2$OCO), 4.48 (s, 2H, CC*H*C), 6.80–6.93 (m, 8H, CCHC*H*), 7.01–7.09 (m, 8H, CC*H*CH).

4.37 Simulation program

4.37.1.1 Interface and data output

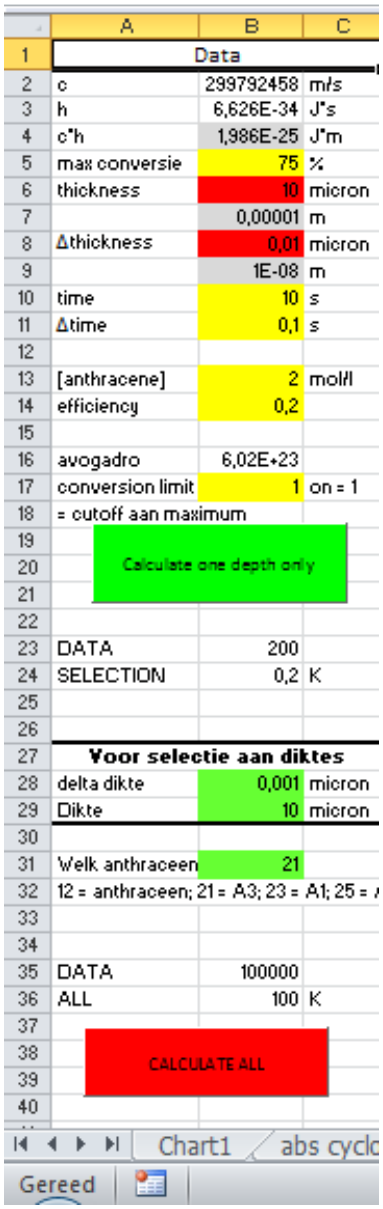
Data
c 299792458 m/s
h 6,626E-34 J*s
c*h 1,986E-25 J*m
max conversie 75 %
thickness 10 micron
0,00001 m
Δthickness 0,01 micron
1E-08 m
time 10 s
Δtime 0,1 s
[anthracene] 2 mol/l
efficiency 0,2
avogadro 6,02E+23
conversion limit 1 on = 1
= cutoff aan maximum
Calculate one depth only
DATA 200
SELECTION 0,2 K
Voor selectie aan diktes
delta dikte 0,001 micron
Dikte 10 micron
Welk anthraceen 21
12 = anthraceen; 21 = A3; 23 = A1; 25 =
DATA 100000
ALL 100 K
CALCULATE ALL
Chart1
abs cyclo
Gereed

	A	B	C	D	E	F	G
1					dikte =	1	micron
2	time (s)	conversie dimee	concentratie in laag ervoo		delta dikte =	0,001	micron
3	0	0	2		tijd =	100	seconden
4	0,1	0,008656458	1,962105278		delta tijd =	0,1	seconden
5	0,2	0,017347868	1,924540794		efficiency =	1	
6	0,3	0,026073099	1,887307855		maximal conversion =	1	
7	0,4	0,034830989	1,850407728		anthraceenderivaat =	A0	
8	0,5	0,043620352	1,81384163				
9	0,6	0,052439975	1,777610736				
10	0,7	0,061288619	1,741716173				
11	0,8	0,070165022	1,706159021				
12	0,9	0,079067897	1,670940311				
13	1	0,087995936	1,636061023				
14	1,1	0,096947807	1,601522091				
15	1,2	0,105922159	1,567324393				
16	1,3	0,114917622	1,533468758				
17	1,4	0,123932804	1,499955963				
18	1,5	0,132966299	1,466786729				
19	1,6	0,142016686	1,433961725				
20	1,7	0,151082524	1,401481566				
21	1,8	0,160162365	1,369346811				
22	1,9	0,169254744	1,337557963				
23	2	0,178358189	1,306115471				
24	2,1	0,187471216	1,275019725				
25	2,2	0,196592337	1,244271062				
26	2,3	0,205720056	1,213869758				

Chart1 | abs cyclohex | emission | 12|d=1|t=100|1|1|2 | Model-data | energie-zonlicht

4.37.1.2 Code at Sheet (buttons)

```
Private Sub CommandButton1_Click()

Call Model4

End Sub

Private Sub CommandButton2_Click()

Call Model4_selectie

End Sub
```

4.37.1.3 General code Model4

```
Sub Model4()Application.ScreenUpdating = False
Application.DisplayAlerts = False
On Error Resume Next
Sheets("Model-resultaten").Delete
Application.DisplayAlerts = True
On Error GoTo 0
Sheets.Add().Name = "Model-resultaten"
Worksheets("Model-resultaten").Range("B1").Value = "thickness (micron)"
Worksheets("Model-resultaten").Range("A2").Value = "time (s)"
dikte = Worksheets("Model-data").Range("B6").Value
delta_dikte = Worksheets("Model-data").Range("B8").Value
tijd = Worksheets("Model-data").Range("B10").Value
delta_tijd = Worksheets("Model-data").Range("B11").Value
max_conversie = Worksheets("Model-data").Range("B5").Value / 100
resolutie_dikte = dikte / delta_dikte
d = 0

For i = 1 To resolutie_dikte
d = d + delta_dikte
Worksheets("Model-resultaten").Cells(2, 1 + i).Value = d
Next i

resolutie_tijd = tijd / delta_tijd
t = 0

For i = 1 To resolutie_tijd
t = t + delta_tijd
Worksheets("Model-resultaten").Cells(2 + i, 1).Value = t
Next i

‘ hier stopt de vormgeving van de worksheet
```

```
efficiency = Worksheets("Model-data").Range("B14").Value
concentration_origineel = Worksheets("Model-data").Range("B13").Value
concentration = concentration_origineel
avogadro = Worksheets("Model-data").Range("B16").Value
For x = 3 To resolutie_tijd + 2
For y = 2 To resolutie_dikte + 1
d = Worksheets("Model-resultaten").Cells(2, y).Value


If y = 2 Then
concentration_gemiddeld = 0
ElseIf x = 3 Then
concentration_gemiddeld = concentration_origineel
Else

concentration_gemiddeld = 0                                    '(gemiddelde) concentratie voor berekening
resterend zonlicht

For j = 1 To y – 2
concentration_tijdelijk = ((1 - Worksheets("Model-resultaten").Cells(x - 1, y - j)) *
concentration_origineel) / (y - 2)
concentration_gemiddeld = concentration_gemiddeld + concentration_tijdelijk
Next j
End If

oude_concentratie = Worksheets("Model-resultaten").Cells(x - 1, y)

If x = 3 Then
concentration = concentration_origineel
ElseIf oude_concentratie > max_conversie Then
concentration = 0
Else
concentration = concentration_origineel * (1 - oude_concentratie)          'concentratie voor absorptive
End If
```

```
For i = 1 To 424 ' 424
energie_foton = Worksheets("Model-data").Cells(2 + i, 5)
epsilon = Worksheets("Model-data").Cells(2 + i, 12)
delta_lambda = Worksheets("Model-data").Cells(2 + i, 17)
zon_origineel = Worksheets("Model-data").Cells(2 + i, 15)

If epsilon < 0 Then
epsilon = 0
Else
End If

E = epsilon * (d - delta_dikte) * concentration_gemiddeld * 10 ^ -4
zon = zon_origineel * (10 ^ -E)                    'resterend zonlicht
A = epsilon * delta_dikte * concentration * 10 ^ -4          'web lambert-beer
absorptie = 1 - 10 ^ -A                            'wet lambert-beer, 1-transmissie
fotonen_energie = absorptie * zon * delta_lambda          'hoeveel fotonen geabsorbeerd (in
J/s*m²)
fotonen_aantal = fotonen_energie / energie_foton * delta_tijd   '
dimerisatie_aantal = efficiency * fotonen_aantal
dimerisatie_som = dimerisatie_som + dimerisatie_aantal
Next i

dimerisatie_relatief = dimerisatie_som / (delta_dikte * concentration_origineel * 1000 * 10 ^ -6 *
avogadro)
dimerisatie_som = 0

If x = 3 Then
Worksheets("Model-resultaten").Cells(x, y) = dimerisatie_relatief
Else
Worksheets("Model-resultaten").Cells(x, y) = dimerisatie_relatief + Worksheets("Model-
resultaten").Cells(x - 1, y)
End If
```

```
If Worksheets("Model-data").Cells(17, 2) = 1 And Worksheets("Model-resultaten").Cells(x, y) > 1 Then
'laatste nieuwe code, voor bij te grote delta's!!!!
Worksheets("Model-resultaten").Cells(x, y) = 1

End If

Next y

Next x

Application.ScreenUpdating = True

End Sub
```

4.37.1.4 General code Model4_selectie

```
Sub Model4_selectie()

Application.ScreenUpdating = False
Application.DisplayAlerts = False
On Error Resume Next
Sheets("Model-resultaten").Delete
Application.DisplayAlerts = True
On Error GoTo 0
Sheets.Add().Name = "Model-resultaten"


efficiency = Worksheets("Model-data").Range("B14").Value
avogadro = Worksheets("Model-data").Range("B16").Value
max_conversie = Worksheets("Model-data").Range("B5").Value / 100
concentration_origineel = Worksheets("Model-data").Range("B13").Value
maxconcentratiedikkelaagervoor = (1 - max_conversie) * concentration_origineel
dikte = Worksheets("Model-data").Range("B29").Value
tijd = Worksheets("Model-data").Range("B10").Value
delta_tijd = Worksheets("Model-data").Range("B11").Value
resolutie_tijd = tijd / delta_tijd
```

```
t = 0
delta_dikte = Worksheets("Model-data").Range("B28").Value          ' waarde delta_dikte, kan aangepast worden
derivaatkeuze = Worksheets("Model-data").Range("B31").Value
Worksheets("Model-resultaten").Range("A2").Value = "time (s)"
Worksheets("Model-resultaten").Cells(2, 3).Value = "concentratie in laag ervoor"
Worksheets("Model-resultaten").Cells(2, 2).Value = "conversie dimeer in laag"
Worksheets("Model-resultaten").Cells(1, 5).Value = "dikte ="
Worksheets("Model-resultaten").Cells(1, 6).Value = dikte
Worksheets("Model-resultaten").Cells(1, 7).Value = "micron"
Worksheets("Model-resultaten").Cells(2, 5).Value = "delta dikte ="
Worksheets("Model-resultaten").Cells(2, 6).Value = delta_dikte
Worksheets("Model-resultaten").Cells(2, 7).Value = "micron"
Worksheets("Model-resultaten").Cells(3, 5).Value = "tijd ="
Worksheets("Model-resultaten").Cells(3, 6).Value = tijd
Worksheets("Model-resultaten").Cells(3, 7).Value = "seconden"
Worksheets("Model-resultaten").Cells(4, 5).Value = "delta tijd ="
Worksheets("Model-resultaten").Cells(4, 6).Value = delta_tijd
Worksheets("Model-resultaten").Cells(4, 7).Value = "seconden"
Worksheets("Model-resultaten").Cells(5, 5).Value = "efficiency ="
Worksheets("Model-resultaten").Cells(5, 6).Value = efficiency
Worksheets("Model-resultaten").Cells(6, 5).Value = "maximal conversion ="
Worksheets("Model-resultaten").Cells(6, 6).Value = max_conversie
Worksheets("Model-resultaten").Cells(7, 5).Value = "anthraceenderivaat ="

If derivaatkeuze = 21 Then
Worksheets("Model-resultaten").Cells(7, 6).Value = "A3"
ElseIf derivaatkeuze = 12 Then
Worksheets("Model-resultaten").Cells(7, 6).Value = "A0"
ElseIf derivaatkeuze = 23 Then
Worksheets("Model-resultaten").Cells(7, 6).Value = "A1"
ElseIf derivaatkeuze = 25 Then
```

```
Worksheets("Model-resultaten").Cells(7, 6).Value = "Anthr-Oct-thioether"
Else
Worksheets("Model-resultaten").Cells(7, 6).Value = derivaatkeuze
End If

Worksheets("Model-resultaten").Cells(3, 1).Value = t
Worksheets("Model-resultaten").Cells(3, 2).Value = 0
Worksheets("Model-resultaten").Cells(3, 3).Value = concentration_origineel

For i = 1 To resolutie_tijd
t = t + delta_tijd
Worksheets("Model-resultaten").Cells(3 + i, 1).Value = t
Next i

' hier stopt de vormgeving van de worksheet

For x = 4 To resolutie_tijd + 3
concentration_gemiddeld = Worksheets("Model-resultaten").Cells(x - 1, 3)        '(gemiddelde)
concentratie in laag op vorig tijdstip
concentration = concentration_origineel * (1 - Worksheets("Model-resultaten").Cells(x - 1, 2))


For i = 1 To 424 ' 424
energie_foton = Worksheets("Model-data").Cells(2 + i, 5)
epsilon = Worksheets("Model-data").Cells(2 + i, derivaatkeuze)
delta_lambda = Worksheets("Model-data").Cells(2 + i, 17)                    ' data
zon_origineel = Worksheets("Model-data").Cells(2 + i, 15)

If epsilon < 0 Then                                                ' negatieve absorptie uitsluiten
epsilon = 0
End If

E = epsilon * dikte * concentration_gemiddeld * 10 ^ -4
absorptie_dikkelaag = 1 - 10 ^ -E                                  'absorptie in dikke laag
fotonen_energie_dikkelaag = absorptie_dikkelaag * zon_origineel * delta_lambda       'hoeveel fotonen
```

```
geabsorbeerd in dikke laag
fotonen_aantal_dikkelaag = fotonen_energie_dikkelaag / energie_foton * delta_tijd
dimerisatie_aantal_dikkelaag = efficiency * fotonen_aantal_dikkelaag
dimerisatie_som_dikkelaag = dimerisatie_som_dikkelaag + dimerisatie_aantal_dikkelaag
zon = zon_origineel * (10 ^ -E)                    'resterend zonlicht
A = epsilon * delta_dikte * concentration * 10 ^ -4          'wet lambert-beer
absorptie = 1 - 10 ^ -A                          'wet lambert-beer, 1-transmissie
fotonen_energie = absorptie * zon * delta_lambda          'hoeveel fotonen geabsorbeerd (in
J/s*m²)
fotonen_aantal = fotonen_energie / energie_foton * delta_tijd   '
dimerisatie_aantal = efficiency * fotonen_aantal
dimerisatie_som = dimerisatie_som + dimerisatie_aantal
Next i

dimerisatie_relatief_dikkelaag = dimerisatie_som_dikkelaag / (dikte * concentration_origineel * 1000 *
10 ^ -6 * avogadro)
dimerisatie_relatief = dimerisatie_som / (delta_dikte * concentration_origineel * 1000 * 10 ^ -6 *
avogadro)
Worksheets("Model-resultaten").Cells(x, 3) = Worksheets("Model-resultaten").Cells(x - 1, 3) -
dimerisatie_relatief_dikkelaag * concentration_origineel

If Worksheets("Model-resultaten").Cells(x, 3) < maxconcentratiedikkelaagervoor Then
Worksheets("Model-resultaten").Cells(x, 3) = maxconcentratiedikkelaagervoor
End If

Worksheets("Model-resultaten").Cells(x, 2) = dimerisatie_relatief + Worksheets("Model-
resultaten").Cells(x - 1, 2)
dimerisatie_som_dikkelaag = 0
dimerisatie_som = 0

If Worksheets("Model-data").Cells(17, 2) = 1 And Worksheets("Model-resultaten").Cells(x, 2) >
max_conversie Then          'laatste nieuwe code, voor bij te grote delta's!!!!
Worksheets("Model-resultaten").Cells(x, 2) = max_conversie
```

```
Worksheets("Model-resultaten").Cells(x, 3) = "-"
x = resolutie_tijd + 3
End If

Next x

ActiveSheet.Name = derivaatkeuze & "|d=" & dikte & "|t=" & tijd & "|" & efficiency & "|" &
max_conversie & "|" & concentration_origineel
Application.ScreenUpdating = True

End Sub
```

5 References

1. Fritzsche, *J. Prakt. Chem.* **1867**, *101* (1), 333-343.
2. Breton, G. W.; Vang, X., *J. Chem. Educ.* **1998**, *75*, 81.
3. (a) Bratschkov, C.; Karpuzova, P.; Müllen, K.; Klapper, M.; Schopov, I., *Polymer Bulletin* **2001**, *46* (5), 345-349; (b) Bruss, J. M.; Sahyun, M. R. V.; Schmidt, E.; Sharma, D. K., *J. Polym. Sci., Part A: Polym. Chem.* **1993**, *31* (4), 987-994; (c) Matsui, J.; Ochi, Y.; Tamaki, K., *Chem. Lett.* **2006**, *35* (1), 80-81.
4. Islangulov, R. R.; Kozlov, D. V.; Castellano, F. N., *Chem Commun* **2005**, (30), 3776-3778.
5. Morris, J. V.; Mahaney, M. A.; Huber, J. R., *J. Phys. Chem.* **1976**, *80*, 969-974.
6. (a) Paul, S.; Stein, S.; Knoll, W.; Müllen, K., *Acta Polymerica* **1996**, *47* (2-3), 92-98; (b) De Schryver, F. C.; Anand, L.; Smets, G.; Switten, J., *Journal of Polymer Science Part B: Polymer Letters* **1971**, *9* (10), 777-780.
7. Froimowicz, P.; Frey, H.; Landfester, K., *Macromol. Rapid Commun.* **2011**, *32*, 468-473.
8. (a) Radl, S. V.; Roth, M.; Gassner, M.; Wolfberger, A.; Lang, A.; Hirschmann, B.; Trimmel, G.; Kern, W.; Griesser, T., *Eur. Polym. J.* **2014**, *52*, 98-104; (b) Rameshbabu, K.; Kim, Y.; Kwon, T.; Yoo, J.; Kim, E., *Tetrahedron Lett.* **2007**, *48*, 4755-4760.
9. Wells, L. A.; Brook, M. A.; Sheardown, H., *Macromol. Biosci.* **2011**, *11*, 988-998.
10. Mitsuishi, M.; Tanuma, T.; Matsui, J.; Chen, J.; Miyashita, T., *Langmuir* **2001**, *17* (24), 7449-7451.
11. Guarini, G. G. T.; Spinicci, R.; Carlini, F. M.; Donati, D., *J. Therm. Anal.* **1973**, *5*, 307-314.
12. Donati, D.; Guarini, G. G. T.; Sarti-Fantoni, P., *J. Therm. Anal.* **1991**, *37*, 1917-1922.
13. Gore, P. H., *J Org Chem* **1957**, *22* (2), 135-138.
14. Ali, M. M.; Sana, S.; Tasneem; Rajanna, K. C.; Saiprakash, P. K., *Synth. Commun.* **2002**, *32* (9), 1351-1356.
15. Meyer, K. H., *Org. Synth.* **1941**, *Coll. Vol. 1*, 1.
16. Pan, K.; Noël, S.; Pinel, C.; Djakovitch, L., *Journal of Organometallic Chemistry* **2008**, *693* (17), 2863-2868.
17. Gore, P. H., *Chemical Reviews* **1955**, *55* (2), 229-281.
18. Groves, J. K., *Chemical Society* Reviews **1972**, *1* (1), 73-97.
19. Bawa, R. A.; Jones, S., *Tetrahedron* **2004**, *60* (12), 2765-2770.
20. Bayliss, M. A. J.; Homer, R. B.; Shepherd, M. J., *J Chem Soc Chem Comm* **1990**, (4), 305-306.
21. Pirkle, W. H.; Finn, J. M., *J Org Chem* **1983**, *48*, 2779–2780.
22. Wang, Y. X.; Zhang, Y. M.; Liu, Y., *J Am Chem Soc* **2015**, *137* (13), 4543-4549.
23. (a) Zanardi, M. M.; Suárez, A. G., Tetrahedron *Letters* **2015**, *56* (24), 3762-3765; (b) Hong, C.; Luo, W.; Yao, D.; Su, Y.-B.; Zhang, X.; Tian, R.-G.; Wang, C.-J., *Bioorganic & Medicinal Chemistry* **2014**, *22* (12), 3213-3219.
24. Uchiyama, Y.; Watanabe, R.; Kurotaki, T.; Kuniya, S.; Kimura, S.; Sawamura, Y.; Ohtsuki, T.; Kikuchi, Y.; Matsuzawa, H.; Uchiyama, K.; Itakura, M.; Kawakami, F.; Maruyama, H., *ACS Omega* **2017**, *2* (7), 3371-3379.
25. Liu, B.; Wang, H.; Zhang, L.; Yang, G.; Liu, X.; Kim, I., *Polym. Chem.* **2013**, *4*, 2428-2431.
26. Jones, R. N., *Chem. Rev.* **1947**, *41* (2), 353-371.
27. Werner, T. C.; Hercules, D. M., *The Journal of Physical Chemistry* **1969**, *73*, 2005–2011.
28. Lai, T. I.; Lim, E. C., *J Am Chem Soc* **1985**, *107* (5), 1134-1137.
29. Hirayama, S., *J Chem Soc Farad T 1* **1982**, *78*, 2411-2421.
30. Ghoneim, N.; Scherrer, D.; Suppan, P., *Journal of Luminescence* **1993**, *55* (5), 271-275.

31. Yamamoto, T.; Yagyu, S.; Tezuka, Y., *J. Am. Chem. Soc.* **2016**, *138* (11), 3904-3911.
32. Ebeid, E. Z. M.; Habib, A. F. M.; Azim, S. A., *React Solid* **1988**, *6* (1), 39-44.
33. Brouwer Albert, M., Standards for photoluminescence quantum yield measurements in solution (IUPAC Technical Report). In *Pure and Applied Chemistry*, **2011**; Vol. 83, p 2213.

Chapter IV: Thermo-degradable and photo-reversible thiol-ene networks

Abstract

Reversible networks based on an alkene-functionalized dimer of 9-anthracenemethanol were synthesized by photo-initiated radical thiol-ene polyaddition, using either a poly(dimethylsiloxane-co-propylmercaptomethylsiloxane) or a novel aliphatic trithiol synthesized from 1,2,4-trivinylcyclohexane in a simple two-step procedure. The obtained networks were analyzed using differential scanning calorimetry, dynamic mechanical analysis, polarization microscopy, X-ray diffraction and (photo)rheology. The two types of networks showed weak endothermic transitions between 50 and 60 °C, which proved to originate either from melting of a crystalline anthracene-dimer phase (trithiol network) or from a liquid crystalline phase (PDMS network) based on X-ray diffraction and polarization microscopy. Using rheology, both types of networks were shown to cleanly decompose into multi-functional anthracene monomers at temperatures above 180 °C. Irradiation of these anthracene monomers resulted in the formation of networks having similar physical properties as the original materials.

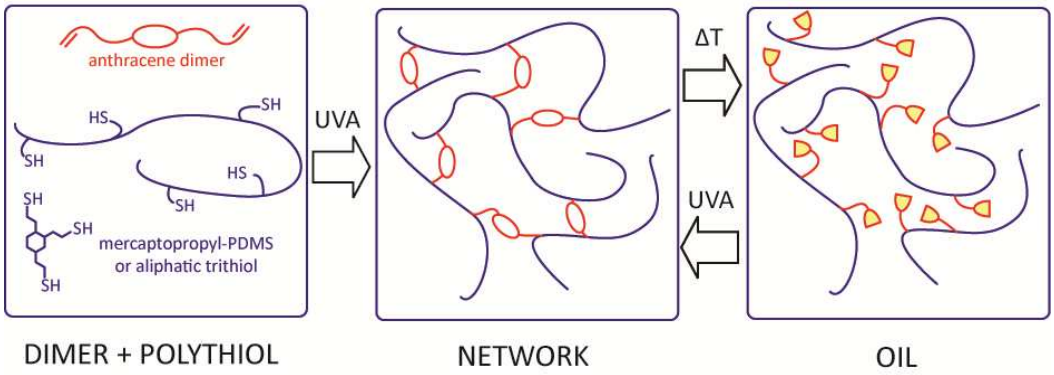

The results discussed in this chapter have been published as:

- Van Damme , J.; van den Berg, O.; Brancart, J.; Vlaminck, L.; Huyck, C.; Van Assche, G.; Van Mele, B.; Du Prez, F. Anthracene-based Thiol-Ene Networks with Thermo-Degradable and Photo-Reversible Properties. *Macromolecules* **2017**, *50*, 1930-1938

Collaborators:

This work was performed in close collaboration with dr. Otto van den Berg (VUB/UGent), who also performed thermal analysis and XRD measurements. Additional thermal analysis experiments at VUB were performed by dr. Joost Brancart.

1 Introduction

Covalently crosslinked materials are used in numerous applications, ranging from coatings, which is the focus in this thesis, over composite materials, to biomedical materials. The presence of covalent crosslinks makes these materials behave in a predominantly elastic manner when exposed to mechanical deformation. However, the permanently crosslinked structure often poses a serious disadvantage when reshaping, recycling or easy removal of the material is required. Introduction of reversible covalent bonds into a network allows for combining the advantages of classical crosslinked materials, e.g., dimensional stability, with the advantages of non-crosslinked oligomers or thermoplastic polymers, e.g., easy processing.

As mentioned in chapter I, the type of reversible covalent bond determines the conditions under which such materials behave as classic thermosets or as thermoplastic materials. A reversible bond can either be dynamic (exchange reaction) or non-dynamic (breaking or forming bonds).[1] In addition to the type of reversible bond, the change in connectivity and the time scale on which this change of connectivity occurs largely determine the material behavior. In case associative exchanges take place, *i.e.*, an exchange reaction where no change in macroscopic connectivity occurs, the material behaves like a strong glass former and is processable over a broad temperature range. In the case that dissociative exchanges occur, e.g., due to a temperature dependent shift of the chemical equilibrium between a connected and an unbound state, large changes in viscosity are observed in the processing of the material as a result of large changes in connectivity.

For networks held together by non-dynamic reversible bonds at the relevant time-scales, activation of the reversibility leads to a net breaking of bonds and possible conversion of an essentially solid material into a viscous liquid. As no reversion takes place when ceasing the stimulus, the connectivity of the material at ambient conditions can be tuned. Activation of the reverse reaction (with another stimulus) leads to the reformation of the network and recovery of the solid properties. Well known examples are materials containing photoreversible bonds such as cinnamate esters,[2] coumarines,[3] and anthracenes.[4] As the 4π-4π photocycloadditions of anthracenes occur using less energetic, longer wavelengths (even visible light) compared to their 2π-2π counterparts, they are preferred in order to avoid side reactions. As proven in chapter III, anthracene dimers are also able to dissociate cleanly at elevated temperatures

through a diradical transition state (Figure IV.1). The synthesized dimer derivatives differ in thermal stability, which depends on the nature (and position) of the substituents.

Therefore, this chapter will focus on the preparation and study of non-dynamic reversible anthracene dimer containing networks, where the bond-forming reaction is a concerted 4π-4π photochemical cycloaddition, and the bond-breaking reaction is a non-concerted thermally activated retro-cycloaddition.[6]

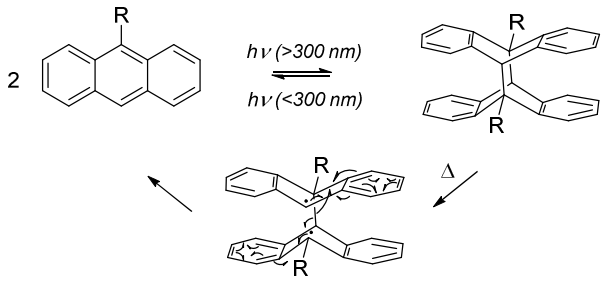

Figure IV.1. Dimerization of anthracene with photochemical 4π-4π concerted cycloaddition and scission of the anthracene dimer back into anthracene, either by a thermally activated (radical) reaction or by a photochemical 4π-4π concerted retro cycloaddition.

This system allows the creation of crosslinked materials that are easy to repair or recycle by heat treatment followed by an irradiation step with UVA light. Unlike other recent work on reversible anthracene networks,[7] the (first) network formation does not occur by anthracene dimerization, but by thiol-ene reactions with anthracene dimers. This approach guarantees the synthesis of networks without free anthracene groups (and thus also no crosslinking gradient) and facilitates incorporation of the reversible bonds in known formulations and thicker materials.

A large number of publications on thiol-ene chemistry involve modification and functionalization of existing (polymer) structures and the preparation of new molecular architectures. Some excellent reviews dealing with this topic were published.[8] In patent literature, thiol-ene polymerization of multifunctional thiols with multifunctional enes and ynes is described for the preparation of materials with different types of functionality. For example, Bowman *et al.* reported the polymerization of several multifunctional unsaturated urethanes, allylethers, acrylates and methacrylates with multifunctional thiols, yielding crosslinked end products exhibiting shape memory properties,[9] which are claimed for medical applications. Other examples of applications of thiol-ene based polymeric structures include the preparation of low gas permeability membranes,[10] sealants,[11] stamps for lithography,[12] degradable

polymeric structures for biomedical[13] and dental applications,[14] liquid crystalline compositions for optical applications,[15] and polymer electrolytes for, e.g., batteries.[16]

Multifunctional thiol crosslinkers can come in different shapes and forms. Silicone-based thiols have been described for different applications,[8a] including fast-cure optical fiber coatings,[17] functionalized microfluidic devices[18] and for the modification of surfaces.[19] In a recent paper, we described the preparation of low-modulus dry silicone gels built on silicone-based thiols.[20] A very common class of readily available tetrafunctional thiol crosslinkers is based on the esters of pentaerythrytol or trimethylolpropane and 2-mercaptoacetic acid or 3-mercaptopropanoic acid. However, the presence of multiple ester moieties in such multithiols can result in a reduced hydrolytic stability. For materials where ester moieties need to be avoided, no economically viable alternative to such tetrathiols is available. In this context, we explored the synthesis of a purely aliphatic multithiol from an available polyunsaturated precursor.

Starting from the synthesized multifunctional thiols and ene-functionalized anthracene dimers, fully reversibly crosslinked polymer networks will be prepared that can be used as a material that can be easily removed after its service-life in applications like coatings or composite materials, by a simple temporarily temperature increase. The reversible bonds can recure the disintegrated materials, potentially allowing recycling.

2 Results and discussion

2.1 Compound selection and synthesis

While anthracene in its monomeric form is prone to radical addition of thiyl radicals at the 9- or 10-positions,[22] the loss of sp^2-hybridization of the same positions after dimerization leads to the loss of thiol-ene reactivity. Therefore, we chose to add the anthracenes to the resin formulations as dimers instead. Introduction of additional double bond functionality, as was often the case in chapter III, allows dimers to be used in the construction of one, two and three-dimensional structures. Since the unfunctionalized anthracene dimer itself is virtually insoluble in any solvent, functionalization of the basic anthracene dimer core is also done to improve and optimize the solubility of the anthracene dimer based compounds in various monomers, co-reactants and solvents. In this context, an anthracene dimer derivative is chosen having long alkyl spacers. Therefore, we chose to incorporate anthracene dimers

(4)$_2$ as reversible bond (Figure IV.2). This specific derivative has a high thermal stability and is easily scalable. This dimer can be applied as bifunctional building block in thiol-ene networks where photoreversibility or thermo-/photoreversibility is required as a property of the final product, without excessive costs or a limited availability of the component. It should be noted that the (benzylic) ester moiety is likely to decrease the acidic stability due to hydrolysis. While this property has not been specifically tested, no hydrolysis of stored compounds has thus far been observed. This is probably due to the apolar character and the high crystallinity of **4** and **(4)$_2$**. Additionally, the benzylic ester moiety of **4** might also lead to faster photo-oxidation. In **(4)$_2$**, the ester group is no longer benzylic, which might limit the eventual industrial application range of the resulting materials.

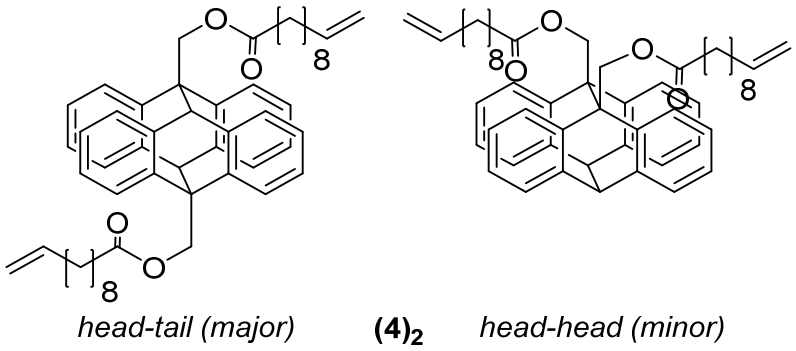

Figure IV.2. Head-tail and head-head forms of **(4)$_2$**.

In order to investigate the basic thermal and photochemical properties of thiol-ene networks prepared from **(4)$_2$**, two different types of thiols were considered, i.e. one that can create well-defined anthracene-dimer based thiol-ene networks with a high concentration of anthracene-dimers and a fixed crosslink functionality of 3, and one that results in a lower concentration anthracene-dimer network with crosslink functionalities mostly between 3 and 6. A first cyclo-aliphatic trithiol was prepared from 1,2,4-trivinylcyclohexane (**51**, Figure IV.3), a relatively inexpensive intermediate that is produced on large scale by isomerization of 1,5,9-cyclododecatriene, which is a precursor of Nylon 12, over a palladium catalyst.[23]

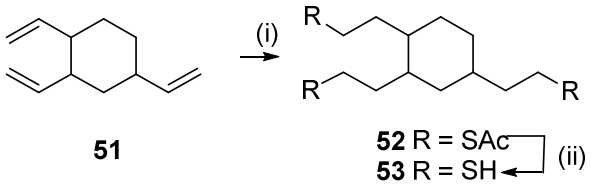

Figure IV.3. Preparation of a mixture of trifunctional thiol isomers: (i) thioacetic acid, DMPA, 365 nm UV, THF, 100 %; (ii) dilute HCl, reflux, 90 %.

Since **51** is supplied as a mixture of several (stereo) isomers, reaction of **51** with thioacetic acid results in a complex mixture of trifunctional thioesters. However, a mixture of isomers is desirable in this case, since the presence of different molecular configurations suppresses crystallization, both in the thiol and in the resulting networks. Indeed, suppression of crystallization in the networks is needed to create sufficient mobility for the dimerization reaction and the thermal/photochemical scission reaction to take place. The reaction between **51** and thioacetic acid proved to be self-initiating and exothermic, requiring efficient cooling. While a conversion of up to 97 % could be accomplished after an hour without initiator or irradiation and cooling using a salty ice bath, a final irradiation in the presence of a photoinitiator (2,2-dimethoxy-2-phenylacetophenone, DMPA) was performed in order to ensure (nearly) full conversion of all available double bonds to the desired end product. The proton NMR spectrum of the resulting mixture of isomers showed broad peaks with slightly overlapping signals between 2.5 and 3 ppm (Figure IV.4). Based on chemical shift, these peaks must correspond to α-CH_2SAc (anti-Markovnikov) and/or α-CHSAc (Markovnikov). Additionally, ^{13}C and HSQC NMR spectra were taken, which exclude the presence of Markovnikov products as there are only CH_2 signals coupling to these peaks in HSQC, nor are there any CH_3 signals present in the ^{13}C NMR (Figure IV.5 and Figure IV.6).

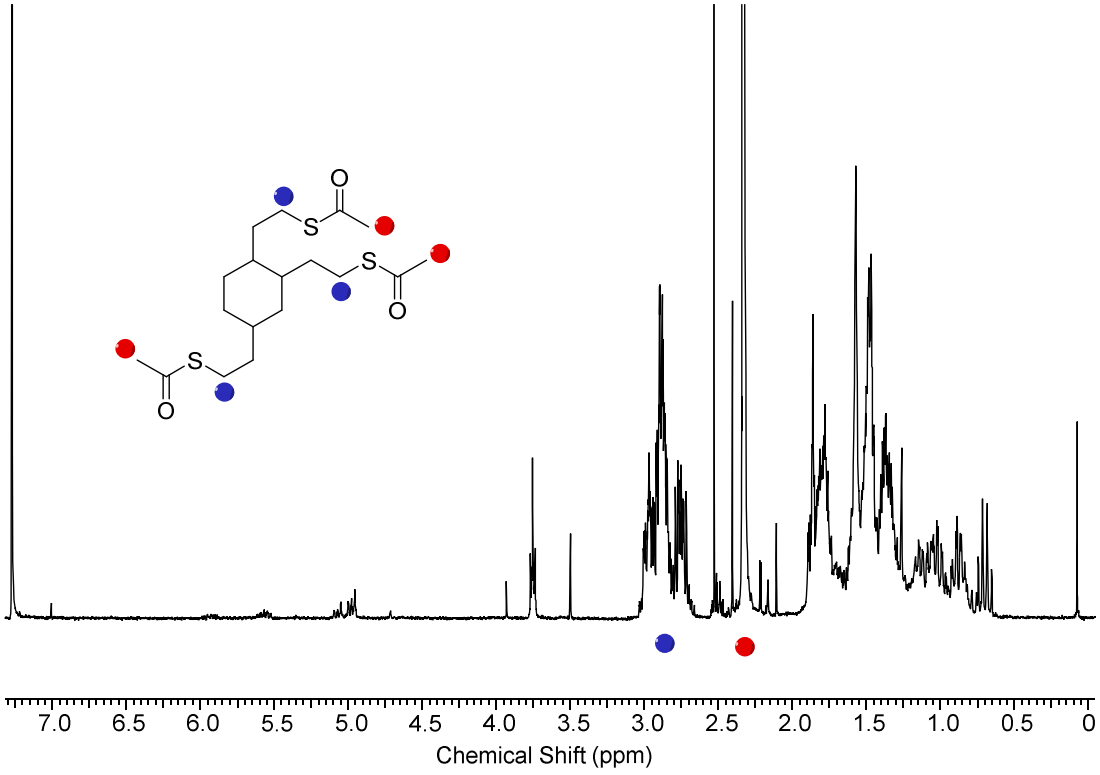

Figure IV.4. ^{1}H NMR of crude trithioacetate mixture.

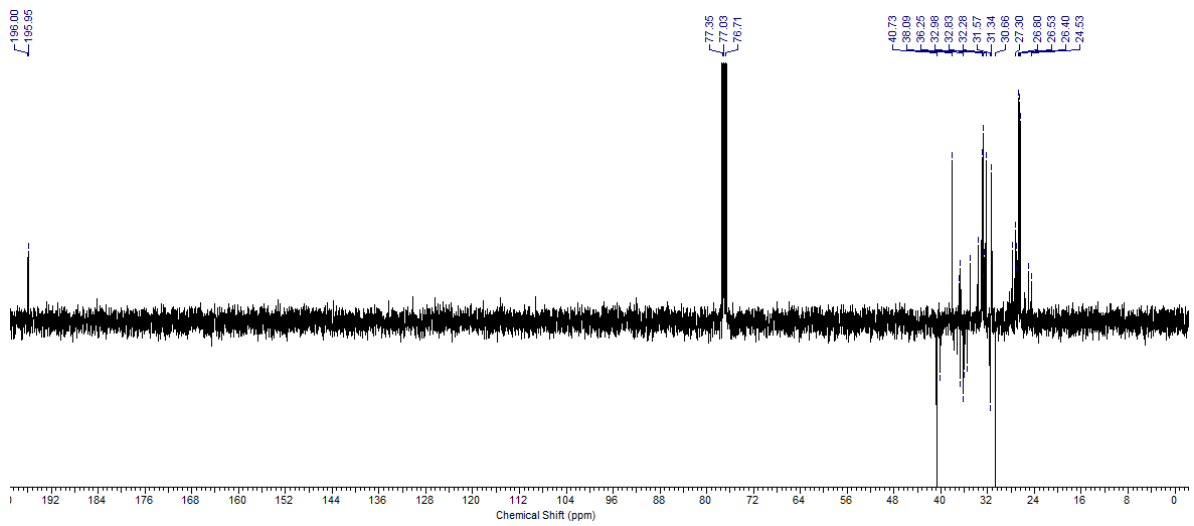

Figure IV.5. ^{13}C NMR of crude trithioacetate mixture.

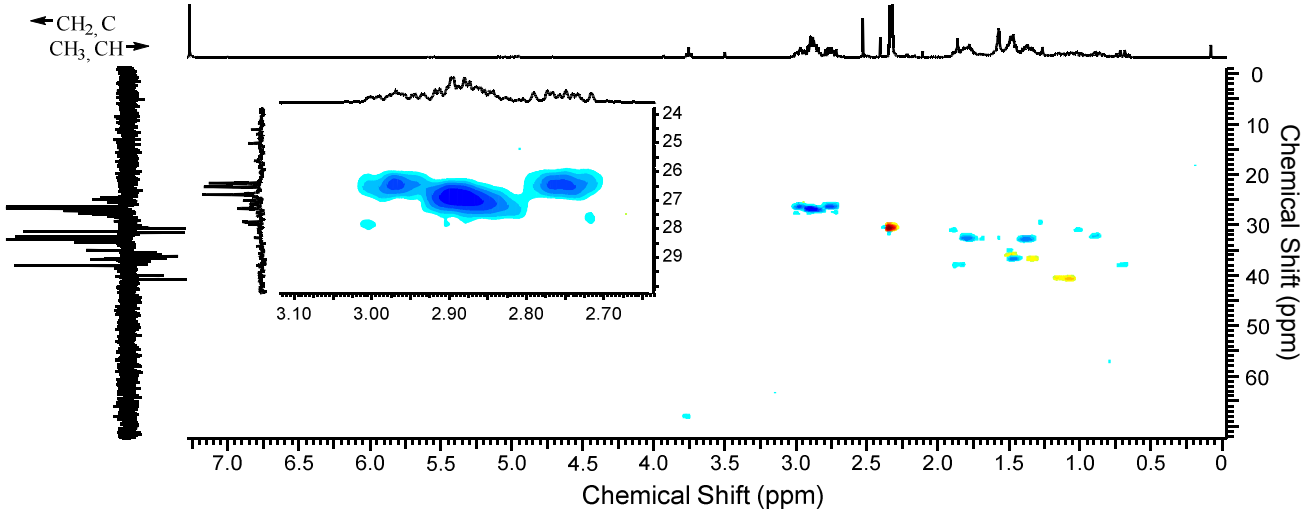

Figure IV.6. HSQC NMR of crude trithioacetate mixture.

Hydrolysis of the trithioacetate mixture **52** with dilute hydrochloric acid and subsequent vacuum distillation provided the free trithiols **53** (^{1}H NMR in Figure IV.7). GC-MS analysis of this complex mixture gave a set of unseparated peaks of identical molecular mass components (M = 264.10 g/mol),

indicative of clean conversion of the trithioacetate into the free trithiol (Figure IV.8) with only a minor impurity of dithiol (M = 230 g/mol).

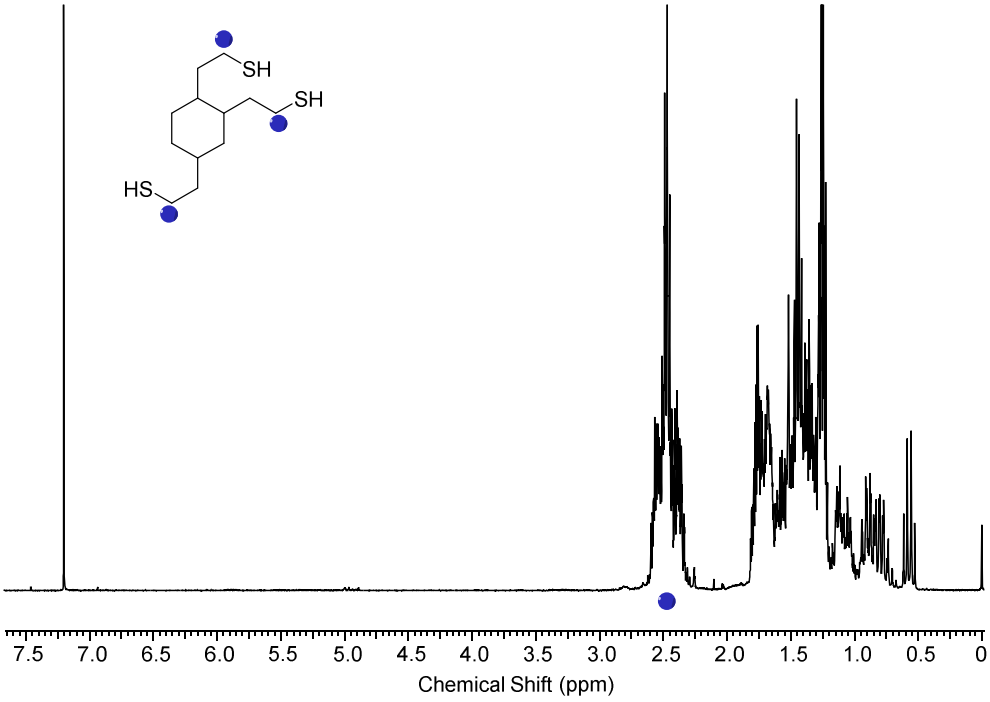

Figure IV.7. ^{1}H NMR of trithiol mixture.

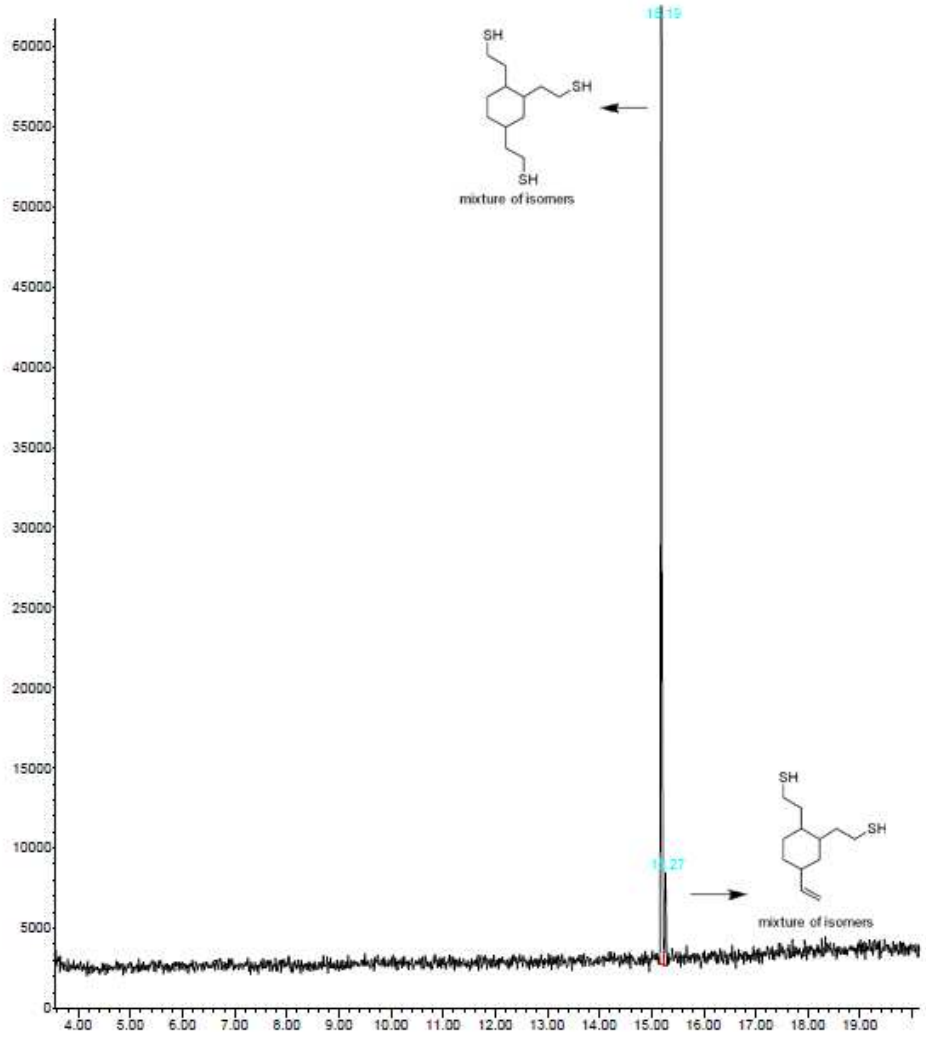

Figure IV.8. GC-MS of trithiol.

As alternative thiol-bearing compound for network synthesis, a readily available thiopropyl functional PDMS (M_n = 6800 g/mol, ~ 5 thiols per PDMS-chain) is chosen. Because of the higher molecular weight to functionality ratio, a lower weight percentage of the (more expensive and solid) dimer is required for equimolarity. Additionally, due to the higher functionality, the minimal anthracene dimer-monomer ratio required to maintain the structural integrity of the network should be lower. The low T_g of PDMS-based networks also ensures enough mobility for reversible reactions to occur within the network.

Preparation of the networks based on the anthracene diene ($(\mathbf{4})_2$) and the synthesized aliphatic trithiol (**53**) or the available thiopropyl functional PDMS (**54**) required the use of a co-solvent in order to create homogeneous mixtures (having 79 wt% and 58 wt% of THF) at room temperature. Higher solid contents are obtainable by using better solvents (e.g. 72 wt% and 47 wt% of $CHCl_3$), increased temperatures and/or appropriate reactive diluents. UV-cure occurred in the presence of DMPA between glass windows separated with 1 mm silicone-rubber spacers. After curing and removal from the mold, the solvent was allowed to evaporate under ambient conditions, resulting in clear, rigid, trithiol-based films (**A**), or in clear, highly elastic thiopropyl-functional-PDMS-based films (**B**) (Figure IV.9).

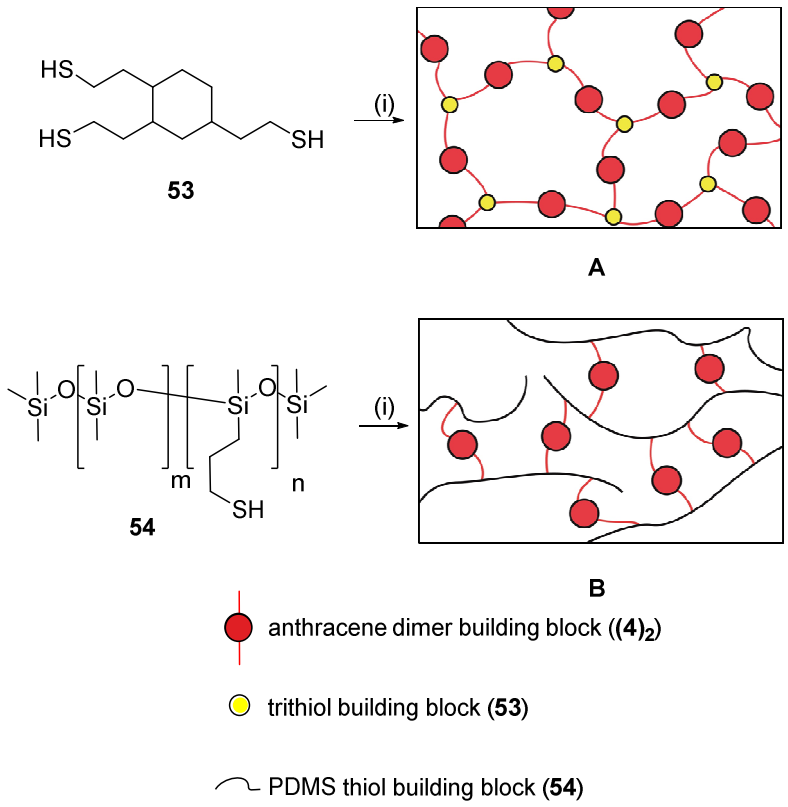

Figure IV.9. Preparation of thiol-ene networks using trithiol **53** and thiol-functionalized PDMS **54**, resulting in a densely crosslinked structure containing well-defined crosslinks (**A**) and a loosely crosslinked structure with ill-defined polymeric crosslinks (**B**). (i) anthracene dimer diene $(\mathbf{4})_2$, DMPA, 365 nm UV (1 h), THF.

2.2 Thermal characterization

Prior to discussing the thermal characterization of the materials, it is worthwhile to shortly discuss the the thermal behavior of **(4)$_2$** in more detail. Pure dimer **(4)$_2$** is characterized by a broad highly structured melting peak at 148 °C measured via differential scanning calorimetry (DSC), which might indicate recrystallization of **(4)$_2$** into thermally more stable crystal structures. While the melting endotherm of **(4)$_2$** is quite obvious, the scission of the dimer into the monomeric anthracene can only be observed as the small exothermic bending of the baseline near 200 °C in the DSC curve of pure **(4)$_2$** (Figure IV.10).

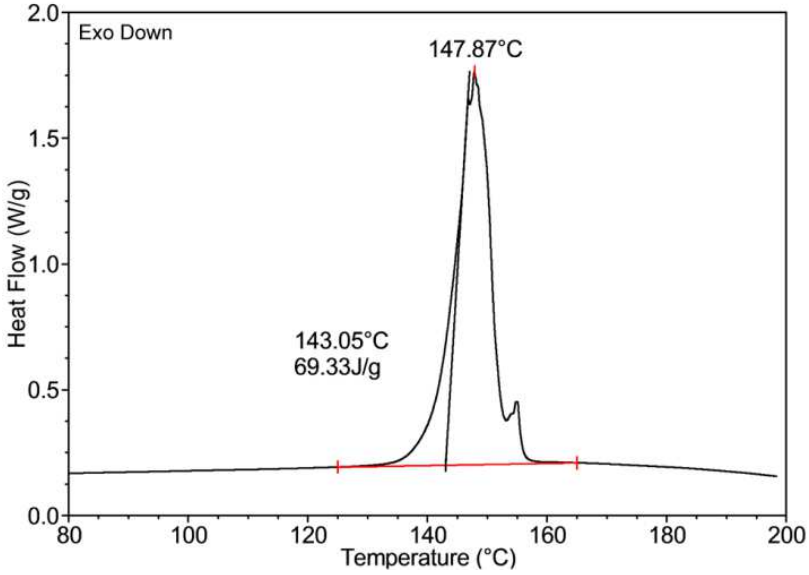

Figure IV.10. DSC curve of **(4)$_2$** (first heating) showing the melting endotherm and a lack of other visible thermal changes in the area where thermal scission of **(4)$_2$** into monomeric anthracene **4** is to be expected according to ^{1}H NMR.

It was previously reported that heating dimer **(4)$_2$** for 10 minutes led to scission into its corresponding monomer **4** starting from temperatures around 160-170 °C, without appreciable competing side reactions.[5] This proves that the melting endotherm of **(4)$_2$** and the scission into **4** do not overlap significantly on the temperature scale of the DSC experiment and that the exothermic bending of the baseline starting from 160-170 °C indeed originates from the scission. Using the Arrhenius parameters of the bulk thermal scission of **(4)$_2$** (ln A = 32.5 & Ea = 148 kJ/mol), the scission conversion at the end of the DSC measurement was calculated to be 24 % and a (small) peak maximum would only be reached at 210 °C. This corresponds to a connectivity x = 0.76, where x = 1 for fully dimerized/crosslinked

systems and x = 0 for fully dissociated systems. This limited conversion, in combination with a (presumably) low scission enthalpy explains the low intensity in the DSC experiment.

Networks based on **(4)$_2$** and trithiol **53** (network **A**) or PDMS multithiol **54** (network **B**), both containing the same type of reversible bonds, were subsequently investigated. While trithiol based network **A** has a high crosslink density, PDMS based network **B** has a low one. After UV cure and evaporation of the THF, first under ambient conditions and next in high vacuum, the samples were measured using differential scanning calorimetry (DSC). The glass transition of network **A** is rather difficult to observe at 10 K/min in the first heating, but could be measured in the second heating, being equal to 14.6 °C (Figure IV.11). As expected, network **B** has a very low glass transition temperature (T_g = -118 °C) because of the flexible PDMS chains and the low crosslinking density (Figure IV.12). Both materials show a weak endothermic peak at around 50-70 °C. Especially for network **A**, it is surprising that any crystallinity is present, as crystallinity in highly crosslinked materials is usually suppressed. However, due to the method of preparation, which involves the use of a good solvent for dissolving all reactants, the initial structure has a much higher degree of molecular mobility than usually observed for materials crosslinked in bulk. In fact, our materials can be described as typical xerogels, formed by crosslinking in concentrated solution, followed by slow air drying, which allows the components to slowly self-assemble to a thermodynamically more stable ordered situation. This is in stark contrast to densely crosslinked networks that are crosslinked in bulk, where mobility is quickly reduced by the formation of the polymer network, freezing to an amorphous material that is far away from thermodynamic equilibrium. Vitrification of the network in bulk will also halt the crosslinking at the point where the bulk-T_g coincides with the reaction temperature, leading to an incomplete reaction. However, even when the overall content of **(4)$_2$** in the networks is taken into account, the observed endotherms are rather small, respectively 16.8 J/(g of **(4)$_2$)** for network **A** and 15.8 J/(g of **(4)$_2$)** for network **B**, or about four times smaller than for pure **(4)$_2$**.

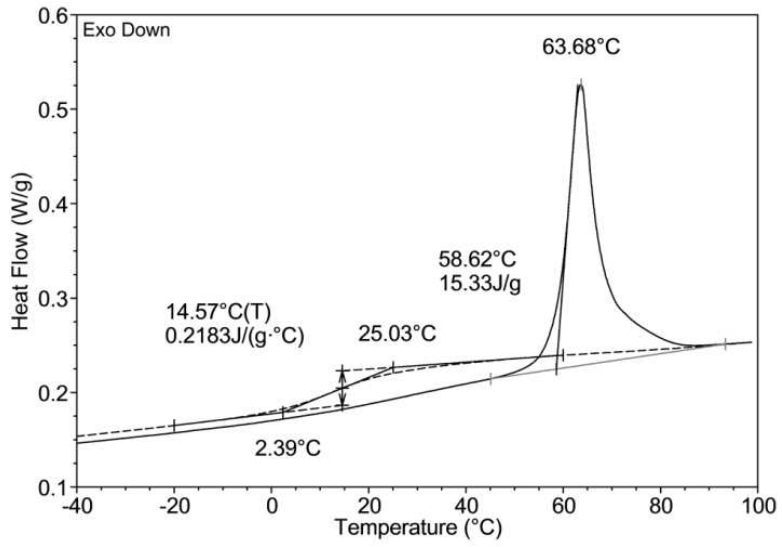

Figure IV.11. DSC curve of network A based on **(4)$_2$** and trithiol **53**. First (full lines) and second (dotted lines) heating at 10 K min^{-1}.

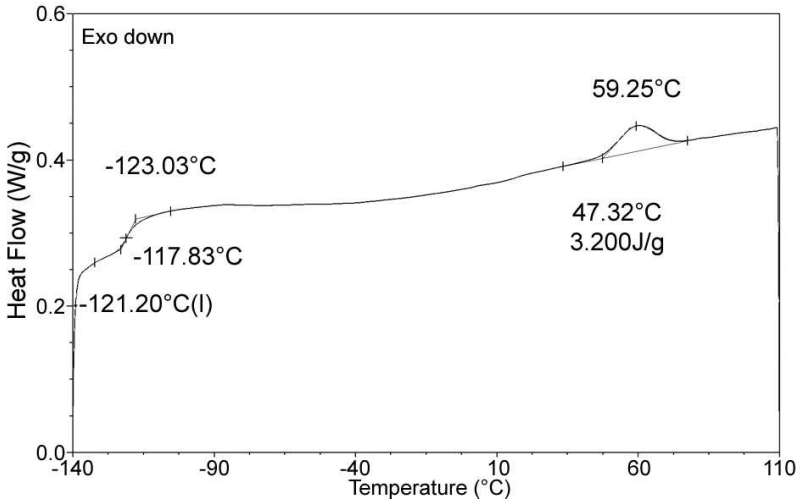

Figure IV.12. DSC curve of network B based on **(4)$_2$** and PDMS **54**. First heating at 10 K min^{-1}.

The reduced melting temperature of the networks **A** and **B**, combined with a decreased melting enthalpy, as compared to the anthracene dimer **(4)$_2$,** might suggest the formation of a mesophase, which could be induced by the presence of mobile spacers and/or a mobile low T_g polymer, such as the PDMS in network **B**, combined with a rigid anisotropic anthracene dimer moiety. In order to determine whether the prepared materials exhibit either crystalline or liquid crystalline order, both networks were characterized using wide-angle X-ray diffraction (Figure IV.13 and Figure IV.14). Both samples were

first analyzed at ambient temperature, after which they were quickly heated to just above the transition temperatures (70 °C), quenched to room temperature, and measured again. Finally the samples were measured 48 hours after quenching. From the first diffraction results, it was found that network **A** based on trithiol **53** shows sharp reflections at 2θ values of 11, 18, and 28 degrees, which correspond with d-spacings of 8 Å, 4.9 Å and 3.2 Å, respectively. While the trithiol-based network **A** displays sharp XRD patterns typical for a crystalline material, the PDMS-based network **B** shows a much more diffuse reflection at 12 degrees, corresponding with a d-spacing of 7.3 Å, which is indicative for a nematic liquid crystalline material that exhibits orientational order without positional order.

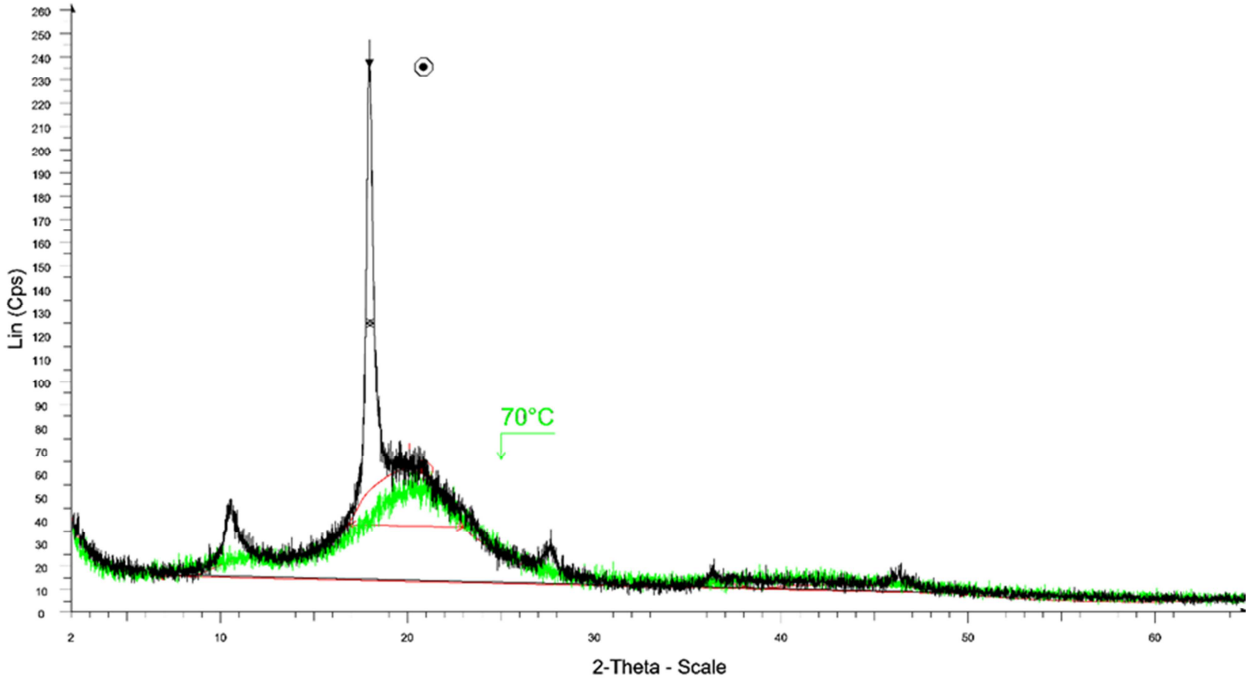

Figure IV.13. Wide angle x ray diffraction pattern of the trithiol based network **A** before heating (black), immediately after a quench from 70 °C (green).

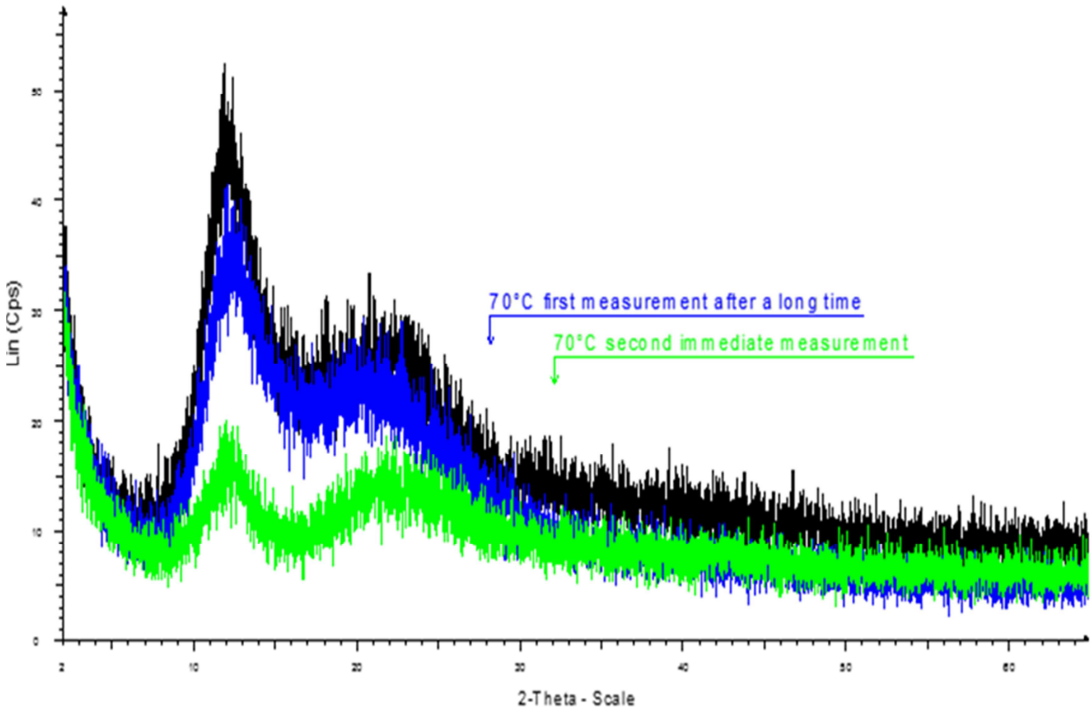

Figure IV.14. Wide angle x ray diffraction pattern of the PDMS based network **B** before heating (black), immediately after a quench from 70 °C (green) and 24 hours after the quench from 70 °C (blue).

The subsequent heating and quenching step initially leads to the formation of amorphous materials at room temperature. However, after resting for 24 hours at room temperature, the PDMS-based material regains its liquid crystalline order, while the trithiol-based material remains amorphous. Polarization microscopy of a freshly prepared sample of **B** exhibited birefringent domains, when observed between crossed polarizers, confirming that **B** is a liquid crystalline rubbery material (Figure IV.15).

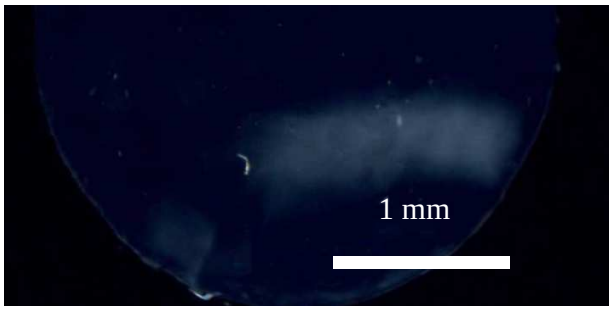

Figure IV.15. Optical micrograph of a thin film (100 µm) of **B** recorded with crossed polarizers.

2.3 Dynamic mechanical analysis and rheology

The visco-elastic behavior of thiol-ene network **A** was characterized using DMA (Figure IV.16). The decrease in storage modulus and maximum in loss modulus, observed around 40 °C, can be attributed to the glass transition of **A**. This is in good correlation to the DSC experiment on network **A**, where a slope in the baseline can be seen in the first heating before the melting occurs. A further increase in temperature above the onset of melting of the crystalline fraction of **A** at 60 °C results in a decrease in storage modulus and loss modulus to a plateau (due to the dimer aggregates) above 100 MPa and around 10 MPa respectively. Near 125 °C the moduli decrease again, resulting in a material that displays an elastomeric behavior with a storage modulus of about 2 MPa.

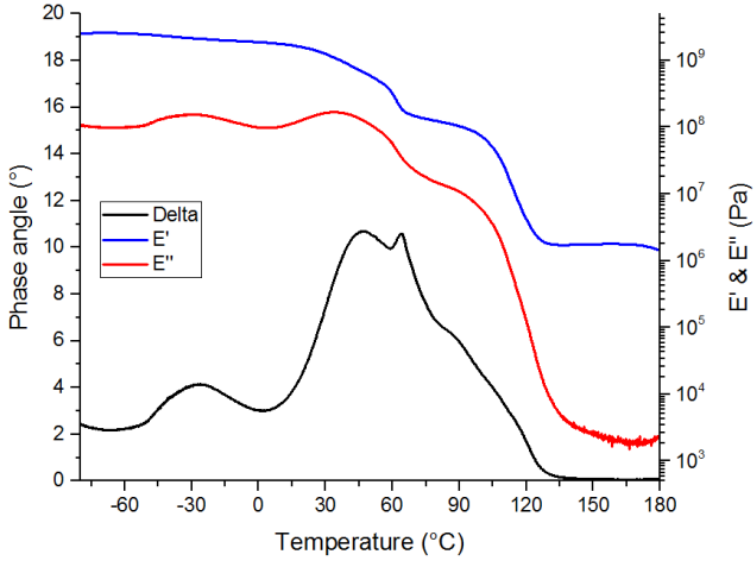

Figure IV.16. DMA plot of network **A** based on **(4)$_2$** and trithiol **53**, first heating at 2.5 K min^{-1} between -80 °C and 180 °C, showing the storage and loss modulus as a function of temperature.

Beyond 180 °C the storage modulus drops sharply, and the sample turns into a highly viscous liquid. The onset thereof can be seen around 165 °C. This transition corresponds with the loss of crosslinking (decrease in connectivity x) due to scission of the dimer units into monomeric anthracene units. The G'-G" crossover, which can be regarded as the point where a material changes from a crosslinked material into a viscous liquid (degelation), could not be studied in DMA as the material liquefied too quickly. We calculated using the acquired Arrhenius parameters that 25 % of the dimers have cleaved at 180 °C, leading to a connectivity x equal to 0.75. This connectivity is indeed still above the minimal connectivity

for a gel x_c of 0.50, according to the Flory-Stockmayer equation (equation 9). This (de)gelation point should be reached upon continuation of the experiment to 189 °C.

$x_c = \frac{1}{f-1}$ with f the number of functional groups and gelation when $x \geq x_c$ Equation 9

The intrinsically low modulus of network **B**, compared to **A**, makes the material more suitable for a visco-elastic characterization by dynamic rheometry. Rheological analysis of a 200 µm thick film of **B** was performed between parallel plates at frequencies between 0.1 and 10 Hz and temperatures from 30 °C up to 200 °C (Figure IV.17). Increasing the temperature leads to a stepwise decrease in both storage and loss moduli between 35 °C and 55 °C, which is slightly below the isotropization point found by DSC (59 °C). However, the heating rate at which the rheological measurement was performed (1 K/min) is one decade slower than the heating rate for the DSC experiment, which explains the small difference in transition temperatures. Between 55 °C and 170 °C the storage modulus of **B** is slightly increasing but remains virtually constant at a low value of 0.1 MPa, while the phase angle stays below 5 degrees; in this temperature range the material shows a typical entropy-elastic behavior. Beyond 170 °C both G' and G" steeply decrease, G' faster than G", until the values become equal at the point where crosslinking is lost, at around 185 °C, and the material starts to behave as a viscoelastic liquid rather than as an elastomer. Using the calculated Arrhenius parameters, a connectivity x of 0.33 remains at this point in the measurement. This is higher than the minimal connectivity for a gel (x = 0.25), which should be reached at 187.4 °C. This underestimation of the connectivity required for a gel can be explained by a significant amount of intramolecular bond formation which occurred due to the considerable dilution during cure.

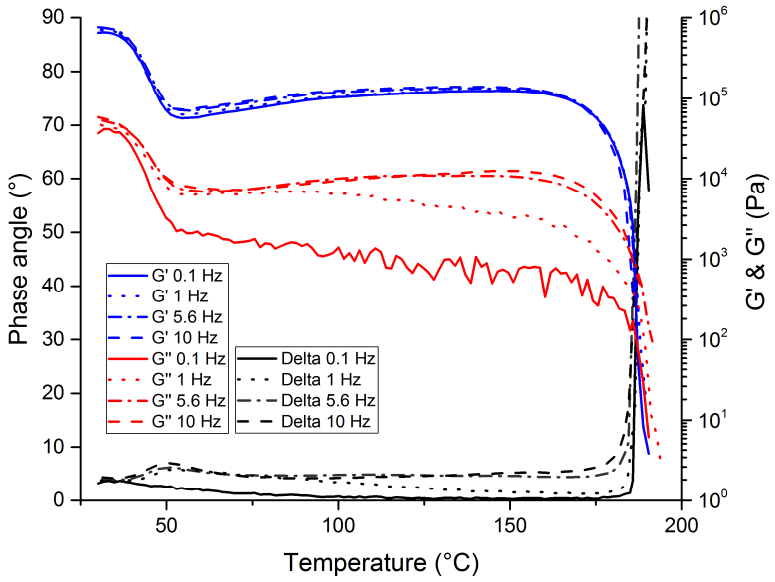

Figure IV.17. Dynamic rheometry curves of network **B** based on **(4)$_2$** and PDMS polythiol **54**: G', G" and phase angle as a function of temperature (1 K min^{-1} heating rate).

The results indicate that the anthracene dimer diene **(4)$_2$** can effectively be used to form crosslinked materials using thiol-ene chemistry. By heating the crosslinked materials above 170 °C, the dimer units split into two anthracene moieties, effectively reversing the crosslinking. The reverse process, *i.e.* the re-establishment of the network, should be possible by UVA-irradiation. In order to establish to what extent this reformation of the network can actually be accomplished, a 200 µm thick sample of thermally degraded **B** (prepared by heating virgin **B** for 10 minutes at 185 °C under argon), was exposed to UVA radiation in a UV rheometry setup, while measuring G', G" and the phase angle at a fixed frequency of 10 Hz and at 60 °C. The results are shown in Figure IV.18.

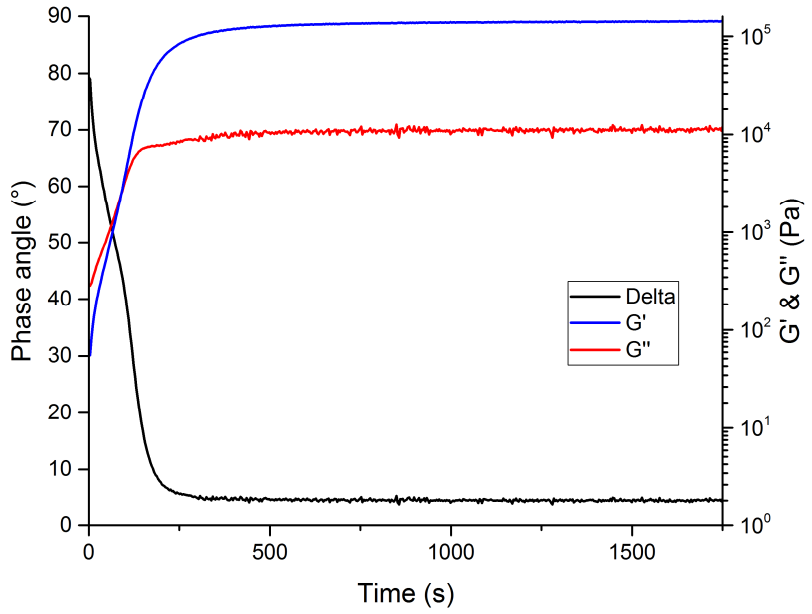

Figure IV.18. Dynamic rheometry curves of thermally degraded network **B** (200 µm thickness) during UVA irradiation (300-400 nm) with an intensity of approximately 2 W cm^{-2} at 60 °C: G', G" and phase angle (10 Hz) as a function of time.

Irradiation clearly re-establishes the material's mechanical integrity (increase in connectivity x). The crossing of G' and G" (gelation), indicating the formation of an elastic solid, occurs after 75 seconds of irradiation at approximately 2 W/cm^2. After 300 seconds of UV-exposure the rheological properties hardly change anymore and a solid rubber film is obtained. At 20 °C, the photochemical dimerization of dissociated **B** is much slower: the G'-G" crossover occurs after more than 20 minutes (Figure IV.19). While a higher temperature does lead to higher mobility, facilitating dimerization, the large reactivity difference has a more significant cause: dissociated **B** is an opaque (highly scattering) viscous liquid at room temperature, and becomes a clear non-scattering liquid around 50 °C, close to where the isotropization occurs. This observation indicates micro-phase separation between the anthracene containing parts of the material and the PDMS. Such phase separation can slow down crosslinking due to the scattering of the UV light, bringing down the effective absorbed dose of UV by the sample.

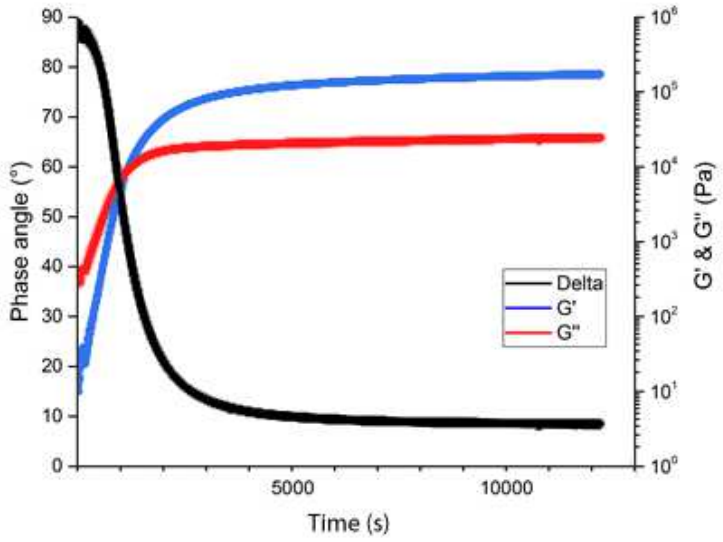

Figure IV.19. G', G" and the phase angle (10 Hz) of a film of thermally degraded **B** (200 µm thickness) as a function of time and a near UV (300-400 nm) intensity of approximately 2 W cm^{-2} at 20 °C.

For the more highly crosslinked network **A**, the photorheological characterization of the network reformation upon UVA exposure at room temperature is quite challenging, as vitrification induces large changes in the modulus upon crosslinking. Besides, the reduction in chain segment mobility upon vitrification can slow down the reactions and can be a limiting factor in the degree of conversion. For this reason, the re-establishment of the network by UVA-irradiation was investigated at 60 °C, above the T_g of network **A**. To thermally decompose network **A** into its liquid anthracene counterpart, a sample of virgin **A** was heated for 10 minutes at 185 °C under argon. The sample was subsequently exposed to UVA radiation at 60 °C in a UV rheometry setup, while measuring G', G" and the phase angle at a fixed frequency of 8 Hz. The results are shown in Figure IV.20.

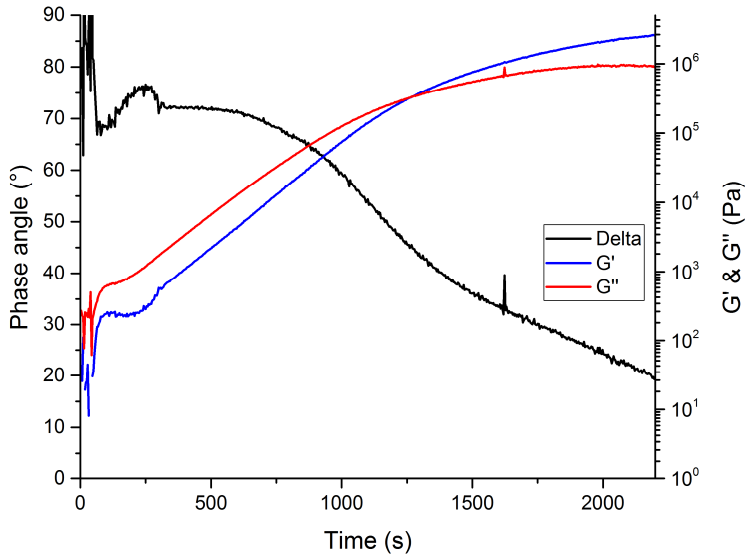

Figure IV.20. Dynamic rheometry curves for a film of thermally degraded **A** (200 µm thickness) during UVA (300-400 nm) irradiation with an intensity of approximately 2 W cm^{-2} at 60 °C: G', G" and phase angle (8 Hz) versus time.

The crossover of G' and G" is found at 1200 s of UVA exposure, which is much later compared to the PDMS-based **B** material. The storage and loss moduli continued to increase after the crossover beyond the measurable range of the rheometer.

The difference in gelation time has several causes. Firstly, a higher minimal connectivity is required for gelation of network **A** (x = 0.50 instead of 0.25). Secondly, the connectivity x before irradiation is not 0 and although the same anthracene chemistry is used, this initial connectivity might also differ between the materials. A third difference is the higher concentration of anthracene groups in network **A**. Due to this higher concentration, more energy (and thus irradiation time) is required for changes in connectivity.

The above results show that the two types of prepared thiol-ene networks containing anthracene dimers as reversible bonds in the interconnecting chains can be effectively split into the anthracene functionalized building blocks by heating to a temperature of 180 °C for 10 minutes under an inert atmosphere. Exposure of the resulting anthracene functionalized building blocks to UVA at slightly elevated temperature (60 °C) gives networks with mechanical properties that are close to the original networks. Exposure to UVA at room temperature resulted, for the two investigated types of materials, into inefficient photocuring reactions, either due to inhomogeneities, in case of the PDMS-based

network, or due to limitations to the conversion because of vitrification, in case of the trithiol-based network.

3 Conclusion

A soluble alkene-functionalized dimer of 9-anthracenemethanol (**(4)$_2$**), prepared from readily available compounds, was combined with two multifunctional thiols, i.e. one well-defined mixture of isomeric trithiols (**53**), prepared from 1,2,4-trivinylcyclohexane in a simple two-step procedure, and an available thiopropyl functionalized PDMS (**54**). The networks formed from these two types of thiols resulted in a hard, crosslinked material (**A**; from trithiol **53**) and a soft, flexible rubber (**B**; from PDMS thiol **54**). All anthracene dimer containing materials, independent from the type of network these were included in, decomposed into anthracene functionalized building blocks in the same temperature range as the parent anthracene dimer (**(4)$_2$**), *i.e.*, above 160 °C. DSC analysis of the two types of networks showed for both materials a weak endothermic transition between 50 °C and 60 °C, which proved to be either melting of a crystalline anthracene-dimer phase (**A**) or a liquid crystalline phase (**B**), based on evidence obtained by XRD measurements, which gave sharp reflections for **A** and a single broad reflection for **B**. Polarization microscopy on **B** confirmed the presence of birefringent domains, typical for a nematic liquid crystalline phase. Above 125 °C and 60 °C, **A** and **B** behave like crosslinked rubbers up to 160-170 °C, the onset of dimer dissociation. Above this point, both materials quickly lose their rubber characteristics and start to behave like viscoelastic liquids. In DSC, thermal dissociation of **(4)$_2$** is only slightly visible and was not visible for the network materials (**A** and **B**). This finding suggests that the splitting of dimer does not involve a significant change in enthalpy under these specific DSC conditions. Thermally dissociated anthracene dimer networks can be readily restored to a state that resembles their original state by irradiation with UVA, provided that the samples are homogeneous and no vitrification takes place during dimerization. In this particular case, for both networks **A** and **B**, a slight heating to 60 °C was needed to prevent vitrification during the dimerization (**A**) or to create a homogeneous non-scattering sample (**B**).

4 Experimental section

4.1 Materials and methods

Nuclear magnetic resonance spectra were recorded on a Bruker Avance 300 (300 MHz), or a Bruker DRX 500 (500 MHz) NMR spectrometer at room temperature. DSC experiments were performed on a TA Instruments Q2000 Differential Scanning Calorimeter, equipped with either a Refrigerated Cooling System (RCS) or a Liquid Nitrogen Cooling System (LNCS). A Tzero calibration was performed at 10 K min^{-1} using sapphire discs and temperature and enthalpy calibrations were performed using indium calibration standards for Tzero hermetic aluminum pans. The instrument was purged using a 25 ml min^{-1} nitrogen gas purge flow. Dynamic Mechanical Analysis (DMA) experiments were performed on a TA Instruments Q800 Dynamic Mechanical Analyzer, equipped with a Liquid Nitrogen Cooling System. All experiments are performed in tension using a film tension set-up (TA Instruments), using rectangular specimens with a width of 2 mm and a thickness of ~1 mm. Dynamic rheometry experiments were performed on a TA Instruments AR-G2 dynamic rheometer equipped with an electrically heated plates setup using disposable aluminum parallel plates. For experiments under UVA irradiation, the lower plate assembly was replaced by a dedicated UV light guide accessory equipped with a disposable acrylic plate and connected to a Lumen Dynamics 100 W Mercury Arc lamp with 320 - 500 nm broad band gap filter + 1 % neutral-density 2.0 filters. Measurements were performed in a 25 mm parallel plate setup using 200 µm thick films. A Mettler-Toledo TGA/SDTA 851e under nitrogen atmosphere was used for thermal dissociation of bulk dimers.

All chemicals were purchased from either ABCR, Sigma-Aldrich, TCI Europe or Acros Organics and were used as such. IR spectra were recorded with a Perkin Elmer FTIR SPECTRUM 1000 and a PIKE Miracle ATR unit. LC-MS analyses were performed on an Agilent Technologies 1100 series LC/MSD system with a diode array detector (DAD) and single quad MS. Analytical reversed phase HPLC-analyses were performed with a Phenomenex Luna C18 (2) column (5 µm, 250 mm × 4.6 mm) and a solvent gradient (0 – 100 % acetonitrile in H_2O in 15 minutes), the eluted compounds were analyzed via UV detection (214 nm). UV dimerization occurred in a Metalight Classic from Primotec, with 12 double 365 nm UV lamps of 9 W each.

4.2 Synthesis of 1,2,4-tris(1-mercaptoethyl)cyclohexane and isomers (54)

1,2,4-Trivinylcyclohexane (mixture of isomers, 100 mL, 0.52 mol) was cooled to -10 °C in an ice-salt bath in a 1 L erlemeyer flask. Under vigorous stirring and continued cooling in the ice-salt bath, thioacetic acid (121.5 mL, 1.55 mol) was slowly added, followed by 2,2-dimethoxy-2-phenylacetophenone (1.5 g, 3.9 mmol). An efficient reflux cooler was then fitted, followed by the removal of the ice-salt cooling bath. After the initial exotherm had subsided, the reaction mixture was brought under argon and was irradiated for 1 hour, using a Metalight irradiation chamber, fitted with 365 nm fluorescent light bulbs. Subsequently hydrochloric acid (2 M, 200 mL) was added and the reaction mixture was then refluxed overnight. Next, the mixture was extracted with diethyl ether (2×200 mL). The combined organic layers were then washed with brine (2×200 ml), dried over magnesium sulfate and concentrated *in vacuo*, yielding a slightly yellow oil that was further purified by vacuum distillation (0.1 mm Hg 130 °C) to yield 1,2,4-tris(2-mercaptoethyl)cyclohexane as a mixture of (stereo) isomers (**54**) (116 g, 85 %).

5 References

1. Kloxin, C. J.; Bowman, C. N., *Chemical Society Reviews* **2013,** *42* (17), 7161-7173.
2. (a) Ali, A. H.; Srinivasan, K. S. V., *Polym. Int.* **1997,** *43* (4), 310-316; (b) Oya, N.; Sukarsaatmadja, P.; Ishida, K.; Yoshie, N., *Polymer Journal* **2012,** *44* (7), 724-729.
3. Nakayama, Y.; Matsuda, T., *J. Polym. Sci. Part A: Polym. Chem.* **2005,** *43* (15), 3324-3336.
4. Xu, J. F.; Chen, Y. Z.; Wu, L. Z.; Tung, C. H.; Yang, Q. Z., *Org. Lett.* **2013,** *15* (24), 6148-6151.
5. Van Damme, J.; Vlaminck, L.; Van Assche, G.; Van Mele, B.; van den Berg, O.; Du Prez, F., *Tetrahedron* **2016,** *72* (29), 4303-4311.
6. Bouas-Laurent, H.; Castellan, A.; Desvergne, J.-P.; Lapouyade, R., *Chem. Soc. Rev.* **2001,** *30* (4), 248-263.
7. Manhart, J.; Ayalur-Karunakaran, S.; Radl, S.; Oesterreicher, A.; Moser, A.; Ganser, C.; Teichert, C.; Pinter, G.; Kern, W.; Griesser, T.; Schlögl, S., *Polymer* **2016,** *102*, 10-20.
8. (a) Hoyle, C. E.; Bowman, C. N., *Angew. Chem. Int. Ed.* **2010,** *49* (9), 1540-1573; (b) Hoyle, C. E.; Lee, T. Y.; Roper, T., *J. Polym. Sci. Part A: Polym. Chem.* **2004,** *42* (21), 5301-5338; (c) Lowe, A. B., *Polym. Chem.* **2010,** *1* (1), 17-36.
9. Bowman, C.; Cramer, N.; Shandas, R.; Nair, D. P. Thiol-vinyl and thiol-yne shape memory polymers for medical use. WO2009132070A2, **2009**.
10. Hoyle, C. E.; Nazarenko, S.; Wei, H. Photocurable thiol-ene copolymer low gas permeability membranes. US20090253805A1, **2009**.
11. Woods, J. G.; Angus, R. O., Jr.; Schall, J. D. Thiol-ene cured oil-resistant polyacrylate sealants for in-place gasketing applications. WO2009137197A2, **2009**.

12. (a) Hawker, C. J.; Campos, L. M.; Meinel, I. Thiol-ene-based poly(alkylsiloxane) materials for lithography. US20090096136A1, **2009**; (b) Campos, L. M.; Truong, T. T.; Shim, D. E.; Dimitriou, M. D.; Shir, D.; Meinel, I.; Gerbec, J. A.; Hahn, H. T.; Rogers, J. A.; Hawker, C. J., *Chem. Mater.* **2009,** *21* (21), 5319-5326.
13. Bowman, C.; Anseth, K.; Hacioglu, B.; Nuttelman, C. Degradable thiol-ene polymers. US7288608B2, **2007**.
14. (a) Bowman, C.; Lu, H.; Stansbury, J. Novel photopolymers and use in dental restorative materials. US20070082966A1, **2007**; (b) Bowman, C. N.; Cramer, N. B. Photopolymerizable resin systems for dental restorative materials. US20090270528A1, **2009**; (c) Rheinberger, V.; Moszner, N.; Salz, U. Polymerized alkoxysilyl derivatives of norbornene and mercaptans as dental materials. DE19619046A1, **1997**.
15. Coates, D.; Nolan, P.; Marden, S. A. Polymer-dispersed liquid-crystal system based on thiolene type polymer matrix precursor. GB2277744A, **1994**.
16. Chen, K.; Huang, H. Polymer electrolyte composition of salt-containing thiol-ene matrix. WO9635238A1, **1996**.
17. Jacobine, A. F., In *Radiation Curing in Polymer Science and Technology III*, Fouassier, J. P.; Rabek, J. F., Eds. Elsevier: London, **1993**; Vol. III.
18. Carlborg, C. F.; Haraldsson, T.; Oberg, K.; Malkoch, M.; van der Wijngaart, W., *Lab Chip* **2011,** *11* (18), 3136-3147.
19. Zhang, J.; Chen, Y.; Brook, M. A., *Langmuir* **2013,** *29* (40), 12432-12442.
20. van den Berg, O.; Nguyen, L. T. T.; Teixeira, R. F. A.; Goethals, F.; Ozdilek, C.; Berghmans, S.; Du Prez, F. E., *Macromolecules* **2014,** *47* (4), 1292-1300.
21. (a) Payamyar, P.; Kaja, K.; Ruiz-Vargas, C.; Stemmer, A.; Murray, D. J.; Johnson, C. J.; King, B. T.; Schiffmann, F.; VandeVondele, J.; Renn, A.; Gotzinger, S.; Ceroni, P.; Schutz, A.; Lee, L. T.; Zheng, Z. K.; Sakamoto, J.; Schluter, A. D., *Adv. Mater.* **2014,** *26* (13), 2052-2058; (b) Goldbach, J. T.; Russell, T. P.; Penelle, J., *Macromolecules* **2002,** *35* (11), 4271-4276; (c) Song, Y. K.; Lee, K. H.; Hong, W. S.; Cho, S. Y.; Yu, H. C.; Chung, C. M., *J. Mater. Chem.* **2012,** *22* (4), 1380-1386.
22. Liu, B.; Wang, H.; Zhang, L.; Yang, G.; Liu, X.; Kim, I., *Polym. Chem.* **2013,** *4*, 2428-2431.
23. Fritz, D.; Walter, F.; Walter, S. Process for the production of 1, 2, 4-trivinylcyclohexane. US2967895A, **1961**.

Chapter V: Reversible polyurethane materials: easy removability, remoldability and stress-relaxation

Abstract

Anthracene dimer diols having very different thermal stabilities have been incorporated in polyurethane networks. The thermal de-crosslinking of these networks was shown to be dependent on the anthracene dimer used, allowing tunable thermal degradation. This scission was studied using (HR-MAS) NMR, DSC and rheometry. The tunable thermal decrosslinking was validated as a technique to easily remove the coatings at their end-of-life. The UV irradiation of the thermally degraded materials allows for recuring the coatings to materials having similar properties. By simultaneous irradiation and heating of (partially) reversibly cross-linked networks, the networks were able to relief internal stress and adopt a new permanent shape.

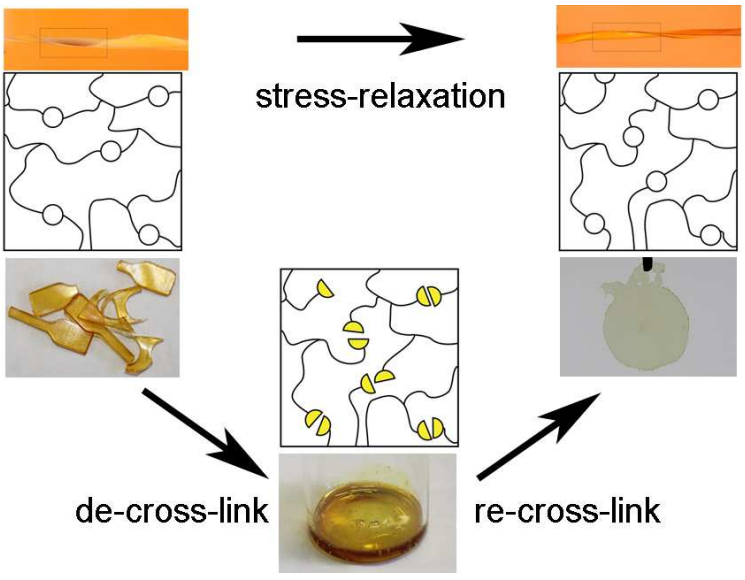

The results discussed in this chapter have been published as:

> Van Damme , J.; van den Berg, O.; Vlaminck, L.; Brancart, J.; Van Assche, G.; Du Prez, F. Anthracene-based polyurethane networks: tunable thermal degradation, photochemical cure and stress-relaxation, Eur. Polym. J. **2018**, doi.org/10.1016/j.eurpolymj.2018.06.018

Collaborators:

The practical workload was shared with Laetitia Vlaminck (master thesis student) and Lea Sollka (internship student).

1 Introduction

In this chapter, we introduce several anthracene derivatives in polyurethane materials (PUs). PUs are commonly used for making foams, elastomers, adhesives and coatings. Their unique properties are a result of hydrogen bridge formation between the repeating carbamate groups. Short repeating units result in hard, crystalline domains which act as physical cross-links. Most often, PU networks are made by polyaddition of polyols with diisocyanates, while the use of polyisocyanates to achieve a cross-linked material is also applied in industrial context. However, isocyanates have harmful effects on human and environment and are progressively banned by Europe (REACH).[1] Attractive alternatives are curing chemistries that form urethanes without using (toxic) isocyanates. For example, polyhydroxyurethanes can be formed by the polyaddition of cyclic carbonates and amines.[2] The urethane bonds can also be made beforehand in precursor molecules, followed by cross-linking using a different chemistry such as acrylate polymerization[3] or thiol-ene addition.[4]

Additionally, the increasing demand on the performance and sustainability of polymer materials, as well as the request for adaptability and additional functionalities, has inspired scientists to incorporate reversible bonds to develop covalently adaptable networks.[5] Depending on the chemistry involved, these reversible bonds may lead to bond exchange while maintaining a constant connectivity (vitrimers)[6] or to a (temporary) change in connectivity.

Self-healing polyurethanes have been developed by incorporating thermoreversible bonds such as Diels-Alder cycloadducts[7] and triazolinedione-ene adducts.[8] Raising the temperature of these materials leads to bond scission and thus a lower connectivity, which is restored upon cooling. This temporary decrease and increase in connectivity allows the formation of new bonds across a damaged area, resulting in a (partial) recuperation of the original properties and longer lifetimes.

Photoreversible bonds formed by coumarine dimerization, have also been incorporated in polyurethane materials.[9] The [2+2] cycloaddition of the pending coumarine groups requires irradiation above 270 nm (e.g. 350 nm), while scission of the formed dimers requires irradiation below 270 nm (e.g. 254 nm). Photochemical scission of the coumarine bonds at cut surfaces, followed by photostimulated cross-linking while pressing the cut surfaces together, led to reattachment with partial restoration of the mechanical properties.

Very recently, Fang and coworkers developed thin self-healing polyurethanes using anthracene dimers as reversible cross-links.[10] For this, they started from prepolymers having pendent anthracene groups, followed by photochemical cure (anthracene dimerization) during 20 minutes. Cracked materials were repaired by heating to 130 °C for 1 hour, which cleaves the dianthracene bonds, followed by anthracene dimerization by 10 minutes irradiation using UVA light.

It was shown in chapter III that the thermal scission of the model dimers is highly tunable by altering the 9-substituent. Additionally, the thermal stability of similar dimers can be raised by the occurrence of melting points at or above the thermal scission temperature region. The thermal scission behavior of the studied derivative was similar when incorporated in cross-linked materials, and thus thermally cleavable materials with a designed scission behavior could be made (chapter IV).

In this chapter, we introduce several alcohol-functionalized anthracene dimers and discuss their thermal stabilities in polyurethane materials. These anthracene dimer building blocks and the polyurethane materials are industrially more relevant, as polyurethanes are more widely spread than thiol-ene cured materials (chapter IV). Additionally, the hydrogen bridges in the polyurethanes may influence the mobility of the (di)anthracene groups and therefore alter the thermal behavior.[11] By using pre-dimerized anthracenes, the derivatives can easily be implemented in existing PU-formulations. It eliminates the necessity of an – often slow and incomplete– photochemical curing step, which limits the material dimensions to thin films and coatings. The mechanical and thermal properties of the synthesized polyurethanes were studied for different types and quantities of reversible bonds. The thermal scission of these materials was evaluated as a method to easily remove coatings. Also, proof of concept trials for stress-relaxation by simultaneous dimerization and dimer scission were performed.

2 Results and discussion

2.1 Material development

2.1.1 Compound selection and synthesis

In chapter III, we have shown that the ester based derivatives (**$(47)_2$** and **$(48)_2$**; Figure V.1) had a high thermal stability, with significant scission occurring above 160 °C. Alternatively, anthracene ethers (**$(28)_2$** and **$(50)_2$**; Figure V.1) had a low thermal stability, with fast scission occurring above 110 °C.

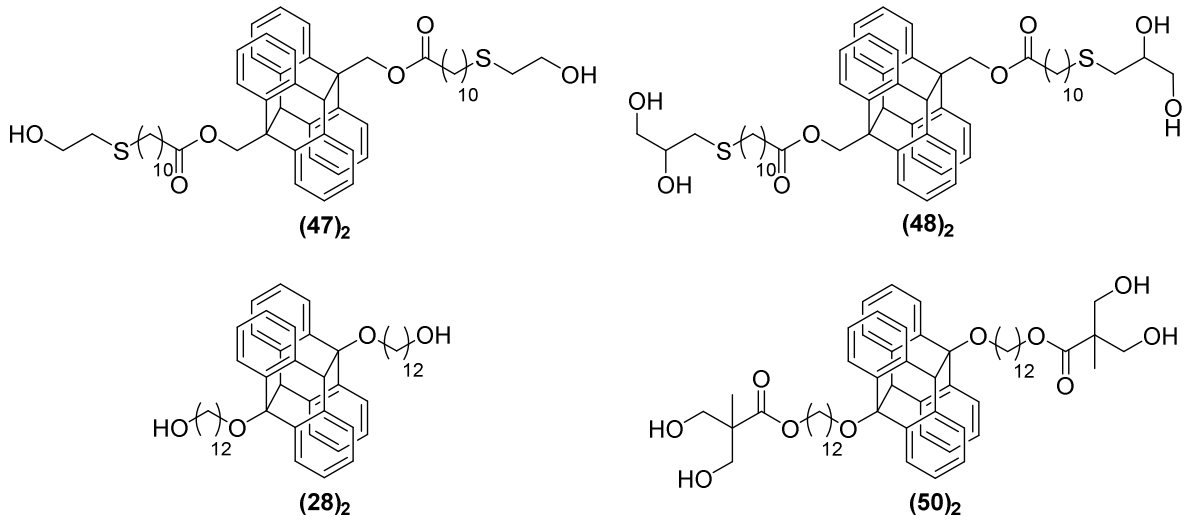

Figure V.1. Structures of the used dimer diols and dimer tetraols.

As anthracene dimers **(47)$_2$** and **(28)$_2$** are bifunctional, a multifunctional cross-linker is required to form a PU-network. While polyols could have been used as cross-linker in combination with diisocyanates, the use of a polyisocyanate, i.e. the isocyanurate trimer of hexamethylene diisocyanate (**56**, HDI-trimer, Figure V.2), was preferred because this reduced the number of parameters, simplifies the synthetic procedure, and ensures a homogeneous cross-linking. Additionally, scission of these networks would lead to monodisperse (triarm) scission products (similar to network A in chapter III). Although this design simplifies the analysis of the reversible bond behavior, it does require a large amount of dimer diols and limits the tunability of the thermal and mechanical material properties. Therefore, additional materials were made with non-reversible bonds by using readily available hydrophobic diols.

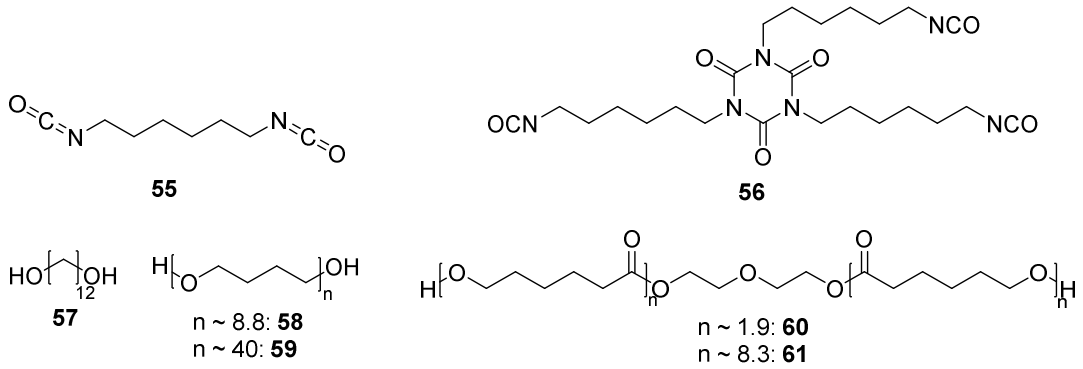

Figure V.2. Structures of the used isocyanates and diols.

First, 1,12-dodecane diol (**57**) was used as non-reversible diol, which has a flexible aliphatic chain. The lack of additional functional groups ensures high stability and hydrophobicity. However, because of the melting point (79-81 °C) and limited solubility (106 g/l THF), relatively large amounts of solvent were required to solubilize these formulation mixtures. Secondly, polytetramethyleneoxide (PTMEO) was used having different molecular weights (i.e. ~ 650 g/mol and ~ 2900 g/mol (**58** and **59**)). However, when keeping a fully cross-linked network consisting solely out of HDI-trimer and PTMEO chains at 120 °C for 2 hours, darkening and liquefaction of the material was observed (Figure V.3). As thermo-oxidation and ether scission occurs in the presence of air and at elevated temperatures, these materials were also dismissed.[12] Finally, polycaprolactone diols having molecular weights of approximately 530 and 2000 g/mol (**60** and **61**) were used successfully as non-reversible chains.

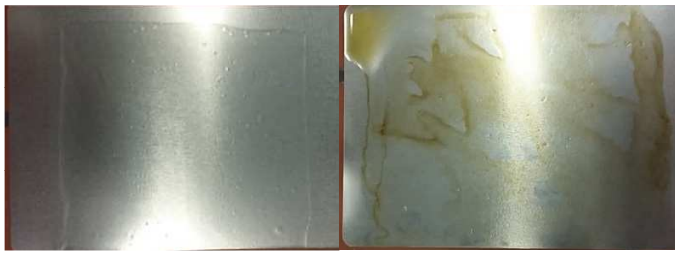

Figure V.3. PU coating made from PTMEO and HDI-trimer. Left: quantitatively cured after overnight heating at 70 °C; right: additional 2 h at 120 °C.

As anthracene dimers **(48)$_2$** and **(50)$_2$** are tetraols, no additional cross-linkers are required and only a diisocyanate is necessary to form networks. Here, the readily available hexamethylene diisocyanate (**55**, HDI) was chosen. This methodology has the benefit that by adding chain extenders, the cross-link densities and other properties can easily be tuned, without creating potentially undesirable non-reversible cross-links. In this work, only two materials are described, consisting of the dimer tetraols and HDI: D48_100 based on dimer **(48)$_2$** and D50_100 based on dimer **(50)$_2$**. All material formulations are given in Table V.1.

Table V.1. Formulations for materials based on **(47)$_2$** or **(28)$_2$** with HDI_3 and **(48)$_2$** or **(50)$_2$** with HDI.

Material	Dimer diol	Non-reversible diol	Isocyanate HDI or HDI_3 (equiv.)	Reversible diol (equiv.)	Non-reversible diol (equiv.)
DOD_0	-	**57**	0.66	0	1
PCL530_0	-	**58**	0.66	0	1
PCL2000_0	-	**59**	0.66	0	1
D47DOD_25	**(47)$_2$**	**57**	0.66	0.25	0.75
D47DOD_50	**(47)$_2$**	**57**	0.66	0.50	0.50
D47DOD_75	**(47)$_2$**	**57**	0.66	0.75	0.25
D47PCL530_50	**(47)$_2$**	**58**	0.66	0.50	0.50
D47PCL2000_25	**(47)$_2$**	**59**	0.66	0.25	0.75
D47PCL2000_50	**(47)$_2$**	**59**	0.66	0.50	0.50
D47_100	**(47)$_2$**	-	0.66	1	0
D28DOD_25	**(28)$_2$**	**57**	0.66	0.25	0.75
D28DOD_50	**(28)$_2$**	**57**	0.66	0.50	0.50
D28DOD_75	**(28)$_2$**	**57**	0.66	0.75	0.25
D28_100	**(28)$_2$**	-	0.66	1	0
D48_100	**(48)$_2$**	-	1	1	0
D50_100	**(50)$_2$**	-	1	1	0

2.1.2 Curing and gel content

All materials were made in a one-pot fashion, using dibutyltin dilaurate as catalyst and a minimal amount of anhydrous THF as solvent. In some instances, dry DMF was chosen as a solvent to avoid using excessive THF, which led to the formation of highly swollen networks resulting in fractures during sample drying. After overnight heating of the samples at 70 °C, full cure was confirmed through the disappearance of the isocyanate stretch peak around 2270 cm^{-1} in infrared spectroscopy.

The gel content of the materials was determined by soxhlet extraction using either THF or acetone as solvent. While THF (307 % for D47PCL2000_50) swelled the materials better than acetone (184 % for for D47PCL2000_50), this led to cracking in some instances. The gel content of the materials reached between 94 % and 99 % with the exception of D48_100 (73%). The low gel content of the latter could be ascribed to incomplete cure of the alcohol groups due to the lower solubility of the (curing) compound and the lower reactivity of the secondary alcohols. This is supported by the presence of a broad infrared absorption peak around 3475 cm^{-1} (Figure V.4).

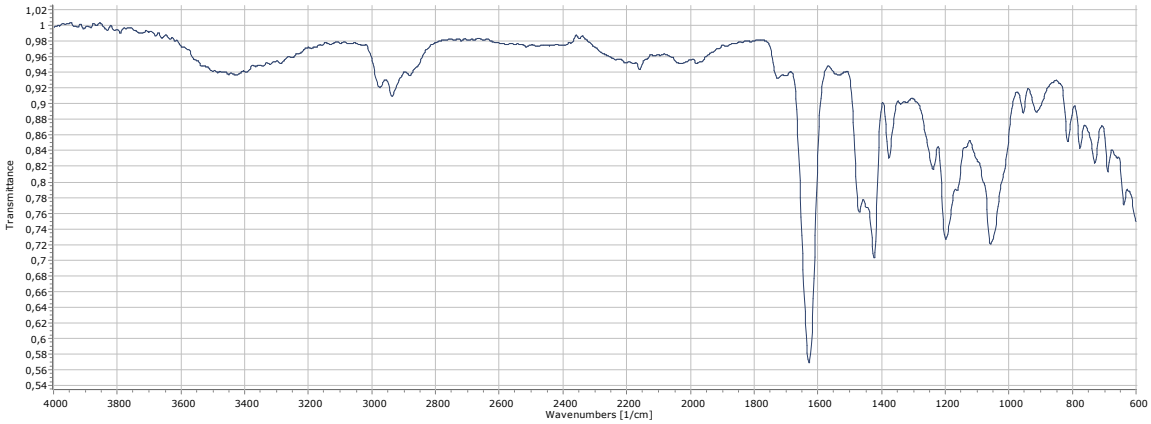

Figure V.4. Infrared spectrum of D48_100 material.

2.1.3 Thermomechanical properties

The thermal stability of the polymers was studied using thermogravimetric analysis (TGA) under nitrogen atmosphere. Material mass loss exceeded 3 % at 218 - 245 °C for the materials based on **(47)$_2$**. While this is lower than for the reference material DOD_0 (279 °C), these temperatures are still higher than what is required for thermally induced dimer scission. The materials based on **(28)$_2$** showed a higher thermal stability, with the mass loss exceeding 3 % at 259 – 294 °C, similar to the reference material. The temperatures at which 3 % mass loss occurred for the materials based on the tetraols **(48)$_2$** and **(50)$_2$** were 249 °C (D48_100) and 286 °C (D50_100), respectively. These values are in line with the results for the materials based **(47)$_2$** and **(28)$_2$**, indicating that the alternative polymer topology does not significantly influence the degradation properties.

The mechanical properties of the 1,12-dodecanol-based materials and the fully reversible networks in the absence of any non-reversible diol were studied by stress-strain measurements using a tensile apparatus. The data thereof are given in Table V.2. All materials were rubbery, with glass transition temperatures (T_g) slightly below room temperature. These relatively low T_g-values are a result of the (long) aliphatic chains of the monomers, which increase the flexibility of the polymer network. These rubbery networks allow for sufficient mobility to accomplish photochemical reversible dianthracene scission/ formation under ambient conditions.

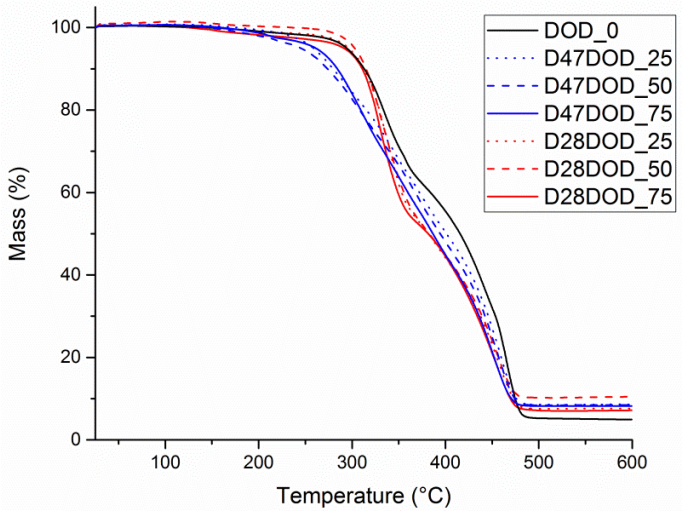

Figure V.5. Thermogravimetric thermograms of the 1,12-dodecanol-based polyurethane materials (under N_2 atmosphere, at 10 K min^{-1}).

The variation in mechanical properties of the materials shows no clear relation to their composition. However, it is noticeable that the use of dimer **(28)$_2$** results in lower T_g's and Young's moduli. This is probably a consequence of the completely aliphatic chains, compared to dimer **(47)$_2$** bearing ester and thioether groups. Nevertheless, full optimization of the mechanical properties lies beyond the scope of this work.

Table V.2. Tensile, DSC and DMTA data.

Material	Strain at break (%)	Stress at break (Mpa)	Young modulus (Mpa)	T_g via DSC (°C)	T_g via DMTA (°C)
DOD_0	290	29	145	13.4	21.0
D47DOD_25	280	8	85	16.5	15.1
D47DOD_50	320	25	50	11.6	25.4
D47DOD_75	230	6	65	13.2	12.3
D47_100	120	12	186	14.2	23.8
D28DOD_25	320	27	20	9.1	8.5
D28DOD_50	240	21	61	5.4	15.2
D28DOD_75	220	17	74	6.9	8.9
D48_100	260	19	15	8.6	9.1
D50_100	194	24	45	11	8.7

2.2 Thermal scission of the anthracene-based networks

2.2.1 Scission and liquefaction of the 1,12-dodecane-based networks

The thermal scission of the anthracene dimer crosslinks of the networks was studied by placing samples in a pre-heated oven for 10 minutes. Dependent on the oven temperature and the network composition, some networks disintegrated and became soluble. The ratio of the remaining dimer bonds r_{dim} was quantified by ^{1}H-NMR spectra of the fully soluble samples (Table V.3 and Table V.4). Using HR-MAS ^{1}H-NMR, the insoluble samples of D47DOD_75 were also measured. Using this data, the total connectivity of the polymer bonds x is derived for each sample (equations 10-12).

$$x = x_{nr} + x_r \qquad \text{Equation 10}$$

$$x_{nr} = \frac{[non-reversible\ bonds]}{[total\ bonds]} = \frac{[dodecane\ diol]}{[dodecane\ diol]+[dimer\ diol]_0} \qquad \text{Equation 11}$$

$$x_{nr} = r_{dim}\ \frac{[dimer\ diol]_0}{[dodecane\ diol]+[dimer\ diol]_0} \qquad \text{Equation 12}$$

Liquid samples had connectivities up to 0.50, while the insoluble samples of D47DOD_75 had connectivities between 0.73 and 0.97. This is in agreement with the Flory-Stockmayer equation (equation 8, chapter IV), which predicts, for this type of architectures, a minimal connectivity of 0.5 to observe gelation.[13] These gel-sol transitions occurred at 180 °C and 120 °C for the materials based on **(47)$_2$** and **(28)$_2$**, respectively. These temperatures are similar to what was observed for the starting compounds,[14] proving that the thermal de-crosslinking of anthracene-based networks is mainly determined by the substituents present on the anthracene rings.

Because of these good similarities, the experimental data are compared to connectivities estimated using the thermal scission activation energies and pre-exponential factors for **(47)$_2$** (E_a = 148 kJ/mol, ln(A/s^{-1}) = 32.5) and **(28)$_2$** (E_a = 92 kJ/mol, ln(A/s^{-1}) = 21.1) determined in chapter III.

Using the Arrhenius parameters the reaction constants are calculated for each temperature using equation:

$$\boldsymbol{k = A * e^{-\frac{E_a}{RT}}} \qquad \text{Equation 13}$$

The concentration for a first order dimer scission reaction after a given time t is given by:

$$[Dimer] = [Dimer]_0 e^{-kt}$$ Equation 14

Therefore, the remaining dimer bond ratio r_{dim} can be calculated as.

$$r_{dim} = e^{-kt}$$ Equation 15

Alternatively, the fraction of cleaved dimer bonds can be calculated as:

$$r_{mono} = 1 - r_{dim} = 1 - e^{-kt}$$ Equation 16

When the temperatures were varying, these calculations were done for each time interval (up to several seconds) between datapoints.

The differences between the experimental and simulated data are probably largely due to the uncontrolled heating and cooling rates of the materials in the oven, as well as scission that happened prior to the experiment. The largest mismatch is found for the materials based on **(28)$_2$**. These experimental samples all have a lower connectivity than simulated. This is partially due to thermal scission occurring during sample cure (at 70 °C) and storing/handling prior to the experiments, as **(28)$_2$** is known to have a relatively low thermal stability.

Also experiments for the tetraol-based networks D48_100 and D50_100 show good similarity between the experimental and simulated dimer content (Table V.3 and Table V.4). D48_100 and D50_100 became soluble after heating for 10 minutes at 190 °C and 130 °C, with r_{dim} values of 0.21 and 0.33, respectively. These temperatures are slightly higher than those for the diol-based networks. This is explained by the different architecture of these materials, i.e. compared to the diol-based networks, the tetraol based networks require the scission of more dimer bonds before the formation of soluble polymer chains.

Table V.3. Ratio of remaining dimer bonds r_{dim} (determined via ^{1}H-NMR and HR-MAS ^{1}H-NMR*), the derived connectivity x and the simulated connectivity x_{sim} after heating of **(47)$_2$**- and **(48)$_2$**-based materials for 10 minutes.

	160 °C	170 °C	180 °C	190 °C	200°C	210°C
r_{dim} D47DOD_25	-	-	-	-	-	-
r_{dim} D47DOD_50	-	-	-	-	-	-
r_{dim} D47DOD_75	0.96*	0.82*	0.64*	0.04	0.02	0
r_{dim} D47_100	-	-	0.23	0.02	0.02	0
r_{dim} D48_100	-	-	-	0.21	0.08	0.03
x D47DOD_25	-	-	-	-	-	-
x D47DOD_50	-	-	-	-	-	-
x D47DOD_75	0.97	0.87	0.73	0.28	0.27	0.25
x D47_100	-	-	0.23	0.02	0.02	0
x D48_100	-	-	-	0.21	0.08	0.03
x_{sim} D47DOD_25	0.98	0.94	0.88	0.80	0.76	0.75
x_{sim} D47DOD_50	0.95	0.88	0.76	0.60	0.52	0.50
x_{sim} D47DOD_75	0.93	0.82	0.63	0.40	0.27	0.25
x_{sim} D47_100	0.90	0.76	0.51	0.20	0.03	0
x_{sim} D48_100	0.90	0.76	0.51	0.20	0.03	0

Table V.4. Ratio of remaining dimer bonds r_{dim} (determined via ^{1}H-NMR) , the derived connectivity x and the simulated connectivity x_{sim} after heating of **(28)$_2$**- and **(50)$_2$**-based materials for 10 minutes.

Material	100 °C	110 °C	120 °C	130 °C	140°C	150°C
r_{dim} D28DOD_25	-	-	-	-	-	-
r_{dim} D28DOD_50	-	-	-	-	0	0
r_{dim} D28DOD_75	-	-	0.20	0.05	0	0
r_{dim} D28_100	-	-	0.18	0.04	0	0
r_{dim} D50_100	-	-	-	0.33	0	0
x D28DOD_25	-	-	-	-	-	-
x D28DOD_50	-	-	-	-	0.50	0.50
x D28DOD_75	-	-	0.40	0.29	0.25	0.25
x D28_100	-	-	0.18	0.04	0	0
x D50_100	-	-	-	0.33	0	0
x_{sim} D28DOD_25	0.97	0.95	0.90	0.84	0.78	0.76
x_{sim} D28DOD_50	0.95	0.89	0.80	0.68	0.57	0.51
x_{sim} D28DOD_75	0.92	0.84	0.69	0.51	0.35	0.27
x_{sim} D28_100	0.89	0.78	0.59	0.35	0.13	0.02
x_{sim} D50_100	0.89	0.78	0.59	0.35	0.13	0.02

2.2.2 Thermal scission of materials based on PCL and $(47)_2$

The thermal scission of the materials based on **$(47)_2$** and using a PCL diol were further studied by differential scanning calorimetry (DSC). As a decrease in cross-linking density resulting from thermal scission would lower the T_g, the scission in a controlled environment can be monitored by determining the T_g of the material.

To study this, D47PCL530_50 samples were heated and cooled in a cyclic manner. They were heated to a selected temperature, kept for 5 minutes, and cooled, except for the last cycle, which had a 20 min isotherm (Figure V.6). After an initial rise in T_g between the first and second heating (e.g. from 5 °C to 12 °C when heating to 150 °C), attributed to the evaporation of moisture or plasticizing small molecules (solvent), the T_g gradually decreased (by 3 K after 1 hour at 150 °C). As can be seen, a significant lowering of the T_g only occurred above 150 °C, indicating that below this temperature the thermal scission is very slow. At higher temperatures, the glass transition temperatures dropped faster (with up to 18 K difference).

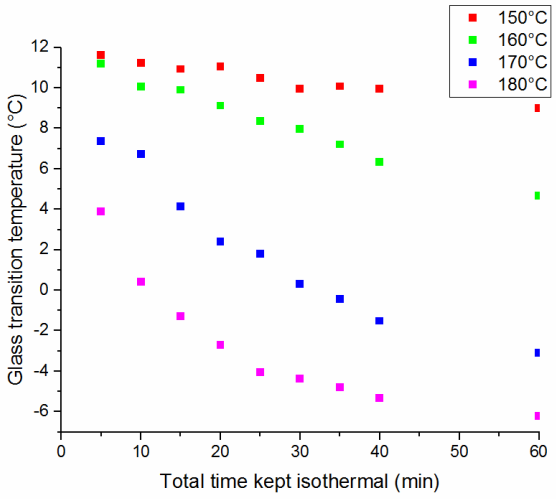

Figure V.6. Glass transition temperatures of D47PCL530_50 after each heating cycle, plotted versus the total time it was kept isothermal.

The acquired T_g's are plotted versus the simulated percentage of cleaved reversible bonds $r_{mono} = 1 - r_{dim}$ in Figure V.7. The monotonously decreasing trend that is acquired illustrates that one can quantitatively follow the cross-linking degree and the thermal scission reaction by DSC measurements.

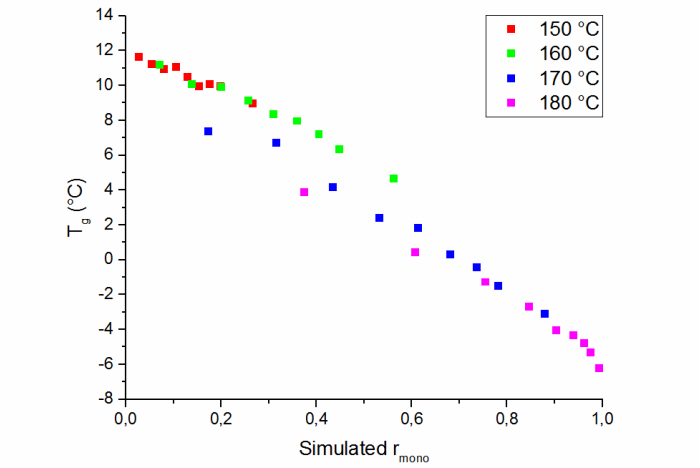

Figure V.7. Glass transition temperatures of heated D47PCL530_50 plotted versus the simulated ratio of cleaved bonds r_{mono}.

Similar experiments with D47PCL2000_50, but with increasingly higher maximum temperatures (100, 120, 140, 160, 180, 190 and 200 °C) showed much less significant lowering of the glass transition by decrosslinking: after the final heating step at 200 °C, corresponding with complete decrosslinking, the T_g has only achieved a total drop of approximately 3.5 °C (Figure V.8). The T_g drop is small because of the higher molecular weight of the PCL chains, resulting in loosely cross-linked materials prior to scission.

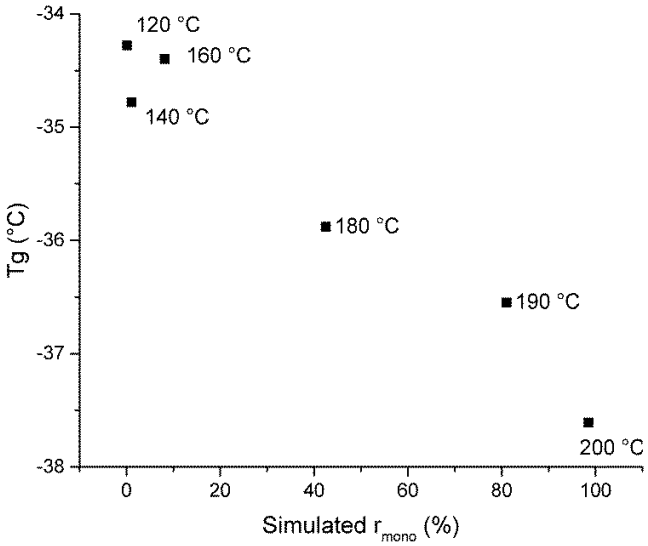

Figure V.8. Glass transition temperatures from cyclic DSC tests of D47PCL2000_50 at a rate of 10 K min^{-1} as a function of the simulated bond scission ratio r_{mono}.

Therefore, another set of experiments was performed on materials having only reversible bonds (D47_100). This was done in the same manner as described above for the D47PCL530_50 materials. The increase of the concentration of reversible bonds (dimers) within the network and its higher initial T_g, in comparison to the partially reversible-based materials (D47PCL530_50 and D47PCL2000_50), results in much larger changes in T_g-values (Figure V.9). Similarly to D47PCL530_50, the initial glass transition increased significantly after the first heating step due to the evaporation of plasticizing molecules. Heating at 150 °C for one hour leads to a significant decrease in T_g of about 8 K, while heating at 170 °C for one hour led to a more significant T_g drop of approximately 36 K at the end of the experiment. Plotting the T_g data versus the calculated ratio of cleaved bonds r_{mono}, again resulted in a nearly linear trend (Figure V.10), allowing for an easy monitoring of the progress of the anthracene dimer scission. Besides, this also indicates that one could control and reversibly change the glass transition of these materials by stimulating the dianthracene bond scission and recuring them by dimerization through exposure to UVA light.

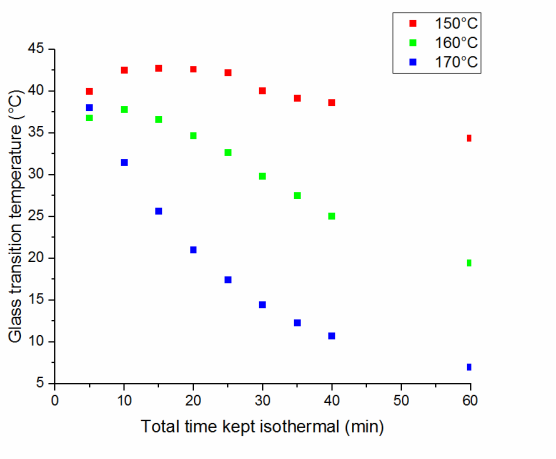

Figure V.9. Glass transition temperatures of D47_100 after each heating cycle, plotted versus the total time it was kept isothermal.

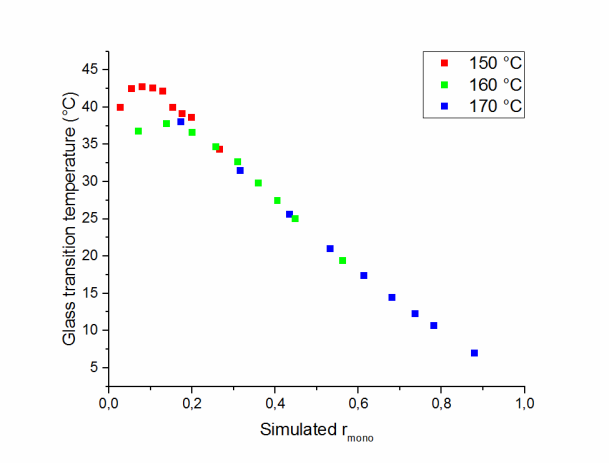

Figure V.10. Glass transition temperatures of heated D47_100 plotted versus the simulated ratio of cleaved bonds r_{mono}.

2.2.3 Rheometry experiments

To illustrate the changes in mechanical properties by thermal scission of the reversible bonds, dynamic rheometry experiments were performed on a material having no thermally cleavable bonds (PCL530_0), a material having reversible bonds but which does not liquefy (D47PCL2000_50) and a material which does (usually) liquefy (D47PCL530_50) (Figure V.11). While both D47PCL2000_50 and D47PCL530_50 theoretically have the same reversible bond fraction (50 %), the D47PCL2000_50 samples probably (coincidentally) have more additional non-reversible crosslinks. This is likely due to moisture-induced polyurea formation, which is common in polyurethanes. Because of these extra cross-links, the material keeps its integrity upon cleaving the reversible bonds. These samples were heated up to 180 °C and the storage and loss modulus (G' and G'') were measured for a 1 % deformation at 1 Hz frequency. As expected, the irreversibly cross-linked PCL530_0 material remains integer and maintains a high storage modulus. In fact, even a mild increase in the storage modulus, along with a decrease in loss modulus occurred during heating up, which is attributed to the evaporation of plasticizing molecules. The PCL2000-based polyurethane having approximately 50 % reversible anthracene bonds shows a small initial increase in storage modulus during heating, followed by a steady decline thereof. After a drop in G' from 900 to 250 kPa over approximately 1 hour, the moduli stabilized. As 1 hour at 180°C corresponds to a simulated thermal scission conversion of approximately 98 %, this drop in G' is clearly due to dianthracene scission. This drop in properties is larger for D47PCL530_50, which after approximately 1 hour resulted in a cross-over between G' and G'', indicating a gel-sol transition, at

which point the sample could no longer be quantitatively measured (after ~4000 s). The estimated percentage of scission of the dianthracene bonds near the cross-over point was 96 %.

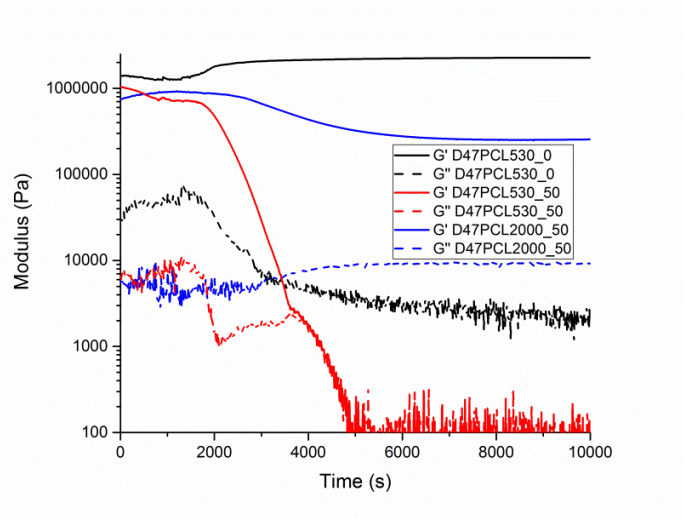

Figure V.11. Storage (full lines) and loss (dashed lines) modulus of PCL530_0, D47PCL530_50 and D47PCL2000_50 upon heating. Heating from 65 to 180 °C at 10 K min^{-1} during the first 2000 seconds, followed by isothermal conditions. After 4000 seconds, the viscosity of D47PCL530_50 became too low for quantitative measurement.

2.2.4 Thermal scission of coatings

This tunable and controllable thermal scission may find appealing application in thermally degradable coatings or protection layers. To validate this potential application, coatings were made from these materials on steel substrates and tested on their hardness and their solvent resistance. As coating material, D47_100 was chosen, as it was expected that this material would lead to the largest property changes because of the reversible nature of all bonds. To successfully apply the material as a coating, a minimal amount of DMF was used as a solvent. Other attempted solvents led to inhomogeneous coatings. As reported in Table V.5, the number of rubs with 2-butanone required to remove the coating first increased from 70 to up to 160 rubs by heating to increasing temperatures. This is attributed to the evaporation of DMF initially present in the material. As this is a good solvent for the material, the material was already swollen, leading to faster mechanical failure and thus faster removal.

The number of rubs required to remove the coating rapidly decreases after heating for 1 hour at 160 °C or 30 minutes at 170 °C. Unlike for other samples, the coating was not simply removed by mechanical

failure starting at the edges and defects, but by loss of integrity throughout the entire coating. Estimations of r_{mono} confirm that this heating is sufficient to break 49 and 57 % of the reversible bonds, respectively. The results of the pencil hardness tests reveal a slight decrease in hardness from 3H to 2H when heating for 1 hour at 140 °C or when heating at 150 °C. Calculations reveal a scission of 9 to 22 % of the bonds for these temperature treatments. After heating for 30 minutes at 160 °C, the hardness dropped to B, with an estimated bond scission of 28 %. Longer heating and higher temperatures led to full loss of the integrity and hardness below 6B. From these results can be concluded that the thermal scission of these coating materials leads to a slow decline in hardness at low thermal scission, followed by a quick loss of properties once the thermal scission becomes extensive by heating the material to 160 °C. This disintegration allows the easy removal of the material from the (undamaged) substrate.

Table V.5. Heating program, 2-butanone rub test and pencil hardness test results with the estimated bond scission ratio.

Temperature	Time (h)	Rubs	Pencil hardness	R_{mono}
Rt		70	3H	0
130 °C	0.5	70	3H	0.02
130 °C	1	90	3H	0.03
140 °C	0.5	60	3H	0.04
140 °C	1	110	2H	0.09
150 °C	0.5	160	2H	0.12
150 °C	1	150	2H	0.22
160 °C	0.5	140	B	0.28
160 °C	1	8	<6B	0.49
170 °C	0.5	4	<6B	0.57

2.3 Recure and stress-relaxation

2.3.1 Recure of $(28)_2$–based networks

As the (thermal) scission of the dimer bonds of these materials regenerates the anthracene moieties, dissociated materials should be curable using UVA light. When possible, this irradiation step should occur under inert atmosphere to avoid the undesirable formation of endoperoxides. This is similar to what was done in chapter IV for thiol-ene materials having 9-anthrylmethyl esters. To test this hypothesis for anthracene ether based polyurethanes, samples of D28DOD_75 were kept at 130 °C for

15 minutes, leading to full liquefaction of the materials (Figure V.13). The resulting viscous oil was pressed between glass plates without using a spacer, to limit the exposure of the material to oxygen during irradiation. Overnight UV irradiation with 365 nm wavelength light led to thin, glassy materials. The high gel content (97 %) indicated good cure.

HR-MAS NMR analysis revealed that 28 % of the anthracene dimers remained unreacted (which corresponds to a total connectivity x of 0.79) (Figure V.12). However, TGA showed a faster degradation: 3 % mass loss was reached near 240 °C, while this was around 290 °C for the virgin samples. This is likely due to the presence of photo-oxidation products of the material, formed during the irradiation step by reaction with dissolved oxygen present in the oil. The remolded samples had a similar stress at break (30 MPa) as the virgin material, but had a higher modulus (285 MPa instead of 110 MPa), a decreased stretch at break (150 % instead of 230 %) and an increased T_g (27 °C and 31 °C instead of 7 °C and 9 °C, using DSC and DMTA respectively). These changes could be attributed to an increased degree of cross-linking due to side reactions, or to the evaporation of plasticizing low molecular weight compounds (e.g. solvent residue) initially present in the virgin material. While the latter could be avoided by increasing the drying time and temperature *in vacuo*, the low thermal scission temperatures of the bonds would probably lead to significant premature bond scission. During the approximately 16 hours of curing and drying of the virgin material at 70 °C, approximately 2 % of the reversible bonds should have cleaved already. Although these experiments confirm the viability of 9-anthryl ether-based polyurethanes as reversible materials with a low thermal dimer scission temperature, the latter does complicate characterization due to (the risk of) possible premature dimer scission.

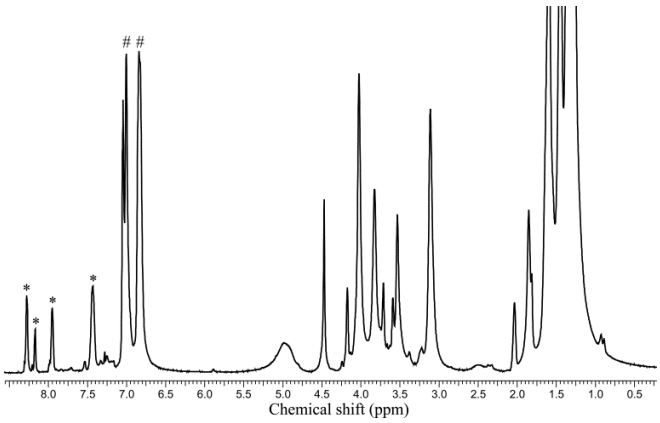

Figure V.12. HR-MAS NMR spectrum of remolded D28DOD_75. Both monomer (*) and dimer (#) peaks are clearly visible.

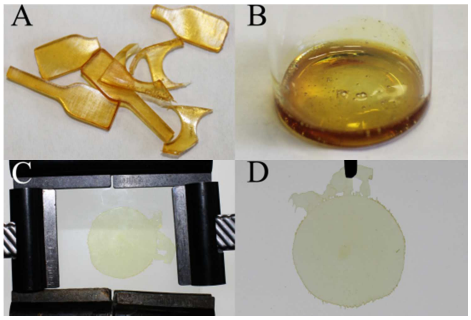

Figure V.13. Samples of D28DOD_75 (A) were liquefied at 130 °C for 15 minutes (B). The oil was put between glass plates (C) and after irradiation with UVA light a glassy material was achieved (D).

2.3.2 Recure of $(47)_2$-based networks and coatings

The UV-curing of previously liquefied samples of D47_100 and D47PCL530_50 was studied using a rheometer equipped with a UV-irradiation setup. After insertion of the liquid samples and removal of air bubbles, the liquids were kept at 70 °C and pressed to a thickness of 100 µm. The samples were irradiated with unfiltered UVA light with varying intensities while following the evolution of the moduli. The thermally degraded D47_100 materials exhibited an increase in G' and decrease in G'', with a crossover occurring after 1 minute when irradiated at the highest intensity (13 W/cm^2) (Figure V.14). Lower intensities led to lower curing rates and later G'-G'' crossovers (e.g. after 11 minutes at 2.75 W/cm^2). When irradiating at the highest intensity while using a filter that only transmits wavelengths around 365 nm, the G'-G'' crossover occurred after 6 minutes. While this leads to a much

lower cross-linking rate, undesirable side reactions occurring at lower wavelengths would be suppressed in this way.

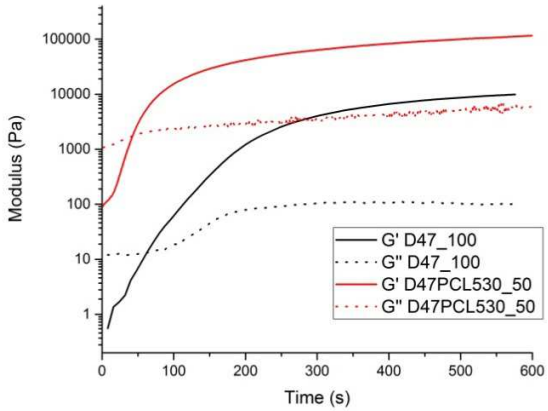

Figure V.14. Cure of a 100 µm film of thermally degraded D47_100 and D47PCL530_50 films at 70 °C by UVA irradiation (13 W/cm^2).

The irradiation of thermally degraded D47PCL530_50 films under the same conditions at an intensity of 13 W/cm^2 led to slightly faster cure (Figure V.14): the G'-G'' crossover was achieved after 45 seconds. This is explained by the different network morphology of these resins. While the D47_100 materials lead to trifunctional triarm structures upon thermal scission, the D47PCL530_50 films lead to a complex mixture of branched, linear and cyclic structures, having higher molecular weights. Despite this complexity, it is safe to assume that these higher molecular weight species have an average anthracene functionality far exceeding 3. The higher functionality of these macromolecular structures thus requires lower dimerization conversions to reach the gelation point.

Heating these (re)cured materials again to 150 – 160 °C leads to a lowering in G' and another cross-over, because of the thermal degelling of the reversible network.[15] Unfortunately, under these conditions only 2 to 3 cure/degradation cycles could be achieved, due to the occurrence of side reactions during the long heating and irradiation steps. This is not surprising, as many anthracene derivatives are known to readily undergo photo-oxidation reactions.[16] The D47PCL530_50 networks eventually led to irreversibly cross-linked networks, while the D47_100 networks became viscous oils. Presumably sufficient irreversible cross-linking reactions occur, which cross-link the D47PCL530_50 materials. In D47_100 (mainly) non-crosslinking anthracene degradation reactions take place, such as endoperoxide formation. These side reactions limit the use of these materials to applications where only a few thermal

scission/dimerization cycles are required, or to conditions where the presence of oxygen can be excluded or limited.

The recuring of the thermally degraded coatings of D47_100 was attempted. The D47_100 coatings were first heated to 160 °C for 1 hour, leading to loss of integrity. The degraded coating was irradiated under a N_2 flush using a 250 W handheld UVA lamp for 10 minutes. Due to the disappearance of fluorescent anthracene moieties, the irradiation leads to an observable change in fluorescence under a UV-lamp. This is easily observed when masking one section upon UVA irradiation (Figure V.15). Solvent rubs and pencil hardness tests confirmed the formation of a polymer coating with similar properties as the original.

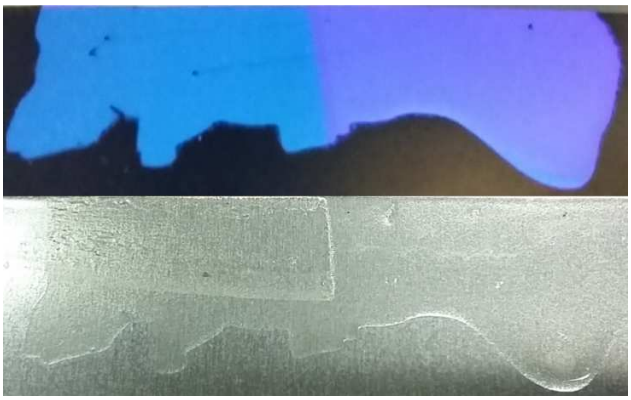

Figure V.15. Fluorescence under UV of a D47_100 coating before (up, left) and after (up, right) recure. Solvent rubbing resulted in exclusive removal of the masked material (bottom).

2.3.3 Stress relaxation

The presence of reversible crosslinks might allow the relief of stress in (coating) materials, while maintaining the integrity of the material. The required exchange of bonds can be achieved by the simultaneous formation and scission of anthracene dimers by UVA irradiation at elevated temperatures.

To avoid loss of integrity of these materials, either by the occurrence of excessive dimer scission or side reactions, stress relaxation experiments were performed on materials having both irreversible cross-links and reversible bonds (e.g. D47PCL2000_25 and D47DOD_25).

Unfortunately, studying these materials via the rheometer proved to be impractical. In order to have a homogeneous material between the plate and the spindle, the originally cross-linked materials (in other

dimensions) had to be decrosslinked, followed by cross-linking in the rheometer. The resulting build-up of side products prior to measuring, in combination with the high temperatures and light intensities required for dynamic exchange over extended times, lead to excessive degradation of the material.

Because of this, stress-relaxation was qualitatively studied using polarized light instead. Stress in polymers can be studied optically because of birefringence under mechanical tension, which is detectable using a polariscope. By shining polarized light through the samples, stripe and color patterns are seen through a polarizing filter, indicating the amount of stress.

This was first tested for materials based on **(47)$_2$**. D47PCL2000_25 films were placed in a tensile apparatus and deformed by elongation. Observation of the films between polarizing filters showed blue-green color, indicating the presence of stress (Figure V.16, up). Subsequently, the samples were irradiated with a hand-held UVA lamp of 250 W with an emission maximum at 365 nm. As this lamp also produced a lot of heat, leading to temperatures above 100 °C, not only dimerization occurred but also some thermal scission. After overnight irradiation, the materials had a red-pink color when observed under polarized light (Figure V.16, down). This indicated some disappearance of stress. However, it was inconclusive whether the material lost stress due to the breaking and reforming of anthracene dimer bonds or by other factors such as slipping at the clamps. Also, the yellowing of the material due to the irradiation influences the observed color throughout the material.

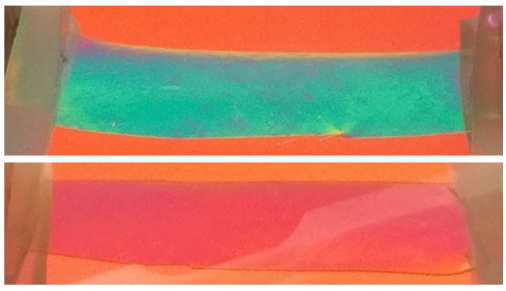

Figure V.16. Elongated D47PCL2000_50 material between polarizing filters before (up) and after (down) heating and irradiation.

Therefore, tests were performed with thin materials based on **(28)$_2$**, which have a lower thermal scission temperature. D28DOD_25 films of 200 µm were placed in a tensile apparatus under torsion (Figure V.17, (a) and (b)). Under polarized light, color changes at several bends were observed, indicating internal stress (Figure V.17, (c)). After overnight irradiation, no significant color gradients were observed (Figure V.17, (d)), indicating that stress relaxation has occurred. After removal from the tensile

apparatus, the materials remained in a twisted shape (Figure V.17, (e) and (f)) even after heating above the T_g. This proved the formation of new crosslinks, which are stress-free in the new, twisted shape. For reference, the same experiments with DOD_0 samples, having no reversible bonds, showed no stress-relaxation using polarized light. As expected, mild heating of these materials above their T_g resulted in a return to the original shape.

The material did, however, become yellow. This is known to be caused in polymers (and anthracenes) by photo-oxidation and degradation products. Excessive coloring is problematic for the esthetics of transparent coatings. In future work, this change in color could be suppressed by (i) changing the light source to a LED that only emits the required wavelengths for stress-relaxation, and (ii) adding selective UV-absorbers and/or oxygen scavengers to the material formulation.

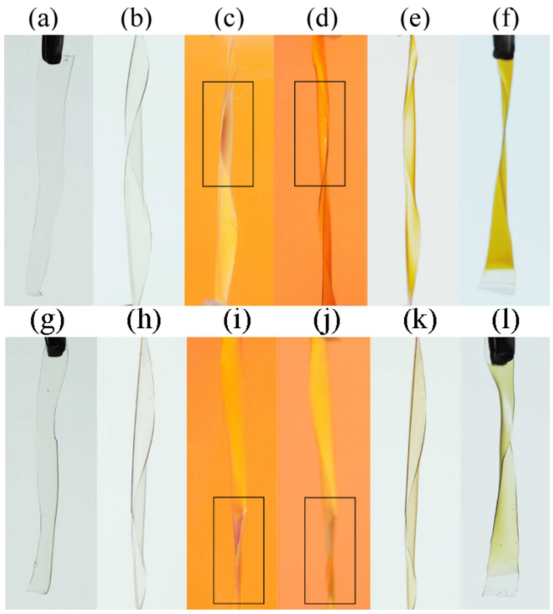

Figure V.17. D28DOD_25 material either treated by heating while irradiating using UVA light (up, a-f) or solely irradiated using UVC light (254 nm) (down, g-l). Samples prior to treatment (a,g), put under torsion (b, h) and observed between polarizing filters (c, j). Samples after treatment observed between polarizers (d, j), under regular lighting (e, k) and with the clamps removed (f, l).

As the scission of anthracene dimers can also occur photochemically, stress-relaxation in D28DOD_25 was attempted overnight using short wavelength UV irradiation only (12 x 9 W lamps) (Figure V.17, g-l). It is well known that irradiating anthracene dimers using 254 nm light results in the scission of the dimer. However, these wavelengths are also absorbed by the anthracene monomers and can lead to

anthracene dimerization. As can be seen in Figure V.17 (j), stress remained present in the material, even though the change in color does suggest some relaxation. After removal of the samples from the tensile apparatus, the samples remained in a twisted shape. The anthracene-free DOD_0 samples showed no change in color between polarizers after irradiation. These materials also quickly returned to their original shape under mild heating. These results suggest the formation of new bonds in D28DOD_25 by irradiation, presumably by anthracene dimer scission, followed by the formation of new (ir)reversible bonds. While the material remains in the new shape upon heating above T_g, significant amounts of stress are still present in the material. This is probably a consequence of the limited penetration depth of the short wavelength UVC irradiation in the sample, preventing the relaxation of stresses in the core of the material.

3 Conclusion

Anthracene ether and anthracene ester dimers were incorporated in polyurethane materials as photo- and thermoreversible bonds. The temperatures at which scission occurred are in good correspondence to the monomer studies in chapter III. Therefore, materials can be made having bonds cleavable at relatively modest (~ 110 °C) or higher (~ 160 °C) temperatures. From these results (and those in chapter IV), we can assume that the other derivatives synthesized in chapter III would similarly tune the thermal behavior of in materials. Depending on the design of the polymer network, i.e. incorporation of more or less reversible bonds, scission led to significant drops in mechanical properties, liquefaction (reversible bonds ≥50%) and controllable T_g drops (up to 40 K). Thermal scission could be used to remove these reversible coatings after heating to a predetermined temperature. UVA irradation of thermally degraded materials led to materials and coatings having similar mechanical properties as the original ones. However, the occurrence of side reactions with oxygen limits this reversibility to a few cycles. Thermally stimulated anthracene scission with simultaneous photostimulated bond formation could be used to induce a (partial) stress relaxation in these covalently adaptable polymer networks, while maintaining structural integrity.

4 Experimental section

4.1 Materials

Chloroform (≥ 99.8 %), zirconium (IV) acetylacetonate (97 %), methanol (99.9 %), diethyl ether (≥ 94.8 %), ethyl acetate (≥ 99.7 %), poly(tetramethylene oxide) (M_n ~ 650 and M_n ~ 2900 g/mol), polycaprolactone diol (M_n ~ 530 and M_n ~ 2000 g/mol), hexamethylene diisocyanate (≥ 98 %), acetone (≥ 99.8 %), 2,2-bis(hydroxyl)methylpropionic acid (98 %) and dibutyltin dilaurate (95 %) were purchased via Sigma-Aldrich. Toluene (99.9 %), 1,12-dodecanediol (99 %), methanesulfonyl chloride (99.5 %), triethyl amine (99%) and methanesulfonyl chloride (99.5 %) were purchased via Acros Organics. Sodium hydrogen carbonate (≥ 99.5 %), sodium chloride (≥ 99 %), magnesium sulfate hydrate (≥ 99 %) and potassium carbonate (≥ 99 %) were purchased via Carl Roth. Silica 60 A° (99.5 %) was purchased via ROCC. Hexamethylene diisocyanate trimer (Desmodur N-3300) was provided by Covestro. Toluene was dried by distillation over sodium prior to use. Anhydrous dimethylformamide, tetrahydrofuran and triethylamine were purchased from Acros Organics and used as such.

4.2 Instruments

IR spectra were recorded with a Perkin Elmer FTIR SPECTRUM 1000 and a PIKE Miracle ATR unit. NMR spectra were recorded with Bruker AVANCE 300 (300 MHz) and Bruker DRX500 (500 MHz) NMR spectrometers. HR-MAS NMR spectroscopy was performed using a Bruker Avance II 700 (700.13 MHz) spectrometer equipped with a HR-MAS probe. Sample materials were cut to small pieces, brought into a 4 mm rotor (50 µL) and deuterated chloroform was added to swell the sample. ^{1}H-NMR spectra were measured at rotational frequency of 6 kHz. LC-MS analyses were performed on an Agilent Technologies 1100 series LC/MSD system with a diode array detector (DAD) and single quad MS. Analytical reversed phase HPLC-analyses were performed with a Phenomenex Luna C18 (2) column (5 µm, 250 mm × 4.6 mm) and a solvent gradient (0 or 75 - 100% acetonitrile in H_2O in 15 minutes), the eluted compounds were analyzed via UV detection (214 nm). Unless mentioned otherwise, photoirradiation occurred under inert atmosphere in a Metalight Classic from Primotec, with 12 double 365 nm or 254 nm UV lamps of 9 W each (intensity measured in the middle ~ 5 mW cm^{-2}). Differential scanning calorimetry (DSC) was performed under nitrogen atmosphere using a DSC1/700 Mettler-Toledo apparatus. The used heating rate was 10 K min^{-1}. Thermogravimetric analyses (TGA) were performed on a Mettler-Toledo TGA/SDTA 851e under nitrogen atmosphere. Samples were heated from

25 to 600 °C, at rate of 10 K min^{-1}. Dynamic mechanical thermal analysis (DMTA) was performed on a Mettler-Toledo DMA/SDTA 861e in shear mode using a force of 5 N, temperature sweep from -50 °C to 50 °C and a frequency of 1 Hz. The data from TGA, DSC and DMTA measurements were analyzed using the STARe software from Mettler-Toledo. Size exclusion chromatography (SEC) was performed on three sequential polymer standards services SEC columns (1x GRAM Analytics 30 Å, 10 µm and 2 x GRAM Analytical 1000 Å, 10 µm) at 35 °C. N,N-Dimethylacetamide containing 0.42 mg L^{-1} LiBr was used as eluent (1 mL min^{-1}). The system was calibrated using PMMA standards (690 g mol^{-1} and 1 944 000 g mol^{-1}) with a narrow dispersity. A Hitachi Column Oven L-7300, a Waters 2414 Refractive index Detector, a Waters 610 Fluid Unit and a Waters 600 controller were used. Mechanical properties were determined using a Tinius Olsen H10KT tensile machine. The dogbone shaped samples with a width of 2 mm were pressed out of films prior to use. The length of the samples in between the clamps was 12 - 14 mm and the elongation speed was 0.5 mm s^{-1}. Solvent rub tests were performed using a cheese cloth drenched in butanone (and refreshed every 20 rubs). Approximately 100 N force was applied on a surface of 1 cm^2. Steel substrates were washed with soap, followed by rinsing with water and acetone and drying before use. The coating resins were doctor bladed, with a gap of 100 µm. Rheology experiments were performed using an Anton Paar MRC 302. For UV-curing and stress-relaxation experiments (on 100 µm thick samples), a 25 mm peltier plate was used and an Omnicure S2000 with mercury lamp of 13.23 W/cm^2 maximum intensity was used with a light guide to the rheometer. In other rheometry measurements, a 8 mm peltier plate was used with samples of 2 mm thickness, using a normal force of 2 N, a frequency of 1 Hz and 1 % deformation. Pencil hardness was determined using an Elcometer 3086 motorized pencil hardness tester in a forward fashion (chip method) with a force of 7.5 N.

4.3 Polyurethane network curing

All compounds were dried by azeotropic evaporation with anhydrous toluene prior to use. A minimal amount of dry solvent (THF or DMF) is added to the alcohols and isocyanates, until a homogenous mixture is acquired. When necessary, this mixture was sonicated. The catalyst (dibutyltin dilaurate, 2 w% of the material solid content) is dissolved in a minor quantity of the anhydrous solvent and added to the mixture. The mixture was heavily stirred for 10 - 20 seconds. The mixture is brought via a syringe in between (rinsed and dried) glass plates, separated with a silicone spacer of 1 mm thickness. This setup is

placed in a pre-heated oven at 35 °C until at least gelation occurred. After gelation, the material is removed from the glass plates and further cured by overnight heating *in vacuo* at 70 °C.

5 References

1. *Annex XV restriction report*; ECHA: 2016.
2. Cornille, A.; Dworakowska, S.; Bogdal, D.; Boutevin, B.; Caillol, S., *European Polymer Journal* **2015,** *66* (Supplement C), 129-138.
3. Xu, H.; Qiu, F.; Wang, Y.; Wu, W.; Yang, D.; Guo, Q., *Progress in Organic Coatings* **2012,** *73* (1), 47-53.
4. (a) Otts, D. B.; Heidenreich, E.; Urban, M. W., *Polymer* **2005,** *46* (19), 8162-8168; (b) Resetco, C.; Hendriks, B.; Badi, N.; Du Prez, F., *Materials Horizons* **2017,** *4* (6), 1041-1053.
5. Bowman, C. N.; Kloxin, C. J., *Angewandte Chemie International Edition* **2012,** *51* (18), 4272-4274.
6. Denissen, W.; Winne, J. M.; Du Prez, F. E., *Chemical Science* **2016,** *7* (1), 30-38.
7. (a) Feng, L.; Yu, Z.; Bian, Y.; Lu, J.; Shi, X.; Chai, C., *Polymer* **2017,** *124* (Supplement C), 48-59; (b) Willocq, B.; Khelifa, F.; Brancart, J.; Van Assche, G.; Dubois, P.; Raquez, J. M., *RSC Advances* **2017,** *7* (76), 48047-48053; (c) Rivero, G.; Nguyen, L.-T. T.; Hillewaere, X. K. D.; Du Prez, F. E., *Macromolecules* **2014,** *47* (6), 2010-2018.
8. Billiet, S.; De Bruycker, K.; Driessen, F.; Goossens, H.; Van Speybroeck, V.; Winne, J. M.; Du Prez, F. E., *Nature Chemistry* **2014,** *6*, 815.
9. (a) Ling, J.; Rong, M. Z.; Zhang, M. Q., *Polymer* **2012,** *53* (13), 2691-2698; (b) Ling, J.; Rong, M. Z.; Zhang, M. Q., *Journal of Materials Chemistry* **2011,** *21* (45), 18373-18380.
10. Fang, Y.; Du, X.; Du, Z.; Wang, H.; Cheng, X., *J. Mater. Chem. A* **2017,** *5* (17), 8010-8017.
11. Tazuke, S.; Tanabe, T., *Macromolecules* **1979,** *12* (5), 848–853.
12. Botelho, G.; Queirós, A.; Gijsman, P., *Polymer Degradation and Stability* **2000,** *68* (1), 35-42.
13. Flory, P. J., *Journal of the American Chemical Society* **1941,** *63* (11), 3091-3096.
14. Van Damme, J.; Vlaminck, L.; Van Assche, G.; Van Mele, B.; van den Berg, O.; Du Prez, F., *Tetrahedron* **2016,** *72* (29), 4303-4311.
15. (a) Diaz, M. M.; Van Assche, G.; Maurer, F. H. J.; Van Mele, B., *Polymer* **2017,** *120*, 176-188; (b) Scheltjens, G.; Diaz, M. M.; Brancart, J.; Van Assche, G.; Van Mele, B., *Reactive and Functional Polymers* **2013,** *73* (2), 413-420.
16. (a) Sigman, M. E.; Zingg, S. P.; Pagni, R. M.; Burns, J. H., *Tetrahedron Letters* **1991,** *32* (41), 5737-5740; (b) Bauch, M.; Klaper, M.; Linker, T., *Journal of Physical Organic Chemistry* **2017,** *30* (4), e3607.

Chapter VI: Novel 2,6-substituted derivatives: synthesis and characterization

Abstract

In this final experimental chapter, a novel functional 2,6-substituted donor-acceptor anthracene derivative is synthesized from readily available compounds. This monomer was equipped with an electron donor and an electron acceptor in conjugation to achieve UV absorption and anthracene dimerization at longer wavelengths and under milder conditions. The compound was shown to have a red-shifted absorption and dimerize much faster compared to most 9-substituted anthracenes. The fast photochemical and relatively slow thermal scission of the dimers were studied and related to the chemical structure.

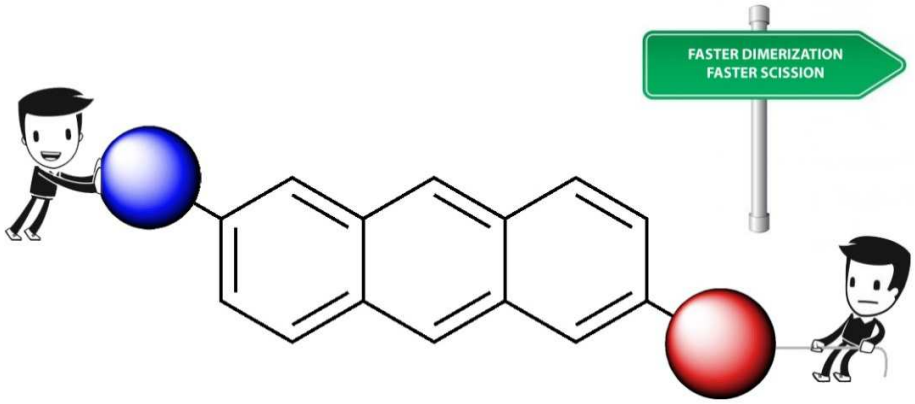

Collaborators:

The synthetic work was performed in collaboration with dr. Otto van den Berg.

1 Introduction

Despite the promising properties of anthracene, as described over the past chapters, the number of publications on anthracene as photoreversible bond in polymers is limited. This fact could be ascribed to the restricted availability of functional derivatives. In fact, the majority of publications use 9-substituted derivatives, many of which are based on 9-anthracenemethanol. In chapter III, we discussed the synthesis of a large series of novel functional 9-substituted anthracene derivatives and evaluated their properties for use in polymer materials. It was shown how different substituents heavily influenced the easy of thermal scission. In the subsequent chapters, we introduced several derivatives into thiol-ene and polyurethane materials and found good similarity between the thermal stability of the dimers and their corresponding materials. We concluded that it is therefore safe to assume that similarly good correlations would exist between the other anthracene dimer derivatives and their corresponding materials.

Despite the promising thermal dissociation properties, not much difference in photochemical reactivity (absorption, dimerization and scission) was found between the different 9-substituted derivatives. While all derivatives had an absorption redshift compared to unsubstituted anthracene, this shift remained limited. Strong shifts were found by Barner-Kowollik and coworkers, who used a larger strongly electron-donating 9-substituent to allow the reversible dimerization to occur at higher wavelengths.[1] However, the larger group might cause more steric hindrance and thus reduce the dimerization rate.

In the endeavor to further tune the photodimerization properties of anthracene, we aimed to develop functional 2,6-substituted anthracenes. The absence of a substituent on the central ring is known to improve the dimerization rate by reducing steric hindrance. Furthermore, we favored to have two different substituents with the assumption that we could count on a shift of the absorption to (much) higher wavelengths because of a synergetic effect of an electron donor and an electron acceptor as substituent in conjugation. These shifts in absorption and fluorescence in donor-π-acceptor anthracenes has previously been demonstrated by Ihmels[2] and Lu *et al.*[3] (absorption to > 500 nm). Initially, inspired by their publications, we aimed to develop a new upscalable synthetic pathway to develop donor-π-acceptor anthracenes from readily available compounds with the possibility to acquire other useful derivatives by small synthetic changes. Similarly to the products in chapter III, the resulting derivative is equipped with an alkyl chain to improve its solubility and can be incorporated as (di)anthracene monomer in existing polymer formulations. The absorption, dimerization and scission properties of this

derivative have been studied, related to its structure and evaluated in the context of reversible bond formation in polymers and polymer materials.

2 Results and discussion

2.1 Synthesis

The followed synthetic pathway of the 2,6-substituted donor-acceptor anthracene derivative first involved the synthesis of a benzyl benzoic acid precursor (Figure VI.1, **67**). Ring closure of this compound would result in an anthrone and reduction thereof in an anthracene. First, m-anisole (**62**) was brominated using bromine in acetic acid. The resulting 2-bromo-5-methoxybenzaldehyde (**63**) underwent a Grignard reaction using 4-chlorophenylmagnesium bromide (**64**), followed by a reduction to remove the benzylic alcohol group using triethylsilane in trifluoroacetic acid. The resulting bromide of **66** was modified to a carboxylic acid group. This was done by making the Grignard reagent using magnesium, followed by a reaction with anhydrous carbon dioxide. The overall yield for the synthesis of this carboxylic acid was 74 %.

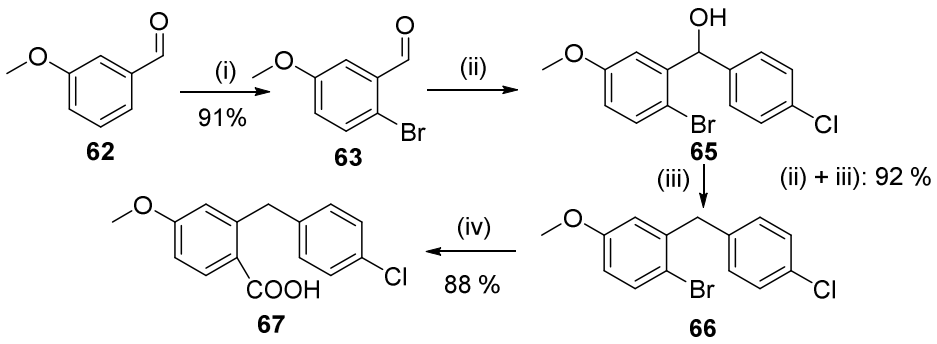

Figure VI.1. Synthesis of the benzyl benzoic acid precursor. (i) Br_2, AcOH, 2 h, rt; 1 h, 70°C; (ii) (1) 4-chlorophenylmagnesium bromide 3, diethyl ether, 1 h, rt, (2) H_3O^+; (iii) triethyl silane, trifluoroacetic acid, 18 h, rt; (iv) (1) magnesium, tetrahydrofuran, (2) CO_2, (3) H_3O^+.

Carboxylic acid **67** was then reduced and modified to the desired anthracene (Figure VI.2). Anthrone **68** was made in high yield by first forming the acid chloride from **67** using thionyl chloride, followed by the removal of excess thionyl chloride and ring closure by Friedel-Crafts acylation using aluminum trichloride in dichloromethane. Anthrone **68** was then reduced to anthracene **69** in high yield using

sodium borohydride in diglyme. In the absence of a protic solvent, anthracenolate anions are formed, which are unable to reduce to the anthracene or reform the anthrone. Therefore, methanol was added to the solution to allow the kinetically trapped anions to equilibrate with the anthrone, resulting in higher yields.[4] The formed 2-chloro-6-methoxyanthracene **69** was used to make 6-methoxyanthracene-2-carboxylic acid by forming the corresponding Grignard reagent, followed by a reaction with carbon dioxide. However, this proved to be rather difficult. No Grignard reagent formation using magnesium pallets was observed. Attempts to achieve magnesium exchange using isopropylmagnesium chloride lithium chloride in THF also did not result in any significant end product formation. Only using freshly prepared Rieke magnesium, chloride activation occurred and a yield of 10 % carboxylic acid **71** was achieved. This issue with the formation of the Grignard reagent was avoided by synthesizing the nitrile **70** instead. This was done in 66 % yield by adding an excess of copper cyanide in N-methyl-2-pyrrolidone and heating the solution to reflux for 30 hours. The resulting crude 6-methoxyanthracene-2-carbonitrile **70** was easily converted into the desirable 6-methoxyanthracene-2-carboxylic acid **71**. The combined yield over these two steps was 57 %, exceeding the results achieved by Grignard reagent formation.

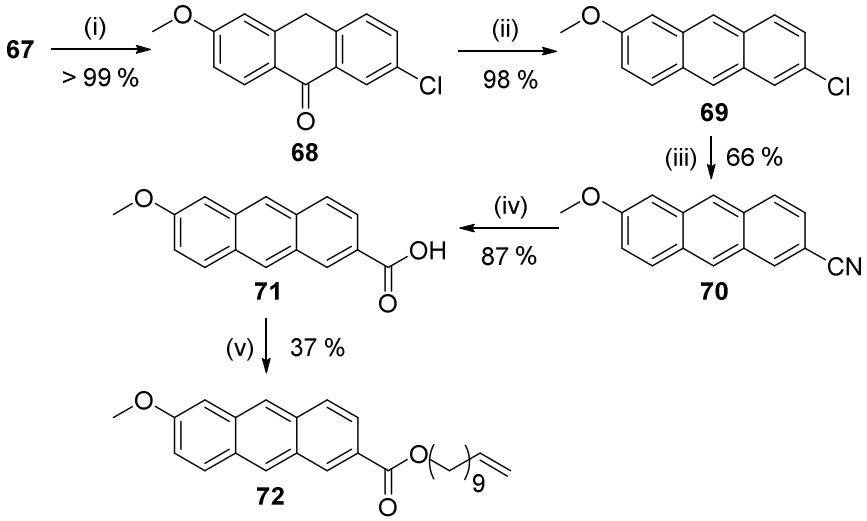

Figure VI.2. Ring closing and final steps to synthesize the anthracene derivatives. (i) (1) $SOCl_2$, 2 h, reflux, (2) $AlCl_3$, 1 h, rt; (ii) $NaBH_4$, diglyme, MeOH; (iii) CuCN, NMP, 30 h, reflux; (iv) KOH, H_2O, MeOH, reflux, overnight; (v)11-bromo-1-undecene, K_2CO_3, DMF, 24 h, rt.

This synthetic pathway to **71**, starting from m-anisaldehyde **62**, had an overall yield of 41 %. The carboxylic acid functionality of **71** allows making an ester bond to a long spacer with a polymerizable

end group. The long spacer improves not only the solubility of the anthracene, but also improves the solubility of the corresponding dimer. The low solubility of anthracene dimers is often a limiting factor for its use in resin formulations. The best result was found by performing an addition of the carboxylate anion to 11-bromo-1-undecene in dimethylformamide. The resulting anthracene ester **72** has an end-standing double bond, which can be used either directly as polymerizable groups (e.g. for thiol-ene polymerization) or can be modified to acquire other polymerizable functional groups such as oxiranes or alcohols (not done).

2.2 UV-vis absorbance and fluorescence

One of the most important properties of any anthracene derivative, which has to undergo (reversible) dimerization, is their absorption in the UV-visible light spectrum. The absorption spectra of anthracenes **69**, **70**, **71** and **72** were measured in ethanol (Figure VI.3 and Table VI.1). As expected, two absorption regions can be distinguished for all derivatives, one below 300 nm and one above 300 nm. These maxima correspond to respectively longitudinal (long axis) and axial (short axis) electron density shifts.[5] While excitation using wavelengths from either of these regions may lead to dimerization, in most cases dimerization is performed using only longer wavelengths (> 300 nm) to avoid competitive scission and possible side reactions.[6] The short wavelength absorption (< 300 nm) is red-shifted for all derivatives, compared to unsubstituted anthracene. This shift comprises up to 20 nm. By having substituents with a stronger electron withdrawing character (which is identified by having larger Hammett values σ_p^+) in conjugation with the methoxy group, larger redshifts were achieved. This observation is in accordance to a recent publication based on *in silico* results.[7] While the shape of this absorption peak for **69** is similar to anthracene, it is much broader for the compounds having electron withdrawing groups (**70**, 7**1** and **72**). This effect is attributed to the higher polarity of the latter compounds, combined with the polar solvent (ethanol), leading to solute-solution interaction.[8] This same interaction also leads to lower molar absorptivities ε_{max} (Table VI.1).

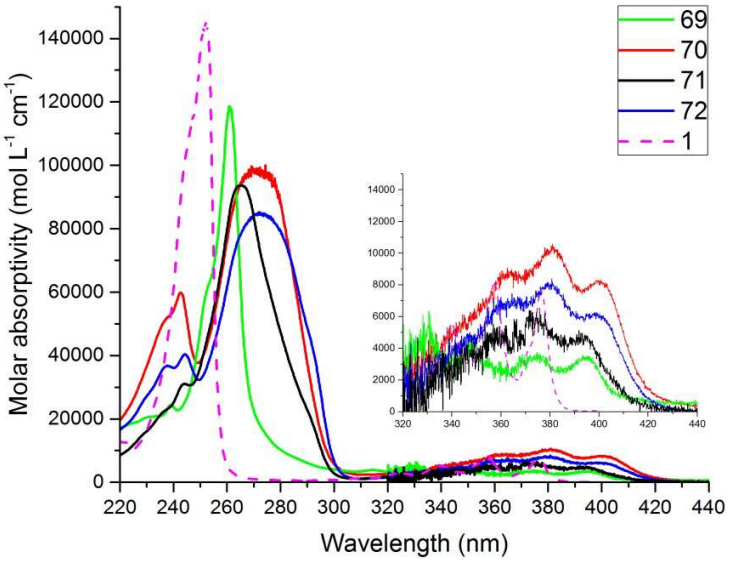

Figure VI.3. Molar absorptivity of anthracene and four 2,6-substituted derivatives in ethanol.

Table VI.1. Absorption maxima (below and above 300 nm) with molar absorptivity in ethanol. Hammett values σ_p^+ of the 6-substituent, taken from ref [9].

	λ_{max} (nm)	ε_{max} (10^3 mol L^{-1} cm^{-1})	λ_{max} (nm)	ε_{max} (10^3 mol L^{-1} cm^{-1})	σ_p^+ of 6-substituent
1	252	140	357	8.2	-
69	261	120	373	3.5	0.11
70	272	98	381	11	0.66
71	265	94	377	5.6	0.42
72	272	85	380	8.1	0.48

The axial absorption (above 300 nm) of the synthesized 2,6-substituted derivatives is also red-shifted up to 24 nm compared to unsubstituted anthracene (Figure VI.3). Again, in combination with the electron donating methoxy group, the conjugated substituents with stronger electron withdrawing properties result in larger red-shifts. The achieved shifts in absorption are higher than previously achieved for 9-substituted anthracenes (up to 12 nm; chapter III), therefore allowing excitation and subsequent dimerization to occur under milder conditions as we aimed for.

The absorption and fluorescence of anthracene derivative **72** in chloroform, ethanol and acetonitrile were measured to study possible solvatochromic effects (Figure VI.4). In all cases, the effects were minor. The emission wavelengths ranged approximately from 400 nm to 600 nm, with peak maxima at

455-460 nm. The emission quantum yields were 0.54 in ethanol and acetonitrile, while being 0.64 in the more apolar chloroform. These high quantum yields allow potential use as polymerizable fluorophore.

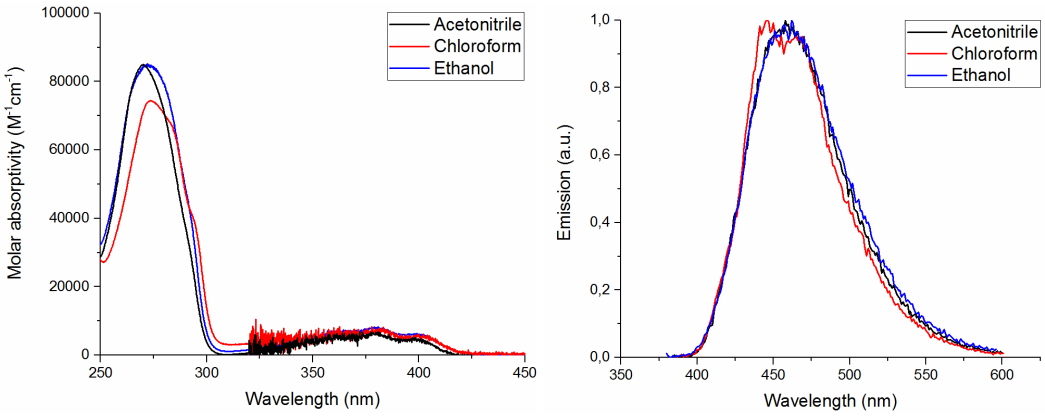

Figure VI.4. Molar absorptivity (left) and emission (right) of **72** in acetonitrile, chloroform and ethanol.

2.3 Photochemical dimerization

By irradiating a solution of anthracene ester **72** with UVA light, the corresponding photodimers **(72)$_2$** are made. Because of the asymmetric structure of **72**, multiple end products are possible (Figure VI.5). This is also observed as the different peaks corresponding to the bridge heads in ^{1}H-NMR around 4.53-4.62 ppm (Figure VI.6). Should only one dimer be formed, 2 singlets of equal integration would have been expected.

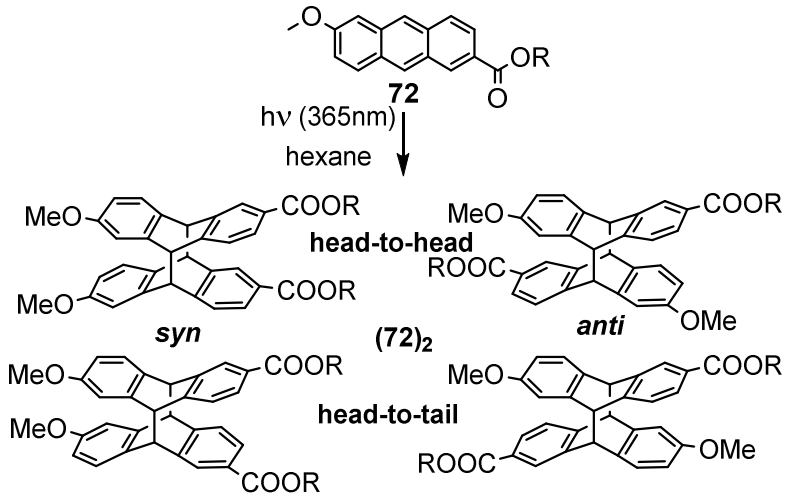

Figure VI.5. Possible photodimerization products **(72)$_2$** from anthracene ester **72**.

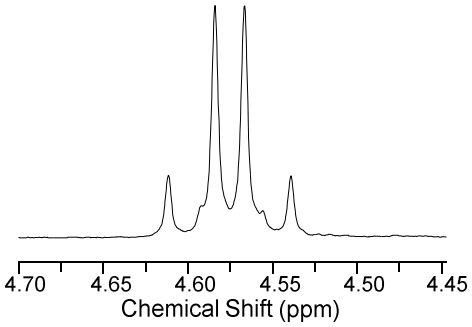

Figure VI.6. Zoom of the ^{1}H-NMR spectrum of photodimers **(72)$_2$**. The peaks originate from the anthracene dimer bridge heads.

The dimerization rate was studied by irradiating 5 and 10 mM solutions of **72** in hexane with UVA light (365 nm; 12 x 9 W), followed by concentration *in vacuo* and quantification via ^{1}H-NMR (Figure VI.7 and Figure VI.8). The dimerization occurred quickly, with 98 % conversion occurring after 1 hour. This is much faster than the previously studied 9-substituted anthracenes, which under the same conditions only had a conversion of 43 to 82 % after 1 hour (chapter III). The superior dimerization kinetics of **72** is largely due to the absence of steric hindering substituents at the 9- and 10-positions.[6, 10] As a result, not only head-tail but also head-head dimerization can easily occur, which is often not the case for the more commonly used 9-substituted anthracenes.

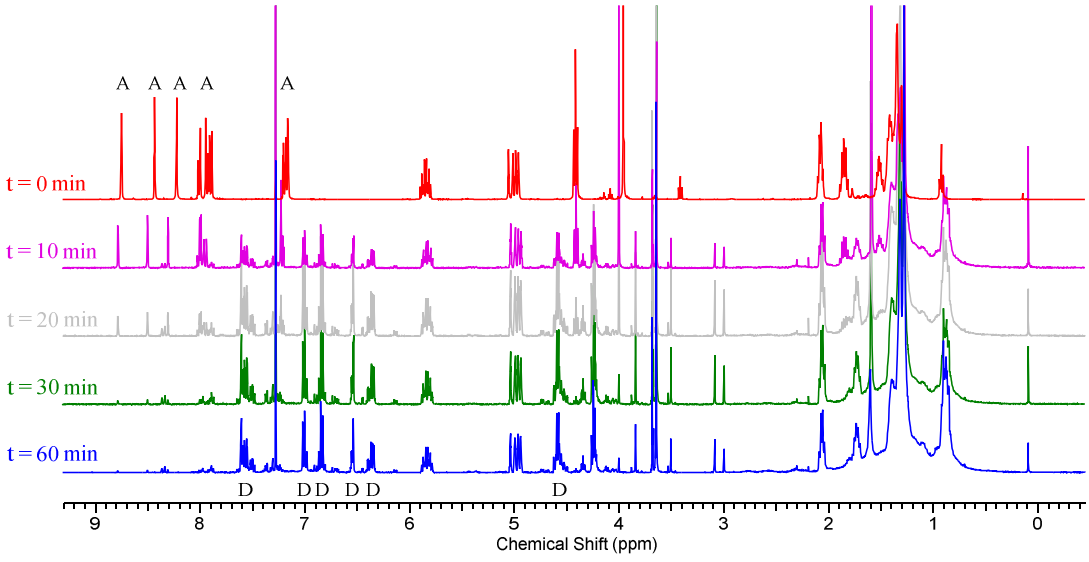

Figure VI.7. ^{1}H-NMR spectra after irradiation (365 nm) of a 5 µM solution of **72** for 0, 10, 20, 30 and 60 minutes. A and D indicate peaks corresponding to the anthracene **72** and dianthracene **(72)$_2$** structures.

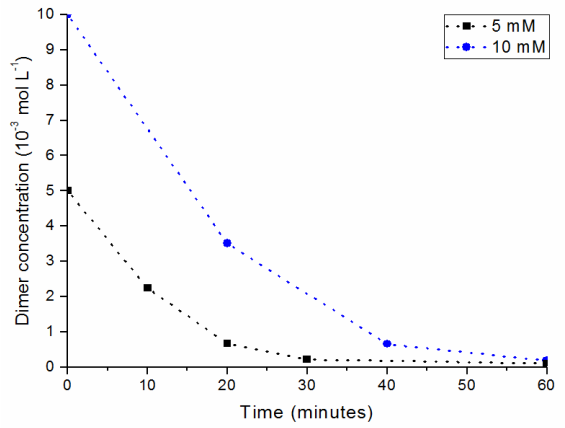

Figure VI.8. Photodimerization (365 nm; 12 x 9 W) of **72** in hexane.

2.4 UV-vis absorption of dimer $(72)_2$ and its photochemical scission

Scission of dianthracenes to their parent anthracenes requires excitation by absorption of photons. As can be seen in Figure VI.9, dimers **$(72)_2$** have a red-shifted absorption, with a large shoulder peak at 232 nm. This redshift is a result of the position of the substituents, which after dimerization remain directly connected to the benzene rings of the dimer structure. This is not the case for 9-substituted anthracenes, which after dimerization no longer have the substituent being part of an aromatic system. This extensive absorption redshift (tailing up to ~310 nm) possibly even allows for scission to occur under sunlight (>280 nm).

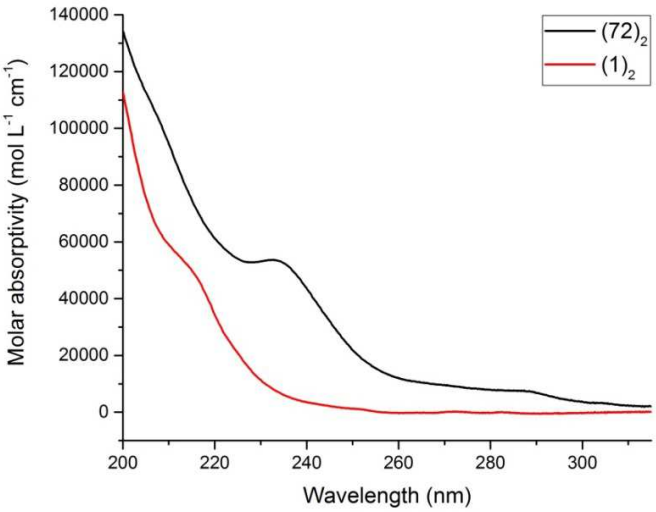

Figure VI.9. UV-vis absorption spectra of the photodimers **$(72)_2$** and unsubstituted dianthracene **$(1)_2$** in acetonitrile.

Photochemical scission of **(72)$_2$** and dianthracene **(1)$_2$** was studied by observing the appearance of the UV-vis absorption peak of **72** as a function of irradiation time (270 nm and 252 nm) (Figure VI.10). The samples were irradiated using 11 lamps of 254 nm (9 W each). It should be noted that for analytical reasons each 5 second interval included starting the UV-lamps. Therefore, the actual irradiation time is lower and the dimerization actually occurs faster upon continuous irradiation. The measured absorptions *A* were normalized to the maximum absorption A_{max} achieved for each sample. From Figure VI.10 it is clear that the photochemical scission of **(72)$_2$** occurs much faster than of dianthracene **(1)$_2$**. In fact, scission of **(72)$_2$** reached its maximum after only 15 seconds, while for **(1)$_2$** the maximum was only achieved after 2 minutes. These superior properties are the result of the achieved absorption redshifts by substitution on the 2- and 6- position. Not only does **(72)$_2$** absorb more light at 254 nm than dianthracene, but the resulting compound **72** also absorbs less of these wavelengths than unsubstituted anthracene.

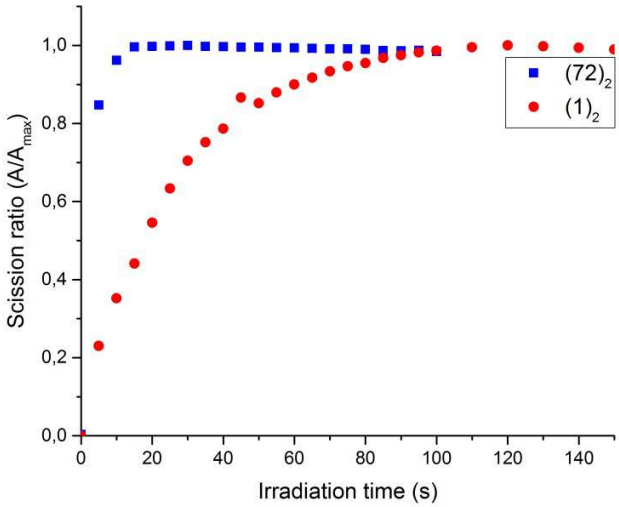

Figure VI.10. Photoscission (254 nm) of 2.8 µM solutions of **(72)$_2$** and dianthracene **(1)$_2$** in acetonitrile.

2.5 Thermal scission in bulk and in solution

The thermal scission of dimers **(72)$_2$** was studied in a solution of a high boiling solvent (tributyrin). The concentration of **72** produced by thermal scission was quantified by measuring the fluorescence of **72** in the samples taken every few minutes. Conversions were normalized to the last sample taken. By plotting the acquired rate constants *k* at different temperatures, the Arrhenius plot could be plotted from which the Arrhenius parameters can be derived (Figure VI.11). The derived activation energy *E* is 156.4 kJ mol^{-1} with a pre-exponential factor A_{exp} of 8.7 10^{14} s^{-1}. This thermal stability is slightly higher than what

was previously reported for a 9-anthracene methanol based derivative (176 kJ mol^{-1} and 1.7 10^{17} s^{-1}), which is clear when comparing scission half-times (Table VI.2).

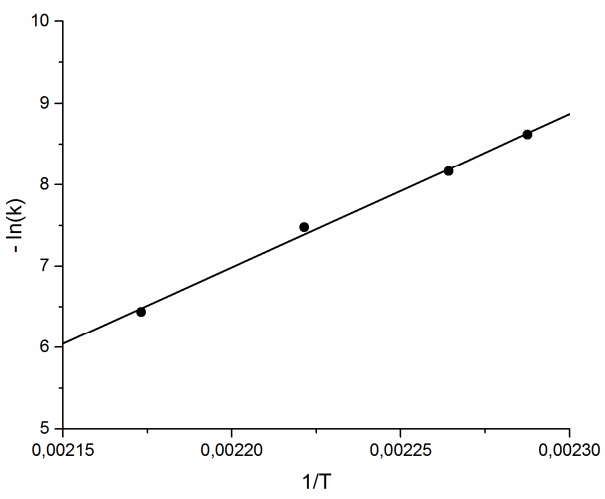

Figure VI.11. Arrhenius plot of the thermal scission of **$(72)_2$**.

Table VI.2. Estimated half-time values of **$(72)_2$** and a stable functional 9-substituted dimer **$(4)_2$.**

	160 °C	170 °C	180 °C	190 °C	200 °C	210 °C
$(72)_2$	1.6 h	36 min	14 min	5.8 min	2.5 min	1.1 min
$(4)_2$	1 h	25 min	10 min	4.4 min	1.9 min	0.9 min

The thermal scission in bulk was studied by ^{1}H-NMR measurements after controlled heating and an isothermal step of 10 minutes as a differential calorimetry scan (DSC) sample. The results thereof are shown in Figure VI.12 and Figure VI.13. These figures show that significant scission only occurs after heating for 10 minutes at 180 °C or higher temperatures. However, calculations using the determined Arrhenius parameters from solution, estimated much lower dimer ratios at 180 °C and lower temperatures. This mismatch between the estimated ratios and the experimental data from bulk is ascribed to the high melting point of **$(72)_2$** (198 °C). The stabilizing effect of the dimer crystal lattice initially slows down the thermal dissociation. A complex thermal behavior is expected by the superposition of thermal dissociation and melting of the dimer. Presumably some thermal scission takes place, resulting in liquid **72**, which dissolves remaining dimer. Nevertheless, this high melting point means that at 180 °C and lower, **$(72)_2$** must have been crystalline, leading to a much slower thermal scission.

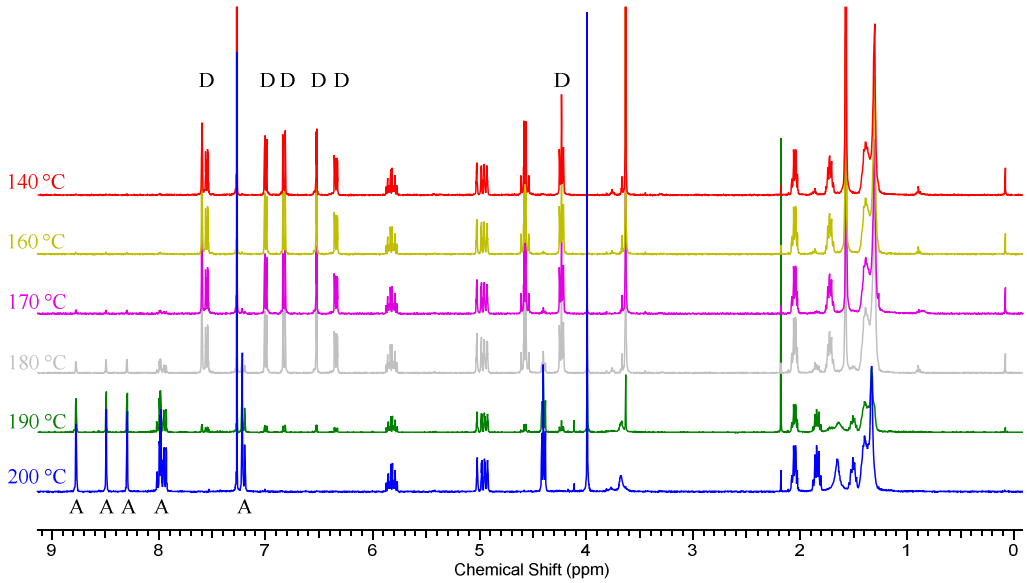

Figure VI.12. ^{1}H-NMR spectra after controlled heating (10 K min^{-1}) of photodimers **(72)$_2$** and 10 minutes isothermal at 140, 160, 170, 180, 190 or 200 °C. A and D indicate peaks corresponding to the anthracene **72** and dianthracene **(72)$_2$** structures.

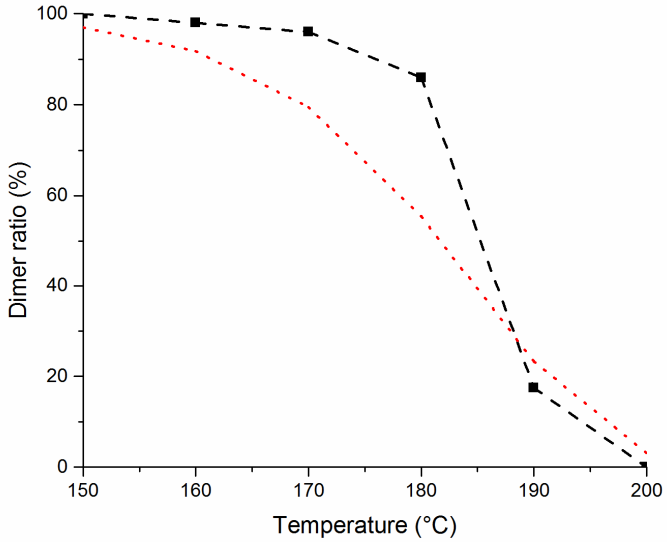

Figure VI.13. Thermal scission of **(72)$_2$** in bulk, determined using ^{1}H-NMR, after controlled heating (10 K min^{-1}) and 10 minutes isothermal. Black squares: experimental data; red dotted line: estimated conversion.

3 Conclusion

A soluble, novel functional 2,6 donor-acceptor anthracene derivative and its dimer were successfully synthesized from readily available compounds. This synthetic route may be adapted to synthesize other derivatives. By using stronger electron withdrawing groups, in combination with the donating methoxy group, larger absorption red-shifts were achieved. This is observed for both the axial (above 300 nm) and longitudinal (below 300 nm) absorptions. In addition, the high fluorescence quantum yield of $\mathbf{(72)_2}$ (0.54 - 0.64) also allows its use as efficient polymerizable fluorophore. As there are no substituents present on the middle ring, dimerization occurs much faster than previously synthesized 9-substituted anthracenes. Furthermore, because of the absorption red-shifts for both monomer and dimer, the compound also exhibits superior photoscission properties. Finally, thermal scission occurs cleanly, but requires high temperatures (> 180 °C). This is especially valid in bulk, where crystallization further increases the thermal stability.

The use of longer substituent chains and the incorporation into (densely) crosslinked polymer networks are known to reduce the crystallization of the anthracene dimers and monomers. A further change of the nature of the 2,6-substituents would allow for the preparation of stimuli-responsive polymers with tailored thermal and photochemical responsiveness that could prove especially useful for applications such as reversible adhesion, stress-relaxation and self-healing materials.

4 Experimental section

4.1 Materials & methods

All chemicals were purchased from either Acros Organics, Sigma-Aldrich or TCI Europe and used as such. IR spectra were recorded using a Perkin Elmer FTIR SPECTRUM 1000 equipped with a PIKE Miracle ATR unit. NMR spectra were recorded with a Bruker Avance-III (400 MHz) NMR spectrometer. Differential scanning calorimetry (DSC) was performed using a DSC1/700 Mettler-Toledo apparatus. The used heating rate was 10 K min^{-1} and all measurements were done under nitrogen flow. This was also used to study the bulk thermal scission behavior of the dimer. Melting points were determined using the IA90000 Melting point apparatus from Electrothermal at a heating rate of 1 K min^{-1}. LC-MS analyses were performed on an Agilent Technologies 1100 series LC/MSD system with a diode array detector (DAD) and single quad MS. Analytical reversed phase HPLC-analyses were

performed with a Phenomenex Luna C18 (2) column (5 µm, 250 mm × 4.6 mm) and a solvent gradient (75 - 100% acetonitrile in H_2O in 15 minutes), the eluted compounds were analyzed via UV detection (214 nm). UV dimerization occurred under inert atmosphere in a Metalight Classic from Primotec, with 12 double 365 nm UV lamps of 9 W each (intensity measured in the middle ~ 5 mW cm^{-2}). For fluorescence analysis, a Cary Eclipse Fluorescence Specrophotometer from Agilent with a Xenon flash lamp was used. Excitation occurred at the absorption peak maxima in the 350-400 nm region and the fluorescence spectrum was measured between up to 600 nm with a 2.5 nm slit and a scan rate of 600 nm min^{-1}. UV-vis absorption was measured using a Specord 200 from AnalyticJena from 200 to 600 nm with a speed of 5 nm s^{-1}, a slit of 2 nm and $\Delta\lambda$ = 0.1 nm. For quantum yield determinations, the concentration of the samples were chosen to ensure a transmission of 90 to 99% at the emission wavelength. 9,10-Diphenylanthracene in ethanol (Φ_f = 0.95) was used as standard in the quantum yield calculations using following equation,

$$\Phi = \Phi_R \frac{Int}{Int_R} \frac{1 - 10^{-A_R}}{1 - 10^{-A}} \frac{\eta^2}{{\eta_R}^2}$$

where "*Int*" is the integrated area under the fluorescence curve, *A* the absorption, η the refractive index of the medium and Φ the fluorescence quantum yield. Subscript "*R*" is used when referring to the standard. The uncertainty on the activation energies and pre-exponential factor was determined using Excel's LINEST function.

4.2 2-bromo-5-methoxybenzaldehyde (63)

To a stirring solution of *m*-anisaldehyde (100 ml, 0.82 mol, 1 equiv.) in acetic acid (300 ml), bromine (50 ml, 0.97 mol, 1.2 equiv.) was slowly added over 30 minutes. The solution was stirred without additional heating for 2 hours, followed by 1 hour heating at 70 °C. The reaction mixture was added to water (1.5 l), resulting in an orange precipitation. After filtration, the solids were washed with water and bicarbonate solution. The crude product was recrystallized in hot ethanol, resulting in 2-bromo-5-methoxybenzaldehyde **63** as an off-white solid (123 g, 0.57 mol, 70 % yield). To recuperate the remaining product dissolved in ethanol, a sodium hydrogen sulfite solution (37.5 %, 250 ml) was added. The formed salts were filtered and washed with ethanol and water. These salts were dissolved in a minimal amount of hot acetic acid. After cooling, bromo-5-methoxybenzaldehyde **63** crystallized out of solution (36 g, 0.17 mol, 21 % yield). Total yield was 91 %. T_m = 73.5 – 75 °C; ^{1}H-NMR (400 MHz,

$CDCl_3$): δ (ppm) = 3.85 (s, 3H, OC<u>H</u>$_3$), 7.04 (dd, 1H, *J*=8.8 Hz, *J*=3.3 Hz, CC<u>H</u>CHCBr), 7.43 (d, 1H, *J*=3.2 Hz, CC<u>H</u>C), 7.53 (d, 1H, *J*=8.8 Hz, CCHC<u>H</u>CBr), 10.32 (s, 1H, C<u>H</u>O); ^{13}C-NMR (100 MHz, $CDCl_3$) : δ (ppm) = 55.7 (CH_3), 112.7 (CH), 118 (C), 123.1 (CH), 134 (C), 134.6 (CH), 159.3 (C), 181.8 (CH); IR ν_{max} cm^{-1}: 3006, 2942, 2874, 2744, 2031, 1896, 1676, 1569, 1467, 1278, 1198, 1060, 1012; GC-MS (*m/z*) 214 $[M]^+$

4.3 (2-bromo-5-methoxyphenyl)(4-chlorophenyl)methanol (65)

Magnesium flakes (14.4 g, 592 mmol, 1.65 equiv.) were crushed and placed in a flame-dried two-neck flask equipped with a reflux cooler under inert atmosphere. Bromine (0.3 ml, 5.8 mmol) was added to the magnesium flakes. The flask was stirred and heated to the boiling point of the bromine for 15 minutes and afterwards cooled using an ice bath. Anhydrous diethyl ether (60 ml) was quickly added. The icebath was removed. A solution of 1-bromo-4-chlorobenzene (74.5 g, 394 mmol, 1.1 equiv.) in anhydrous diethyl ether (120 ml) was slowly added at a rate which kept the exothermic reaction at reflux conditions. This solution was stirred for 1 hour at room temperature, after which a solution of 2-bromo-5-methoxybenzaldehyde **63** (77 g, 358 mmol, 1 equiv.) in anhydrous diethyl ether (320 ml) was slowly added. After all aldehyde was added, the mixture was stirred for 1 hour at room temperature. The reaction mixture was carefully poured in a 1 M HCl solution (1 l). The organic phase was separated and combined with diethyl ether washings of the aqueous phase (2 x 100 ml). After drying using sodium sulfate, the organic fractions were concentrated *in vacuo*. This crude liquid (2-bromo-5-methoxyphenyl)(4-chlorophenyl)methanol **65** (120 g) was used as such in the next step. For analytical characterization, a small amount was purified using column chromatography (eluens: hexane:ethyl acetate). ^{1}H-NMR (400 MHz, $CDCl_3$): δ (ppm) = 2.38 (d, 1H, *J*=3.8 Hz, CHO<u>H</u>), 3.80 (s, 3H, OC<u>H</u>$_3$), 6.13 (d, 1H, *J*=3.8 Hz, C<u>H</u>OH), 6.74 (dd, 1H, *J*=8.7 Hz, *J*=3.1 Hz, CC<u>H</u>CHCBr), 7.12 (d, 1H, *J*=3.1 Hz, CC<u>H</u>C), 7.29 - 7.38 (m, 4H, CC<u>H</u>C<u>H</u>CCl), 7.43 (d, 1H, *J*=8.8 Hz, CCHC<u>H</u>CBr); ^{13}C-NMR (100 MHz, $CDCl_3$): δ (ppm) = 55.5 (CH_3), 74.1 (CH), 112.8 (C), 113.9 (CH), 115.1 (CH), 128.4 (CH), 128.6 (CH), 133.5 (CH), 133.6 (C), 140.4 (C), 143.1 (C), 159.3 (C); IR ν_{max} cm^{-1}: 3730, 3625, 3584, 3002, 2936, 2836, 2360, 1594, 1469, 1417, 1291, 1236, 1159, 1130, 1090, 1049, 1013; LC-MS (*m/z*) 309.0 $[M\text{-}OH]^+$; HRMS (*m/z* for $[M\text{-}OH]^+$) calcd.: 308.9682; found: 308.9673

4.4 1-bromo-2-(4-chlorobenzyl)-4-methoxybenzene (66)

Crude (2-bromo-5-methoxyphenyl)(4-chlorophenyl)methanol **65** (120 g, theoretically 358 mmol, 1 equiv.) was dissolved with triethyl silane (57.5 ml, 360 mmol, 1 equiv.) in dichloromethane (500 ml). While this solution stirred, trifluoroacetic acid was slowly added (250 ml). The reaction was stirred for 18 hours at room temperature. The reaction mixture was concentrated *in vacuo* and purified via column chromatography (hexane:ethyl acetate 95:5). This yielded the pure 1-bromo-2-(4-chlorobenzyl)-4-methoxybenzene **66** as a colorless liquid (103 g, 331 mmol, 92 % yield). ^{1}H-NMR (400 MHz, $CDCl_3$): δ (ppm) = 3.76 (s, 3H, OC$\underline{H}_3$), 4.05 (s, 2H, C$\underline{H}_2$), 6.67 - 6.71 (m, 2H,CC$\underline{H}$C + CC$\underline{H}$CHCBr), 7.12 - 7.17 (m, 2H, CC$\underline{H}$CHCl), 7.26 - 7.30 (m, 2H, CC$\underline{H}$CHCl), 7.44 - 7.50 (m, 1H, CCHC$\underline{H}$CBr); ^{13}C-NMR (100 MHz, $CDCl_3$): δ (ppm) = 41.2 (CH_2), 55.4 (CH_3), 113.5 (CH), 115.2 (C), 117 (CH), 128.6 (CH), 130.3 (CH), 132.1 (C), 133.4 (CH), 137.8 (C), 140.8 (C), 159 (C); IR ν_{max} cm^{-1}: 2934, 2834, 1894, 1572, 1471, 1238, 1158, 1089; GC-MS (*m/z*) 310 $[M]^+$

4.5 2-(4-chlorobenzyl)-4-methoxybenzoic acid (67)

Magnesium flakes (4.7 g, 193 mmol, 1.5 equiv.) were crushed and placed in a flame-dried two-neck flask equipped with a reflux cooler under inert atmosphere. Anhydrous tetrahydrofuran (20 ml) was added to the flask, followed by a small iodine crystal. While this mixture stirred, a solution of 1-bromo-2-(4-chlorobenzyl)-4-methoxybenzene **66** (40 g, 128 mmol, 1 equiv.) in anhydrous tetrahydrofuran (80 ml) was prepared. This solution of **66** was carefully added to the magnesium over 1 hour while maintaining reflux conditions using external heating. The mixture was left to stir for another 45 minutes at room temperature. Dried CO_2 gas was slowly added to the atmosphere just above the solution surface using a syringe, while heavily stirring the solution. This resulted in an exothermic response. This CO_2 originated from subliming dry ice and the formed gas was dried by bubbling twice through concentrated sulfuric acid before it reached the reaction mixture. After 1 hour, the solution had cooled down and the CO_2 flush was stopped. The reaction mixture was stirred for another 40 hour under CO_2 atmosphere. The reaction mixture was poured in dilute HCl solution (1 M, 400 ml). The yellow precipitation was filtered off and dissolved in a dilute NaOH solution (1 M, 400 ml). Concentrated HCl solution (12 M) was added to the basic solution to a pH of approximately 2. The precipitated solid was filtered off and dried, rendering pure 2-(4-chlorobenzyl)-4-methoxybenzoic acid **67** (31 g, 113 mmol, 88 %). T_m = 144 – 155 °C; ^{1}H-NMR (400 MHz, DMSO-*d6*): δ (ppm) = 3.78 (s, 3H, OC$\underline{H}_3$), 4.35 (s, 2H, C$\underline{H}_2$), 6.85 (d, 1H,

J=2.6 Hz, CC<u>H</u>C), 6.89 (dd, 1H, *J*=8.7, *J*=2.7 Hz, CC<u>H</u>CHCCO), 7.14 - 7.19 (m, 2H, CC<u>H</u>CHCCl), 7.27 - 7.32 (m, 2H, CCHC<u>H</u>CCl), 7.87 (d, 1H, *J*=8.67 Hz, CCHC<u>H</u>CCO); ^{13}C-NMR (100 MHz, DMSO-*d6*): δ (ppm) = 38.1 (CH_2), 55.3 (CH_3), 111.5 (CH), 117.2 (CH), 122.0 (C), 128.1 (CH), 130.4 (CH), 133.2 (CH), 140.2 (C), 144.1 (C), 161.9 (C), 167.9 (C); IR ν_{max} cm^{-1}: 3000, 2937, 2836, 2637, 2560, 2361, 2173, 2027, 1682, 1601, 1487, 1406, 1244, 1148, 1078, 1032; LC-MS (*m*/*z*) 275.1 [M-H]$^-$; HRMS (*m/z* for [M-H]$^-$) calcd.: 275.0475; found: 275.0487

4.6 2-chloro-6-methoxyanthracen-9(10*H*)-one (68)

2-(4-chlorobenzyl)-4-methoxybenzoic acid **67** (18.35 g, 66.3 mmol, 1 equiv.) was added to thionyl chloride (200 ml). After adding a catalytic amount of dimethyl formamide, this reaction mixture was heated to reflux conditions for 2 hours. The formed acid chloride was concentrated *in vacuo*. Anhydrous dichloromethane was added, followed by aluminum trichloride (13.3 g, 99.8 mmol, 1.5 equiv.). After 1 hour of stirring at room temperature, the reaction mixture was poured on ice. When this mixture reached room temperature, the organic phase was separated from the aqueous phase. The aqueous phase was extracted with chloroform (2 x 100 ml). The combined organic fractions were dried using sodium sulfate and concentrated *in vacuo* to give 2-chloro-6-methoxyanthracen-9(10*H*)-one **68** as a brown solid (17.1 g, 66.1 mmol, 100 %). T_m = 162 – 165.5 °C; ^{1}H-NMR (400 MHz, $CDCl_3$): δ (ppm) = 3.91 (s, 3H, OC<u>H</u>$_3$), 4.27 (s, 2H, C<u>H</u>$_2$), 6.89 (s, 1H, CC<u>H</u>COCH$_3$), 7.00 (dd, 1H, *J*=8.8 Hz, *J*=2.1 Hz, CCHC<u>H</u>COCH$_3$), 7.38 (d, 1H, *J*=8.3 Hz, CC<u>H</u>CHCCl), 7.51 (dd, 1H, *J*=8.2 Hz, *J*=2.1 Hz, CCHC<u>H</u>CCl), 8.27-8.35 (m, 2H, CC<u>H</u>CCl + CC<u>H</u>CHCOCH$_3$); ^{13}C-NMR (100 MHz, $CDCl_3$): δ (ppm) = 32.1 (CH_2), 55.5 (CH_3), 111.9 (CH), 114.4 (CH), 125.2 (C), 127.1 (CH), 129.8 (CH), 130.1 (CH), 132.4 (CH), 133.2 (C), 133.4 (C), 138.4 (C), 142.6 (C), 163.4 (C), 182.0 (C); IR ν_{max} cm^{-1}: 3064, 2942, 2840, 2033, 1591, 1478, 1408, 1272, 1167, 1113, 1030; LC-MS (*m*/*z*) 259.0 [M+H]+; HRMS (m/z for [M]+) calcd.: 258.0448; found: 258.0443

4.7 2-chloro-6-methoxyanthracene (69)

2-Chloro-6-methoxyanthracen-9(10*H*)-one **68** (18.4 g, 71.1 mmol, 1 equiv.) was dissolved in diglyme (350 ml). To this solution, sodium borohydride (18.0 g, 476 mmol, 6.7 equiv.) was added, which made the solution color dark red. The solution was stirred for 30 minutes at room temperature. The reaction flask was placed in an ice bath and anhydrous methanol (360 ml) was slowly added over 45 minutes.

This resulted in gas formation and disappearance of the red color. After another 15 minutes, more sodium borohydride (9.0 g, 238 mmol, 3.3 equiv.) was slowly added, causing additional gas formation. The reaction mixture was stirred overnight at room temperature. To the reaction mixture, acetic acid (700 ml) was added, followed by concentrated HCl solution (12 M, 100 ml). This mixture was stirred for 2 hours. Water (3 l) was added to the reaction mixture, resulting in the precipitation of 2-chloro-6-methoxyanthracene **69** as a yellow solid (16.9 g, 69.6 mmol, 98 %). T_m = 213 – 214 °C; ^{1}H-NMR (400 MHz, DMSO-d6): δ(ppm) = 3.93 (s, 3H, OC$\underline{H}_3$), 7.23 (dd, 1H, *J*=9.2 Hz, *J*=2.4 Hz, CCHC$\underline{H}$CO), 7.40 (d, 1H, *J*=2.4 Hz, CC$\underline{H}$CO),7.46 (dd, 1H, *J*=9.0 Hz, *J*=2.1 Hz, CCHC$\underline{H}$CCl), 8.00 (d, 1H, *J*=9.3 Hz, CC$\underline{H}$CHCO), 8.07 (d, 1H, *J*=9.3 Hz, CC$\underline{H}$CHCCl), 8.15 (d, 1H, *J*=1.6 Hz, CC$\underline{H}$CCl), 8.46 (s, 1H, CC$\underline{H}$C)8.48 (s, 1H, CC$\underline{H}$C); ^{1}H-NMR (400 MHz, $CDCl_3$): δ(ppm) = 3.98 (s, 3H, OC$\underline{H}_3$), 7.16 - 7.24 (m, 2H, CCHC$\underline{H}$CO + CC$\underline{H}$CO), 7.37 (dd, 1H, *J*=9.0 Hz, *J*=2.0 Hz, CCHC$\underline{H}$CCl), 7.89 (d, 2H, *J*=9.4 Hz, CC$\underline{H}$CHCO + CC$\underline{H}$CHCCl), 7.95 (d, 1H, *J*=2.0 Hz, CC$\underline{H}$CCl), 8.26 (m, 2H, CC$\underline{H}$C); ^{13}C-NMR (100 MHz, $CDCl_3$): δ(ppm) = 55.3 (CH_3), 103.6 (CH), 121.2 (CH), 124.4 (CH), 125.4 (CH), 126.4 (CH), 126.7 (CH), 128.8 (C), 129.3 (CH), 129.7 (CH), 130.0 (C), 130.2 (C), 130.4 (C), 132.8 (C), 157.4 (C); IR ν_{max} cm^{-1}: 3010, 2841, 2428, 2049, 1980, 1930, 1774 1618, 1466, 1343, 1269, 1175, 1027; GC-MS (m/z) 242 $[M]^+$

4.8 6-methoxyanthracene-2-carbonitrile (70)

2-Chloro-6-methoxyanthracene **69** (1.0 g, 4.1 mmol, 1 equiv.) was dissolved in N-methyl-2-pyrrolidone (10 ml). To this solution, copper cyanide was added (0.74 g, 8.3 mmol, 2 equiv.). The reaction mixture was heated to reflux conditions for 30 hours. The mixture was then poured in a saturated bicarbonate solution (100 ml), followed by an extraction using diethyl ether (2x 25 ml) and toluene (2 x 25 ml). The organic phases were combined, dried using sodium sulfate and concentrated *in vacuo*, rendering 6-methoxyanthracene-2-carbonitrile **70** (0.63 g, 2.7 mmol, 66 %) as a yellow solid. The crude product was used as such in the next step. For characterization, some product was purified using column chromatography. T_m = 184 – 189 °C; ^{1}H-NMR (400 MHz, $CDCl_3$): δ(ppm) = 4.00 (s, 3H, OC$\underline{H}_3$), 7.21-7.28 (m, 2H, CCHC$\underline{H}$CO + CC$\underline{H}$CO), 7.51 (dd, 1H, *J*=8.7 Hz, *J*=1.5 Hz, CCHC$\underline{H}$CCN), 7.95 (d, 1H, *J*=9.0 Hz, CC$\underline{H}$CHCO), 8.00 (d, 1H, *J*=8.8 Hz, CC$\underline{H}$CHCCN), 8.30 (s, 1H, CC$\underline{H}$CCHCO), 8.40 (m, 1H, CC$\underline{H}$CCN), 8.42 (s, 1H, CC$\underline{H}$CCHCCN); ^{13}C-NMR (100 MHz, $CDCl_3$): δ(ppm) = 55.4 (CH_3), 103.6 (CH), 107.7 (C), 119.6 (C), 121.9 (CH), 124.6 (CH), 124.8 (CH), 127.8 (CH), 128.4 (C), 129.0 (CH), 130.1 (CH), 132.1 (C), 134.8 (C), 135.7 (CH), 158.6 (C); IR ν_{max} cm^{-1}: 3077, 2914, 2848, 2428, 2357,

2195, 2043, 1983, 1846, 1717, 1630, 1467, 1419, 1245, 1101, 1025; HRMS (*m/z* for $[M]^+$) calcd.: 233.0841; found: 233.0833

4.9 6-methoxyanthracene-2-carboxylic acid (71)

6-Methoxyanthracene-2-carbonitrile **70** (0.63 g, 2.7 mmol, 1 equiv.) was added to a mixture of methanol (95 ml), water (25 ml) and potassium hydroxide (25 g). The reaction mixture was heated overnight at reflux temperature. After cooling down, water (350 ml) was added, followed by slow addition of concentrated HCl solution (50 ml). After extraction with dichloromethane (3 x 200 ml), the organic phases were combined, dried with sodium sulfate and concentrated *in vacuo*. The resulting solid was recrystallized twice in acetic acid, rendering pure 6-methoxyanthracene-2-carboxylic acid **71** as a yellow powder. (0.60 g, 2.4 mmol, 87 %). T_m > 300 °C; ^{1}H-NMR (400 MHz, DMSO-*d6*): δ (ppm) = 3.94 (s, 3H, OC$\underline{H}_3$), 7.25 (dd, 1H, *J*=9.2 Hz, *J*=2.5 Hz, CCHC$\underline{H}$CO), 7.44 (d, 1H, *J*=2.4 Hz, CC$\underline{H}$CO), 7.90 (dd,1H, *J*=8.7 Hz, *J*=1.6 Hz, CCHC$\underline{H}$CCOOH), 8.05 (d, 1H, *J*=9.5 Hz, CC$\underline{H}$CHCO), 8.08 (d, 1H, *J*=9.4 Hz, CC$\underline{H}$CHCCOOH), 8.47 (s, 1H, CC$\underline{H}$C), 8.72 (s, 1H, CC$\underline{H}$C), 8.74 (m, 1H, CC$\underline{H}$CCOOH), 12.99 (br. s, 1H, COO$\underline{H}$); ^{13}C-NMR (100 MHz, DMSO-*d6*): δ (ppm) = 55.3 (CH_3), 103.9 (CH), 121.0 (CH), 123.9 (CH), 124.3 (CH), 126.5 (C), 127.9 (CH), 128.1 (C), 128.5 (C), 128.6 (CH), 130.1 (CH), 131.8 (CH), 132.7 (C), 134.0 (C), 157.7 (C), 167.5 (C); IR ν_{max} cm^{-1}: 2975, 2837, 2522, 2178, 2048, 1856, 1677, 1476, 1420, 1285, 1216, 1027; LC-MS (*m*/*z*) 251.1 $[M-H]^-$; HRMS (*m/z* for $[M-H]^-$) calcd.: 251.0708; found: 251.0712

4.10 undec-10-en-1-yl 6-methoxyanthracene-2-carboxylate (72)

6-Methoxyanthracene-2-carboxylic acid **71** (774 mg, 3.07 mmol, 1 equiv.) was dissolved in anhydrous dimethyl formamide (30 ml). To this solution, potassium carbonate (0.5 g, 3.65 mmol, 1.2 equiv.) and 11-bromo-1-undecene (1.4 g, 6 mmol, 2 equiv.) were added. The reaction mixture was stirred for 24 hours. The reaction mixture was concentrated *in vacuo* and purified using column chromatography (hexane:ethyl acetate 95:5) to the pure undec-10-en-1-yl 6-methoxyanthracene-2-carboxylate **72** (465 mg, 1.15 mmol, 37 %). T_m = 100 – 102.5 °C; ^{1}H-NMR (400 MHz, $CDCl_3$): δ (ppm) = 1.25 - 1.45 (m, 10H, $CH_2C\underline{H}_2CH_2$), 1.46 - 1.55 (m, 2H, $OCH_2CH_2C\underline{H}_2$), 1.80 - 1.89 (m, 2H, $OCH_2C\underline{H}_2CH_2$), 2.02 - 2.11 (m, 2H, $CH_2C\underline{H}_2CH{=}CH_2$), 3.95 (s, 3H, OC$\underline{H}_3$), 4.41 (t, 2H, *J*=6.7 Hz, $OC\underline{H}_2CH_2$), 4.93 - 5.06 (m, 2H, $CH_2CH{=}C\underline{H}_2$), 5.84 (ddt, 1H, *J*=17.0 Hz, *J*=10.3 Hz, *J*=6.7 Hz, $CH_2C\underline{H}{=}CH_2$), 7.13 - 7.21 (m, 2H,

CC<u>H</u>CO + CCHC<u>H</u>CO), 7.89 (d, 1H, *J*=9.3 Hz, CC<u>H</u>CHCO), 7.93 (d, 1H, *J*=8.9 Hz, CC<u>H</u>CHCCOOR), 8.00 (dd, 1H, *J*=9.0 Hz, *J*=1.8 Hz, CCHC<u>H</u>CCOOR), 8.22 (s, 1H, CC<u>H</u>C), 8.42 (s, 1 H, CC<u>H</u>C), 8.73 – 8.75 (m, 1H, CC<u>H</u>CCOOR); ^{13}C-NMR (100 MHz, $CDCl_3$): δ(ppm) 26.0 (CH_2), 28.8 (CH_2), 28.9 (CH_2), 29.1 (CH_2), 29.3 (CH_2), 29.4 (CH_2), 29.4 (CH_2), 33.7 (CH_2), 55.2 (CH_3), 65.1 (CH_2), 103.5 (CH), 114.1 (CH_2), 121.0 (CH), 123.9 (CH), 124.2 (CH), 126.2 (C), 127.6 (CH), 128.5 (CH), 128.9 (C), 130.0 (CH), 132.1 (CH), 133.1 (C), 134.2 (C), 139.1 (CH), 158.0 (C), 166.8 (C); IR ν_{max} cm^{-1}: 3077, 2914, 2848, 2428, 2357, 2195, 2043, 1983, 1846, 1717, 1630, 1467, 1419, 1245, 1101, 1025; LC-MS (*m*/*z*) 405.2 $[M+H]^+$; HRMS (*m/z* for $[M+H]^+$) calcd.: 405.2430; found: 405.2421

4.11 General procedure to form anthracene ester dimer ((72)$_2$)

Undec-10-en-1-yl 6-methoxyanthracene-2-carboxylate **72** (20.4 mg, 50 µmol) was dissolved in a minimal amount of hexane (10 ml) and irradiated using UVA light (365 nm; 12 x 9 W) for 1 hour. The reaction mixture was concentrated *in vacuo* to render anthracene ester dimers **(72)$_2$** (98 % pure). Recrystallization in hexane yields completely pure dimers. T_m = 197.5 – 198 °C; ^{1}H-NMR (400 MHz, $CDCl_3$): δ(ppm) = 1.22 - 1.46 (m, 24H, $CH_2C\underline{H}_2CH_2$), 1.72 (quin, 4H, J=7.1 Hz, $CH_2C\underline{H}_2CH_2$), 2.05 (q, 4H, J=6.8 Hz, $CH_2C\underline{H}_2CH{=}CH_2$), 3.63 (s, 6H, $OC\underline{H}_3$), 4.23 (t, 4H, J=6.7 Hz, $OC\underline{H}_2CH_2$), 4.53 – 4.62 (m, 4H, CC<u>H</u>C), 4.92 – 4.96 (m, 2H, $CH_2CH{=}C\underline{H}_2$), 4.97 - 5.04 (m, 2H, $CH_2CH{=}C\underline{H}_2$), 5.82 (ddt, 2H, *J*=17.0 Hz, *J*=10.3 Hz, *J*=6.7 Hz, $CH_2C\underline{H}{=}CH_2$), 6.34 (dd, 2H, *J*=8.2 Hz, *J*=2.4 Hz, CCHC<u>H</u>CO), 6.53 (d, 2H, *J*=2.6 Hz, CC<u>H</u>CO), 6.82 (d, 2H, *J*=8.2 Hz, CC<u>H</u>CHCO), 7.00 (d, 2H, *J*=7.7 Hz, CC<u>H</u>CHCCOOR), 7.55 (dd, 2H, *J*=7.7 Hz, J=1.7 Hz, CCHC<u>H</u>CCOOR), 7.60 (d, 2H, *J*=1.5 Hz, CC<u>H</u>CCOOR); ^{13}C-NMR (100 MHz, $CDCl_3$): δ (ppm) = 26.0 (CH_2), 28.7 (CH_2), 28.9 (CH_2), 29.1 (CH_2), 29.3 (CH_2), 29.4 (CH_2), 29.5 (CH_2), 33.8 (CH_2), 52.5 (CH), 53.8 (CH), 55.3 (CH_3), 64.9 (CH_2), 110.6 (CH), 113.5 (CH), 114.1 (CH_2), 127.0 (CH), 127.4 (CH), 127.7 (C), 127.8 (CH), 134.8 (C), 139.2 (CH), 143.7 (C), 144.1 (C), 148.8 (C), 157.8 (C), 166.6 (C); IR ν_{max} cm^{-1}: 2919, 2851, 1705, 1608, 1492, 1437, 1266, 1210, 1162, 1091, 1038; HRMS (*m/z* for $[M+H]^+$) calcd.: 809.4781; found: 809.4762

5 References

1. Claus, T. K.; Telitel, S.; Welle, A.; Bastmeyer, M.; Vogt, A. P.; Delaittre, G.; Barner-Kowollik, C., *Chemical Communications* **2017,** *53* (10), 1599-1602.
2. Ihmels, H., *European Journal of Organic Chemistry* **1999,** *1999* (7), 1595-1600.
3. Lu, Z.; Lord, S. J.; Wang, H.; Moerner, W. E.; Twieg, R. J., *The Journal of Organic Chemistry* **2006,** *71* (26), 9651-9657.
4. Marquardt, D. J.; McCormick, F. A., *Tetrahedron Letters* **1994,** *35* (8), 1131-1134.
5. Jones, R. N., *Chemical Reviews* **1947,** *41* (2), 353-371.
6. Bouas-Laurent, H.; Castellan, A.; Desvergne, J.-P.; Lapouyade, R., *Chemical Society Reviews* **2000,** *29* (1), 43-55.
7. Abou-Hatab, S.; Spata, V. A.; Matsika, S., *The Journal of Physical Chemistry A* **2017,** *121* (6), 1213-1222.
8. Mennucci, B., The Simulation of UV-Vis Spectroscopy with Computational Methods. In *Computational Spectroscopy*.
9. Hansch, C.; Leo, A.; Taft, R. W., *Chemical Reviews* **1991,** *91* (2), 165-195.
10. Mukae, M.; Ihara, T.; Tabara, M.; Jyo, A., *Organic & Biomolecular Chemistry* **2009,** *7* (7), 1349-1354.

Chapter VII: General conclusions & perspectives

1 Conclusions

In this PhD research, we aimed for the development of anthracene-based materials that are reversibly crosslinked. While we initially looked for recyclability, remendability and stress-relaxation, our findings proved to also be fundamental in nature and applicable for many (smart) polymer systems.

In this context, first a large series of novel 9-substituted anthracene derivatives was synthesized (chapter III). While these substituents were carefully chosen to improve solubility and add a suitable polymerizable group for polymerization, the development thereof was largely driven by the desire to tune the reversible dimerization. By being able to tune these properties at the molecular level, we aimed for the control of properties at a material level.

Many synthetic routes have been explored, leading to the successful synthesis of a novel series of anthracenes with shifted UV-vis absorption. From these results, we could clearly see the correlation between the red shift and the nature of the substituent: stronger electron donating groups lead to larger shifts. Extremely large red shifts, which would be desirable to allow the dimerization to occur under milder conditions or (more efficiently) under sunlight, could not be accomplished. Knowing this, larger shifts could be accomplished by having multiple and/or stronger donating substituents, e.g. as was demonstrated recently by Barner-Kowollik.[1] Another option, which was one of the project aims, was to design anthracene building blocks that are having both an electron donor and an electron acceptor as substituents in conjugation (at the 2- and 6-position). In chapter VI, we synthesized several of these donor-π-acceptor anthracenes, one of which was equipped with a spacer and polymerizable group. While the shifts thereof were larger than for the monosubstituted derivatives, a maximal red shift of only 24 nm was accomplished. Presumably, the electron donor (methoxy) and acceptor (ester group) are not sufficiently strong. A next step could be to replace the methoxy group by a dialkylamine, resulting in a much stronger donor.

The dimerization in solution upon irradiation with 365 nm lamps was studied, which revealed the large reactivity difference between the 9-substituted anthracenes and unsubstituted anthracene (slow

dimerization) and the 2,6-substituted anthracenes (fast dimerization). The fast dimerization of the latter compound is presumably due to less steric hindrance and a better spectral overlap.

The photochemical scission of all compounds typically occurred quickly (under dilute conditions), though the scission rate of the 2,6-substituted anthracene far exceeded that of the other compounds. As both photochemical reaction rates of the 2,6-substituted anthracene is superior, it is the preferred compound for fully photoreversible systems.

Alternatively, when thermal scission is desired, the 9-substituted anthracenes are more interesting because, depending on the substituent, the scission temperature (50% scission after 10 minutes) can be finetuned between 180 °C to 110 °C. It should be emphasized that this reaction typically occurs without side reactions, in contrast to photochemical scission. For some dimers, large differences in thermal stability in bulk and solution was found, which is related to the stabilizing effect of the crystal lattice.

This effect of crystallinity is also important when incorporating these derivatives in materials. Polymer coatings were made by reacting a dimer di-ene with polythiols (chapter IV) and dimer diols and tetraols with (tri)isocyanates (chapter V). The thiol-ene networks were surprisingly crystalline, which is partially ascribed to the low solid content of the curing resin. Nevertheless, the aliphatic and silicone thiol-ene networks were thermally degradable at similar time- and temperature scales as the used dimer. By altering the macromolecular architecture of the networks, the loss of integrity by thermal degradation can be tuned. This thermal degradation also worked predictably in different material types and for different dimers. The extent of scission has been studied by rheometry and differential scanning calorimetry. Studying the scission in coatings was more difficult because of abrupt property changes (solvent resistance and hardness) and less temperature control. Cleaved coatings were extremely easily removed once passing their (de)gel point, which might prove interesting in airspace industry for example where coatings need to be carefully and rapidly removed on a regular basis.

Thermally disintegrated materials were recurable, but only for up to a few cycles. The limiting factor is mainly the photo-oxidative formation of endoperoxides and other byproducts. While this is inherent to the chemistry, future research to find stable compounds is necessary to expand the industrial application range.

Stress-relaxation was shown to occur by stimulating both bond breaking and bond formation, either simultaneously or in separate steps. Nevertheless, the limited oxidative stability and oxygen-rich testing set-ups limit the extent thereof to a one-time (partial) stress relaxation.

To conclude, by using different substituents on anthracene moieties, the photodimerization as well as the scission can be accelerated (or slowed down), thereby expanding its applicability. This chemistry is especially interesting when limited reversibility is acceptable.

2 Future perspectives

After this PhD research, many challenges still exist, some of which are discussed below. One important challenge is optimizing the oxidative stability. While the presence of oxygen can often be avoided or limited in a laboratory environment, this is often not an option for industrial applications and thus is problematic in applications such as recycling, self-healing and stress-relaxation. While explorative work surrounding this issue has been performed, a full study with variable derivatives, wavelengths, solvents (and polymer matrices) and oxygen scavengers would be recommended.

While the mechanical scission of anthracene dimers lay beyond the scope of the performed research, it is interesting on both a fundamental and applied level. Considering the strong influence of the nature of the 9-substituent on the thermal scission, 9-substituents are likely to also influence the mechanical scission. The strong fluorescence of (many of) the formed anthracenes would make them excellent damage and stress reporter molecules.

Further studies on donor-π-acceptor anthracenes are worthwhile, although shorter synthetic routes are desired for industrial application. Assuming the latter is possible, strong charge-transfer absorption red-shifts of both monomer and dimer might allow using only visible light to stimulate both dimerization and dimer scission in materials. As a stronger donating group, the methoxy group could be replaced by a dialkyl amine for example.[2] On the other hand, a potentially suitable electron acceptor could be a functional (protonated) oxazoline group.[3] Substitution can also be done at other positions, such as the 1- and 4-position or the 2- and 3-position. Both types would result in the substituents still being in conjugation after dimerization, probably allowing intramolecular charge transfer behavior by the dimers. Because of steric hindrance during dimerization, 1,4-substitution is not recommended.

Thus far the dimerization between identical anthracenes was studied. However, tuning of dimer properties can also be done by making heterodimers. While this strategy makes the materials more complex, it allows tunability using only a limited number of compounds.

The photochemical scission of anthracene dimers occurred very efficiently, but is thus far limited to surfaces and dilute samples. By using different LEDs as light source, scission might also be accomplished for thicker materials. Important is to excite at a wavelength at which the anthracene dimers absorb (slightly), but the formed anthracenes and other compounds do not.

Similar to the recent work of Sumerlin and coworkers,[4] anthracene dimerization can be used to develop materials that undergo stimulated macromolecular metamorphosis. This would be especially interesting when making the combination with the anthracene-maleimide click chemistry.

Once a high reversibility of the anthracene dimerization can be ensured (by hampering any oxidative side reactions), self-healing and stress-relaxation by anthracene chemistry could become industrially relevant and thus be further explored with an industrial partner. In this context, as coatings are often highly cross-linked materials and anthracene dimers are expensive compounds in relation to industrially used crosslinkers, the relation should be studied between the ratio of reversible bonds and the desired coating properties.

3 References

1. Claus, T. K.; Telitel, S.; Welle, A.; Bastmeyer, M.; Vogt, A. P.; Delaittre, G.; Barner-Kowollik, C., *Chem Commun* **2017,** *53* (10), 1599-1602.
2. de Miranda, M. G.; de Oliveira, M. F. G.; Lopes, R. S. C.; da Silva, A. J. R.; Albert, A. L. M.; Lopes, C. C., *Tetrahedron Letters* **2013,** *54* (21), 2587-2590.
3. Ihmels, H.; Meiswinkel, A.; Mohrschladt, C. J., *Organic Letters* **2000,** *2* (18), 2865-2867.
4. Sun, H.; Kabb, C. P.; Dai, Y.; Hill, M. R.; Ghiviriga, I.; Bapat, A. P.; Sumerlin, B. S., *Nature Chemistry* **2017,** *9*, 817.

Nederlandse samenvatting

Algemene inleiding

Coatings (en verven) zijn dunne lagen materiaal die het oppervlak bedekken van grotere objecten, ook substraten genoemd. In de meeste omstandigheden is de coating er om het substraat te beschermen of voorzien van andere eigenschappen. Dit laatste kan corrosiebescherming zijn, een hogere krasweerstand, het geven van een mat of glanzend oppervlak,… Polymeergebaseerde coatings kunnen zowel elastisch zijn, glasachtig of kristallijn. Elk van deze kunnen op hun beurt thermoplastisch zijn (en dus opnieuw vloeibaar gemaakt worden), of thermohard. De meeste coatings zijn thermoharders, gezien deze een hogere solventweerstand hebben, alsook een hogere temperatuurbestendigheid.

Ondanks het lange en wijdverspreide gebruik van coatings, blijven er heel wat uitdagingen over. Sommigen hiervan zijn gerelateerd met het aanbrengen van nieuwe eigenschappen, terwijl anderen gaan om het verhogen van de duurzaamheid. Enkele voorbeelden van uitdagingen zijn het falen door interne spanningen, degradatie door zonlicht en het moeilijk verwijderen van oude coatings.

Stress of interne spanningen ontstaan door gehinderde krimp bij het uitharden van het materiaal. De permanente vernetting bij thermoharders verhindert het optreden van kruip en dus ook het relaxeren van de interne spanningen. Bijgevolg blijven vernette coatings in een gespannen toestand. De hoeveelheid spanning kan (tijdelijk) verlagen of verhogen door vervormingen, temperatuursveranderingen, oplosmiddelen,..

Zonlicht bestaat onder andere uit ultraviolet licht, met golflengtes van 295 tot 400 nanometer. Blootstelling van polymeermaterialen (en dus ook zeker coatings) aan dit UV licht leidt tot het optreden van zijreacties die extra vernetting, verkorte polymeerketens en kleurveranderingen veroorzaken. Vaak worden UV-absorberende additieven toegevoegd aan coatingformulaties om deze ongewenste effecten te beperken.

Hoge taaiheid en adhesie zijn gewenste eigenschappen bij alle coatings, maar vormen een hindernis bij het verwijderen van oude coatings. Heden wordt dit mechanisch gedaan door schuren of zandstralen, of chemisch door gebruik te maken van oplosmiddelen en agressieve chemicaliën.

Doel

Het doel van het uitgevoerde onderzoek was het ontwikkelen en evalueren van antraceen-baseerde coatings. Specifiek gaat het om het gebruiken van de dimerisatie-eigenschappen van antraceen als reversibele vernetting. Een antraceenmolecule absorbeert UV licht (zoals aanwezig in zonlicht) en reageert vervolgens met een andere antraceenmolecule tot een dimeer. Bij blootstelling aan UV licht met een kortere golflengte en/of warmte, splitsen deze dimeren zich opnieuw tot de oorspronkelijke antracenen.

Door deze antraceendimeren als vernettingspunten te gebruiken, kan een materiaal steeds wisselen van een onvernette toestand (thermoplast) naar een vernette toestand (thermoharder). Door het (gedeeltelijk of geheel) wisselen tussen deze toestanden kan een thermoharder gemaakt worden waar de spanningen uit verdwijnen. Anderzijds kan ook een thermoharder gemaakt worden die gemakkelijk te verwijderen is door het eerst om te zetten naar een (vloeibaar) thermoplast.

Antraceen heeft op zijn aromatische structuur veel posities waar substituenten aanwezig kunnen zijn, waarvan geweten is dat ze de absorptie-eigenschappen beïnvloeden (zie hoofdstuk II). Door substituenten toe te voegen, kan de energie vereist voor exciteren (door absorptie van een UV foton) en het daarop volgende dimeriseren verlaagd worden. Daarom werd gekozen om gebruik te maken van antraceen als reversible binding, en deze aan te passen door het rationeel toevoegen van substituenten om zo mildere dimeriseringsomstandigheden mogelijk te maken (met minder zijreacties en degradatie tot gevolg). Daarenboven wensten we ook de golflengtes vereist voor het splitsen van de dimeren verlengen, eventueel zelfs tot in de regio van het zonlicht. Ook de invloed van de substituenten op het thermisch splitsen van de antraceendimeren werd onderzocht. Aangezien de dissociatie van ongesubstitueerd antraceen hoge temperaturen vereist van bij de 200 °C, zou een verlaging in de temperatuur hiervan dit mechanisme toepasbaarder maken.

Het modificeren van de antraceengroepen gebeurde op twee manieren. Eerst werden 9-gesubstitueerde antracenen gemaakt, gezien er reeds 9-gesubstitueerde antracenen commercieel beschikbaar waren die als startmateriaal gebruikt konden worden. Deze 9-positie werkt ook als ankerpunt voor een keten met functionele eindgroep, wat nodig is voor incorporatie in een polymeermateriaal. Belangrijk is ook de lengte van deze keten, gezien langere ketens de flexibiliteit van de antraceengroep in het materiaal verhogen. Tevens verhogen deze ook de oplosbaarheid van de moleculen in de hars, waardoor minder

oplosmiddelen nodig zijn. Een andere strategie bestond uit het maken van 2- en 6-gesubstitueerde derivaten, met zowel een elektrondonor en een elektronacceptor in conjugatie. Het synergetisch effect kan leiden tot efficiënte intramoleculaire ladingsoverdracht en lichtabsorptie (en dimeriseren) in het zichtbare licht. De positionering van de substituenten kan de dimeriseringssnelheid verhogen door een lagere sterische hinder. Het plaatsen van substituenten op de benzeenringen van de gevormde dimeren zou ook het absorptiespectrum (en splitsen) van de dimeren beïnvloeden.

Het was van belang dat de antracenen gemakkelijk in materialen kunnen gebracht worden. Het liefst door het toevoegen van de dimere vormen aan bestaande formulaties. Tijdens het materiaalonderzoek lag de focus op de reversibele dimerisatie en het resulterend (on)vernetten. Belangrijk was ook de invloed van de netwerkstructuren op de finale eigenschappen. Dit had het doel om de materiaaleigenschappen te kunnen verfijnen door rationele selectie van het antraceentype en de macromoleculaire architectuur.

Overzicht

Het werk werd onderverdeeld en besproken in deze thesis als volgt:

In hoofdstuk I staat een korte inleiding betreffende coatings en de uitdagingen hieromtrent. Reversibele reacties werden kort besproken met focus op reversibele addities.

In hoofdstuk II is de reversibele antraceenchemie besproken, gevolgd door een uitgebreide bespreking over de bestaande literatuur betreffende antraceenbevattende polymeren. Deze bespreking begint met polymeren die antracenen bevatten als niet-reactieve groep. Ze functioneerden veelal als geleidende of fluorescerende groep. Daarna worden polymeren besproken waarbij antracenen gebruikt werden voor polymerisering, post-polymerisering modificatie, (reversibele) polymeer-polymeerkoppeling en (reversibele) vernetting. Deze reacties zijn vaak Diels-Alderreacties of antraceenfotodimerisatie.

In hoofdstuk III wordt de synthese en karakterisering van nieuwe 9-gesubstitueerde derivaten besproken. Deze derivaten zijn bruikbaar in formulaties en verschillen voornamelijk in de aard de substituent op de 9-positie. Deze variatie beïnvloedt voornamelijk de absorptie en fluorescentie van de monomeren, alsook de thermische stabiliteit van de dimeren.

In hoofdstuk IV is een van de antraceenderivaten gebruikt om thermisch degradeerbare en opnieuw vernetbare thiol-eennetwerken te ontwikkelen. De interessante thermomechanische eigenschappen die hieruit afkomstig zijn worden grondig bestudeerd.

In hoofdstuk V worden polyurethaanmaterialen en –coatings gemaakt met antraceenderivaten. De eigenschappen werden verder verfijnd door niet-reversibele knooppunten toe te voegen. De reversibele vernetting werd bestudeerd en gevalideerd voor gemakkelijk verwijderbare coatings en voor stressrelaxatie.

In hoofdstuk VI wordt de synthese en karakterisering van 2,6-gesubstitueerde antracenen besproken die een elektrondonor en een elektronacceptor in conjugatie hebben. De invloed van dit substitutiepatroon werd bestudeerd op een vergelijkbare wijze als in hoofdstuk III. Een specifiek 2,6-gesubstitueerd antraceen werd volledige gekarakteriseerd voor gebruik in materialen.

In hoofdstuk VII worden de conclusies van het onderzoek gegeven, alsook een vooruitblik naar toekomstig werk.

Besluit

Verschillende synthetische routes zijn onderzocht in hoofdstuk III, leidende tot de succesvolle synthese van een reeks nieuwe antraceenderivaten met naar het rood verschoven absorptiespectra (hoofdstuk III). Deze resultaten toonden een duidelijke relatie aan tussen de mate van verschuiving en de natuur van het substituent: sterker elektrondonerende groepen leidden tot grotere verschuivingen. Extreem grote verschuivingen werden niet kregen bij de gemaakte 2,6-gesubstitueerde antracenen (hoofdstuk VI). Waarschijnlijk zijn de elektrondonor (methoxy groep) en de elektronacceptor (ester) niet sterk genoeg.

De dimerisatiestudie in oplossing met UV lampen (emissiepiek bij 365 nm) toonde een groot verschil in reactiesnelheid aan tussen ongesubstitueerd antraceen en de 9-gesubstitueerde antracenen enerzijds (trage dimerisatie) en het 2,6-gesubstitueerde antraceen anderzijds (snelle dimerisatie). Dit verschil is waarschijnlijk te wijten aan minder sterische hinder en een betere spectrale overlap bij het 2,6-gesubstitueerd antraceen. De fotochemische dissociatie van alle dimeren verliep snel (in sterk verdunde concentratie), maar verliep veel sneller voor het 2,6-gesubstitueerde derivaat. Wanneer thermische dissociatie gewenst is, zijn de 9-gesubstitueerde derivaten zeer interessant, gezien afhankelijk van de substituent de dissociatietemperatuur (50% dissociatie in 10 minuten) varieerde tussen 180 °C en 110 °C. Bij sommige dimeren ontstond een groot verschil tussen de dissociatie verdunde (opgeloste) en onverdunde toestand. Dit effect is vermoedelijk door een stabiliserend effect van het kristalrooster.

Dit effect van de kristalliniteit is ook van belang bij het incorporeren van deze derivaten in materialen. Polymeercoatings werden gemaakt door een dimeer-dieen te laten reageren met polythiolen (hoofdstuk IV) en dimer diolen en tetraolen met (tri)isocyanaten (hoofdstuk V). De thiol-eennetwerken waren verrassend kristallijn, wat gedeeltelijk ten gevolge is van de lage vaste stof in het uithardende hars. De alifatische en silicone thiol-eennetwerken waren thermisch degradeerbaar bij vergelijkbare temperaturen als bij de gebruikte dimeren. Door de macromoleculaire architectuur van de netwerken te wijzigen, kan het verlies van mechanische integriteit bij thermische degradatie gewijzigd worden. Het bestuderen van thermische dissociatie in coatings was moeilijker dan dikkere stalen, door de abrupte eigenschapsveranderingen (solventresistentie en hardheid) en een lagere temperatuurscontrole. Thermisch gedegradeerde coatings konden zeer gemakkelijk verwijderd worden eenmaal het gelpunt bereikt werd, wat interessant is voor bv. de luchtvaartindustrie. Thermisch gedissocieerde materialen konden opnieuw vernet worden voor enkele cycli. De beperking hierin is voornamelijk door het optreden van foto-oxidatie. Interne spanning verdween bij gelijktijdig of stapsgewijs breken en vormen van bindingen. De beperkte oxidatieve stabiliteit en de zuurstofrijke testopstellingen limiteerden dit proces weliswaar tot een eenmalige (gedeeltelijke) stress relaxatie.

Vooruitzichten

Na dit onderzoek blijven er heel wat uitdagingen over. Een belangrijk punt is het optimaliseren van de foto-oxidatieve stabiliteit. Ook al kan de aanwezigheid van zuurstof vermeden worden in een laboratorium, is dit vaak geen optie bij industriële toepassing. Een uitbreiding op het exploratieve werk dat hieromtrent uitgevoerd werd is aan te raden. Belangrijke parameters zijn de substituenten, golflengtes, oplosmiddelen (en polymeermatrices) en aanwezigheid van stabilisatoren en zuurstofscavengers.

Het mechanisch splitsen van antraceendimeren lag buiten de opzet van dit onderzoek, maar is interessant op zowel fundamenteel als toegepast niveau. De sterke invloed van de 9-substituent op de thermische dissociatie geeft reden om te vermoeden dat dit ook mechanische dissociatie zal beïnvloeden.

Verdere studies op donor-acceptorantracenen zijn een mogelijkheid, maar voor industriële toepasbaarheid is een kortere synthetische route vereist. Er van uit gaande dat dit mogelijk is, zou mits sterkere donoren en acceptoren een verschuiving van de absorptie tot het zichtbare spectrum mogelijk zijn. Andere substitutiepatronen in conjugatie zijn ook te overwegen.

Naast de bestudeerde dimeren tussen identieke antracenen, is het interessant om de eigenschappen van heterodimeren te bestuderen. Zo kan mogelijk de eigenschappen verder gevarieerd worden met slechts een beperkt aantal beschikbare antraceenderivaten.

De fotochemische dissociatie van de dimeren verliep vlot, maar is beperkt tot oppervlaktes en verdunde stalen. Door verschillende LED's te gebruiken, kan splitsing mogelijk optreden bij dikkere stalen. Belangrijk is het om te bestralen bij een golflengte waarbij de dimeren (zwak) absorberen, maar de gevormde antracenen niet.

Deze chemie kan tevens ook gebruikt worden om materialen te ontwikkelen waarvan de macromoleculaire structuur verandert door een stimulus. Dit wordt zeker interessant wanneer de combinatie wordt gemaakt met de antraceen-maleimide "klik" cycloadditie.

Eenmaal een hoge reversibiteit van de antraceendimerisatie verkregen kan worden, kan zelf-herstel en stress-relaxatie industrieel relevant worden en verder bestudeerd worden. Gezien deze derivaten relatief duur zijn om te synthetiseren, is het belangrijk om de vereiste hoeveelheid zo laag mogelijk te houden.

List of publications

Discussed in this thesis:

- Van Damme, J.; Vlaminck, L.; Van Assche, G.; Van Mele, B.; van den Berg; O.; Du Prez, F. Synthesis and evaluation of 9-substituted anthracenes with potential in reversible polymer systems. *Tetrahedron* **2016**, *72* (29), 4303-4311
- Van Damme , J.; van den Berg, O.; Brancart, J.; Vlaminck, L.; Huyck, C.; Van Assche, G.; Van Mele, B.; Du Prez, F. Anthracene-based Thiol-Ene Networks with Thermo-Degradable and Photo-Reversible Properties. *Macromolecules* **2017**, *50*, 1930-1938
- Van Damme, J.; van den Berg, O.; Vlaminck, L.; Brancart, J.; Van Assche, G.; Du Prez, F. Anthracene-based polyurethane networks: tunable thermal degradation, photochemical cure and stress-relaxation. *European Polymer Journal* **2018,** doi.org/10.1016/j.eurpolymj.2018.06.018
- Van Damme, J.; Du Prez, F. Anthracene-containing polymers toward high-end applications. *Progress in Polymer Science* **2018**, *18*, 92-119
- Chattopadhyay, S.; Van Damme, J.; van den Berg, O.; Du Prez, F. Anthracene-based colloidal polymer nanoparticles: their photochemical ligation and waterborne coating applications. *Part. Part. Syst. Charact.* **2018**, 1800030 (doi: 10.1002/ppsc.201800030)